From virus protection to cell isolation and biomarker discovery with aptamers

Shahrokh Ghobadloo

Thesis submitted to the
Faculty of Graduate and Postdoctoral Studies
in partial fulfillment of the requirements for the
Doctorate in Philosophy degree in Chemistry

Department of Chemistry and Biomolecular Sciences
Faculty of Science
University of Ottawa

Abstract

New affinity molecules such as nucleic acid aptamers are in demand in the science and medical fields. Current aptamer selection technologies can generate unique aptamers with desired properties to targets of interest. My thesis describes a series of investigations on the protection of an oncolytic virus, the isolation of target cells from biological fluids, and aptamer-facilitated biomarker discovery.

We tested individual aptamers and constructed a tetramer aptamer structure (quadramer) to increase virus infectivity. The quadramer protects vesicular stomatitis virus (VSV) during freeze–thaw cycles, shields the virus from neutralizing antibodies and increases viral active units. In addition to aptamers, we screened carbohydrate-based ice recrystallization inhibitors for the possible elimination of the cold chain of Vaccinia virus, VSV, and Herpes virus-1. N-octyl-gluconamide provides the longest shelf life for Vaccinia virus and Herpes virus-1 as tested according to the World Health Organization's requirements for viral vaccines efficiency during transportation and distribution.

We generated switchable aptamers capable of isolating cells expressing LIFR, NRP1, DLL4, uPAR, or PTCH1. These aptamers bind to the receptor positive cells in the presence of Mg^{2+} and Ca^{2+}, and release the pure cells upon addition of EDTA. The aptamers were applied for a sequential positive immunomagnetic isolation of cells from mice bone marrow. We also utilized fluorescence-activated cell sorting (FACS) in our aptamer selections to develop switchable aptamers to positive isolation of monocytes from human blood. Moreover, we have selected non-switchable aptamers as an affinity probe to the cells expressing Axl receptor for immunofluorescent analysis and cell sorting.

We determined aptamers to CD107a and applied them for biomarker discovery with mass spectrometry and found that CD107a was co-expressing with PD-1. Furthermore, we identified CD91 as binding partners to our aptamers in human monocytes using FACS and orbitrap mass spectrometry.

Acknowledgements

First and foremost, I would like to thank my supervisor, Professor Maxim Berezovski, for teaching and providing opportunities to learn, participate and grow in broad and diverse fields. I have been fortunate to have him as my supervisor.

Thanks to Dr. Ana Gargaun for editing the thesis and her great collaboration in the experiments.

I appreciate the Mitacs Accelerate PhD Fellowship and STEMCELL Technologies Canada Inc. for their generous support of my PhD studies. Dr. Samuel Clarke and his great team, from STEMCELL Technologies Canada Inc., whose expertise and time have been much appreciated.

Thanks to Ryan Girgrah for proof reading. Thanks to Dr. Darija Muharemagic, my first day at Dr. Berezovski's lab started in collaboration with her as a former PhD student. I would like to appreciate collaborators without whom my projects would not have been possible: Dr. Gleb Mironov, Nadia Al-Youssef, Dr. Nasrin Khan, Evan Bushnik, Dr. Amin Nozari, Thao Nguyen, Dr. Anya Zamay, and Afnan Azizi. Thanks to Ben Kingston and Bani Malhotra from Dr. Clarke's team for supporting the projects. Thanks to Theresa Falls for her help with mice experiments. Thanks to Dr. Pavel Milman for valuable scientific discussions and comments. Thanks to Dr. Reza Nokhbeh for supports. I am grateful to Dr. John C. Bell and Dr. Fabrice Le Boeuf for providing herpes virus type I, Vaccinia virus and vesicular stomatitis virus expressing fluorescent proteins. I thank Dr. Marie-Andrée Akimenko and Jing Zhang for providing the mice for the experiments.

I would like to thank Dr. Robert Ben and his team for giving me insight into carbohydrate-based ice recrystallization inhibitors. I would like to acknowledge Dominic Therrien and Andrew Ochalski for providing training. I would also like to thank the administrative staff at the University: Josée, Manon, Lorraine Houle, Cindy Strasbourg, Annette, Linda and Geneviève.

I would particularly like to thank the wonderful undergraduate students working with me on the research projects: Rebecca Katherine Casselman, Sarah McLaughlin, Mohamed Wehbe, Noreen Ahmed, Nadine Ahmed, Marco Cavar, Kaylee Fiset, Angelique, Connie and Jenny.

To my wife and my son

Sanna and Arian Ghobadloo

Table of Contents

List of Tables

List of Figures

List of Abbreviation

Symbol	Description
bp	Base pair
BSA	Bovine serum albumin
CEV	Cell-associated enveloped virion
CE	Capillary electrophoresis
DLL4	Notch ligand Delta-like 4
DMEM	Dulbecco's modified Eagle medium
DNA	Deoxyribonucleic acid
DPBS	Dulbecco's Phosphate Buffered Saline
FACS	Fluorescence-activated cell sorting
GFP	Green fluorescent protein
HSV-1	Herpes simplex virus type 1
IEV	Intracellular enveloped virion
IMV	Intracellular enveloped virion
IRIs	Ice recrystallization inhibitors
LC	Liquid chromatography
LIFR1	Leukemia inhibitory factor receptor 1
MACS	Magnetic activated cell sorting
mRNA	Messenger RNA
MS	Mass spectrometry

nAbs	Neutralizing antibodies
NOGal	N-octyl-D-gluoconamide
NOGlc	N-octyl-D-gluconamide
NRP1	Neuropilin-1 receptor
OGG-Gal	Ornithine–glycine–glycine-galactose
PBS	Phosphate-buffered saline
PCR	Polymerase chain reaction
PD-1	Programmed cell death protein 1
PFU	Plaque-forming units
PTCH1	Patched 1
qCE	Quantitative capillary electrophoresis
RFP	Red fluorescent protein
RNA	Ribonucleic acid
SDS	Sodium dodecyl sulfate
SELEX	Systematic evolution of ligands by exponential enrichment
uPAR	urokinase plasminogen activator receptor
VSV	Vesicular Stomatitis virus
WHO	World Health Organization
YFP	Yellow fluorescent protein

Chapter 1

Introduction

1.1. Nucleic acids

Deoxyribonucleic acid (DNA) and ribonucleic acid (RNA) are polymers of nucleotides.[1] Both DNA and RNA nucleic acids have the purines adenine (A) and guanine (G) and the pyrimidine cytosine (C). DNA has the pyrimidine thymine (T), which is replaced by the pyrimidine uracil (U) in RNA. Nucleotides have three parts: a five-carbon sugar, a nitrogenous base, and a phosphate group (**Figure 1.1**).[2] Cytosine is complementary to guanine with three hydrogen bonds, and adenine is complementary to thymine with two hydrogen bonds. One of the main differences between RNA and DNA is the 2'-OH group on the sugar unit (RNA has an OH group). The difference between uracil and thymine is a methyl group at C5.

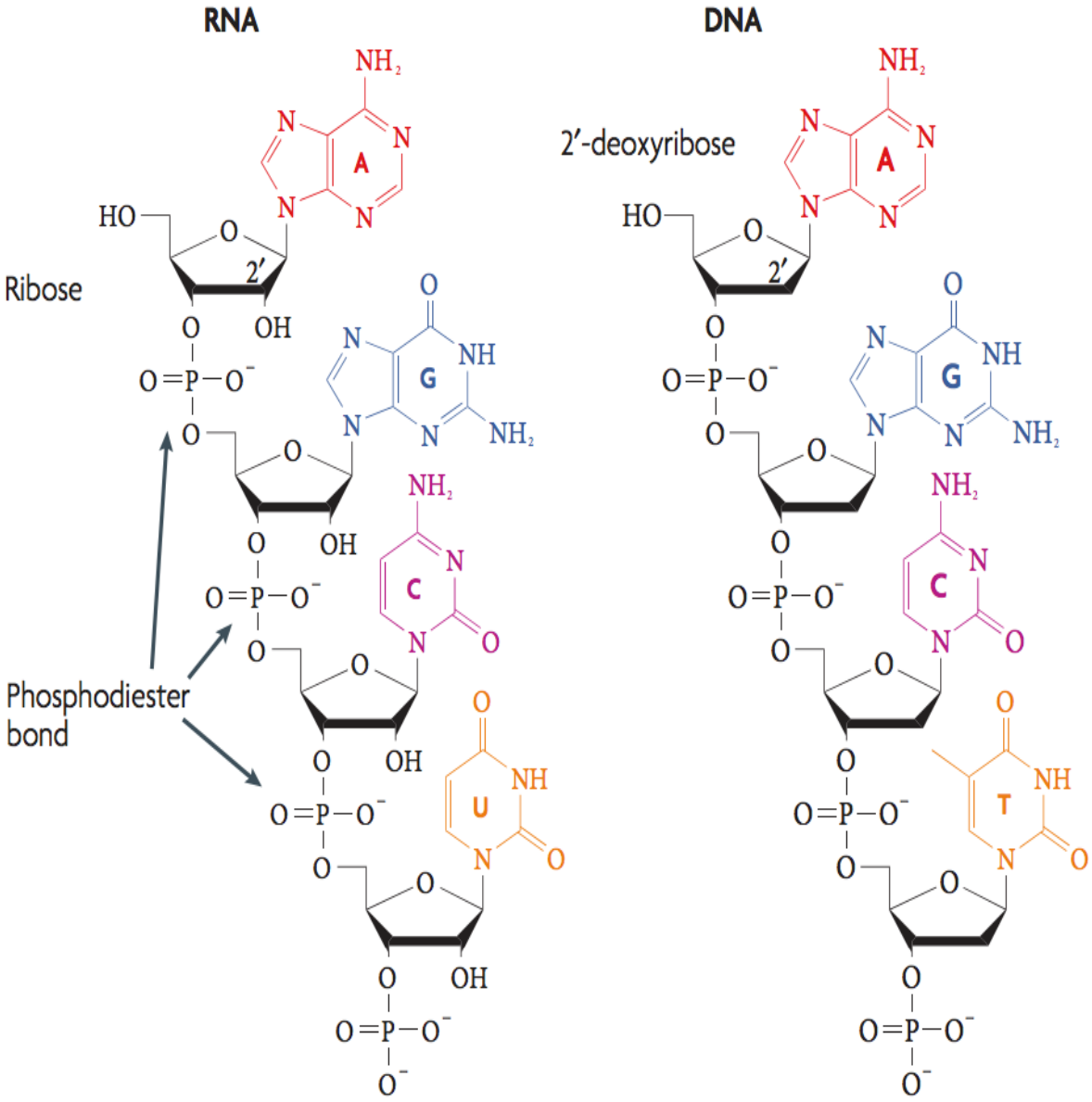

Figure 1.1. Chemical structure of deoxyribonucleic acid (DNA) and ribonucleic acid (RNA). The five-carbon sugar in RNA is ribose, which in DNA is replaced with 2′-deoxyribose. The figure reprinted with permission from[2].

Nucleic acids, in addition to expressing and passing on genetic information, have biochemical roles through their binding to other molecules, depending on their contiguous conditions. Hydrogen bonds, aromatic-aromatic interactions (π stacking), van der Waals forces, shape complementarity, hydration, and surrounding ions are main factors that determine nucleic acids' structures, such as loop, bugle, hairpin, stem, and G-quadruplex.[3] Nucleotides individually contribute unique dynamics to the nucleic acid molecules. Double-stranded DNA has a double helix structure with forms of A, B, and Z. The most typical structure of DNA is the double-stranded B-form (right-handed). Type Z is left-handed, while A is right-handed; they are also different in the sizes of grooves.[2] In single-stranded nucleic acids, unpaired nucleotides make bulged loops. Guanine-rich sequences cause G-quadruplex structures, where four guanines are a core of the structure in a rotational manner. The G-quadruplex structures are stabilized by a monovalent such as K^+.[4] The structural conformations (such as hairpins and quadruplexes) impact nucleic acid recognition.

1.2. Nucleic acids and protein interactions

Reagents that interact with high specificity and affinity are important in the scientific and medical fields. Nucleic acids (DNA and RNA) are built from nucleotides that contain three chemical groups: a phosphate group, a sugar molecule and a nitrogenous aromatic base. Four different nitrogenous aromatic bases in RNA or DNA are capable of providing specific binding affinity to amino acids. Various sequences of nucleotides give shape to a single strand of nucleic acid by binding with other molecules through hydrogen bonding, dipole, ionic, Van der Waals forces, hydrophobic effect, solvent interactions and entropic forces.[5-7] Nucleic acids make discrete structures through stacking interactions of the bases and hydrogen bonds.[8, 9] Nucleic acid

conformations transit easily because of their phosphodiester backbone flexibility to rotate.[5, 9-11] Thus, single-stranded nucleotides recognise and interact with other molecules through noncovalent bonding and have "induced conformation" because of their flexibility in rotation[7, 10, 11], which is different than the "lock and key" mechanism of antibodies.[10, 12, 13] Nucleic acids orient in shape to "key and lock fit" or to induce shape through the affinity of nucleotides to specific amino acids to fit in their epitope.[14] Nucleic acid interactions can be specific or nonspecific. For instance, histone proteins and DNA have a non-specific interaction which is the result of the negatively charged sugar phosphate backbone of DNA and the functional groups on histone regardless of the DNA sequence.[7, 13] Specific interactions are dependent on the primary protein structure and the nucleotide sequence. Protein-nucleic acid interaction is more complex than a simple molecular docking process. Some proteins and nucleic acids change conformations in the presence of each other.[13, 15] The conformational changes can also affect the properties of the protein.[13, 16] In general, specific protein-nucleic acid interactions can be divided into two sets: nucleotide-specific interactions and shape interactions. The former set of interactions occur through hydrogen bonds and hydrophobic interactions while the latter interactions need sequence-dependent structure and deformability in addition to hydrophobic or hydrogen bonds to have specificity.[13, 17] Cations also affect nucleic acid-protein interaction; divalent cations such as Mg^{2+} are more effective than monovalent Na^{+} as they stabilize the backbone.[18] These nucleic acid interaction properties empower us to generate DNA or RNA as affinity tools with the desired function and properties to a specific purpose, which are called aptamers.

In 1990, two laboratories published their discovery of aptamers independently [19, 20]. After this breakthrough, aptamer technologies have been growing for diagnostic, therapeutic and analytic purposes. Aptamers have drawn attention because of their unique advantages such as: small size,

not animal or cell dependent, ease to be modified, economical, and ease to be labeled. Aptamers are selected against a specific target from a library of approximately 10^{15} different sequences. [20-23] One of the most interesting advantages of aptamer technology is the ability to develop a highly tuned aptamer with unique properties and functions by changing the selection procedure. The selection procedure called Systematic Evolution of Ligands by Exponential Enrichment (SELEX).

1.3. Systematic Evolution of Ligands by Exponential Enrichment (SELEX) technology

For the first time, in 1990, Tuerk and Gold [19] and Ellington and Szostak [24] independently developed the "Evolution of Ligands by Exponential Enrichment" (SELEX) method to generate single-strand oligonucleotides, RNA or DNA, from a mixed library. SELEX is based on the Darwinian evolution of single-stranded oligonucleotides. The selected single-strand of RNA or DNA with affinity and specificity to a specific target has been named an aptamer. The library is a chemically synthesized oligonucleotide library. Each oligonucleotide includes a random region of nucleotides flanked by a fixed region with reverse complementary to primers for amplification. The classical SELEX includes cycles of several steps, which starts by incubating a target with the synthesized single strand oligonucleotide library (**Figure 1.2)**. After non-binding oligonucleotides are washed away, the bound oligonucleotides are recovered and amplified. Each additional cycle of aptamer selection provides a more stringent evolutionary selection of oligonucleotides with high binding affinity.

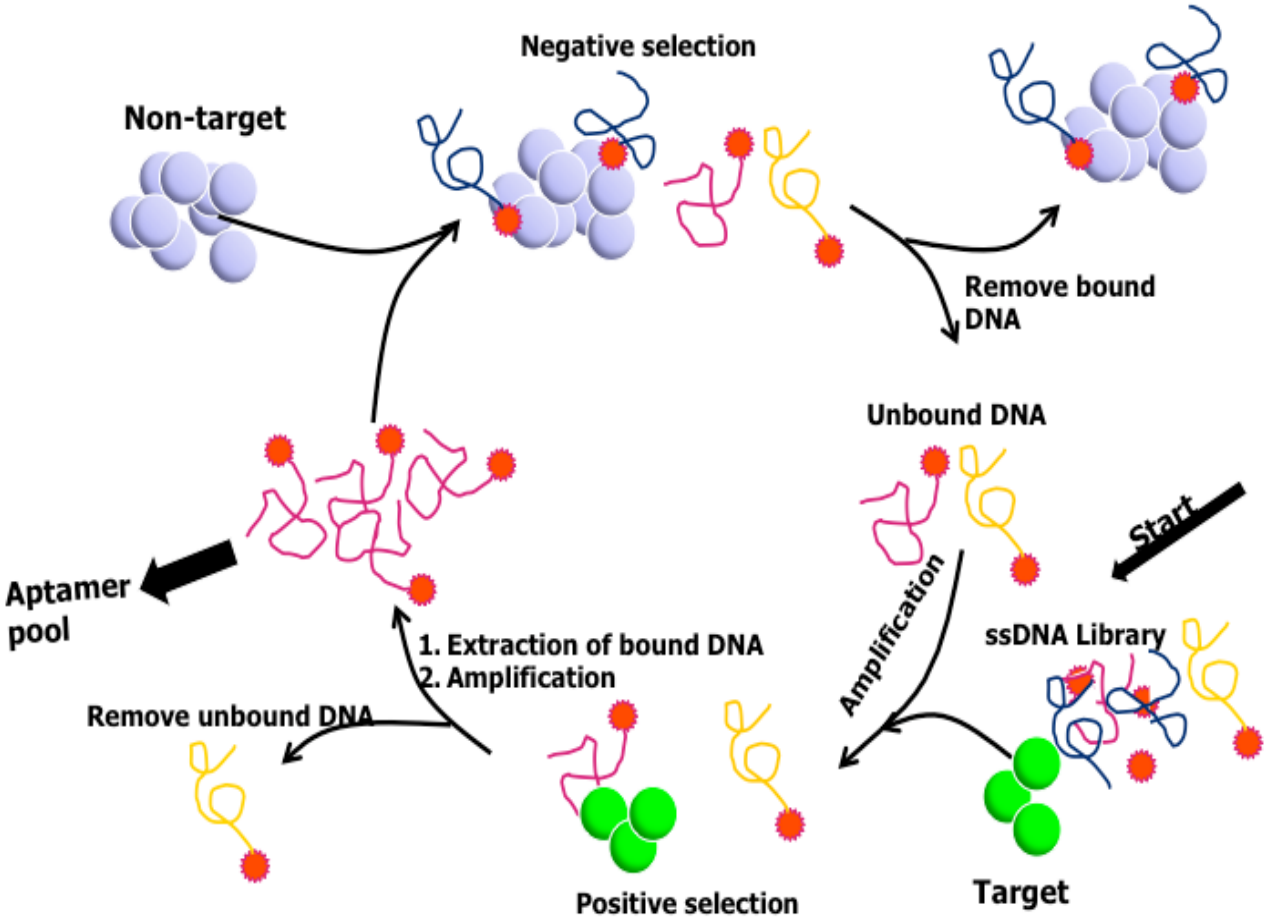

Figure 1.2. Schematic representation of DNA aptamer selection using the SELEX method. Single strand nucleotides with specific binding to a target are evolved and enriched during each cycle of aptamer selection. The specific binding pool is subjected to sequencing.

To recover as many single-stranded oligonucleotides with binding affinity as possible, the first cycle has a longer incubation time and fewer washes. To increase the evolutionary selection pressure, the incubation time is decreased, and the number of washes is increased gradually in each round of selection. In the SELEX procedure for DNA aptamers, the output of each cycle is amplified by PCR, and single-stranded DNA molecules are isolated and purified for the next round of selection. In the selection of RNA aptamers, the resulting RNA of each cycle was reversely transcribed, amplified, and then transcribed for the next round of selection. Adding

negative selections after three cycles eliminates the non-specific binding oligonucleotides. The specific binding affinity of the single-strand oligonucleotides from each round is evaluated, and the pools with the highest specificity and affinity are subjected to sequencing. The resulting single stranded DNA or RNA sequences with specific binding affinity are called aptamers. Since the 1990s, arrays of modifications have been applied to the traditional SELEX to obtain more efficient, specific, and high-binding affinity aptamers with desired functions.

The single-stranded oligonucleotide library is one of the main subjects of modification. Oligomers are made of four different nucleotides, while polypeptides contain twenty different amino acids. To increase the diversity in oligonucleotides addition of functional groups and artificial nucleotides have been used [23, 25]. For example, Dom Zichi's group incorporated modified deoxyuridine triphosphates (dUTPs) to diversify their DNA libraries[26, 27]. More specifically, they modified nucleotide triphosphate analogs at the 5'-position of dUTP with 5-benzylaminocarbony-dU, 5-naphthlmethylaminocarbonyl-dU, 5-tryptaminocarbonyl-dU, and 5-isobutylaminocarbonyl-dU[26]. Bruce E. Eaton's group added conformational flexible functionality groups such as amino acids and alkyls to Uridine-triphosphate (UTPs) to make the oligonucleotide library compatible with proteins and increase the binding of an aptamer to proteins.[27, 28] Adding such functional groups can also provide the oligonucleotides with more torsional freedom than proteins. [27]

Besides modifications to the library, the SELEX procedure itself is also highly altered. To increase the aptamer selection speed, lower the volumes, and remove contaminations, high purity targets such as recombinant proteins can be used. In this case, the target is immobilized on a solid phase. One drawback to this approach is that as a result of immobilization and fusion of the target the epitopes exposed to aptamers may differ than when they are in their natural

environment. Furthermore, the selected aptamer may be contaminated with aptamers, which have a high-affinity, and cross-reactivity to the solid support. One of the most common solid support systems used are magnetic beads [29].

To remove non-specific aptamers to a counter-selection is applied. The capillary electrophoresis-SELEX has been developed for the efficient separation of unbound oligonucleotides from bound aptamers to their target [30]. The principal of this method is electrophoretic mobility. The capillary electrophoresis-SELEX reduces the number of aptamer selection cycles [30], but it is limited to a small volume and the capillary electrophoresis conditions such as charge and solutions.

Cell-SELEX has been developed to employ the generated aptamers in therapy and cancer research, differentiate cells from each other, discover biomarkers, and target recognition. In this method, oligonucleotides are developed with binding affinity to the cell surface targets in their native state (Figure 1.3). Prior knowledge of the target identity is not necessary; the target molecule can be identified after the aptamer selection.[31] The limitation of this approach is the effect of the cell membrane's and the aptamers' negative charge. The negative charge of the membrane and aptamers can repulse them and direct the aptamers to more positive proteins on the cell membrane.[31]

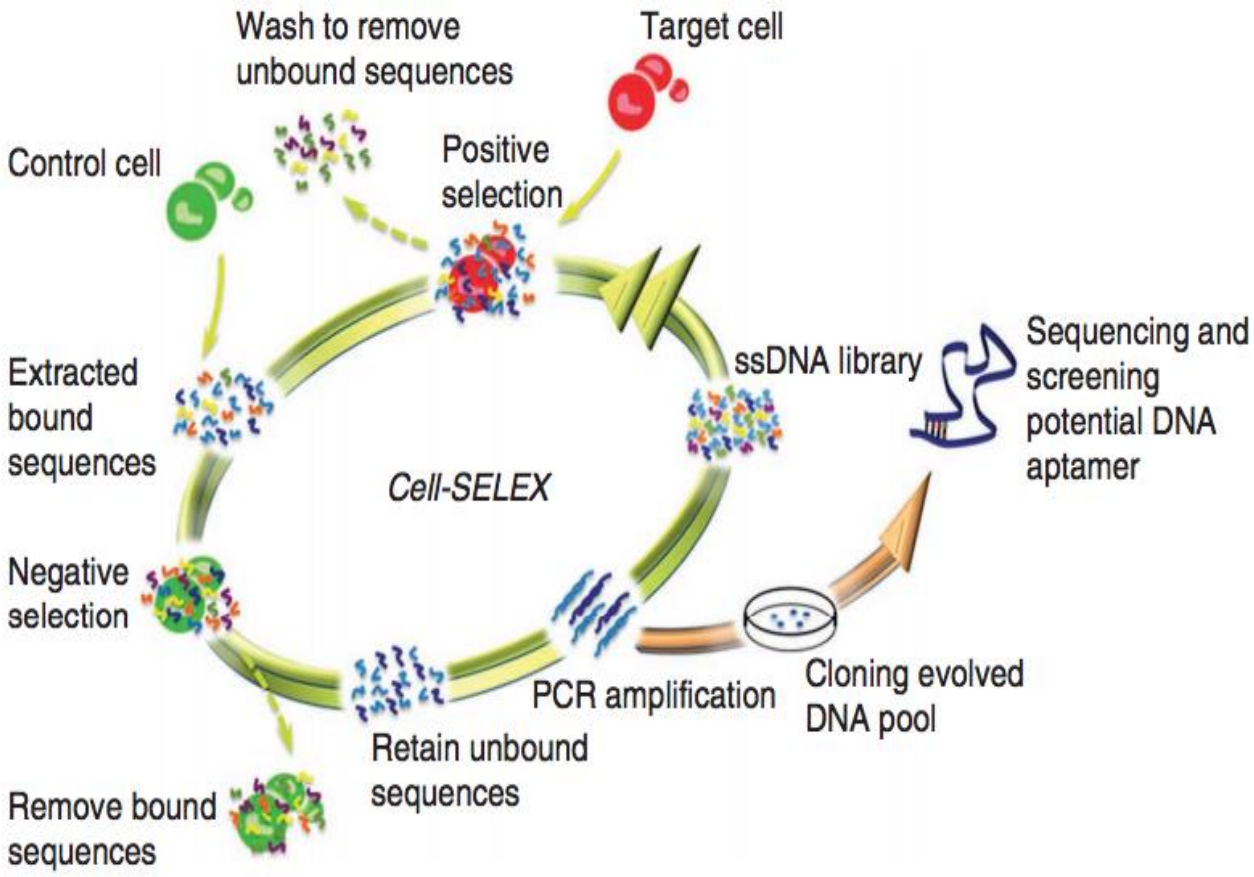

Figure 1.3. Schematic representation of aptamer selection to a specific cell using SELEX method (Cell-SELEX). The figure reprinted with permission from[31].

The sequencing of the selected oligonucleotides pools was another crucial area that that has been modified. Identification of the aptamer sequences from the aptamer pools with the highest affinity is a crucial step in the aptamer selection process. Initially, cloning was used to sequence aptamers. Nowadays, high throughput sequencing has emerged as a more promising method. [32] This method has the advantage of a comprehensive understanding of the functional motifs and abundance of each possible aptamer. High-throughput sequencing provides the possibility of analyzing a million sequences whereas clone sequencing can only analyze a maximum of several hundred clones.

Although there has been much progress, investigations on aptamer selection technology are still needed to improve affinity and specific binding of the developed aptamer, non-specific binding of aptamers to dead cells, and fluctuation of aptamer-specific binding with changing conditions. Moreover, aptamer structures are affected by interactions with other molecules in the solution.

1.4. Cations govern aptamer conformational structures

The structure and conformation of aptamers are the main parameters that govern their binding affinity. Cations govern the conformational structure of all nucleic acids, including DNA aptamers. The negative charges of the phosphate groups on nucleic acids need to be shielded with cations; this interaction influences the conformational structure of nucleic acids. Amanda Beck et al. tested the effect of divalent ions on triplex DNA stabilization, using Circular Dichroism (CD). They reported that positively charged cations increase the stability of the DNA structure. They tested the conformational transition of the DNA structure with changing cation concentrations.[33, 34] The influence of cations is changed depending on their size and charge.

Divalent cations have a higher effect on DNA conformation than monovalent cations. In an experiment which compared the influence of Na+ and Mg^{2+} on DNA conformation, a 1000 times higher concentration of Na+ was as effective as Mg^{2+} to stabilize triplex DNA.[33]

In addition to the charge of cations, their size is another major governing factor of the conformational stability of DNA. The Watson-Crick DNA structure stabilization and conformation can be changed by the concentration of small metal ions.[35] The stability of the DNA structure decreases with the increasing size of divalent cations. Small cations contribute a

stronger Columbic electrostatic potential interaction because they easily fit in grooves and cause a closer distance interaction to the phosphate groups. The size also affects charge density. Mg^{2+} provides significantly higher DNA melting temptation, as compared to other divalent cations. The charge density of Mg^{2+} is greater than Ca^{2+} because of the smaller size of Mg^{2+}.

Charge and size also affects the hydration of ions. Smaller ions, more than larger ions, were hydrated.[35, 36] The freedom of cations contributes to their influence on DNA conformation. A cations' hydration affects their availability.

In conclusion, due to the negative charges of the phosphate groups, cations interact with nucleic acids and govern their structure. Ionic size, charge density, binding site on DNA, and ion hydration are the main factors that determine DNA conformation. Based on this, our objective was to use Mg^{2+} and Ca^{2+} to engineer the aptamer evolutionary selection process to generate switchable aptamers. We modified SELEX where the aptamer binding step was done in the presence of calcium chloride and magnesium chloride. In addition, the elution of the bound aptamers was done by adding EDTA; EDTA chelates Ca^{2+} and Mg^{2+} which can change the conformation of the aptamers' structure and in turn can affect their binding.

1.5. Affinity and Avidity of Aptamers

Strong and specific binding to a target is an essential property of aptamers. The strength of binding is often-called affinity and expressed as dissociation constant (K_d). Affinity is depended on the interaction between aptamer paratopes and target epitope. Avidity reflects several affinities in a structure of aptamers, which have a multiple binding sites with several epitopes. Avidity of aptamer structures is approximately the average affinity of all target epitopes and aptamer paratopes. Avidity is determined by the number of binding sites on the aptamer structure

to a target and their structural arrangement. Constructing a structure with multiple aptamers can increase specific binding.

1.6. Aptamer applications

The advantages of aptamer technologies such as their flexibility to generate aptamer with desired functions have provided a wide range of opportunities in aptamer applications such as therapeutic, diagnostic, and viral applications and targeted drug delivery. [37]

Diverse strategies have been used to employ aptamers in therapy. One strategy is using aptamers as antagonists to block signaling pathways. In this approach, an aptamer with a high binding affinity is applied to block receptor-ligand or protein-protein interactions. For example, Pegaptanib, a single-stranded oligonucleotide is used to treat macular degeneration by binding to the vascular epidermal growth factor and blocking its effects.[38]

The application of aptamers for analytical purposes is an area that has captured the attention of chemists. Aptamers were successfully applied in chromatography, where they were immobilized as ligands on a solid support [39], and they were also used as biosensors for Vaccinia virus [40]. Another common clinical application of aptamers is for the detection of microorganisms such as those responsible for bacterial and viral infections [41]. In 2006, Gopinath et al. reported specific aptamers for the identification of several viral strains. They were able to classify the human influenza A virus subtype H3N2 with discrimination ability [42].

Another application is to use aptamers for targeting the cell membrane molecules. The aptamers to the cell membrane molecules can be generated through Cell-SELEX method without prior knowledge of the molecules. The molecules can be proteins, lipids, and carbohydrates.

Cell-SELEX also is able to generate aptamers to meet cell membrane molecules and distinguish molecular differences between two types of cells. The molecule differences can be identified using mass spectrometry methods. This approach can be used as a biomarker discovery technique and called Aptamer facilitated Biomarker Discovery (AptaBiD).[43] The logic behind it is that Cell-SELEX develops aptamers for molecular targets, which are exclusive to positive cells and absent in the cells used in the negative aptamer selection. The biotinylated aptamer can be applied to pull down its own target from cell membranes using streptavidin-coated magnetic beads. Thus, mass spectrometry can identify the aptamers' target molecule[43], which result in biomarker identification and discovery. Biomarkers are quantifiable characteristics, which determine a person's physiologic or pathologic state, and response to a biological process.[44, 45] Biomarkers are also crucial for monitoring a person's state during medical treatment. Biomarkers are often membrane molecules found on target cells. [45, 46] Various methods for discovering biomarkers are: western blotting, mRNA screening by quantitative PCR and two-dimensional gel electrophoresis followed by mass spectrometry.[45, 46] Recent developments in aptamer technology have enabled discovery of more accurate and sensitive biomarkers. Aptamer technologies empower the discovery of cell membrane biomarkers in heterogeneous tissues and generate probes with high specificity. This is because aptamers with exclusive binding to target cells have a unique molecular structure when bound to the biomarker. The diverse structures of nucleic acids, which are a result of the random nucleotide sequences, are a promising approach to distinguishing different antigen in two heterogeneous samples or identifing an antigen on a cell type in a heterogeneous mixture of cells such as blood or bone marrow. Cell-SELEX enables the selection of aptamers against unknown receptors exclusive to a particular cell population in a mixture of cells.[43] The selected aptamer can isolate the target molecule unique to the cell

population by employing biotin-streptavidin magnet technology.[43] Employing Fluorescence-Activated Cell Sorting (FACS) for cell- SELEX allows to exclusively detect biomarkers of specific cell types in heterogeneous tissues such as bone marrow or blood. The aptamer can then be used to isolate the cell unique target followed by identification by mass spectrometry.

Aptamers as a molecular probes are further area of success for aptamers applications. Fluorescence aptamers have been shown as molecular probes to study membrane targets on live cells such as microscopic and flow cytometric analysis as well as surface energy transfer (SET) studies. Aptamer can provide better resolution because of their small size. For example, a conjugated aptamer Sgc8 with gold nanoparticles was used to analyze the distance of two targets on cell membranes using SET.[47]

Aptamers also have been applied as a vehicle for therapeutic reagents to target intracellular proteins.[48] Aptamers mainly internalize cells through receptor-mediated endocytosis.[49] The specificity of Sgc8 aptamer to its target inside cell was confirmed when experiments had been done on target cells in comparison to controls at 37°C.

Aptamer technology is also going to open a wide area of applications in the isolation of discrete cell types from heterogeneous suspensions in medicine and research such as cell therapy, capturing circulating tumor cells, and isolating specific cells from bone marrow, tissue engineering, regenerative medicine and diagnosis.[50-53] Clinics need cell purification with high efficiency and purity as per the standards of the Food and Drug Administration.[54] As a result, a wide range of cell sorting and purification methods has been developed. Current cell isolation methods are classified into four groups: cell density and size, cell morphology, cell adherence, cell immunophenotypic, and cell elasticity in response to acoustic waves.[55, 56] More work needs to be done in order to improve these approaches to increase the viability, purity, and

functionality of the isolated cells. Antibody-based cell purification methods enable the removal of target cells from a large heterogeneous sample faster and with higher purity than other techniques. Due to their high specificity, antibodies have so far shown to be the most efficient and reliable. For example, antibodies facilitate cell isolation in fluorescence-activated cell sorting (FACS) and magnetic activated cell sorting (MACS). Flow cytometry and cell sorting instruments are capable of examining cells in a wide range of fluorescence and light scattering signals correlated to cellular physiology, cell morphology, surface and intracellular protein expression. The quality of cell purification methods is based on isolated cell purity, recovery, viability and yield.[57] Common biological samples are bone marrow, peripheral blood, and tumor.[58] The major challenges in cell isolation from these types of samples are removal of additives and the antibodies bonded with the cells, which can change cell function and contaminate downstream applications. Cell isolation can be achieved through two main strategies: "negative isolation" or "positive isolation".[59] In negative isolation, non-target cells are eliminated from the cell mixture. Negative isolation is chosen when the isolated target on the cell needs to be left unmodified or no specific antibody is available for the target cells. Moreover, negative isolation is applied for enrichment of target cells. Positive isolation is a direct method for isolating cells from a heterogeneous sample. In this approach, the target cells are labeled and isolated. One challenge of positive cell isolation is that the cells of interest may be affected due to interactions with ligands or antibodies during the isolation process. In the positive isolation, additives, ligands or antibodies, remain in the final sample with the cells after isolation and persist throughout the duration of any downstream experiments; this can cause clustering of receptors, triggering of signaling pathways or blocking of receptor functions. For cell therapy, pure and viable cells, free of antibodies and other additives, are necessary.[60, 61] To accomplish

the isolation of pure cells free of additives, antibody, and beads contamination, we aimed to generate switchable aptamers via a positive cell isolation method. We were successful in selecting switchable aptamers, which bind to target cells in the presence of Mg^{2+}/Ca^{2+} and the aptamers release, the purified cells upon addition of EDTA in solution.

1.7. Thesis outline

We sought to harness the power of aptamer technology for discovering novel biomarkers, detecting and isolating target cells from heterogeneous tissues, protecting oncolytic virus infectivity from neutralizing antibodies, and stabilizing virus infectivity. Furthermore, we screened and evaluated carbohydrate-based small molecule ice recrystallization inhibitors to preserve the potency of viruses. Chapters 2 to 8 of this thesis are divided based on the outcomes of specific objectives.

Chapter 2 had two objectives. The first one was to evaluate the selected aptamers with binding affinity to VSV and its neutralizing antibodies (nAbs) to protect VSV infectivity from nAbs. The second objective was to construct a structure to increase the number of binding sites, which results in high avidity, to better protect VSV potency from nAbs. The VSV neutralizing antibody is the main obstacle of oncolytic virotherapy. Dr. Anna Zamay and Dr. Darija Muharemagic developed the aptamers at Dr. Berezovski's lab. Plaque-forming assays were done in collaboration with Dr. Darija Muharemagic. The developed aptamers' application was successful and increased the oncolytic virus infectivity in the presence of neutralizing antibodies in vitro.

In Chapter 3, the objective was to evaluate the efficiency of monomeric and quadrameric aptamers from Chapter 2 for stabilizing VSV potency during multiple freeze-thaw cycles and increasing the number of active units of viral particles. The results unveiled a new application of aptamers that can be used to preserve a virus from freezing damage.

In the previous chapters, we evaluated a new application of the developed aptamers technology to protect an oncolytic virus, VSV, from neutralizing antibodies and from damage due to storage to increase the active viral units. To increase complexity of our aptamer research we moved from small viruses to cells. In Chapters 4 to 6, we generated EDTA switchable aptamers for positive cell isolation. We pursued this goal because the main challenge of current immunomagnetic positive cell isolation is the persistence of bound antibodies and magnetic beads, which may not only alter cellular viability but also contaminate any downstream applications. We employed Cell-SELEX with some modifications; we incubated the cells with the single strand DNA in the presence of Ca^{2+}/Mg^{2+} and recovered the bound single strand DNAs to generate EDTA switchable aptamers to the cells expressing specific receptors. The outcomes of this method were three groups of aptamers. The first group contains the aptamers (Chapter 4) selected for the cells expressing Notch ligand Delta-like 4 (DLL4), leukemia inhibitory factor receptor (LIFR), neuropilin-1 receptor (NRP1), urokinase plasminogen activator receptor (uPAR), and Patched 1 receptor (PTCH1). The aptamers released the pure and intact cells upon addition of EDTA. However, we could not identify molecular binding partners for the aptamers. The second group (Chapter 5) includes an aptamer to cells expressing Axl tyrosine kinase. Even though we aimed to generate EDTA switchable aptamers using the modified Cell-SELEX method in Chapter 4, the generated aptamer does not leave the cells by adding EDTA. The aptamer facilitated biomarker discovery approach coupled with the liquid chromatography Orbitrap Fusion Tribrid mass spectrometer (LC-MS) identified Axl tyrosine kinase as a possible molecular target of the aptamer. The third group comprises the aptamer generated against cells expressing PD1, and CD107a was recognized as a potential target of the aptamer (Chapter 6).

As a result of lessons learned from previous studies (Chapters 2 to 6) and understanding the influence of experimental conditions and environment (such as ions, proteins, and other cells in the solution) on aptamers as well as cross reactivity of aptamers with other molecules, we generated EDTA switchable aptamers to primary cells from human blood, monocytes, in their native state environment in Chapter 7. For this purpose, we developed DNA aptamers by Fluorescence Activated Cell Sorting (FACS) and SELEX. The developed aptamer was employed in biomarker detection using an LC-Orbitrap Fusion Tribrid mass spectrometer. CD91 was identified as a possible target of the aptamer and an exclusive biomarker of monocytes in whole blood leukocytes.

The last chapter consists of research done in parallel with studying the aptamers' efficiency as a cryoprotectant of the Vesicular Stomatitis virus (VSV) in Chapter 3. We sought to evaluate the impact of carbohydrate-based ice recrystallization inhibitors (IRIs) on the potency of viral vectors for possible elimination of the cold chain and apply them to stabilize the potency of Vaccinia virus, Vesicular Stomatitis virus (VSV), and Herpes virus-1 (HSV-1). The leading and novel outcome of this research was the discovery of the *N*-octyl-*D*-gluconamide effect of increasing the shelf life of Vaccinia virus at room temperature from four days to more than forty days and of the Herpes virus-1 from a day to more than nine days, according to the strict requirements of the World Health Organization.

Chapter 2

Aptamers to shield oncolytic viruses

2.1. Objective

The first objective was to evaluate the selected aptamers with binding affinity to VSV and its neutralizing antibodies (nAbs) to protect VSV infectivity from nAbs. The second objective was to design and construct an aptamer construct, a quadramer, to increase avidity and better protect VSV potency from nAbs. Dr. Anna Zamay and Dr. Darija Muharemagic in Dr. Berezovski's group developed the DNA aptamers used in this study.[62]

Shahrokh M. Ghobadloo with Dr. Maxim V. Berezovski (supervisor) designed the research and Shahrokh M. Ghobadloo performed the experiments. Plaque forming assays were done in collaboration with Dr. Darija Muharemagic.

2.2. Background

Cancer is classified as the third cause of death worldwide by the World Health Organization (WHO).[63] The main characteristics of cancer include prolific invasion and metastasis.[64] Cancer stem cells are tumor-initiating cells that also cause tumor metastasis; they are resistant to current therapies such as chemotherapies and radiotherapies.[65] Cancer stem cells are able to reprogram themselves to make epithelial to mesenchyme transition, which leads to metastasis. Oncolytic viruses are capable of accurately targeting and killing both cancer and cancer stem cells without affecting healthy cells. Oncolytic virus therapy is one the most promising breakthroughs because it targets tumor cells with defects in their interferon response system while leaving healthy tissue unaffected.[66-68] The virus lyses tumor cells and directs the immune system to the infected cancer cells using immune checkpoints.[66-69]

One of the most promising oncolytic viruses is Vesicular Stomatitis virus (VSV). VSV is a bullet-shaped, prototypic, negative-sense RNA virus.[70, 71] VSV integrates no part of its genome into its host genome.[72] Its 11 kb genome codes five genes: nucleocapsid protein, phosphoprotein, matrix protein, glycoprotein and large polymerase.[73] VSV is a suitable oncolytic virus because glycoproteins on VSV facilitate infection in a wide range of cells. Also, VSV induces apoptosis in transformed cells within a few hours because of its rapid life cycle.[74, 75] The interferon system of most tumor cells is diminished.[75] Interferons regulate the cell cycle, apoptosis and antiviral responses. As a result, a virus with a replication system that is sensitive to interferon-induced anti-viral responses can grow only in cancer cells.[75] For example, wild type VSV suppresses interferon induction whereas VSVΔ51 induces the interferon system and its replication is also strongly suppressed by the interferon system.[75] The matrix protein of wild type VSV blocks the system that induces interferons in host cells. However, the deletion of the methionine at amino

acid position 51 leads to a defective VSV matrix protein that is not able to survive in healthy cells and results in selective targeting of cancer cells. The virus will target only the tumor cells, which lack in interferons.[67, 73-76] The main obstacle to using oncolytic viruses in cancer therapy are the neutralizing antibodies (nAbs) produced by the patient's immune system.[77]

The first requirement for oncolytic therapy is that the virus must infect the cancerous cells; thus their infectivity should be protected from nAbs until they reach tumor cells. Wide ranges of strategies were applied such as using polymers to protect virus vectors in blood from neutralizing antibodies.[78] To guard the therapeutic viral infectivity against nAbs, polymer-coating with polyethylene glycol[79] and poly-[N-(2-hydroxypropyl) methacrylamide][80] have been attempted but proven unsuccessful. Even though polymers were able to increase the half-life of the coated viruses, but they significantly decrease the virus ability to infect cells and also polymer coating cause aggregation of viruses.[81] Another approach was using other virus proteins. The used strategies were not efficient because they blocked the virus and cells interaction to infect cells.

We hypothesized that the aptamers with binding affinity to VSV could shield the virus from nAbs while preserving its infectivity, and aptamers with binding affinity to nAbs could block the neutralizing antibodies. Moreover, constructing a quadramer structure of aptamers made of multiple shield aptamers can increase binding avidity and would lead to more effective shielding of the virus (**Figure 2.9**). We employed aptamers with binding affinity to VSV to protect the virus from nAbs and aptamers with binding affinity to nAbs for blocking purposes. Aptamers with binding affinity to VSV and its naturalizing antibodies were selected in Dr. Berezovski's lab by Dr. Anna Zamay and Dr. Darija Muharemagic.[82, 83] They developed aptamers to VSV[83] (**Figure 2.1**) and to neutralizing antibodies[82] (**Figure 2.2**) using competitive

SELEX. To select aptamers to neutralizing antibodies, they mobilized the antibodies on protein G-coated magnetic beads. The binding of the aptamers was evaluated via flow cytometry and electrochemical immunosensing displacement assays.

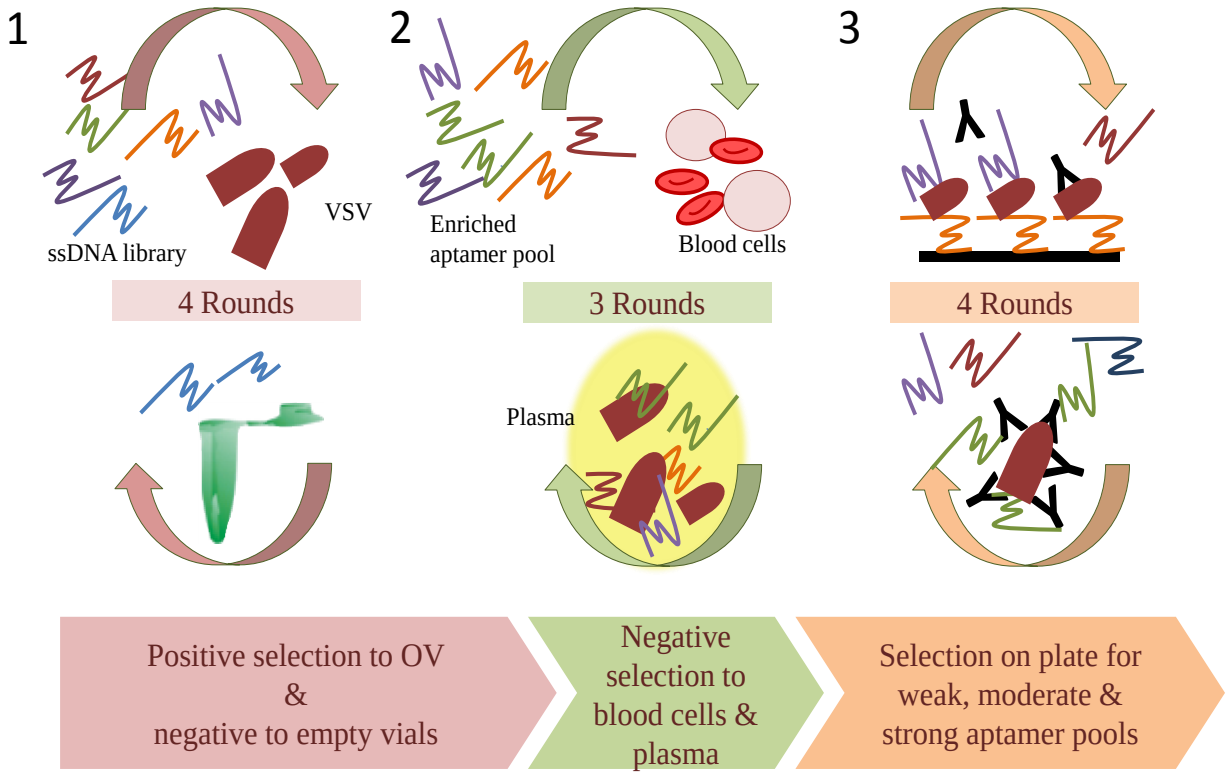

Figure 2.1. Selection aptamers to VSV. The aptamers were selected against VSV through eleven cycle of SELEX strategy; the aptamer selections started with four positive selection cycles and continue with three rounds of negative selection. The figure reprinted with permission from[83].

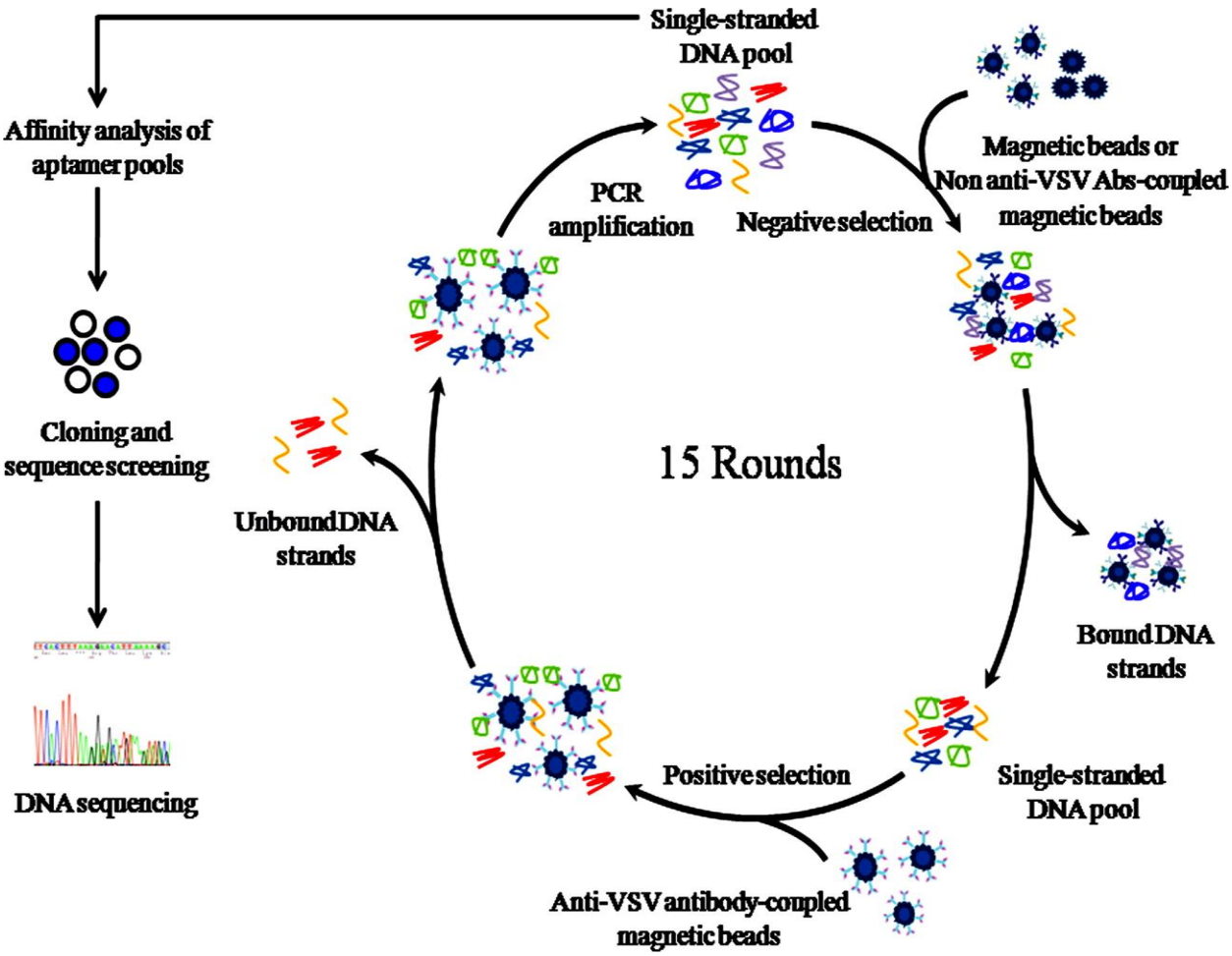

Figure 2.2. DNA aptamers selection procedure to VSV neutralizing antibodies. The figure reprinted with permission from [82].

We investigated the efficiency of aptamers to protect VSV infectivity in the presence of nAbs *in vitro* and *in vivo*. We also examined a quadramer structure of aptamers with binding affinity to VSV. The goal of this study was to determine whether aptamers can preserve the infectivity of VSV in the presence of nAbs.

2.3. Materials and methods

Vesicular Stomatitis Virus preparation

The VSV was prepared and purified as previously described by Diallo et al.[85] Briefly, Vero African green monkey kidney cells were seeded at 1 x 10^4 cells per cm^2 in FBS supplemented with DMEM in 150-mm cell culture petri dishes. Once they have reached around 95% of confluency, the cells were infected with the VSV virus at on multiplicity of infection (MOI) of ~0.01. After 24 hours, the supernatant was collected, centrifuged to remove the cell debris, and filtered through a 0.2 µm membrane. The virus was then pelleted using a centrifuge, resuspended in Dulbecco's phosphate-buffered saline (PBS), and purified with a sucrose gradient.

Cell and culture Conditions

Vero cells were maintained in Dulbecco's modified Eagle's medium supplemented with 10% fetal bovine serum (FBS; Gibco BRL, Gaithersburg, MD)

DNA aptamers[84]

All oligonucleotides were synthesized by Integrated DNA Technologies (Iowa, USA). To prepare a pool of single aptamers, each aptamer was incubated at 95°C for 5 minutes, followed by mixing with an equimolar amount of each aptamer. For incubation with VSV, the aptamer pool was used at a final concentration of 8 µM.

VSV coating with the aptamers and quadramers[84]

Four groups were made for assays: untreated VSV as a control, aptamer- and quadramer-treated VSV. The forth group was to test VSV with single strand DNA library. For each group, 75 µL of virus (3×10^9 PFU) was aliquoted. Then, we added PBS (15 µL) to the control group, a pool of aptamers (15 µL), quadramers (15 µL) and single strand DNA library (15 µL). The mixtures were incubated for 60 min at 37°C.

Assessment of VSV infectivity[84]

After each experiment, each sample group containing the virus was quantified using the Vero cell line (0.4×10^6 per well) in twelve-well culture plates. After infecting the cells with serial dilutions of each sample in serum free media, the plates were incubated for 1 hour at 37°C in a 5% CO_2 humidified incubator. Afterward, all the medium was removed, and the cells were overlaid with 1 mL of 0.5% low melting agarose with 1 x DMEM supplemented with 10% FBS. After 24 hours incubation, cells positive for YFP fluorescence were visualized using Alfa Innotech Imaging System, Version 3.0.3.0. Additionally, a standard plaque assay was performed, where the plates were fixed with methanol–acetic acid fixative (3:1 ratio) and stained with Coomassie blue solution; consequently the white plaques were counted.

Aptamer pool and quadramer effect on VSV infectivity in the presence of nAbs [84]

First, VSV was incubated with the pooled aptamers, quadramer and ssDNA library (as control). They were then individually mixed with serum containing nAbs for 1 h at 37 °C; they were then added onto a monolayer of Vero cells. After 1 h cells were washed, and 1% agarose in DMEM was added, and the plates were incubated for 24 hours. The infectivity of VSV in each

experiment was counted by fluorescent imaging of YFP expression in the infected Vero cells as a plaque assay.

Table 2.1. The sequence of the aptamers against VSV.[62]

Name	Sequence
M-50	F-CCATCACCCTATTATCTCATTATCTCGTTTTCCCTATGCG-cR
S-39	F-GCACTTCACTTCTCCTCTGACTGTAACCACGC-cR
Z-1	F-GTGGGGGTCCTGTGGTTGGTGTGGTGGTGAGATGTGGTGG-cR
Z-20	F-CCATCACCCTATTATCTCATTATCTCGTTTTCCCTATGCG-cR
Z-21	F-CGGGAACCAAATCACGTCCTAGATTGTGATGAACCTCGGC-cR
Z-22	F-GCGACAACACGGACGGTTGAGACTTTAATTCTGCTCACGG-cR
Z-23	F-GGGACCTATCAGGCGATGTGAAAACTCTTATACCACTGG-cR
Z-24	F-GGCGGTCCCTTCTTTTTGTGTTTATGTTGTTCTCTTTTCG-cR
Z-25	F-CCGCAACCGAGCTTCGACCTACACTTACGATGTGTCCCAC-cR
Z-28	F-CCACCATGCACGACCCACGCAATGACAGTAACACACCTCG-cR
Z-29	F-CACATCCTACGTTTGCCACGCGCTACTCCGCCATCTACCC-cR

F is CTCCTCTGACTGTAACCACG (the forward PCR primer), and cR is GCATAGGTAGTCCAGAAGCC (the reverse complement of the reverse PCR primer).

Table 2.2. The sequence of the aptamers against VSV antibodies.[82]

Name	Sequence
C1L	CCCAGAAACAGCACCCTTACATCGACTGGACCTTCCGCG
C3L	ACTAGGACGCTTGGGAGGGGGGGTGGGGTGTCCGGTCGCG
C5L	TGTGCCAAAGAGAGTGGTGGGGGGGTGGGCGGAACTCGCG
C9L	ACCGCCTTCCACCGTTCTCCACCACCCCTCAAACAACCCT
C10L	CCACCGAGCCTACCACATGTGACATCCCAGGACATAGCTG
C1s	CCCAGAAACAGCACCCTTACATCGACTGGACCTTCCGCG
C3s	ACTAGGACGCTTGGGAGGGGGGGTGGGGTGTCCGGTCGCG
C4s	CCGGGGAATCTAGGGGAGGGCGGGTGGGTCAATTGAGCCG

C5s	TGTGCCAAAGAGAGTGGTGGGGGGGTGGGCGGAACTCGCG
C7s	CCAACCACACATCCTTCCATCGACATGGACCCACCGTTCC
C9s	ACCGCCTTCCACCGTTCTCCACCACCCCTCAAACAACCCT
C10s	CCACCGAGCCTACCACATGTGACATCCCAGGACATAGCTG

Aptamers with L suffix have CTCCTCTGACTGTAACCACG (the forward PCR primer) at 5' and GCATAGGTAGTCCAGAAGCC (the reverse complement of the reverse PCR primer) at 3'.

In Vivo Toxicity of Aptamers and Quadramers in Mice[84]

Nine male BL6 mice of 10 weeks of age were obtained and divided into three groups. Two groups (three mice per group) were injected through the tail vein with VSV (5×10^4 PFU) previously incubated with either the aptamer pool or with the quadramer (400 μg) in 10 μL PBS. Three mice, the third group, were injected with VSV (5×10^4 PFU in 10 μL PBS) without the aptamer pool and quadramer as controls. Mice were monitored (5 days) for the development of external symptoms of toxicity, such as ruffled fur, loss of appetite, and body weight loss, according to the Canadian Council on Animal Care guidelines.[86]

2.4. Results and discussion

Evaluation of anti-VSV aptamers shielding ability of VSV

The DNA aptamers with binding affinity to VSV (**Figure 2.3)** were shown to protect VSV survival and infectivity in the presence of nAbs, which is a determining factor for oncolytic virus and vaccine efficiency. For this purpose, the effectiveness of the aptamers to protect VSV from nAbs was evaluated using plaque-forming unit assays. We examined the infectivity of VSV incubated with the aptamers (**Table 2.1**) and ssDNA library as a control in the presence of serum containing nAbs on Vero cells. Briefly, aptamers with a final concentration of (1 μM) were

incubated with VSV coding yellow fluorescent protein for 60 min at 37 °C. Then, serum containing nAbs was added and incubated for additional one hour at 37 °C and then added to a monolayer of Vero cells. After one-hour incubation, cells were washed with PBS and were overlayed with agarose in DMEM. The plates were incubated for 24 hours in an incubator.[84] The capability of aptamers to protect VSV was determined by fluorescent imaging of yellow fluorescent protein expression in the infected Vero cells using a standard plaque assay (**Figure 2.4**). The experiments were repeated five times. The averages and standard deviations were calculated using Microsoft Excel, version 2011. As shown in **Figure 2.5**, nAbs fully inhibited cell infection of un-coated VSV, but VSV coated with aptamers infected cells. VSV coated with Z-23 provided more than 25% recovery of VSV infection in the presence of nAbs in serum while VSV incubated with ssDNA as a control had 5% of the infectivity. Interestingly, the pool of aptamers, which contains multiple aptamers, had the highest protective effect on VSV infectivity in cell experiments. This can be explained by the fact that each aptamer sequence has different binding epitopes. As a result, the pooled aptamers have the ability to block more neutralizing sites of polyclonal nAbs than single sequences alone.

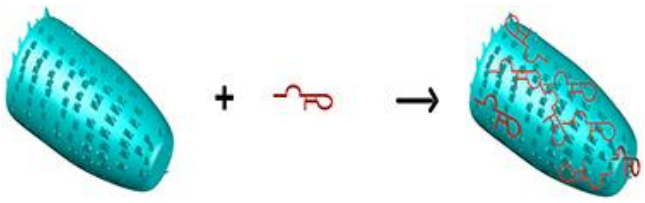

Figure 2.3. Schematic representation of binding vesicular stomatitis virus (VSV) with an aptamer. Reproduced with permission from[84].

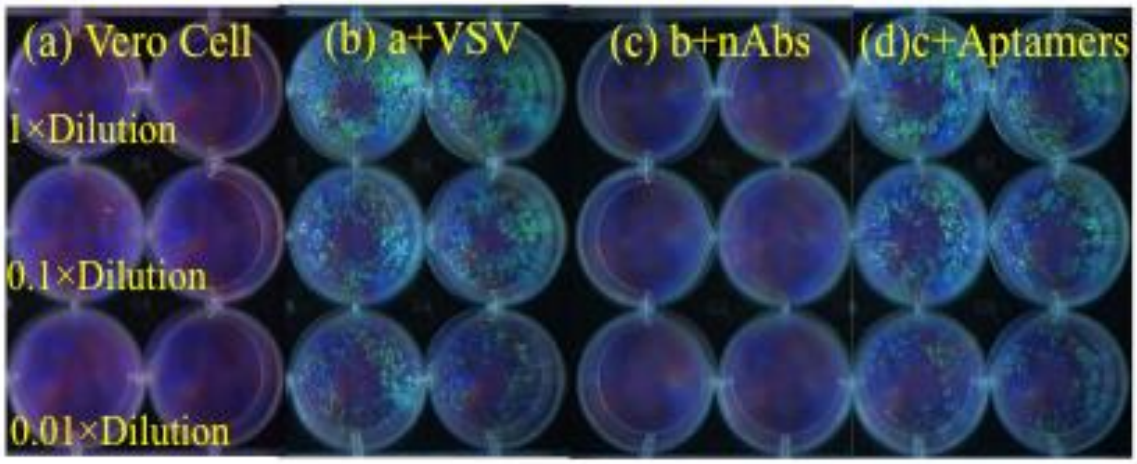

Figure 2.4. Schematic representation of the plaque-forming assay. (a) Vero cells; (b) Vero cells infected with VSV; (c) Vero cells infected with VSV in the presence of serum containing nAbs; and (d) Vero cells infected with VSV in the presence of serum containing nAbs and an aptamer. The plaque forming assay was done with several dilutions (1x, 0.1x, 0.01x). The well with 50-100 plaques was used in the calculation.

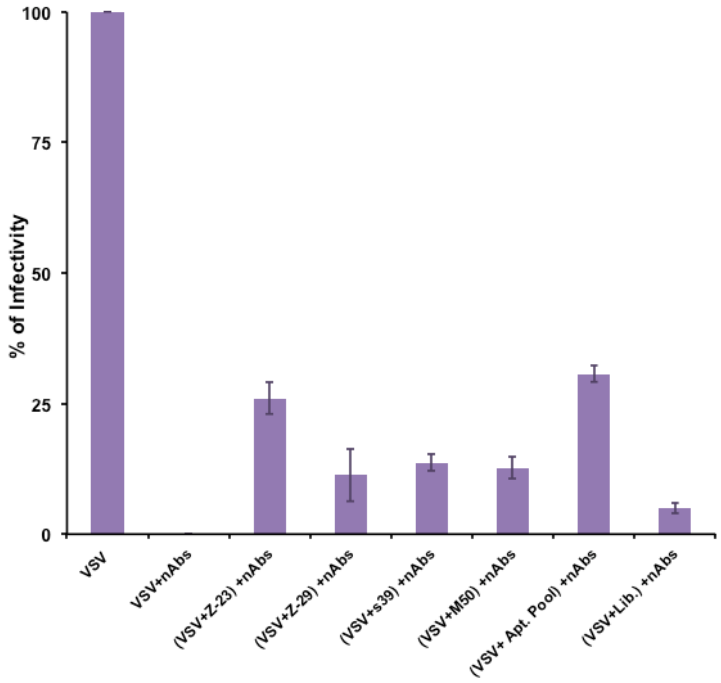

Figure 2.5. Assessment of coated VSV infectivity in the presence of serum containing nAbs. VSV was treated with different aptamers and the pool, which consisted of an equimolar mixture of all aptamers. The infectivity of the subject VSV measured through plaque forming assay in the presence of nAbs. The VSV sample without nAbs was rated 100% infectivity, and the virus with nAbs and without any plaque

formation reveals 0% infectivity. ssDNA library (Lib.) was used as a control. Error bars indicate standard deviation (Microsoft Excel, version 2011). The student's independent T-test P-value for Z-23, Z-29, s39, M50 and Pool to library were 0.003, 0.702, 0.002, 0.011 and 0.076, respectively. The P-value for VSV treated with Pool to Aptamer Z23 was 0.096.

Protecting VSV from neutralizing antibodies

The aptamers with the binding abilities to antibodies against VSV were developed by Dr. Darija Muharemagic in our laboratory.[82] The aptamers, which bind to the antibodies, can obstruct the binding of the antibody to VSV. Cell-based experiments were performed to evaluate the capability of the aptamers to block nAbs effect on VSV. The infectivity of VSV coding yellow fluorescent protein was measured through plaque forming assay in the presence of serum containing nAbs treated with the discussed aptamers, as well as the ssDNA library as a control. The serum, containing nAbs, after incubation with individual aptamers and a pool of aptamers for one hour at 37 °C, were mixed with VSV for an extra hour and then added on a monolayer of Vero cells. A layer of 1% agarose dissolved in DMEM was overlaid after washing the cells with PBS. After 24 hours, the efficiency of aptamers was determined by fluorescent imaging of yellow fluorescent protein expression on the infected Vero cells. Each experiment was performed in triplicates. The plaques were counted and the number of particles to form plaques per mL in each sample was calculated. The average and standard deviations were calculated using Microsoft Excel, version 2011. As shown in **Figure 2.6**, the serum completely inhibited cell infection by VSV, but addition of aptamers to the serum recovered the infectivity of VSV. Aptamer C5S in the serum provided the highest recovery of VSV infection (18%). More importantly, the pool of aptamers recovered 24% of VSV infectivity. nAbs are polyclonal antibodies, and the pool of aptamers is a mixture of multiple aptamers with different binding sites on nAbs. Using a pool of aptamers makes blocking more paratopes achievable.

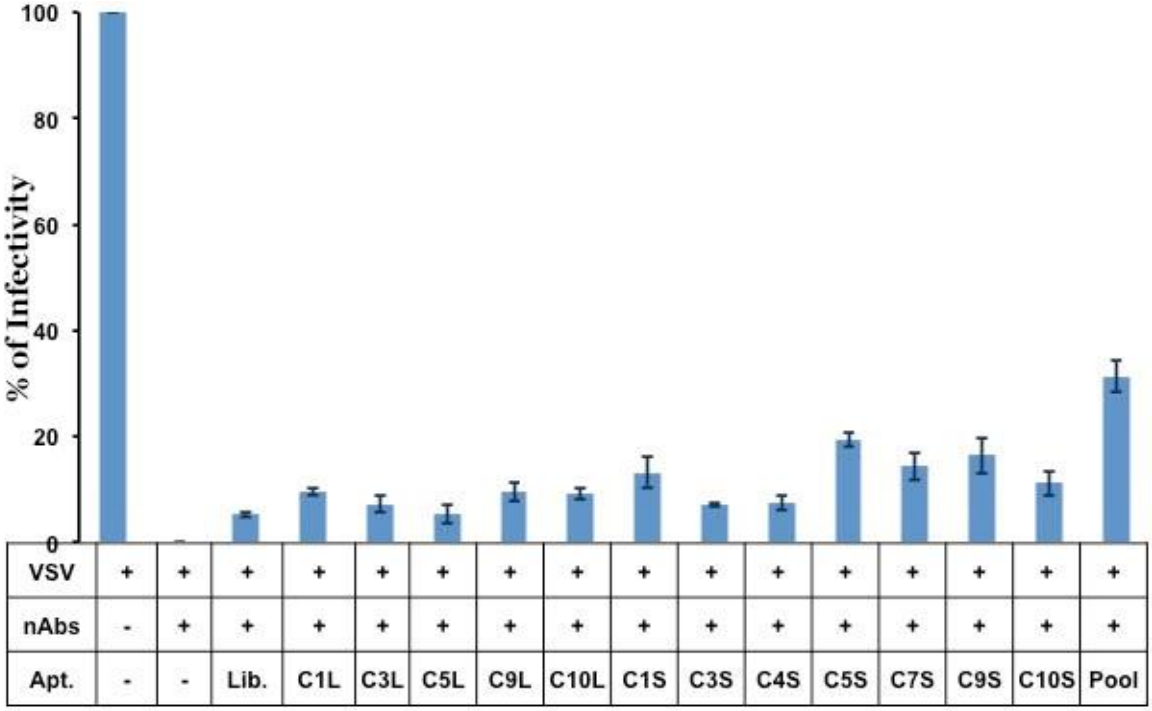

Figure 2.6. Assessment of efficiencies of aptamers and the pool of the aptamers, in equimolar mixture, to guard nAbs effect on VSV infectivity. To quantify the protection effect of aptamers, plaques forming standard assay was applied to evaluate VSV infectivity. The VSV sample without nAbs considered of 100% infectivity and the VSV with nAbs and without any plaque formation reveals 0% infectivity.[82] ssDNA library (Lib.) was used as a control. Error bars indicate standard deviation (Microsoft Excel, version 2011). The pool had signigicant VSV infectivity recovery in compare to library with the student's independent T-test P-value <0.01).

Anti-VSV aptamers and anti-nAb aptamers shielding assessment

In the two previous sections, the ability of an individual aptamer and a pool of aptamers to protect VSV from nAbs in serum was examined. Aptamer Z-23 and the pool of aptamers had the strongest ability to protect VSV from nAbs (**Figure 2.5**). The pool of aptamers included all the aptamers against nAbs: aptamers Z-23, Z-29, S39, and M50 (equimolar ratio of the individual aptamers in mixtures). As for aptamers with binding affinity to nAbs, the pool of aptamers proved the highest protection efficiency (**Figure 2.6**).

To evaluate the efficiency of pools of aptamers (anti-VSV and anti-nAbs) to block both paratopes and epitopes, the standard plaque-forming assay was performed five times in duplicates. The assay examined VSV infectivity after incubation with the pool of aptamers against VSV in the presence of nAbs which were previously incubated with the pool of aptamers against nAbs. The averages and standard deviations were calculated using Microsoft Excel, version 2011. As shown in **Figure 2.7**, VSV coated with the pool of anti-VSV aptamers incubated with nAbs treated with anti-nAbs pool of aptamers increased the virus infectivity to over 61%. This resulted in the highest VSV recovery because the highest amount of paratopes were blocked on nAbs by the pool of anti-nAbs aptamers and the highest amount of epitopes on VSV were covered by the pool of aptamers at the same time.

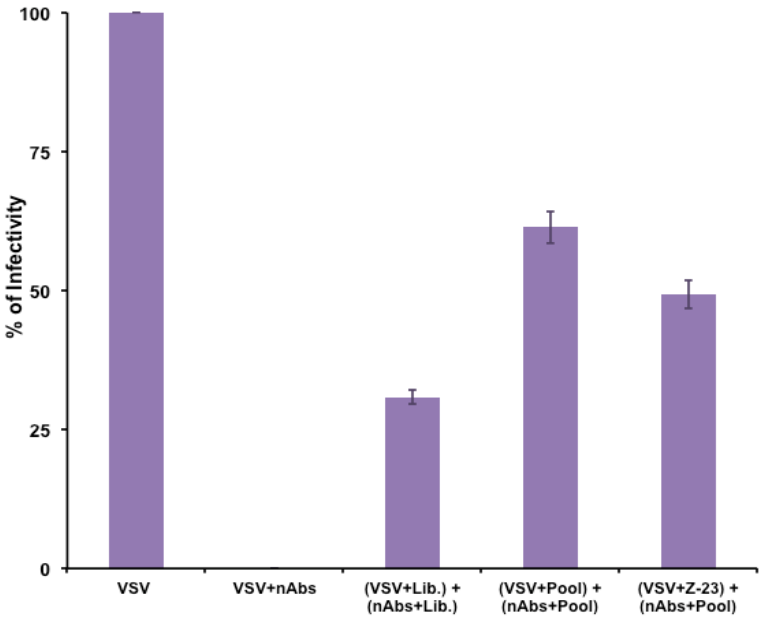

Figure 2.7. To quantify the protection effect of aptamers, plaques forming standard assay was used to assess VSV infectivity. The VSV sample without nAbs was rated 100% infectivity, and the virus with nAbs and without any plaque formation reveals 0% infectivity. The viruses were coated by pool of aptamers (1 μM) against VSV and serum containing nAbs was treated with pool (1 μM) of aptamers against nAbs. ssDNA library (lib.) was used as a control. Error bars indicate standard deviation

(Microsoft Excel, version 2011). The student's independent T-test P-value for pool and aptamer z23 to DNA library were 0.0007 and 0.0016, respectively. The P-value for VSV treated with pool of aptamers to Z23 was 0.0054.

The titration experiment with the pools of aptamers was conducted three times in duplicates to define the optimum concentration of aptamers pools to shield VSV infectivity from nAbs. Both VSV and serum containing nAbs were incubated with their corresponding aptamer pools with the concentration series from 1 to 10 µM. As shown in **Figure 2.8**, the infectivity rises with increasing concentrations of aptamer pools and reaches the highest infectivity (61%) at 1µM.

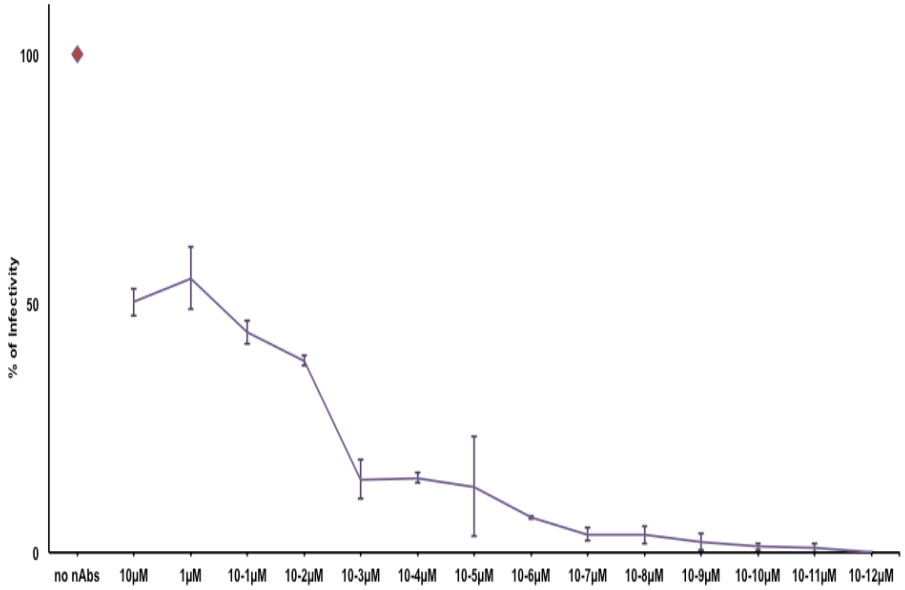

Figure 2.8. The effect of aptamer pools titration on VSV infectivity. Plaque-forming standard assay was used to to quantify the serial dilution effect of aptamers pools on VSV infectivity recovery. The pool of aptamer for VSV and nAbs in the range of concentration from 10 µM to 10^{-12} µM were incubated with their respective targets and added to a monolayer of Vero cells. Each aptamer dose was done in triplicates. The positive control is VSV without nAbs which was rated 100% infectivity. Reproduced with permission from[83]. Error bars indicate standard deviation (Microsoft Excel, version 2011).

An anti-VSV aptamer quadramer to increase protection of VSV

Strong target specific binding is a central requirement of aptamers. Avidity is an accumulation of several affinities in a structure including several aptamers with several binding site; as a result, avidity is stronger than affinity. Making a structure of several binding site with turning affinity to avidity is strategy to provide a strong binding. To increase the avidity of VSV and related aptamers, a quadramer was designed (**Figure 2.9**). A quadramer was constructed by connecting four aptamers with an oligonucleotide bridge. The bridge connecting four aptamers together consists of two oligonucleotide strands joined by a central complementary sequence (**Figure 2.10**). The end of the bridge consists of a complementary side supporting the annealing of an aptamer. To construct the quadramer, after heating at 95°C, the sides of the bridge were mixed equally, followed by mixing them with the aptamer pool of four aptamers in equimolar amounts. Consequently, the complex results in four aptamers annealing to each bridge construction.[84]

The shielding efficiency of the quadramers was evaluated using the plaque forming assays with VSV treated with quadramers in serum carrying nAbs. The averages of three experiments done in duplicates and standard deviations were calculated using Microsoft Excel, version 2011. The results show that while nAbs neutralized uncoated-VSV infectivity, VSV coated with the quadramer (0.25 μM) recovered the infectivity about 75% (**Figure 2.11**). Constructing the quadramer from the pool increased the infectivity from 25% to 75%.[84]

The dosage effect of quadramer on guarding VSV against nAbs was conducted to determine the optimum concentration of quadramer to shield VSV infectivity from nAbs. The experiment was done three times in duplicates. First, the quadramer was constructed. Then, VSV was incubated with the quadramer in the final concentrations of 0.125, 0.25 and 0.5 μM. The

VSV infectivity was measured after incubating with serum containing nAbs by plaque forming assay. The infectivity of VSV treated with the pool of aptamers (1 µM) against VSV in the presence of nAbs and VSV without any treatment, were used as controls. The infectivity of VSV treated with the aptamer pool (1 µM) was 28%. The infectivity of VSV treated with quadramer increased with increasing the concentrations of the aptamer pools and reached the highest infectivity (76%) at 0.5 µM; this trend slows down from 0.25 µM up to 0.50 µM, the final concentration of quadramer incubated with VSV (**Figure 2.12**).

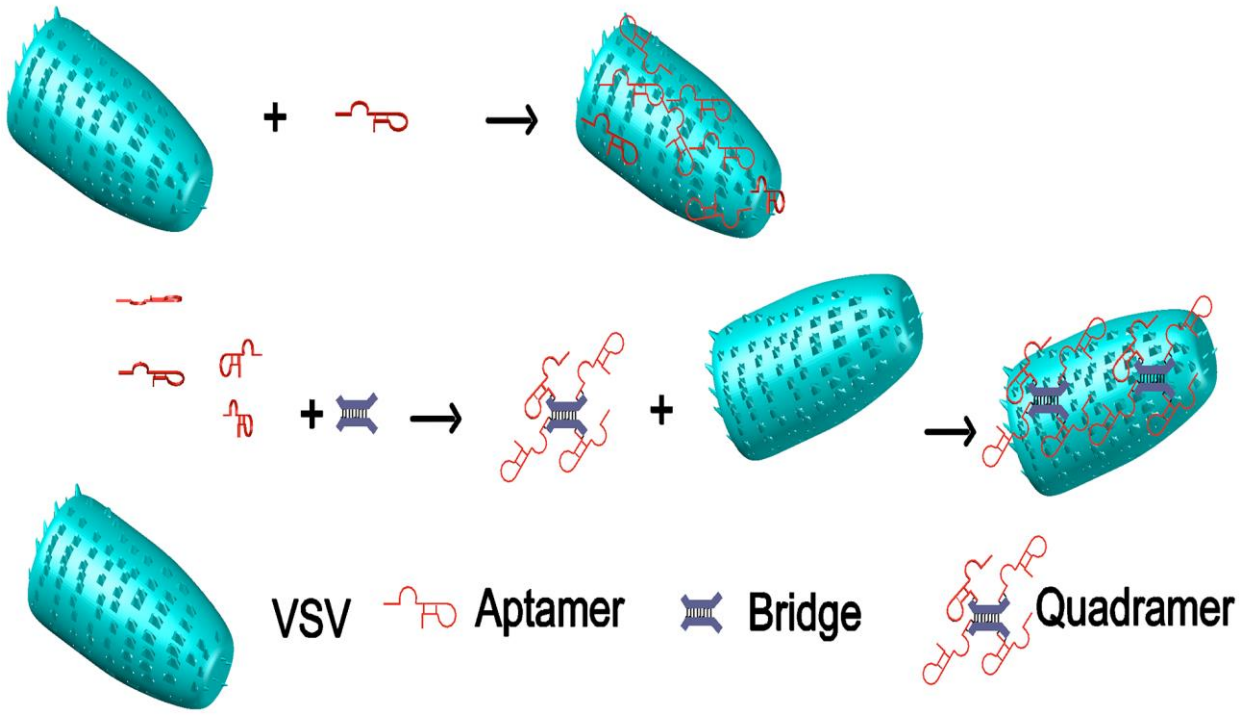

Figure 2.9. Schematic representation of binding VSV with quadramers. Reproduced with permission from [84].

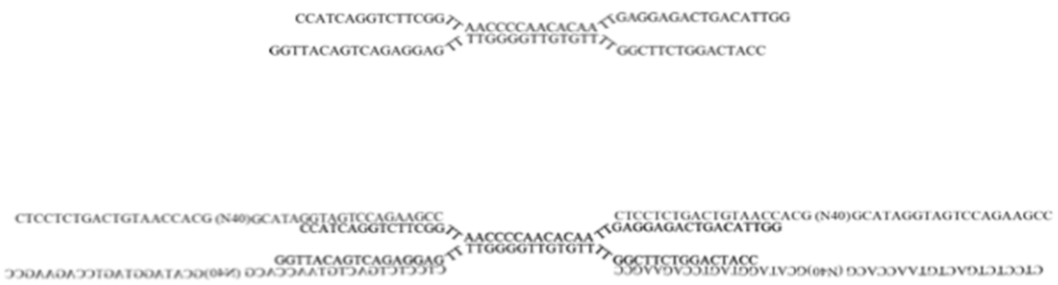

Figure 2.10. Scheme of a quadramer and bridge. The oligonucleotide bridge mediates the formation of the quadramer. Reproduced with permission from [84].

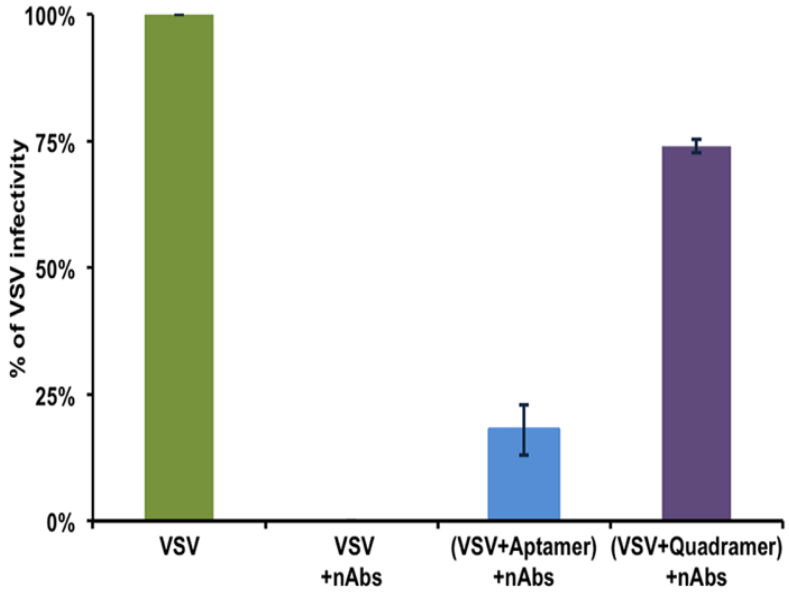

Figure 2.11. Evaluation of the capabilities of aptamer pool (equimolar mixture of Z23, Z29, S39, M50) and quadramer to shield VSV infectivity in the presence of nAbs. The VSV sample without nAbs was ranked 100% infectivity, and the virus with nAbs and without any plaque formation ranked 0% infectivity. Reproduced with permission from [84]. The P-value for VSV treated with quadramer incompare to the monomeric aptamers was lower than 0.01. Error bars indicate standard deviation (Microsoft Excel, version 2011).

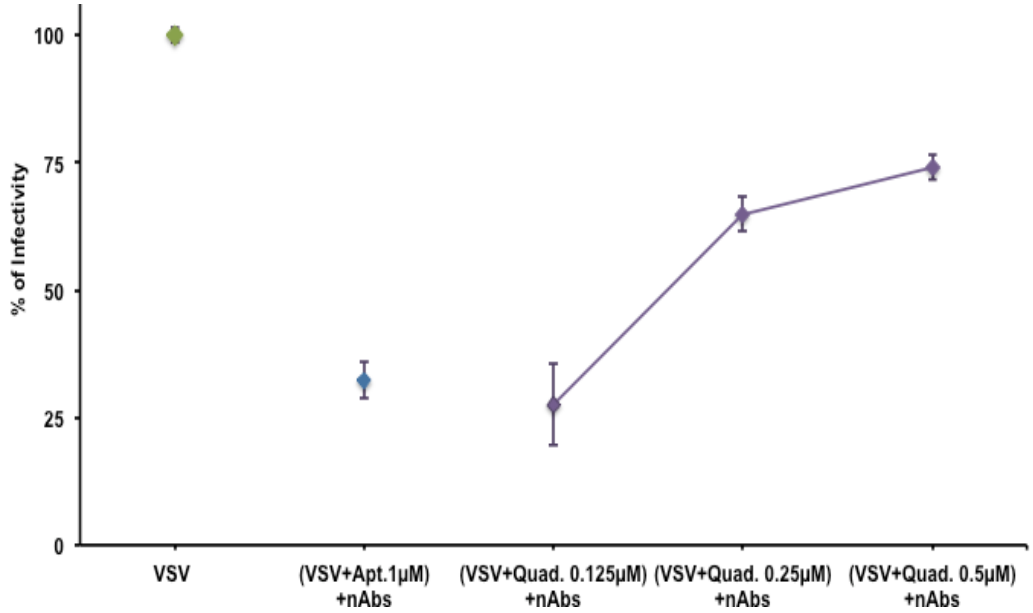

Figure 2.12. The effect of constructed quadramer dosage on guarding VSV infectivity in the presence of nAbs using plaque forming assays. The infectivity of VSV treated with 0.125, 0.25 and 0.5 μM of quadramer was measured in the presence of nAbs along with controls, VSV without nAbs and VSV coated with a 1 μM pool of aptamers. The infectivity of VSV without nAbs was rated 100% of infectivity. Reproduced with permission from [84]. Error bars indicate standard deviation (Microsoft Excel, version 2011).

We also used streptavidin to obtain quadramers of the aptamers to enhance the avidity of VSV. As such, 5'-biotinylated aptamers were mixed with streptavidin (4:1 ratio) and plaque-forming assays were performed (**Figure 2.13**). The shielding efficacy of this approach to protect VSV in the presence of nAbs was compared to quadramers. These structures were made with a pool of aptamers and Z-23 independently. While untreated VSV infectivity in the presence of nAbs was 0%, shielded VSV with both, biotinylated-quadramer and streptavidin (P-value=0.038 compared to VSV treated with Z-23) and biotinylated-Z-23 and streptavidin (P-value=0.033 compared to VSV treated with biotinylated Z-23), at a concentration of 0.25 μM each yielded a similar recovery of approximately 79% of the infectivity of non-treated VSV.

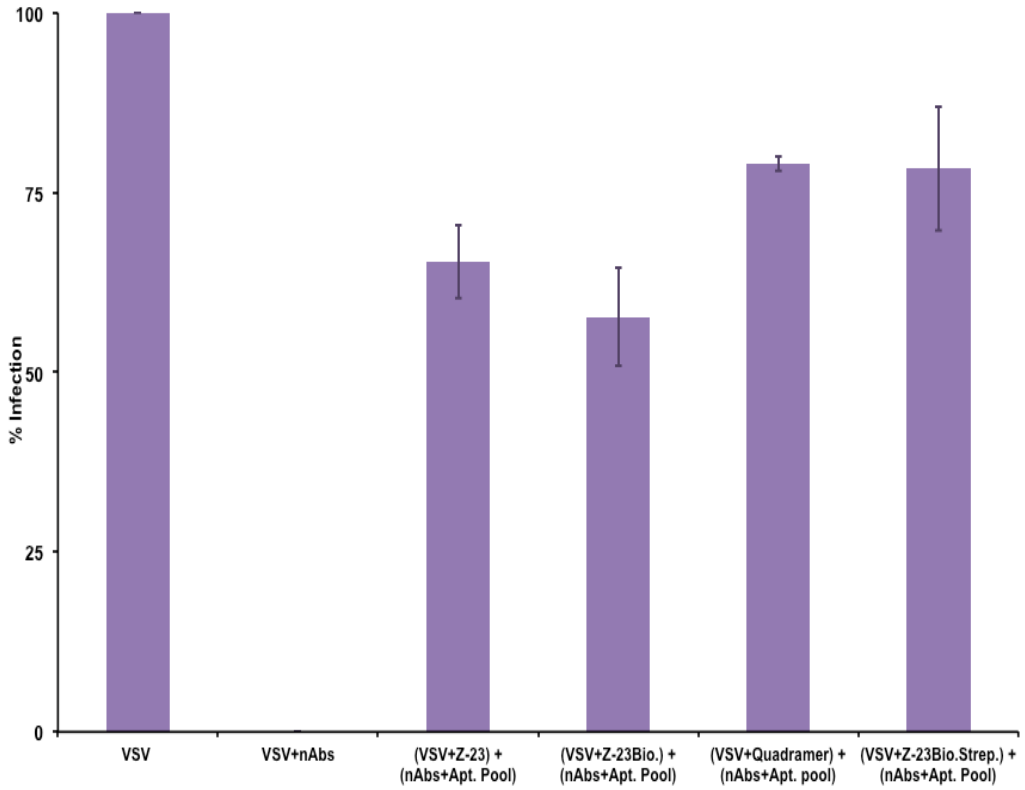

Figure 2.13. Assessment quadramers and streptavidin joined 5' biotinylated aptamer to protect VSV infectivity from nAbs. Quadramers and streptavidin joined structure made from a pool of aptamers and Z-23 independently. The aptamer pool was an equimolar mixture of Z-23, Z-29, S-39, M-50. The VSV without nAbs was standardized as 100% infectivity. The other test samples with aptamer pools, quadramers and streptavidin joined aptamers have been completed after incubating with serum carrying nAbs. Error bars indicate standard deviation (Microsoft Excel, version 2011). The student's independent T-test for quadramer treated VSV to VSV treated Z-23 was 0.038 and for the biotinylated-quadramer with streptavidin compared to biotinylated Z-23 with streptavidin was 0.033.

To monitor the *in vivo* toxicity of aptamers on the mice, the aptamer pool and the quadramer individually (400 μg) were intravenously administered (i.v.) through the tail vein of BL6 male mice (10 weeks old), two times (day 1 and day 2), according to the Canadian Council on Animal Care guidelines[86]. They were observed for the visible symptoms of toxicity for five

days after the administration of the aptamers and quadramer. The mice did not develop any sign of ruffled fur, diarrhea, loss of appetite, lethargy, or lose any weight.[84] Each group consisted of three BL6 mice, and they were all injected with either VSV or with VSV previously incubated with the aptamer pool or with the quadramer (400 µg).

In vivo evolution of quadramer and aptamer for protection of VSV

We performed three mice experiments to examine the *in vivo* efficacy of the aptamers and quadramers to protect VSV and block nAbs. VSV expressing firefly luciferase injection was used. The *in vivo* experiments were performed on four groups of male, ten weeks old mice, and three mice in each group for both immunized and non-immunized mice against VSV. The first group had an injection of VSV coated with the relevant pool of aptamers. The second group had an injection of the pool of aptamers against nAbs before injecting VSV. The third group was injected with both, pool of aptamers against nAbs and then with VSV coated with the aptamer pool. The fourth group of mice was injected with VSV incubated with ssDNA library. All virus and aptamers injections were done via the tail vein. On day three, the non-immunized mice displayed the firefly luciferase expression in their tumor while immunized mice did not present luciferase expression in their tumor. The mice were sacrificed to extract tumors to test possible VSV infection. The cytosol of the cells was obtained and tested using plaque forming assays. The results showed no VSV infection in any of the tumors of the immunized mice. The same procedure was later repeated with the quadramers instead of the pools of aptamers to coat VSV. The results revealed that the aptamers and quadramer were not able to protect VSV infectivity in any of the immunized mice.

2.5. Conclusion

Here, the protection capacity of aptamers with binding affinity to VSV and anti-VSV nAbs was assessed. Cell-based *in vitro* experiments using plaque-forming assays were employed to test several aptamers and respective pool of aptamers. While the efficacy of Z-23 to protect VSV and that of C5s to block nAbs were higher than other aptamers, the pool of aptamers provided significantly greater recovery of VSV infectivity. We later designed constructed a quadramer structure of aptamers. The protection efficiency of the constructed quadramer on VSV infectivity was about three times higher than single aptamer (76%). We also built a quadramer structure using biotinylated-aptamers and streptavidin that protects VSV from nAbs similarly to quadramer as shown by plaque forming assays. Unfortunately, none of these approaches were effective at protecting VSV in the bloodstream of immunized mice. This may be due to the aptamers' inability to protect the virus as it interacts with other cells, proteins and enzymes. These aptamers are good candidates for further investigation and should be considered alongside other approaches to protect VSV infectivity as an oncolytic virus in future research.

Chapter 3

Aptamer-facilitated cryoprotection of viruses

3.1. Objectives

The objective was to evaluate and apply the aptamers with affinity binding and the constructed structure of aptamers with high avidity, quadramer of aptamers, to stabilize vesicular stomatitis virus (VSV) potency more efficiently. Here, the aptamers and constructed quadramer were tested to protect viral activity during multiple freeze−thaw cycles and increase active unit of viral particles.

Shahrokh M. Ghobadloo with Dr. Maxim V. Berezovski (supervisor) designed the research and Shahrokh M. Ghobadloo performed the experiments. Shahrokh M. Ghobadloo drafted the manuscript, and Dr. Berezovski conducted further contributions to it. Dr. Ana Gargaun designed and performed capillary electrophoresis analysis and wrote the related parts in the article. Rebecca Katherine Casselman as honors student assisted me for the experiments. Dr. Darija Muharemagic provided valuable comments and measured the apparent dissociation constant (K_d) for the quadramer.

3.2. Background

Vaccination saves millions of lives each year. Main portions of vaccines are biological products, which contain attenuated viruses. Cryoprotection of viral vectors is essential for the development of vaccines and anticancer therapeutics. Due to temperature sensitivity, many viruses should be stored frozen[87]. One of the significant obstacles to global vaccination programs is viral vaccines thermostability.[88, 89] To protect vaccine potency, vaccines have to be stored and transported in a narrow range of temperatures, which is referred to as the vaccine "cold chain".[90] According to the World Health Organization (WHO), maintenance of the cold chain is the most challenging part from manufacturing to distribution.[90] This cold chain system represents a significant economic and logistical burden, estimated to be as high as 80% of the entire financial cost[91]. Freezing also aggregate and damage vaccines.[92-95] Damage due to storage issues accounts approximately 80% of the entire financial cost.[91, 96] A major portion of vaccines (75–100%) loses its efficacy during distribution because of non-ideal storing and transportation conditions.[94, 96]

The WHO has regulated that, less than 1 Log_{10} reduction in the original titer is accepted to consider the vaccine to be effective [97, 98].

Vesicular stomatitis virus (VSV) is innocuous and useful to stimulate immunity. Thus, VSV is a suitable option as a vaccine vector [99-101]. Moreover, VSV has been developed as a vaccine shuttle for other viral pathogens, such as Ebola virus,[102] HIV-1,[103] hepatitis B[104] and C.[105] Instability of VSV especially after freeze-thaw cycles limits its utilization as a viral vector.[106] Unfortunately, the reported cryoprotective agents have not provided satisfactory stabilization.[96, 107-113] Freeze-thaw cycles in particular have a deleterious effect on VSV. Stabilization of VSV is essential for the development of VSV-based vaccines.[87] VSV is an enveloped RNA rhabdovirus with a lipid envelope enfolding a nucleocapsid.[70] The developed and reported methods such as utilizing silk films, DMSO, metal ions, albumin, gelatin and carbohydrate-based stabilizers have issues in efficiency, application, toxicity or immune responses.[94-97, 107, 108, 114-120] The goal of this study was to determine whether aptamers can preserve the infectivity of VSV after multiple freeze-thaw cycles and in the presence of nAbs (**Scheme 3.1**).

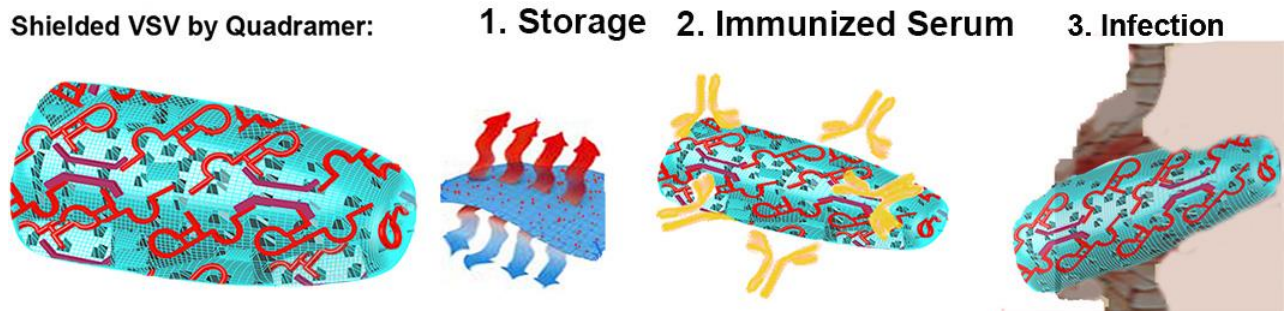

Scheme 3.1. Shielded VSV by quadramers to protect from the cold chain and neutralizing antibody and increase infectivity. Reprinted with permission from[84].

3.3. Materials and methods

Vesicular Stomatitis Virus preparation

The vesicular stomatitis virus was prepared and purified as previously described by Diallo et al[121]. Briefly, Vero African green monkey kidney cells were seeded at 1 x 10^4 cells per cm^2 in fetal bovine serum (FBS; Gibco BRL, Gaithersburg, MD) supplemented with Dulbecco's modified Eagle's medium (DMEM) in 150 mm cell culture petri dishes. Once they reached around 95% confluence, the cells were infected with the VSV virus at a multiplicity of infection (MOI) of ~0.01. After 24 h, the supernatant was collected, centrifuged and filtered through a 0.2 µm membrane to remove cell debris. The virus was then pelleted by centrifugation, resuspended in phosphate buffered saline (PBS), and purified with a sucrose gradient.

Cell and Culture Conditions

Vero cells were maintained in DMEM supplemented with 10% FBS.

DNA Aptamers

All oligonucleotides were synthesized by Integrated DNA Technologies (Iowa, USA). To prepare a pool of different single aptamers, each aptamer was incubated at 95°C for 5 minutes, followed by mixing with an equimolar amount of each. For incubation with VSV, the aptamer pool was used at a final concentration of 8 µM.

Quadramer

We employed the same quadramer, which have been discussed in the chapter 2 in this study (**Figure 2.9**). The bridge linking the four aptamers together consists of two oligonucleotide strands connected by a central complementary sequence (**Figure 2.10**). Each end of the bridge consists of a complementary flank allowing the annealing of an aptamer. To prepare the quadramer, after heating at 95°C, the sides of the bridge were mixed equally, followed by mixing with the aptamer pool of four clones in equimolar amounts. Subsequently, the complex results in four aptamers annealing to each bridge construct.

VSV coating with the aptamers and quadramers

Three groups of VSV were made for assays: untreated VSV as a control, aptamer- and quadramer-treated VSV. For each group, 75 µL of virus (3×10^9 PFU) was used together with the aptamer pool (15 µL) and the quadramer (15 µL), except the control assay, which contained PBS (15 µL). The mixtures were incubated for 60 min at 37°C.

Freeze-Thaw Cycles

For testing the dosage effect of the aptamer pool and the quadramer, 3×10^9 PFUs of VSV with nine dilutions of the aptamer pool and the quadramer, as well as nine control samples with PBS were used. The samples were succumbed to 30 freeze-thaw cycles. To study the effects of freezing and thawing cycles, after determination of the optimal DNA concentration to be used, seven samples for each VSV group (54×10^5 PFUs) were prepared and exposed to 0, 10, 20, 30, 40, 50 and 60 freeze-thaw cycles. The virus groups were tittered for VSV infectivity after each set of 10 freeze-thaw rounds.

Assessment of VSV infectivity

After each set of 10 freeze-thaw cycle experiments, the samples containing the virus were titered using the Vero cell line at 4×10^5 per well in 12-well culture plates. After infecting the cells with serial dilutions of each sample in serum free media, the plates were incubated for 1 hour at 37°C in a 5% CO_2 humidified incubator. After that, the medium was removed and the cells overlaid with 1 mL of 0.5% low melting agarose in 1 x DMEM supplemented with 10% FBS. After 24 hours incubation, YFP expressing (fluorescent) cells were visualized using Alfa Innotech Imaging System, Version 3.0. Furthermore, a standard plaque assay was performed using the 12-well plates fixed with methanol–acetic acid fixative (3:1 ratio) and stained with Coomassie blue solution, and subsequently, the white plaques were counted.

Active unit test

Equimolar concentrations of YFP and RFP-expressing VSV were incubated with the aptamer pool and the quadramer for one hour at 37°C and used to infect cells plated on a chamber slide. After 1 hour of infection, cells were washed and overlaid with 0.5% low melting agarose with DMEM and supplemented with 10% FBS. After 24 hour incubation at 37°C in a 5% CO_2 humidified incubator, cells were washed and analyzed by fluorescence microscopy. The cells expressing YFP, RFP, or both YFP and RFP were counted and analyzed (**Figure 4.4**).

***In vivo* toxicity of aptamers and quadramers in mice**

Nine male BL6 mice of 10 weeks of age were obtained and divided into three groups. Two groups (three mice per group) were injected through the tail vein with VSV (5×10^4 PFU)

previously incubated with either the aptamer pool or with the quadramer (400 µg) in 10 µl PBS. Three mice, the third group, were injected with VSV (5×10^4 PFU in 10 µl PBS) without the aptamer pool and quadramer as controls. Mice were monitored (five days) for the development of visible symptoms of toxicity such as ruffled fur, loss of appetite, body weight loss, according to the Canadian Council on Animal Care guidelines[19].

Aptamer pool and quadramer effect on VSV infectivity in the presence of nAbs

Rabbit serum containing nAbs was added to the sample groups with VSV together with the aptamer pool and quadramer for 1 hour at 37 °C and were then added to a monolayer of Vero cells. After 1 hour cells were washed, 1% agarose in DMEM was added, and the plates were incubated for 24 hours. The infectivity of VSV in each experiment was counted by fluorescent imaging of GFP expression in the infected Vero cells.

3.4. Results and discussion

We used anti-VSV DNA aptamer clones Z23, Z29, S39, M50 (**Table 2.1**) that were previously selected in our laboratory and had shown high affinity to VSV[62]. To increase VSV infectivity and serum stability, we designed a quadramer, which was made by connecting four aptamers (equimolar mixture of all above- mentioned aptamers), with an oligonucleotide bridge (**Figure 2.9 and Scheme 1**).

We measured the apparent dissociation constant (K_d) for monomeric pool and quadramer using the approach described by K. Sefah et al[31]. The K_d for a monomeric pool of four clones was 71±15nM, and quadramer had an affinity of 22±9 nM. The protective role of the aptamers and

quadramers in viral activity was assessed using the plaque-forming and virus cells co-infection assays after freeze-thaw cycles.

We investigated the dosage effect of an equimolar pool of the aptamer clones and quadramers on VSV stability after 30 freeze-thaw cycles. Dosage effect experiments indicated that increasing the concentration of both the aptamer pool and quadramers above 400 pM improved VSV infectivity (**Figure 3.1B**). We also studied the effect of the number of freeze-thaw cycles on the infectivity of VSV ($54x10^5$ plague-forming units, PFU) with the aptamer pool (1 μM), quadramer (0.25 μM), non-specific DNA library (1 μM) and compared with the pure virus only. To this end, the three VSV groups were subjected to 0, 10, 20, 30, 40, 50 and 60 freeze-thaw cycles in duplicate (**Figure 3.2**). The infectivity of quadramer- and aptamer pool-protected virus was 1.4 and 0.7 log higher, respectively than the pure virus after 60 freeze-thaw cycles. Fascinatingly, just adding quadramers to the virus without freezing (0th cycle) increased the virus infectivity by 30% (**Figure 3.2** inset), which can be ascribed to the ability of quadramers to increase virus active units.

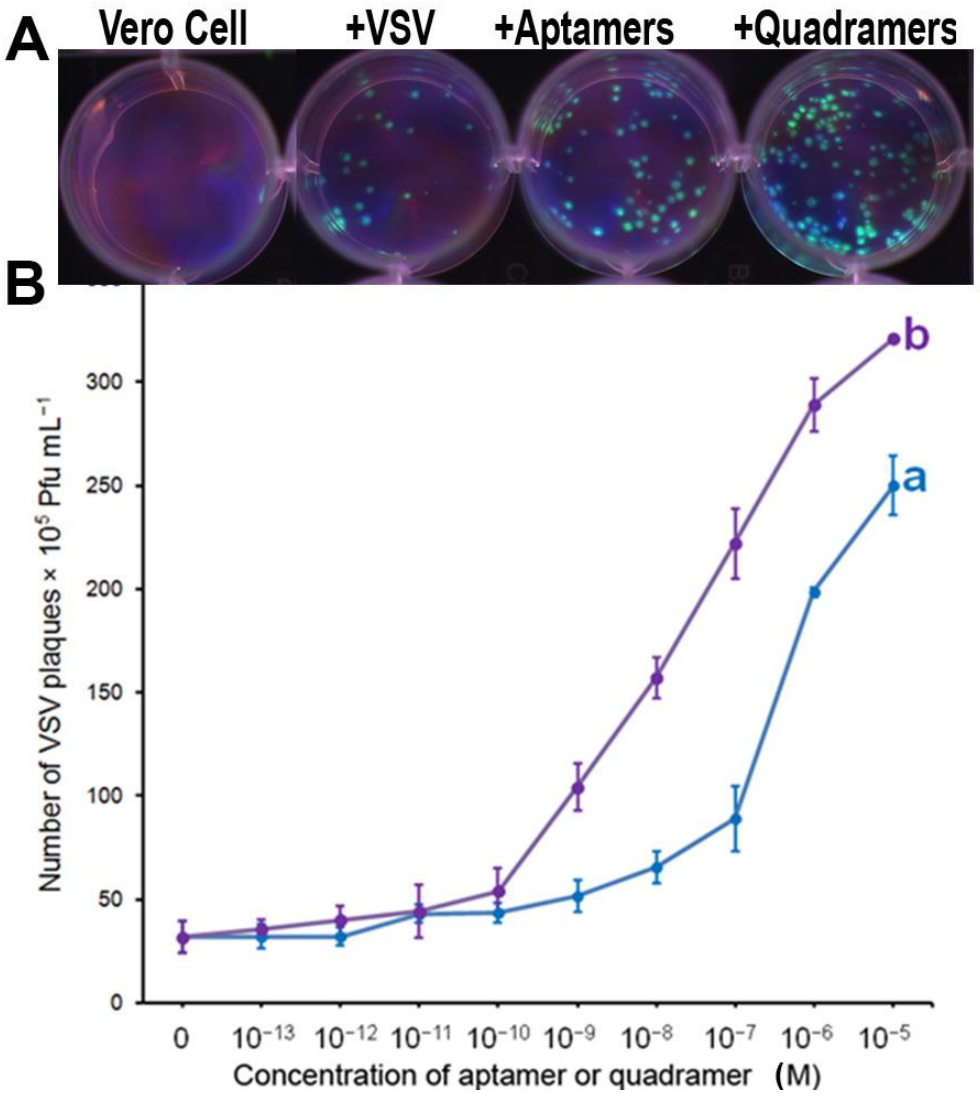

Figure 3.1. A) Schematic representation of the plaque-forming assay when Vero cells infected with YFP-coding VSV. B) Dosage effect assessment. Number of plaques formed by VSV treated with different concentrations of an equimolar mixture of aptamers (a) and quadramer (b) both after 30 freeze-thaw cycles. Error bars indicate standard deviation (Microsoft Excel, version 2011). Reprinted with permission from[84] (Part B).

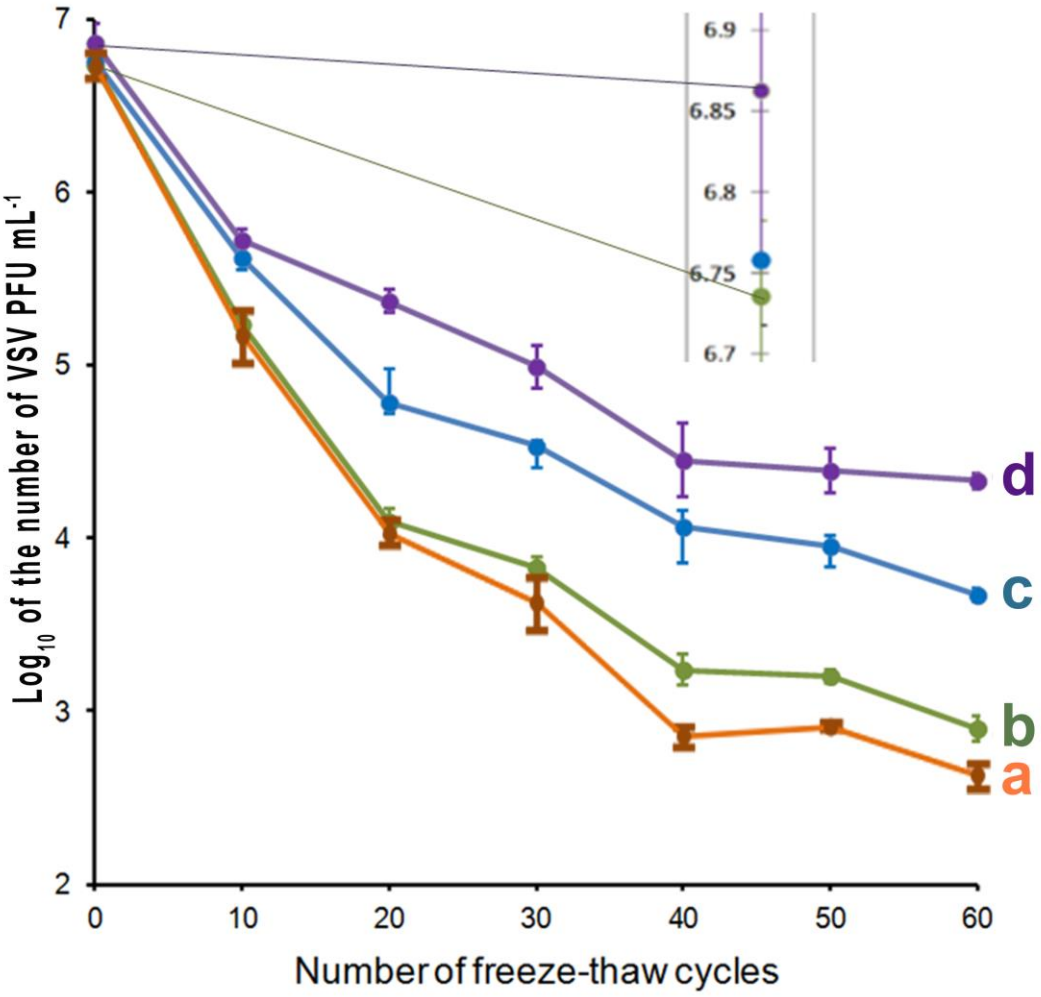

Figure 3.2. VSV infectivity correlation curve for DNA library (a), pure virus (b), with an aptamer pool (c), with the quadramer (d) depending on the number of freeze-thaw cycles. The inset represents the initial infectivity before any freeze-thaw (0th cycle). Error bars indicate standard deviation (Microsoft Excel, version 2011). Reprinted with permission from[84].

The stabilization effect of aptamers was confirmed by viral quantitative capillary electrophoresis (viral qCE)[122], where the intact virus particles were separated from free RNA released during virus degradation (**Figure 3.3**) after a cycle of freeze-thaw. The areas corresponding to the intact virus particles were then calculated and displayed in a bar graph (**Figure 3.3B**). From the electropherograms, the areas of virus peaks show that treating VSV with quadramers protects about 3 times more efficiently than the untreated virus.

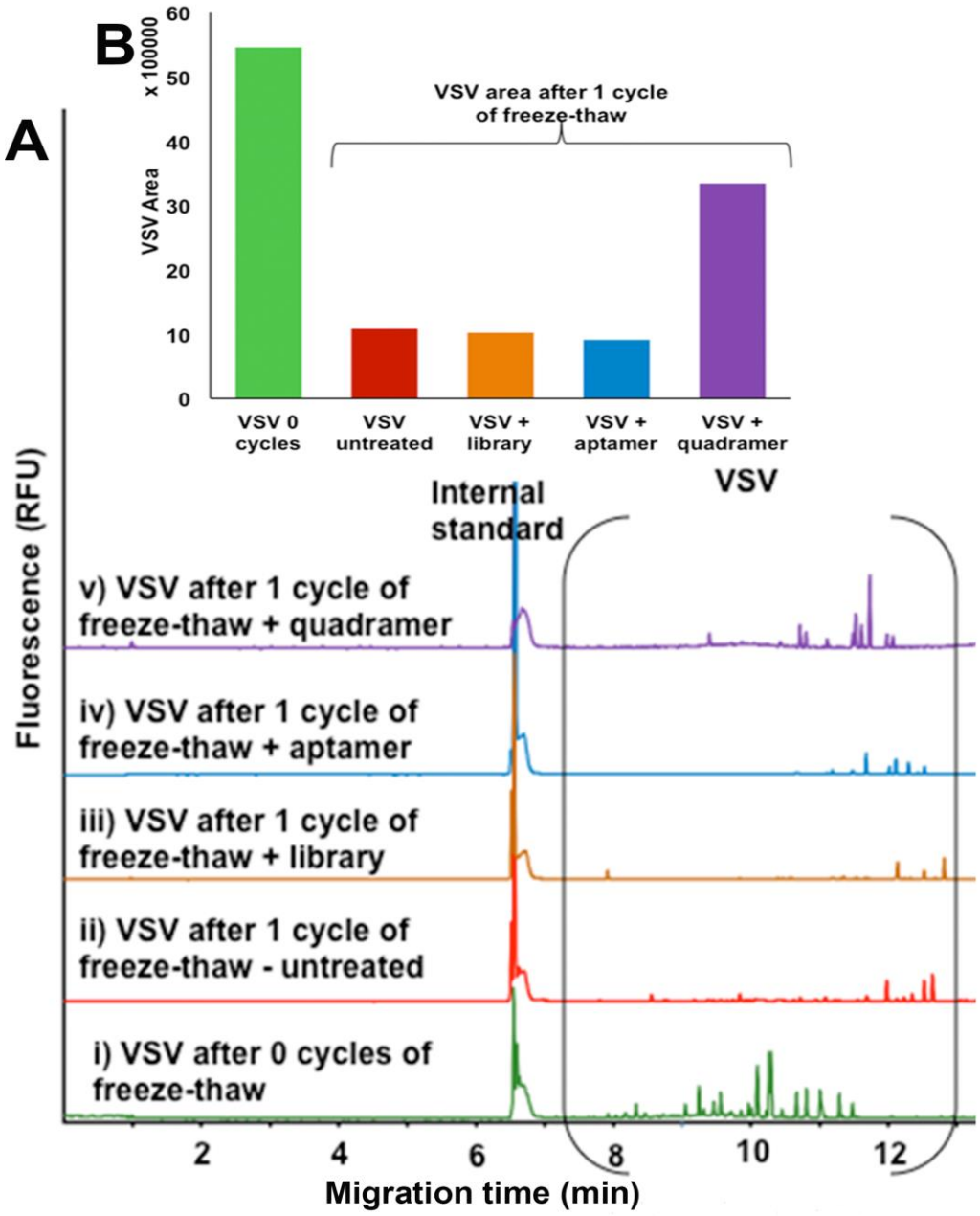

Figure 3.3. A) Electropherograms for VSV separated by capillary electrophoresis and detected by laser-induced fluorescence. VSV was stained with YOYO-1 dye. CE separations were performed in a 60 cm long capillary under 250 V cm^{-1} in 25 mM borax buffer at 15 °C. i) fresh, not frozen VSV, ii-v) VSV after 1 cycle of freeze-thaw, untreated, treated with the library, an aptamer, and a quadramer, respectively. B) Areas of intact virus peaks for all experiments. Reprinted with permission from[84].

The effect of quadramers and the aptamer pool on VSV active units *in vitro* was also evaluated using a mixture of viruses coding yellow fluorescent protein (YFP) and red fluorescent protein (RFP) and by detecting the expression of the corresponding fluorescent proteins in Vero cells (**Figure 3.4A**). Galasso G. et al. using electron microscopy confirmed that in the infection of a monolayer of cells by viruses with a low multiplicity of infection (MOI), the ratio of virus to the cells, one active viral particle could infect one cell and an aggregation several infectious particles lead only one cell infection.[123] The co-infection of cells by virus particles was observed when YFP and RFP were both expressed in the same cells. Overlapping YFP and RFP signals were detected in 27±2.1%, 16±1.9% and 11±1.4% of cells infected with the pure virus, treated with aptamer pool, and quadramer, following one cycle of freeze-thawing, respectively. The results show the relatively increase virus active units exhibited in quadramer-treated VSV (**Figure 3.4B**). These may be explained by repulsion of virus particles from each other after binding to negatively-charged DNA aptamers. The aptamers prevent interaction of surface proteins and keep virus particles suspended in solution. It was previously reported that treating VSV with trypsin in order to remove the sticky part of the glycoprotein leads to a increase virus active units as well[124, 125]. Interesting to note, that the aptamer-based coating does not suppress virus capability to infect cells due to the non-covalent and reversible nature of aptamer interaction with the virus.

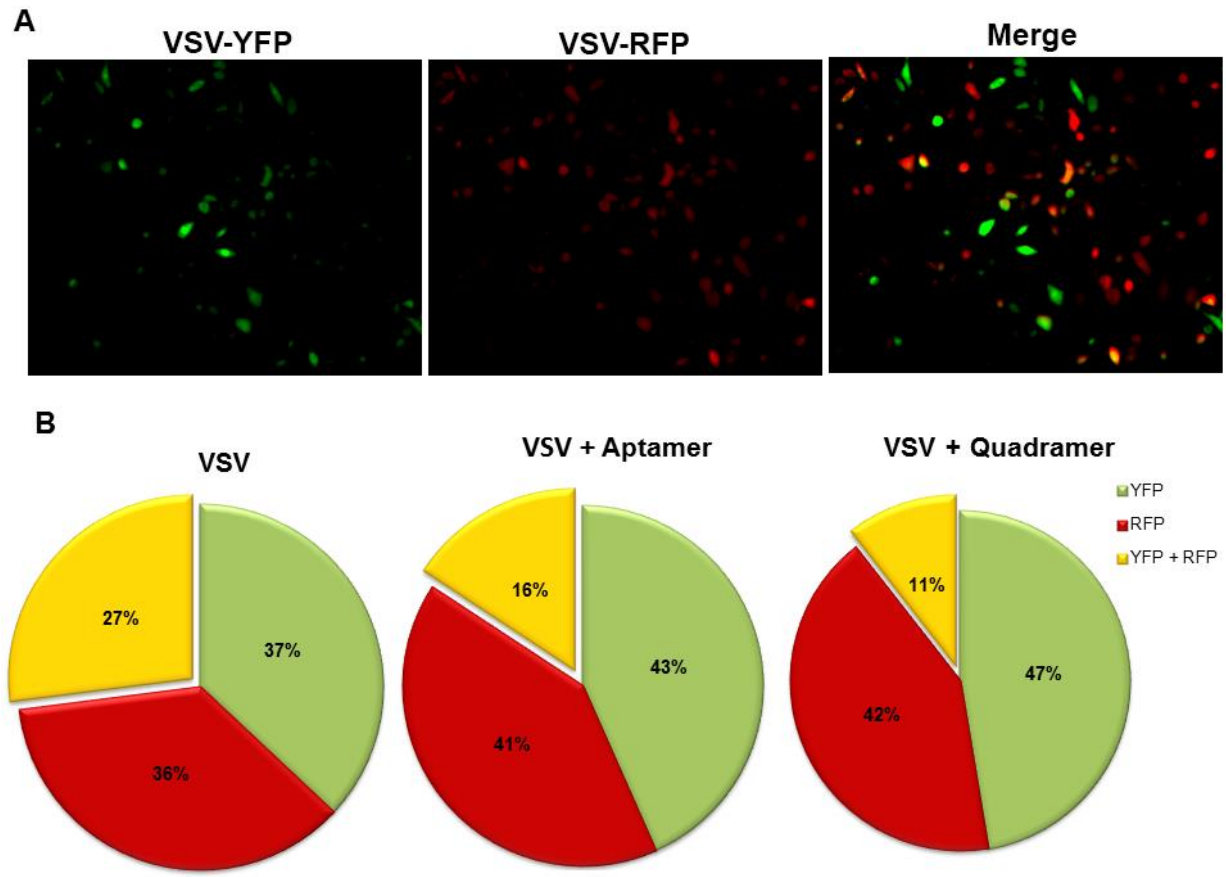

Figure 3.4. Cells infected with a mixture consisting of equal amounts of VSVs coding YFP and RFP; A) Fluorescent imaging of YFP and RFP in Vero cells after 24 hrs of virus infection; B) Percentage of cells expressing YFP, RFP, and both after infection with pure VSV, aptamer- and quadramer-treated virus following one cycle freezing. Less co-infection of the viruses expressing YFP and RFP is observed in the presence of quadramers. Reprinted with permission from[84].

Viral vectors survival and infectivity in the presence of nAbs is a major factor for vaccine efficiency. Therefore, in addition to cryoprotection, we evaluated the aptamers and quadramers competence to shield VSV from neutralizing antibodies. We measured the infectivity of VSV after incubation with the aptamer pool (1 μM) and quadramer (0.25 μM) as well as control groups in the presence of rabbit serum containing nAbs on Vero cells. While nAbs neutralized the virus infectivity, incubated VSV with aptamer pool and quadramer retrieved the infectivity

about 25% and 75% respectively (**Figure 3.5**). In order to check the in-vivo toxicity, 400 µg of both the aptamer pool alone and the quadramer with VSV were intravenously administered (i.v.) through the tail vein two times (day 1 and day 2) into three BL6 male mice (10 weeks old) in two groups, according to the Canadian Council on Animal Care guidelines[19]. They were examined for the visible symptoms of toxicity for five days after the administration. The mice did not develop diarrhea, lethargy, ruffle fur, loss of appetite or lose any weight.

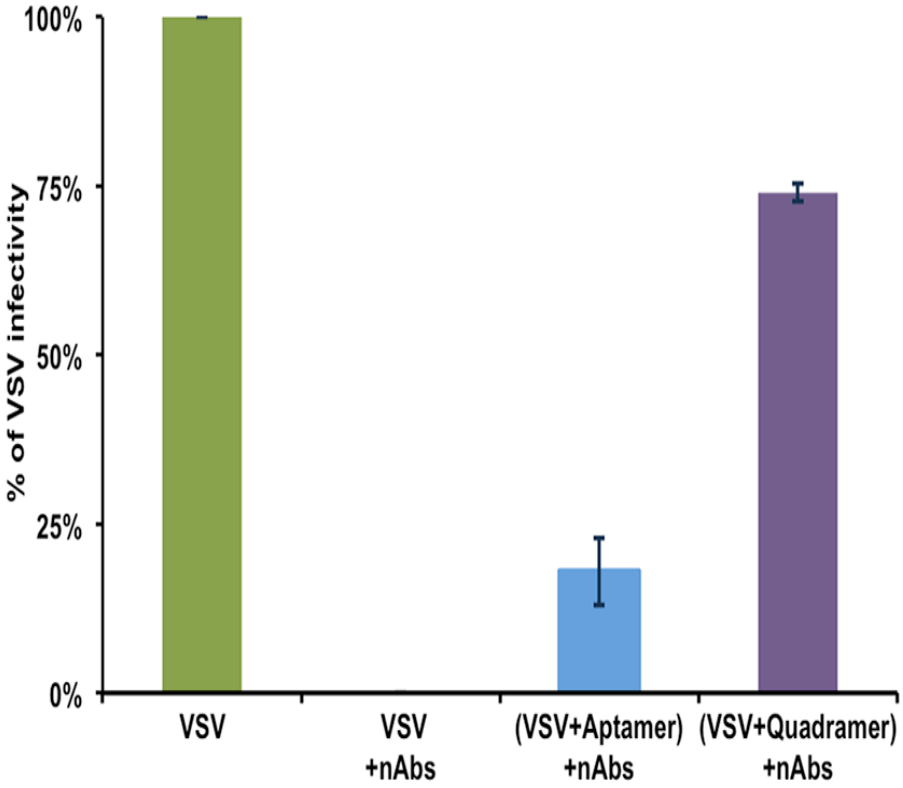

Figure 3.5. Comparison of the efficiencies of an equimolar mixture of aptamers and quadramer to protect VSV infectivity in the presence of VSV neutralizing antibody. Reprinted with permission from[84].

3.5. Conclusion

In conclusion, we have modified anti-VSV aptamers by bridging them together to form tetrameric counterparts and were able to achieve 1.4 log increase of viral infectivity after 60 freeze-thaw cycles in a plaque-forming assay. Adding these aptamers to VSV increase viral active units and protects its infectivity from neutralizing antibody. The findings of this study opened new doors for aptamer applications as virus cryo- and antibody- protectors. These types of aptamers can potentially be applied *in vivo*, in combination with the oncolytic virus, to prevent clearance of the virus and thus increase its oncolytic efficiency without toxic effect.

Chapter 4

Aptamers with switchable binding for positive isolation of cells

4.1. Objective

Positive immunomagnetic isolation is the most direct and specific way to separate intact target cells from a heterogeneous cell population. One challenge, after cells isolation is the persistence of bound antibodies and magnetic beads, which may alter not only cellular viability but also complicate any downstream applications. Here, we aimed to develop DNA aptamers with switchable binding to transmembrane proteins: Notch ligand Delta-like 4 (DLL4), leukemia

inhibitory factor receptor (LIFR), neuropilin-1 receptor (NRP1), urokinase plasminogen activator receptor (uPAR) and Patched 1 receptor (PTCH1), which act as effective substitutes to antibodies without alterations in cellular viability. The switchable aptamers need to bind selectively to the receptor positive cells in the presence of Mg^{2+} and Ca^{2+} ions and release the pure and intact cells upon addition of EDTA, allowing for cell separation in a facile and non-toxic manner with reagents readily available to any standard laboratory.

Contributions

Shahrokh M. Ghobadloo and Dr. Maxim V. Berezovski (supervisor) conceived the idea and designed the research. Shahrokh M. Ghobadloo performed experiments. Nadia Al-Youssef assisted in evaluating aptamers using flow cytometry.

4.2. Background

The isolation of discrete cell types from heterogeneous suspensions such as bone marrow, blood or digested tissue is an essential step in cell-based research, diagnostics, molecular analysis of cells, tissue engineering and cell-based therapeutics [52, 53]. Among the current cell separation methods, the immunomagnetic approach, due to the high specificity of antibodies, has so far shown to be the most efficient and reliable. Gentle, tube-based magnetic separation is the technology of choice to isolate high yields of pure, viable and functional cells. It is divided into two main strategies: “negative isolation” where unwanted or negative (-) cells are removed or depleted, or “positive isolation” where the target positive (+) cells are collected.[59]

In negative isolation, the (-) cells are magnetically labeled, retained in a magnetic separator, and eliminated from the cell mixture. This method is preferred either when no specific antibody is available for the target cells or when labeling of the target cells is not desirable. Additionally, if target cells in a mixture are present in very low concentrations negative isolation may result in low yield and purity as target cells are inefficiently isolated and unwittingly lost. Positive isolation is a fast and gentle way to isolate the (+) cells from a complex mixture. The (+) cells are magnetically labeled, retained in a magnetic separator and finally eluted as the enriched fraction after removal of the magnet.

The challenge when performing positive cell isolation is that the cells of interest may be affected and/or altered during the isolation process. In most systems, the antibody-coated magnetic beads, required for isolation, remain with the cells and persist throughout the duration of any downstream experiments. This can lead to clustering of receptors, triggering of signaling pathways or blocking of receptor functions. Positive cell isolation without antibody and bead removal is used for some downstream applications, such as nucleic acid or protein analysis. However, for cell therapy and the injection of cells into a patient, it is necessary to obtain pure and viable cells that preclude the retention of bound antibodies. Current detachment technologies utilize anti-antibodies or peptides, these recognize the variable region of the primary antibody and disrupt the binding of the primary antibody and the surface antigen [60, 61].

To achieve the isolation of pure cells in high yield without antibody and beads contamination, we present a universal isolation technology utilizing switchable aptamers (SwAps). These small (~30 kDa), single-stranded DNA oligonucleotides carry the blueprint for their synthesis in their primary sequence, allowing them to be synthesized by chemical or enzymatic procedures. They fold into well-defined three-dimensional structures; with high affinity and specificity for their

targets. Aptamers are often viewed as “synthetic antibodies” with applications ranging from target detection to drug discovery and delivery. In many respects, aptamers are superior to antibodies. They can be chemically synthesized in high purity at low cost (1000s times cheaper than for monoclonal antibodies), and are considered a synthetic chemical product, and not a biological product, which can be easily manipulated and purified.

The switchable aptamers bind to the target cells in the presence of Mg^{2+}/Ca^{2+} and release the pure and intact cells after the addition of EDTA into solution (**Figure 4.1)**.

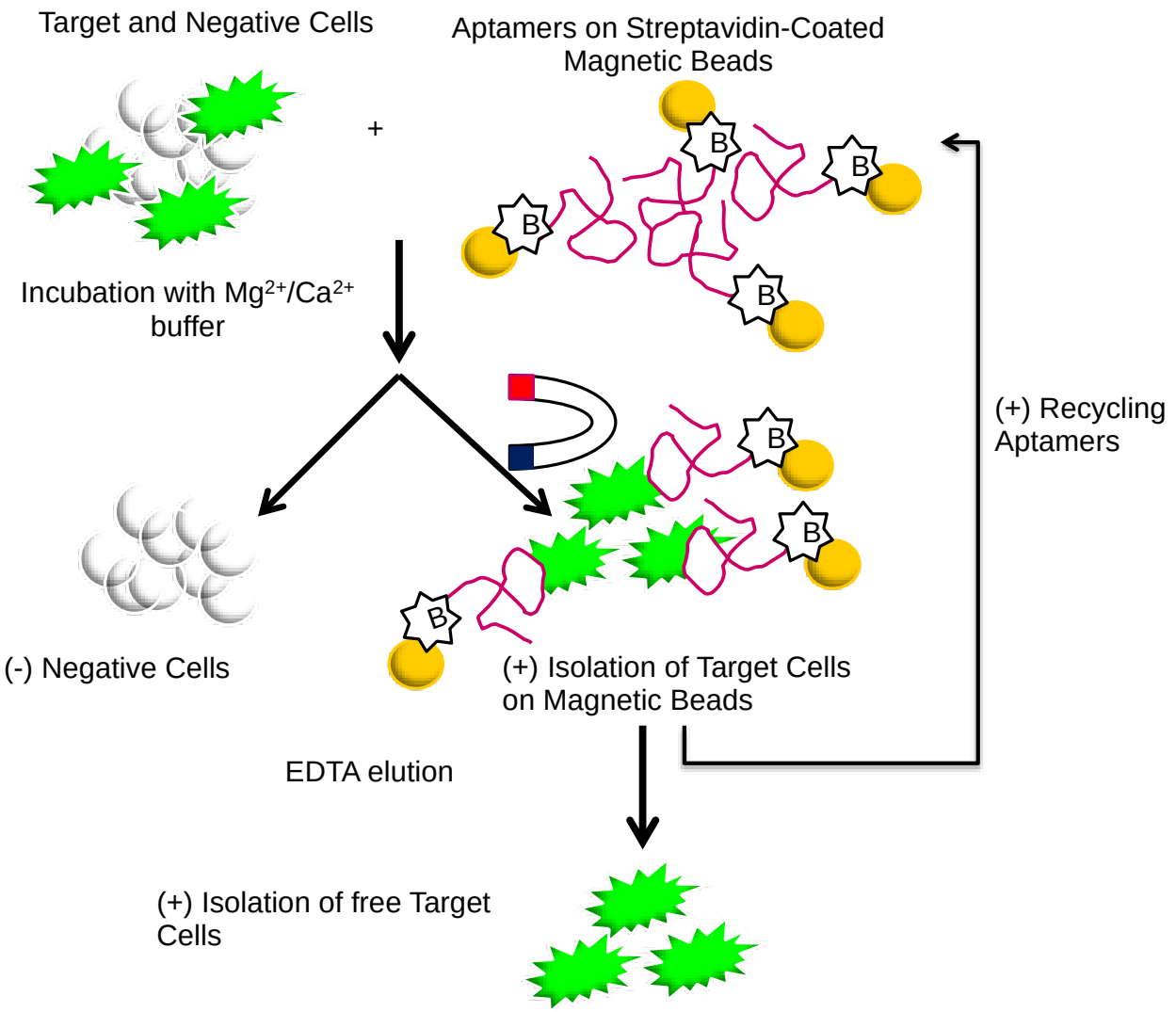

Figure 4.1. The biotinylated switchable aptamers bind to the target cells in the presence of Mg^{2+}/Ca^{2+} and followed by magnetic cell sorting using streptavidin coated magnetic beads. Adding EDTA release the pure and intact cells.

We have selected aptamers to five individual human cell surface protein targets: Notch ligand Delta-like 4 (DLL4) [126], leukemia inhibitory factor receptor (LIFR) [127], neuropilin-1 receptor (NRP1) [128], urokinase plasminogen activator receptor (uPAR) [129], and Patched 1 receptor (PTCH1) [130]. DLL4 is a cell-surface protein, which binds to Notch receptors. It is expressed on endothelial and recruited bone marrow-derived vascular precursor cell where it is

involved in vascular maturation and angiogenesis[131]. LIFR is a transmembrane receptor which binds LIF; its roles are in self-renewal, survival, and differentiation[132]. NRP1, a transmembrane glycoprotein, is involved in vascular development and is expressed in bone marrow stromal cells, pancreatic, placental and tumor cells[133]. uPAR, a glycosylated extracellular receptor expressed in hematopoietic cells and some non-hematopoietic cells. Its role is in regulating angiogenesis and tumor progression [134]. PTCH 1 is hedgehog receptor and acts as a negative regulator of the hedgehog signaling pathway. PTCH 1 is a critical receptor involved in the development of T- and B-lymphoid lineages [135].

4.3. Materials and methods

Cell lines

The human embryonic kidney (HEK293) cell line was purchased from Clontech Laboratories and maintained in Dulbecco's modified Eagle medium supplemented with 10% fetal bovine serum. The transfected cells expressing DLL4, LIFR, NRP1, uPAR and PTCH1 were maintained with Doxycycline (500 ng/mL) fortified complete media.

Antibodies

Anti-PTCH1 (MAB41051) and anti-Neuropilin-1 Alexa Fluor 700 (FAB3870N) were purchased from R&D Systems. Anti-Neuropilin-1 FITC (354512) was obtained from Biolegend. Anti-LYPD6 (PA5-24832) and anti-DLL4 (PA5-26963) were purchased from Thermo Scientific and Anti-LIFR (sc-20752) from Santa Cruz Biotechnology. Anti-PTCH1 (946-960) was purchased from Sigma-Aldrich. Anti-Neuropilin-1 (EPR3113) and secondary antibody to rat

IgG-FITC (ab6115) were provided from Abcam. Anti-rabbit IgG-Dylight 488 (DI-1488) were obtained from Vector Laboratories.

Bone marrow cell isolation

Fresh bone marrow was extracted from 8 week old BL6 male mice. Mice were maintained and euthanized according to the Canadian Council on Animal Care guidelines[86].

Construction genes into the pLVX-TRE3G Vector

Bacteria containing pReceiver vectors with open reading frame of DLL4 (NM_019074.3; Product ID# U1091), LIFR (NM_001127671.1; Product ID# A0537), NRP1 (NM_001024629.2; Product ID# Z1914), uPAR (NM_002659.3; Product ID#A0851) and PTCH1 (bc043542; Product ID# E1069) were obtained from GeneCopoeia, Inc. Bacteria were cultured in selective growth media, the vectors extracted and used to provide cDNAs of DLL4, LIFR, NRP1, uPAR and PTCH1 using CloneAmp HiFi PCR Premix (Clontech Laboratories, Inc. Cat. # 639298) and related specific primers with 15 bp extensions homologous to the pLVX-TRE3G vector ends **(Table 4.1)**. For cloning, we incubated pLVX-TRE3G vector with MluI (New England Biolabs, cat# R0198S) and EcoRI ((New England Biolabs, cat# R0101S) restriction enzymes at 37°C for 3 hours to generate linearized vector. The linearized vector was purified using 1% Agarose gel and extracted with the GeneJet Extraction Kit (Thermo Scientific, Cat#K0692). The cloning of the PCR products into pLVX-TRE3G was carried out by using Fusion HD Cloning Kits (Clontech Laboratories, Inc. Cat. #639648).

Table 4.1. The primers of cDNAs.

cDNA	Forward Primer	Reverse Primer
uPAR	gcccccgggacgcgtatgggtcacccgccgctg	ctacccggtagaattcttaggtccagaggagagtgcctcc
DLL4	gcccccgggacgcgtatggcggcagcgtcc	ctacccggtagaattcttatacctccgtggcaatgacaca
PTCH1	gcccccgggacgcgtatggggaaggctactggccggaa	ctacccggtagaattcttacaggaggtatgctgtcccaga
LIFR	gcccccgggacgcgtatgatggatatttacgtatgtttg	ctacccggtagaattcttaatcgtttggtttgttctga
NRP1	gcccccgggacgcgtatggagaggggggctgccgct	ctacccggtagaattcgggttgcggccgactcgag

Transformation

We mixed competent cells (50 µl) with cloned pLVX-TRE3G reaction mixture (2.5 ng). The mixture placed on ice for 30 min. Tubes were then heat shocked for 45 seconds at 42°C and then placed on ice for an additional 1–2 min. Afterward, Super Optimal Broth with Catabolite repression (SOC) medium was added bringing the final volume to 500 µl. The cell mixture was cultured on agar medium supplemented with ampicillin (100 µg/ml).

Lentivirus production and transduction

A lenti-X^{TM} Tet-On 3G Inducible Expression System was used (Clontech, Cat#631187) for lentiviral production. DLL4, LIFR, NRP1, uPAR and PTCH1 were subcloned into the pLVX-TRE3G vector using the In-Fusion HD (Clontech, Cat# 638909). Lentiviruses were generated by transfecting 293T cells using pLVX-TRE3G- DLL4, -LIFR, -NRP1, - uPAR and -PTCH1 separately with the Lenti-X HTX Packaging System (Clontech, Cat#631187). Virus particles were harvested 48 hours after transfection. HEK293 cells were infected with the

pLVX-Tet3G and selected with G418 (Clontech; Cat#631307) (1 mg/mL). Five 10 cm plates of the chosen cells separately were infected with the pLVX-TRE3G-DLL4, -LIFR, -NRP1, - uPAR and -PTCH1 viruses and selected with puromycin (Clontech; Cat#631305) (25 μg/mL). Doxycycline (Clontech) was added to the cultures at 500 ng/mL to induce appropriate the corresponding receptors expression.

Immunofluorescence staining

Cells were fixed with 4% paraformaldehyde, permeated with 0.25% Triton X-100 (Sigma, St. Louis, MO), and blocked with 10% fetal bovine serum (Gibco, CA). The cells were incubated with the corresponding primary antibodies at room temperature for 1 hour. The cells were then incubated with fluorochrome-conjugated secondary antibodies for 1 hour. After the cells had been rinsed, they were counterstained with 4′,6′-diamidino-2-phenylindole (DAPI; Sigma), and analyzed under a fluorescence microscope or confocal microscope (Nikon).

Confirmation of the target on cell membrane: Flow cytometric analysis

Non-transfected transfected and induced cells were made into single-cell suspensions and stained with the corresponding primary and fluorochrome-conjugated secondary antibodies. The primary antibody for DLL4, LIFR, NRP1, uPAR and PTCH1 respectively were from Thermo Scientific (PA5-26963), Santa Cruz Biotechnology (sc-20752), Abcam (ab81321), Thermo Scientific (PA5-24832) and SIGMA-ALDRICH (946-960). The samples were analyzed on a Beckman Coulter FC500 flow cytometer.

DNA aptamer selection

For aptamer selection, we used a single-stranded DNA library with 100 base lengths including a 60 variable internal region flanked by two 20mer PCR primer sequences which originated from Liu's laboratory at Harvard University[136]; the library was made with 5′ CTCCTCTGACTGTAACCACG78787878666678787878786667878787878666678787878666 678787878 GCATAGGTAGTCCAGAAGCC3′ where 6 is a combination that makes 1 : 1 : 1 : 1 A/C/G/T, 7 is a combination that makes 45 : 5 : 45 : 5 A/C/G/T, and 8 is a combination that makes 5 : 45 : 5 : 45 A/C/G/T. The library in PBS with Ca^{2+} (0.9 mM) and Mg^{2+} (0.49 mM) was applied to selection. After denaturation at 95°C and 10 minutes the sample was snap cooled on ice. DNA was then incubated with the target positive cells to allow DNA sequences to bind to positive cells' membranes for 1 hour at 37°C. Then the cells were rinsed using PBS and spun down at 200 RCF using tabletop centrifuge. The supernatant containing unbound DNAs was removed, after which the DNA sequences bound to the cell surface were eluted by heating at 95°C for 5 minutes. The recovered DNA was then incubated with non-transfected HEK293T cells as a negative selection to remove non-specific DNA. Incubation was performed for 1 hour at 37°C. To collect sequences, only DNA in the supernatant was retained. Both non-transfected cells, as well as any bound DNA, was discarded. Each round of positive selection was followed by one round of negative selection for a total of 10 rounds. DNA collected after the selection was amplified by PCR for the next round.

Twenty-five cycles of PCR were carried out for the amplification of single-stranded DNA using Thermo Scientific Phire Hot Start II DNA Polymerase (Thermo Scientific). In addition to the DNA template, 50 μL of the PCR reaction mixture contained 1x Phire Reaction Buffer, 3% Dimethyl sulfoxide (DMSO), 200 μM dNTPs, 1 μL of the Phire Hot Start II DNA Polymerase

(Thermo Scientific), 0.5 µM of 5'-Cy5-labeled forward primer and 0.5 µM 5´-phosphorylated reverse primer were used. The following settings were used for the thermal cycler: melting at 95 °C for 30 s, annealing at 58°C for 15 s, and extending at 72°C for 10 s. After PCR, Lambda Exonuclease (New England Biolabs, Cat#M0262S) was used, according to manufacturer protocol, to digest the 5´-phosphorylated reverse strand producing single stranded DNA.

After multi-round selection, aptamer pools became enriched for sequences that possess significant binding. These pools were used in EDTA switchable cell-SELEX. For this method of selection, after incubation with positive cells, aptamers are eluted using 10 mM EDTA instead of heating. Liberated sequences are collected for subsequent rounds of selection.

Next-generation sequencing and phylogenetic tree analysis

PCR using Illumina specific barcodes was performed with pool 10 of all targets. DNA was purified using 4% ultraPure Agarose gel (Invitrogen) and the GeneJET Gel Extraction Kit (Thermo Scientific, Canada). All samples were mixed in equimolar amounts (each 200 ng) and sequenced by Eurofins MWG Operon LLC, a Eurofins Genomics company, in a single lane of an Illumina MiSeq paired-end for 150 bases. We obtained a total number of 17.61 million reads by Illumina sequencing, which were subsequently sorted according to their barcodes. The barcodes were not equally distributed even though an equimolar mixture of barcoded and purified PCR products for the sequencing pool. The data, in fastq files, were uploaded onto the Galaxy project platform (https://usegalaxy.org)(1) and converted to FASTA. To find the abundance of each sequence, the FASTA data was collapsed. The most abundance sequences were analyzed for common motif using MEME (http://meme.nbcr.net/meme/) and phylogenetic tree analysis using Clustal Omega (http://www.ebi.ac.uk/Tools/msa/clustalo/).

Flow cytometric assay of the aptamer binding affinity

Target receptor positive and negative cells (10^5 cells) were incubated with related Cy5-conjugated aptamers (0, 1, 10, 100, 200 and 300 nM) at room temperature for 30 minutes, and then washed and analyzed by flow cytometry. After deducting the mean fluorescence value of the control sample, the average fluorescence intensity (MFI) of positive cells bound with Cy5-aptamers were used to the equilibrium dissociation constants (Kd). The apparent Kds of the aptamer−cell interaction were calculated based on the dependence of fluorescence intensity binding and aptamer concentration according to the formula $Y = B_{max}X/(Kd + X)$, where the Y is the bound fraction, the Bmax represents the saturated binding, and the X is for the concentration of ligand.

Capture assay of aptamers

Biotinylated switchable aptamer sequences, specific to cells expressing DLL4, LIFR, NRP1, uPAR and PTCH1 in PBS with Ca^{2+} (0.9 mM) and Mg^{2+} (0.49 mM), were added to the cells and incubated at room temperature for 1 hour. The cells were washed with PBS ($+Ca^{2+}/Mg^{2+}$) and then incubated with streptavidin magnetic beads (Thermo Scientific, cat#88817) in PBS ($+Ca^{2+}/Mg^{2+}$) at room temperature for an additional 1 hour. To isolate captured cells, the tubes were exposed to a magnet holder; the solution was decanted, and the tubes were washed to discard non-bound cells. To purify the isolated cells from magnetic beads and aptamers, EDTA (10 mM) in PBS without Ca^{2+}/Mg^{2+} was added to each tube. After 30 minutes, the tubes were placed into a magnet holder and the free cells collected for further assays including viability, target receptor expression and phenotype identification tests.

Phenotype identification of the isolated mice bone marrow cells

ALDH is potently expressed in stem and progenitor cell types including hematopoietic progenitors and mesenchymal cells [137]. CD44 is found on bone marrow mesenchymal stem cells, hematopoietic stem cells, immune cells of both lymphoid and myeloid origin, as well as megakaryocytic lineage, erythroid lineage, endothelial lineage, mature T cells and B cells [138-141]. CD24 is expressed on granulocytes in a pattern that is similar to CD11b, but it is not expressed on monocytes [142]. CD20 is a marker of naïve and mature B cells [143]. CD11b is a marker at the myelocytic stage of differentiation and is not expressed on mesenchymal stem cells [142, 144]. CD52 is broadly expressed on lymphocytes [145]. B cells, activated T cells and a subset of dendritic cells express CD45R [146]. CD45R is not presented on mesenchymal stem cells, mature erythrocytes, platelets and plasma cell. Bone marrow cells were isolated and purified using aptamers and assayed for phenotype using the markers above (ALDH, CD44, CD24, CD20, CD11b, CD52, and CD45R). The purified cells were washed with PBS containing Ca^{2+}/Mg^{2+}. The ALDEFLUOR kit (StemCell Technologies, cat#01700) was used to test the isolated mice bone marrow cells for ALDH enzymatic activity according to the manufacturer's instructions. Briefly, the cells were incubated with ALDH substrate in ALDEFLUOR buffer. As a negative control, with the same conditions, a sample of the cells was incubated with dimethylamino benzaldehyde, a specific ALDH inhibitor. Also, the cells were stained with conjugated Alexa Flour 488 anti-mouse CD11b antibody (Stem Cell Technologies, cat#60001AD), conjugated PE anti-mouse CD45R antibody, FITC conjugated CD20 antibody (Thermo Scientific Pierce, cat# MA1-82402), FITC conjugated CD52 (Thermo Scientific Pierce, cat#MA1-82162), APC-conjugated

CD44 (BD Pharmingen, cat#559942) and PE-conjugated CD24 (BD Pharmingen, cat#555428) to elucidate identity. All samples were analyzed by Beckman Coulter FC500 Flow Cytometer.

4.4. Results and discussion

Cell-SELEX [147] is an *in vitro* evolution approach of affinity ligands that does not require target purification; it needs only two types of cells: receptor positive (+) cells, which express the protein of interest, and receptor negative (-) cells, which do not. In the case of transmembrane proteins, cell-SELEX generates aptamers capable of recognizing the target protein in its natural folding and modification state presented in its physiological environment [147-149]. The (+) cells were prepared by transduction of a (-) cell line, human embryonic kidney (HEK293), lacking the proteins mentioned above using a lent viral-based gene transfer system (**Figure 4.2**).

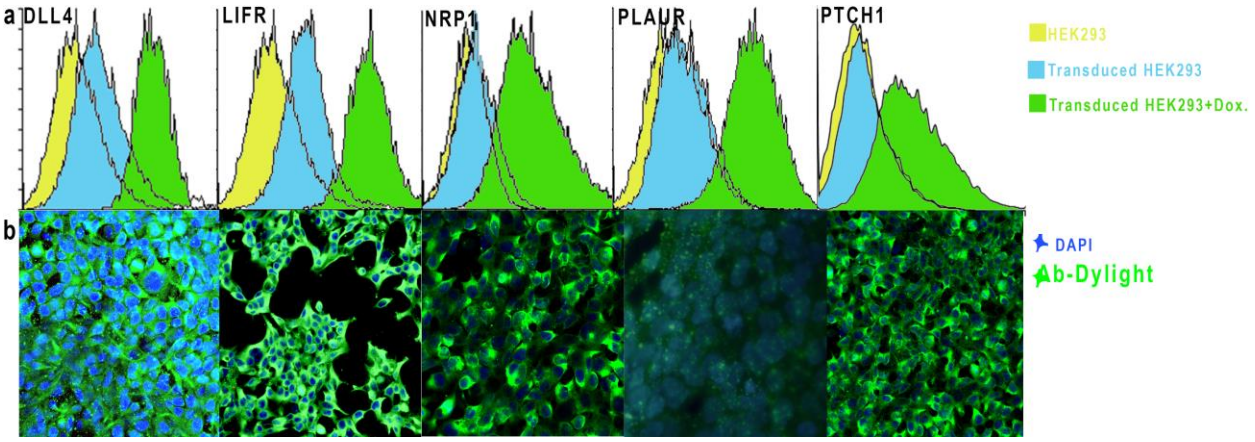

Figure 4.2. Expression of target proteins in HEK293 cells. (a) Flow cytometry analysis of non-transfected, transfected either non-induced or induced with doxycyclin of HEK293 cells expressing DLL4, LIFR, NRP1, uPAR and PTCH1 with the corresponding antibody. Flow cytometry was performed on surface exposed protein (without permeabilization) (b) Immunofluorescence of induced transfected HEK293 cells expressing DLL4, LIFR, NRP1, uPAR and PTCH1 with corresponding antibodies. Microscopy was performed on total fractions with permeabilization. All the photos except PLAUR were

captured by Zeiss Axiophot fluorescence microscope (20X magnification). The photo for PLAUR was campture by Nikon A1RsiMP confocal microscope at 25X magnification.

After twelve rounds of cell-SELEX, the evolved aptamer pools displayed stronger binding to (+) cells compared with initial DNA library **(Figure 4.3)**.

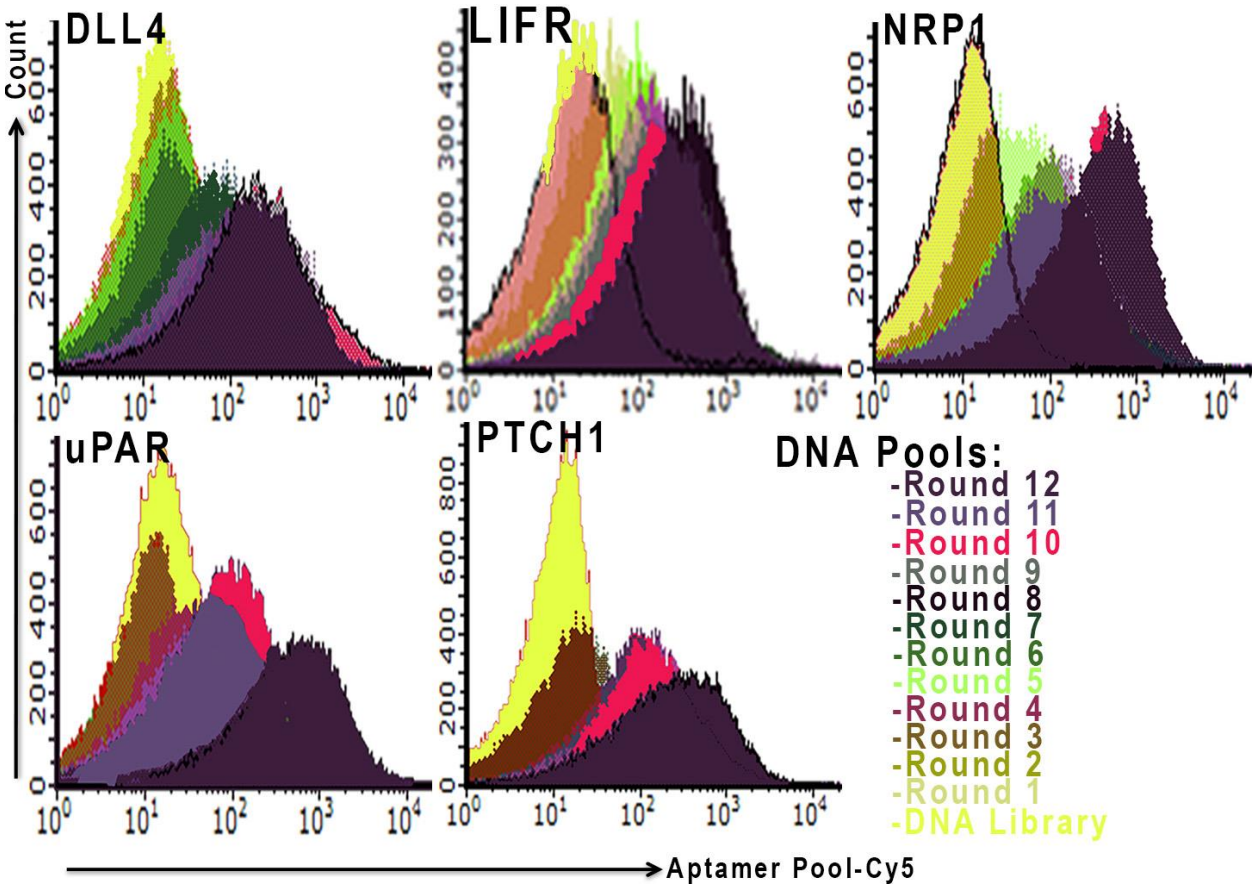

Figure 4.3. Binding of selected aptamer pools to (+) cells.Cy5-labeled aptamer pools (20 0nM) were incubated with corresponding target (+) cells in 200 μL of PBS with Ca^{2+}/Mg^{2+} for 30 min. After washing and re-suspension in 500 μL of PBS with Ca^{2+}/Mg^{2+}, cell fluorescence was determined by flow cytometry. The Cy5-labeled ssDNA library was used as a control for nonspecific binding.

The resulting aptamer pools for the five target proteins were sequenced by the next-generation sequencing (NGS). **Figure 4.4** represents quality check electropherograms of the DNA pools subjected to NGS by bioanalyzer.

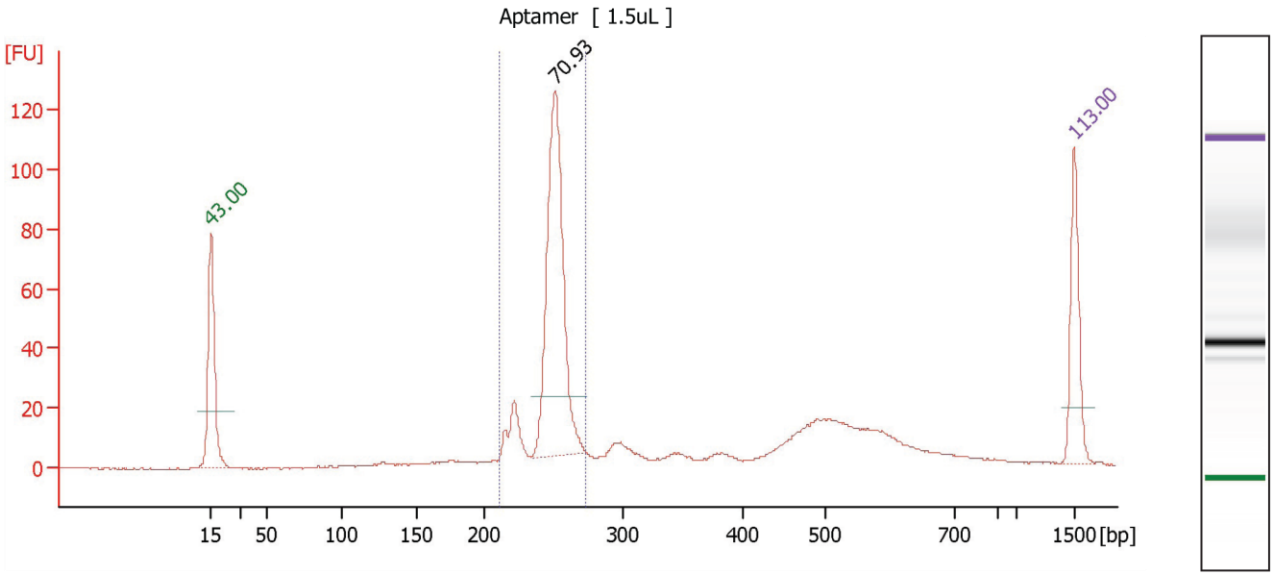

Overall Results for sample 1 : Aptamer

Number of peaks found:	1	Area 1:	266.6

Peak table for sample 1 : Aptamer

Peak	Size [bp]	Conc. [ng/µl]	Molarity [nmol/l]	Observations
1	15	4.20	424.2	Lower Marker
2	251	8.15	49.2	
3	1,500	2.10	2.1	Upper Marker

Region table for sample 1 : Aptamer

From [bp]	To [bp]	Area	% of Total	Average Size [bp]	Size distribution in CV [%]	Conc. [ng/µl]	Color
211	273	266.6	50	248	4.7	10.14	

Figure 4.4. Electropherograms of bioanalyser for the pools subjected to next generation sequencing (provided by eurofins MWG); FU stand for fluorescence units.

NGS data derived from cell-SELEX pools were filtered, clustered, and analyzed using Galaxy (https://usegalaxy.org)[150]. They were grouped based on the common motif. **Table 4.2** shows the most abundant DNA sequences from every group after align.

Table 4.2. Multiple sequence alignment of the selected aptamers against DDL4, LIFR, NRP1, PLAUR (Upar) and PTCH1.

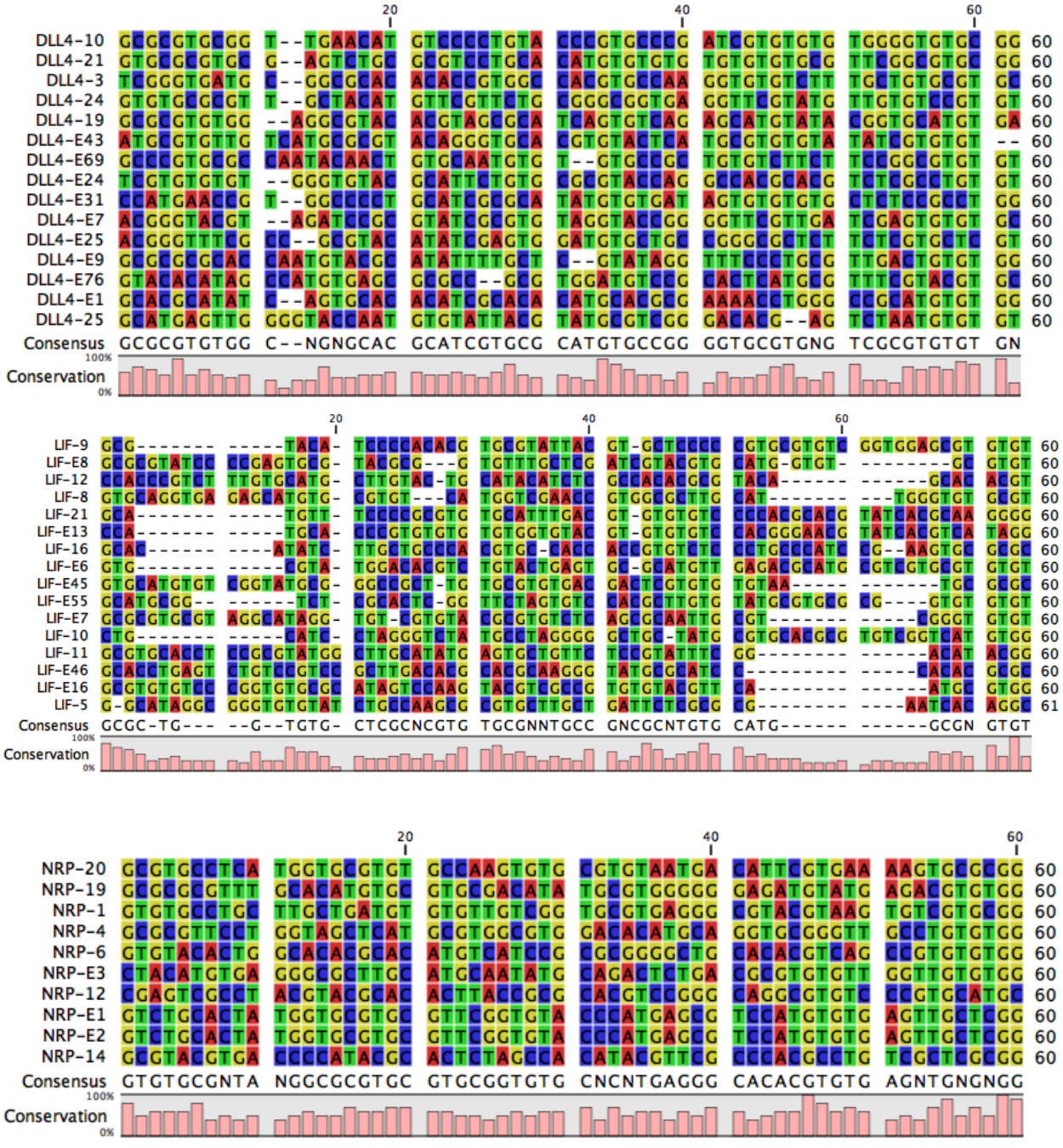

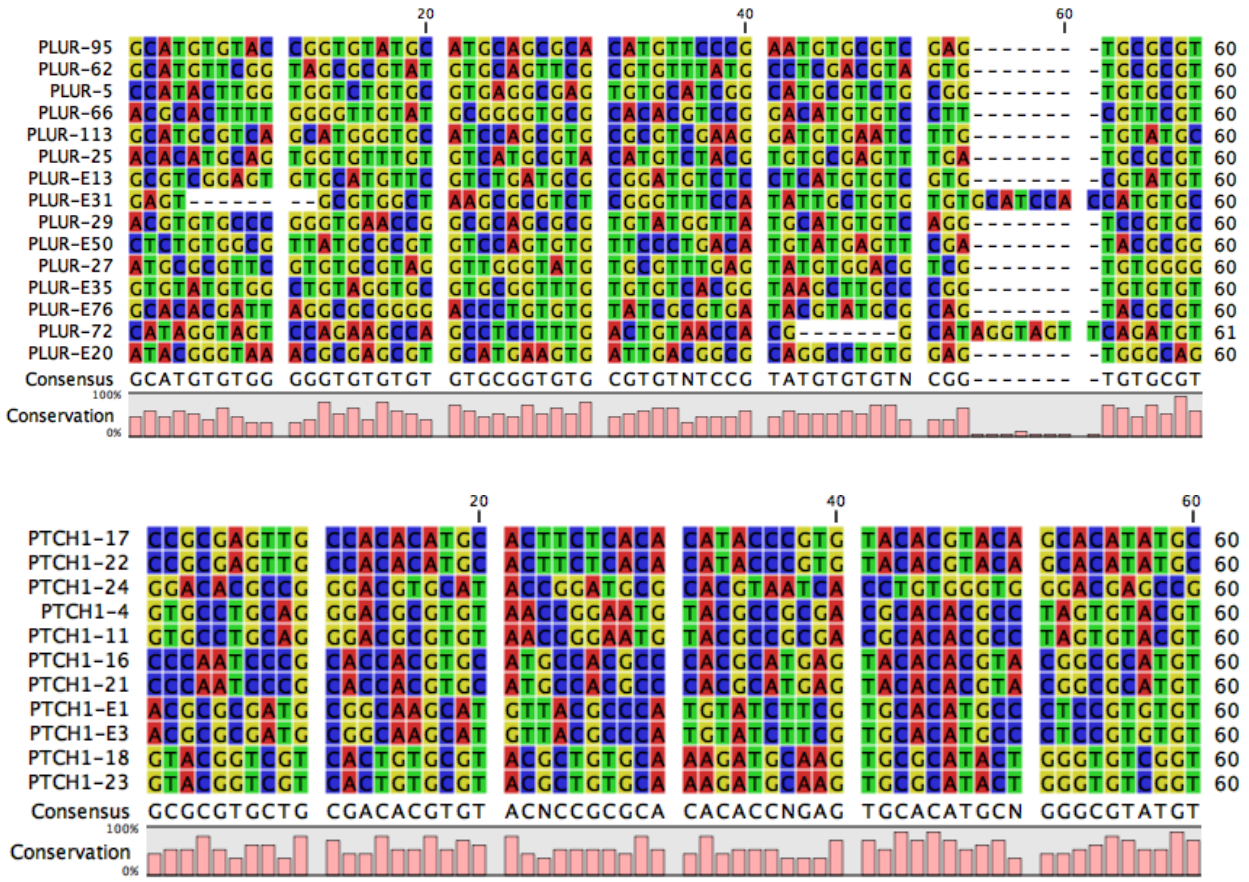

Afterward, we chemically synthesized four fluorescently labeled aptamers with common motifs for each target and tested their individual cellular binding by flow cytometry (**Figures 4.5 and 4.6**) and microscopy (**Figures 4.7 and 4.8**). **Figure 4.5** represents the binding of the aptamers to the HEK293 cells expressing the target receptors, DLL4, NRP1, LIFR, uPAR (PLAUR) and PTCH1 using flow cytometric analysis. The aptamers without binding or nonspecific binding are presented in the figures. The same cell line, HEK293, without expressing the receptors was used as a control. Furthermore, the binding of individual aptamer to a mixture of the five cells expressing the receptors was tested in this experiment.

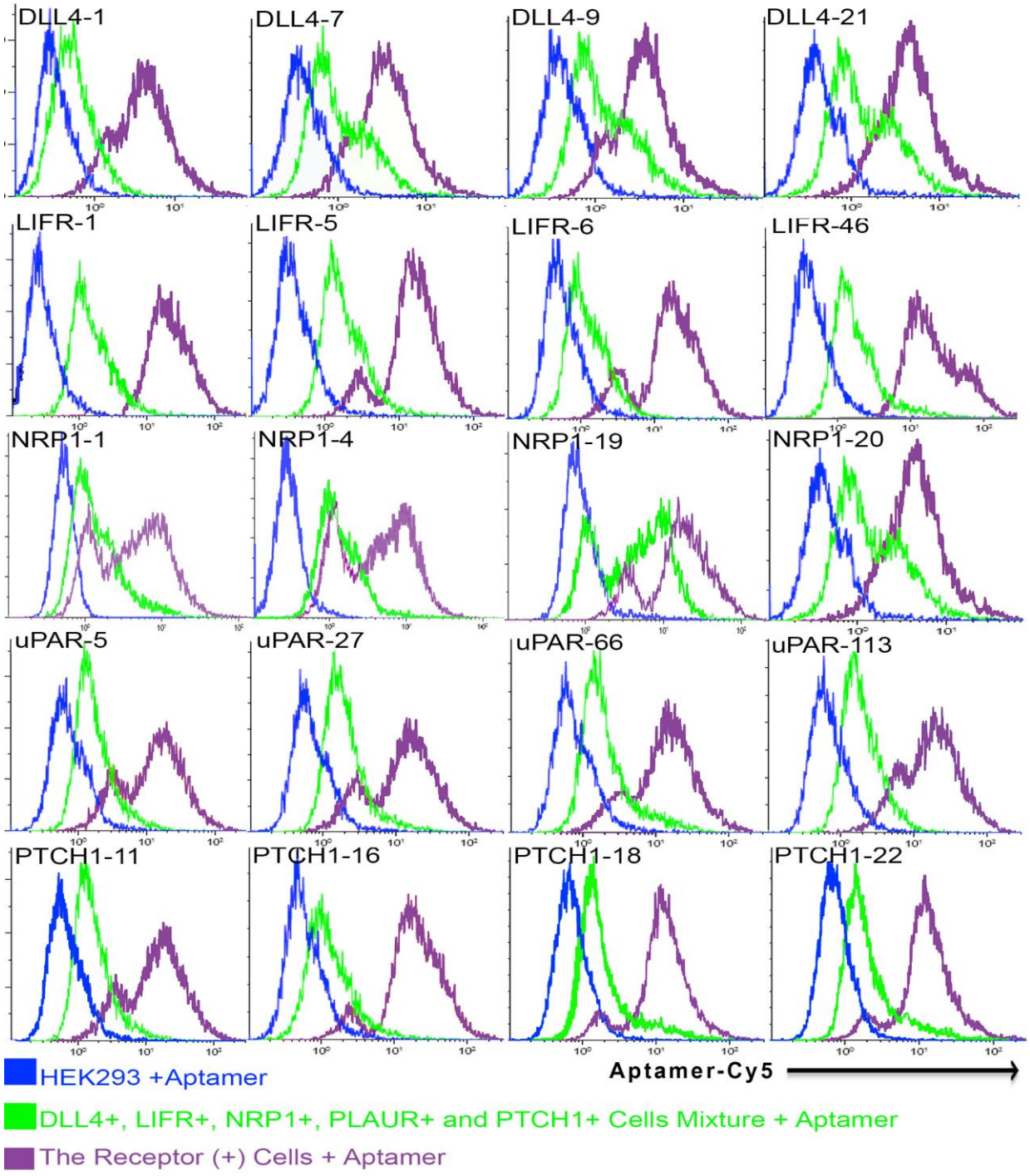

Figure 4.5. Cross-reactivity of aptamer clones to cells. Cy5-labeled aptamer clones (200 nM) were incubated with a mixture of DLL4+, LIFR+, NRP1+, uPAR+, PTCH1+ cells in PBS with Ca^{2+}/ Mg^{2+}. HEK293 cells were used as a negative control, corresponding (+) cells – as a positive control and green represents the the mixture of the five cells.

To study the dosage effect of the aptamers' binding to the target cells and measure the apparent K_d for each clone, the receptor (+) cells were incubated with corresponding aptamer clones at various concentrations in PBS with Ca^{2+}/Mg^{2+} at room temperature for 30 minutes, washed and analyzed using flow cytometry (**Figure 4.6**). The lowest apparent K_d belongs to Aptamer LIFR-1 with 2 nM, and the highest apparent K_d belongs to Aptamer LIFR-46 with 117 nM.

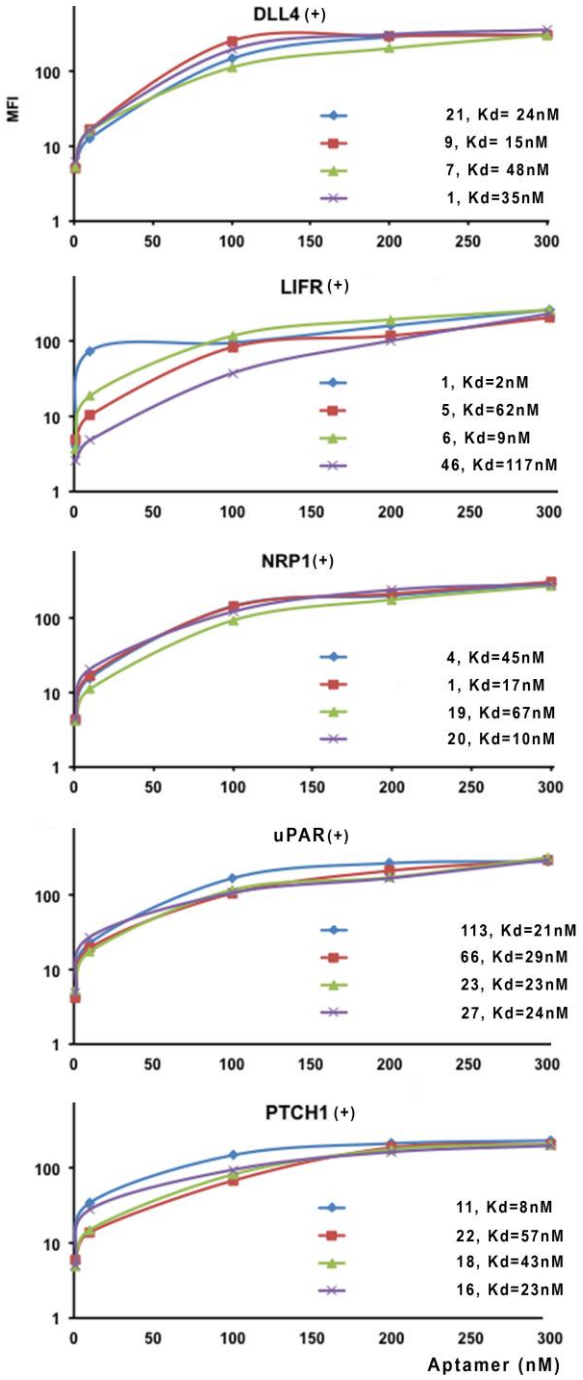

Figure 4.6. Titration curves of aptamer-cell interactions. The (+) cells were incubated with corresponding aptamer clones at various concentrations in PBS with Ca^{2+}/Mg^{2+} at room temperature for 30 minutes, washed and analyzed using flow cytometry to measure the apparent K_d for each clone.

The co-binding of the related antibodies and aptamers to live HEK 293 cells expressing the target receptors was studied with a fluorescent microscope (**Figure 4.7 and 4.8**). As an example, to show the quantity of the aptamers and antibodies co-localization, a particular part of one of the photos (Apt-PTCH1-16 and PTCH1 antibody) were zoomed in **Figure 4.8**.

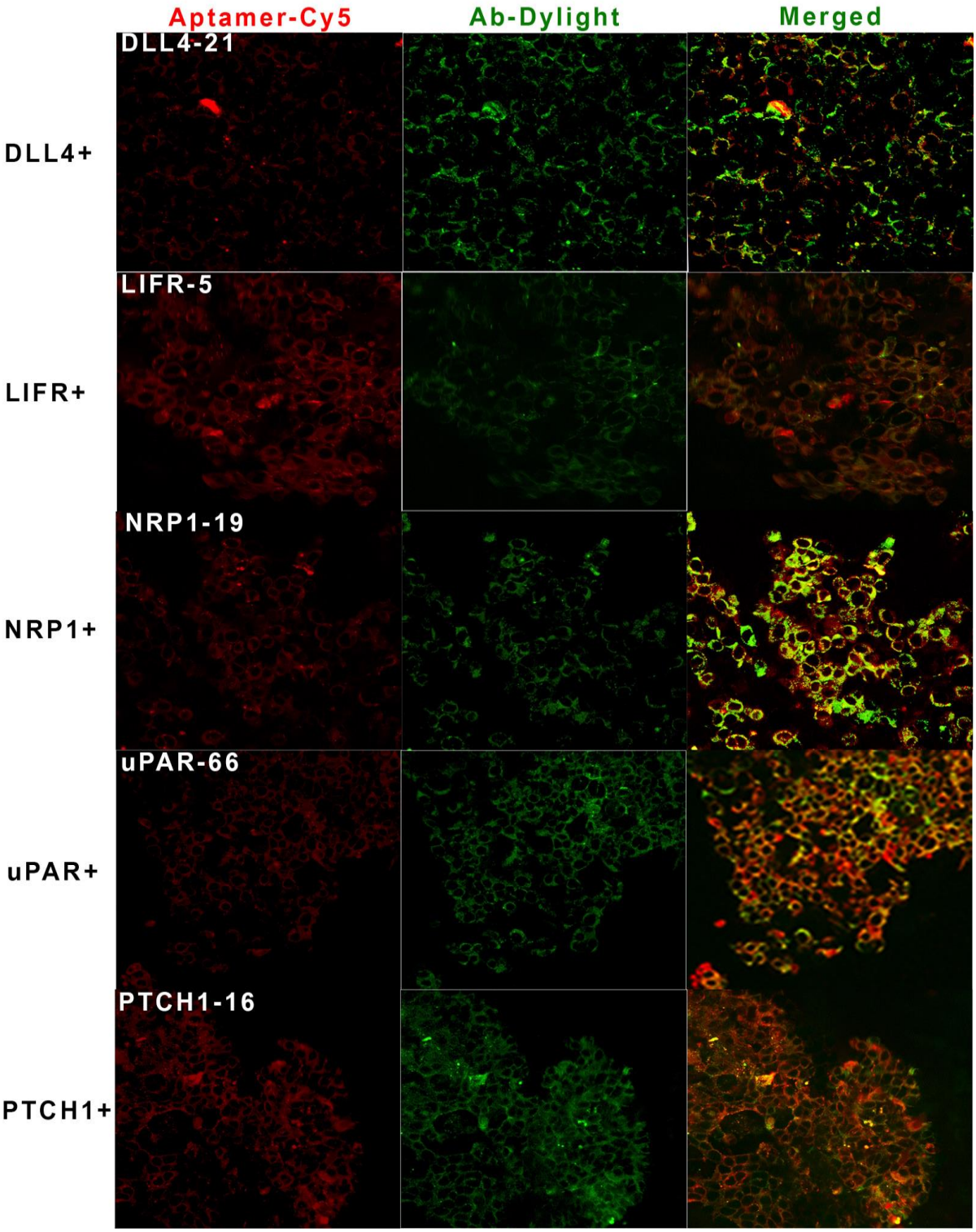

Figure 4.7. Microscopic study of aptamers binding to live cells cells (25X Confocal Microscope). Live cells expressing DLL4, LIFR, NRP1, uPAR, and PTCH1 were incubated with corresponding Cy5 aptamers and with the corresponding antibodies. Photos were captured by Nikon A1RsiMP confocal microscope at 25X magnification.

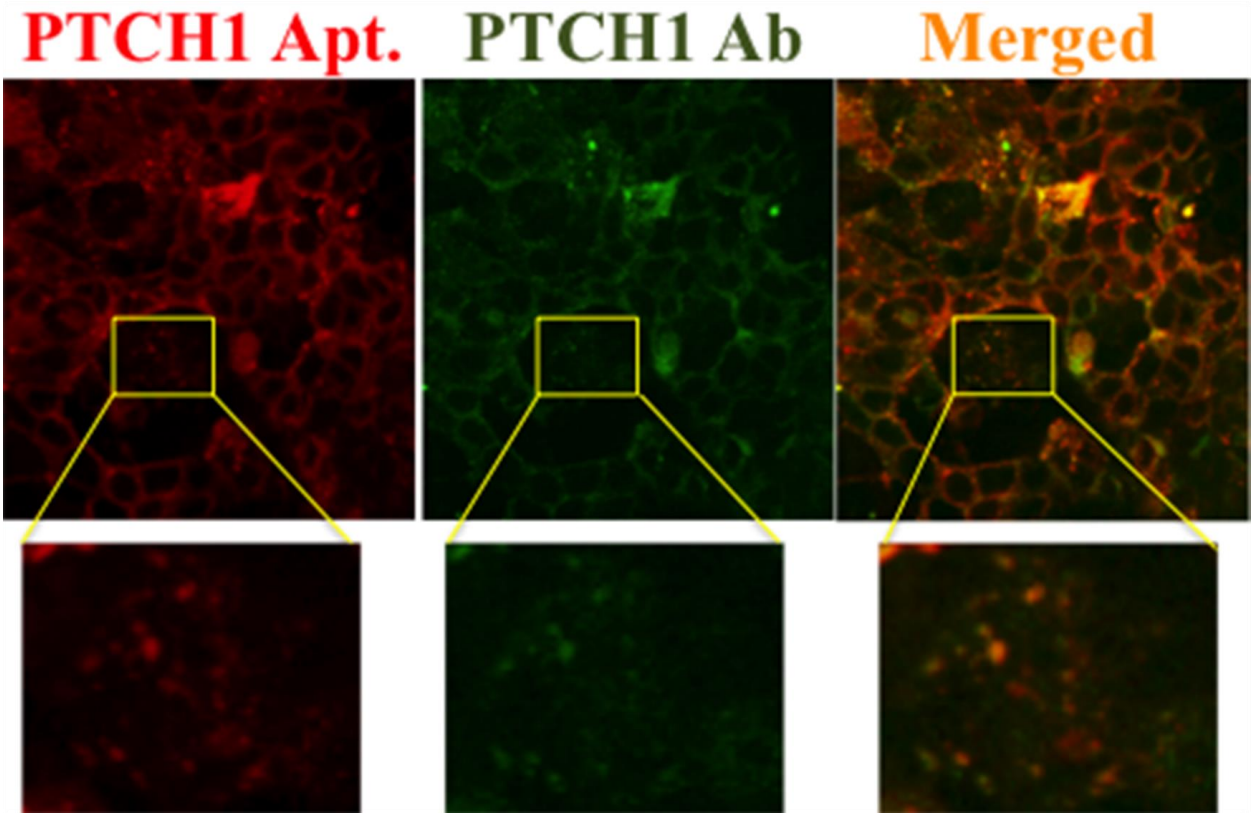

4.8. As an example a zoomed photos of the last photo of Figure 4.7. to evaluate the patern of colocalizaions of the antibody and aptamer. Live cells stained with Cy5 labeled Apt-PTCH1-16, primary antibody against PTCH1 and secondary antibody labeled with dylight 488. Photos were captured by Nikon A1RsiMP confocal microscope at 25X magnification.

To confirm switchable binding of aptamers to (+) cells, we incubated individual aptamers with the cells in PBS buffer containing $Ca^{2+}$and Mg^{2+} for 30 minutes. After washing, the cells were split into two tubes, one containing PBS with Ca^{2+}/Mg^{2+} the other with PBS with 10 mM EDTA; the divided cells were then analyzed by flow cytometry **(Figure 4.9)**.

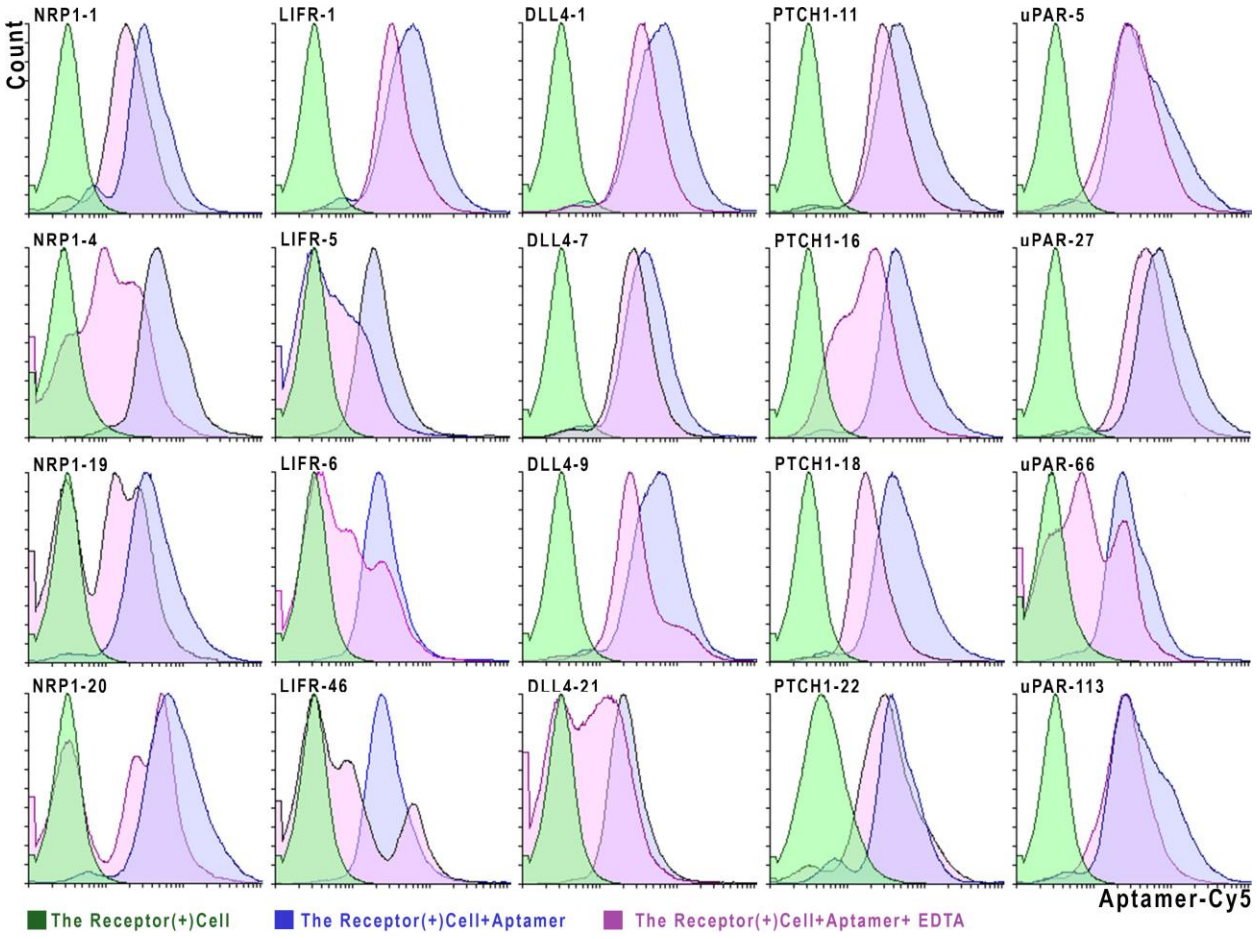

Figure 4.9. The impact of EDTA on aptamer binding. Target (+) cells (green) stained with 200 nM corresponding Cy5-aptamers in PBS with Ca^{2+}/Mg^{2+} and analyzed before (blue) and after (pink) the addition of 10 mM EDTA.

The results demonstrated that the binding of the following aptamer clones: NRP1-19E, LIFR-5E, DLL4-21E, PTCH1-16E and uPAR-66E to the corresponding (+) cells, in the presence of EDTA, was reduced more than other clones and are therefore capable of being utilized in cell separation. In these experiments, we did not wash the cell after addition of EDTA because we were interested in observing the effect of EDTA alone on the aptamers binding' without washing the cells.

Positive cell separation was examined with both HEK293 cell line and mice bone marrow. First, we employed biotinylated switchable aptamers and streptavidin coated magnetic

beads to isolate one type of (+) cells from a mixture of (DLL4+, LIFR+, NRP1+, uPAR+ and PTCH1+) HEK293 cells. The cells before and after separation have been visualized by bright field microscopy (**Figure 4.10**).

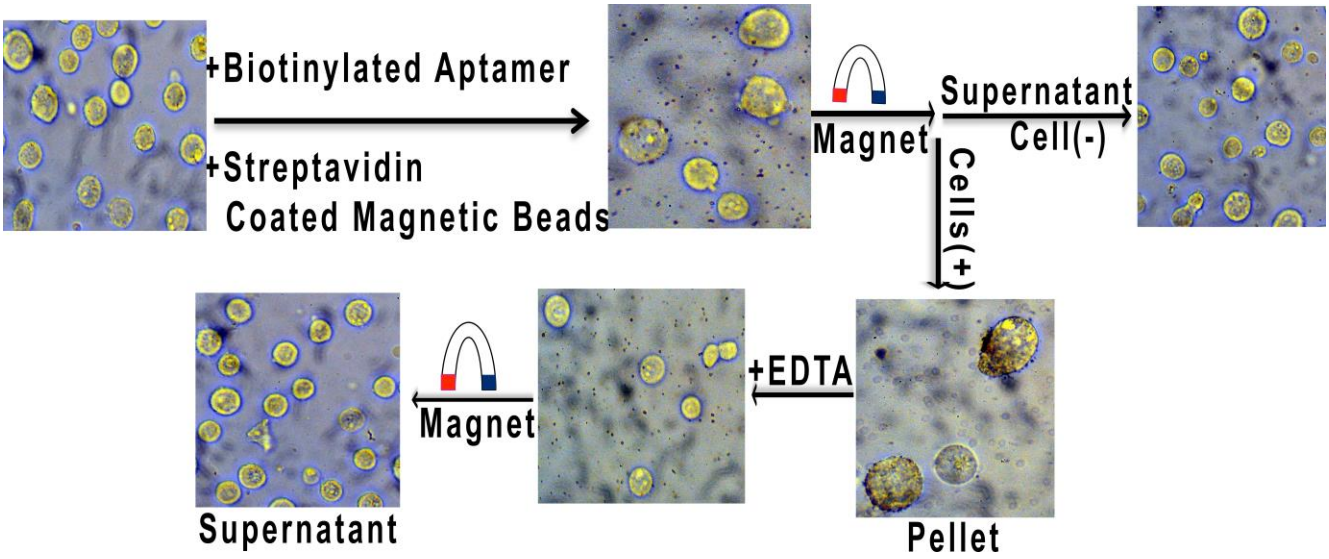

Figure 4.10. Picture of the receptor (+) cell isolation from a mixture of cells using aptamers and streptavidin-coated magnetic beads.

The purity of the captured cells was analyzed by antibody staining using flow cytometry (**Figure 4.11A**). The data demonstrated enriching of the target cells after magnetic bead separation by 2-4 times.

We were interested in determining whether our aptamers could isolate receptor (+) cells from a very heterogeneous population such as bone marrow. Bone marrow cells have been the focus of intense research because of their potential application in regenerative medicine and research [151, 152]. We incubated mice bone marrow cells with switchable aptamers in PBS with Ca^{2+}/Mg^{2+} and streptavidin-coated magnetic beads. The captured cells were washed and released

by adding 10 mM EDTA in PBS. DLL4-21E, LIFR-5E, NRP1-19E, uPAR-66E and PTCH1-16E aptamers respectively isolated 9%, 4%, 3%, 3% and 11% of total bone marrow cells. The cells viabilities after process were over 93%(**Table 4.3)**. Whole and purified mice bone marrow cells were examined using flow cytometry with the use of monoclonal antibodies and Cy5-labeled aptamers against DLL4, LIFR, NRP1, uPAR and PTCH1 (**Figure 4.11B**).

Table 4.3. The percentage of viable cells isolated from mice bone marrow

Sample	Cell Viability %
Total Bone Marrow Cells	100.00
Cells Purified by DLL4-21	99.70
Cells Purified by LIFR-5	98.20
Cells Purified by uPAR -66	86.20
Cells Purified by NRP1-19	98.78
Cells Purified by PTCH1-16	98.77

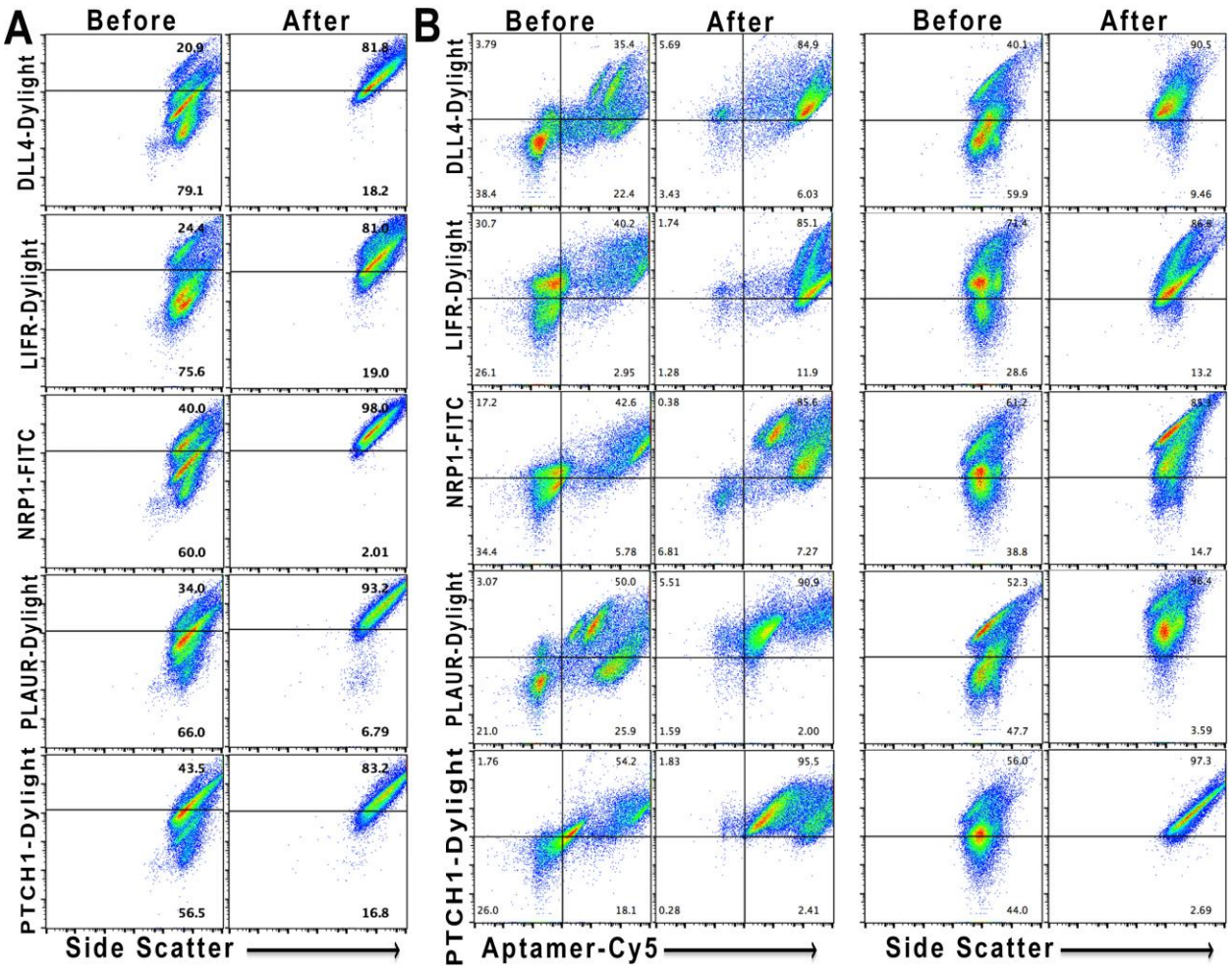

Figure 4.11. Flow cytometric analysis of the cells before and after purifications.**(A)** Flow cytometric analysis of the mixture of the five HEK293 cells expressing DLL4, LIFR, NRP1, uPAR and PTCH1 before and after purification. The mixture of the cells before and after purification by DLL4-21, LIFR-5, uPAR-66, NRP1-19 and PTCH1-1 were incubated with related antibody and followed by flow cytometric analysis. The dot plots compared antibody- Dylight or -FITC vs. side scatter of the same results before and after isolation. **(B) Flow cytometric analysis of mice bone marrow before and after purification.** Mice bone marrow cells before and after purification by DLL4-21, LIFR-5, uPAR-66, NRP1-19, and PTCH1-1 were incubated with the corresponding aptamer-Cy5 and antibody, followed by flow cytometric analysis. The left side is the flow cytometry dot plots comparing antibody- Dylight or -FITC vs. aptamer-cy5 and the right side are the dot plots comparing antibody- Dylight or –FITC vs. side scatter of the same results before and after isolation. Results of the bone marrow separation are presented in **Figure 6.12** and **Table 4.4.**

Table 4.4: The percentage of the ALDH+, CD44+, CD20+, CD11B+, CD52+ and CD45R+ in the purified mice bone marrow cells by the switchable aptamers.

	ALDH+	CD44+	CD24+	CD20+	CD11b+	CD52+	CD45R+
B. M.	0.85	12.7	19.6	29.3	28.8	30.4	28.6
DLL4-21	16	18.1	12.9	21	22.2	16.8	28.4
LIFR-5	19.6	27.9	8.67	41.4	27.6	19	40.7
NRP1-19	11.3	9.54	4.01	10.2	11.1	12.8	19.4
uPAR-66	7.94	22.2	7.99	33.3	16.8	24.8	29.3
PTCH1-16	6.44	27.1	11.8	23.4	14.5	20.1	43.7

The aptamer DLL4-21E enriched cell populations of ALDH+ and CD44+ cells while depleted CD24+, CD20+, CD52+ and CD11b+. LIFR-5E enriched ALDH+, CD44+, CD20+ and CD45R+ cells while depleted CD44+ and CD52+ cells in extracted bone marrow cells. NRP1-19E extracted bone marrow cell has a high population of ALDH+ cells with a low population of the other makers. uPAR-66E captured more ALDH+, CD44+ and CD20+ cells. PTCH1-16E fished out more ALDH+, CD44+, and CD45+ cells.

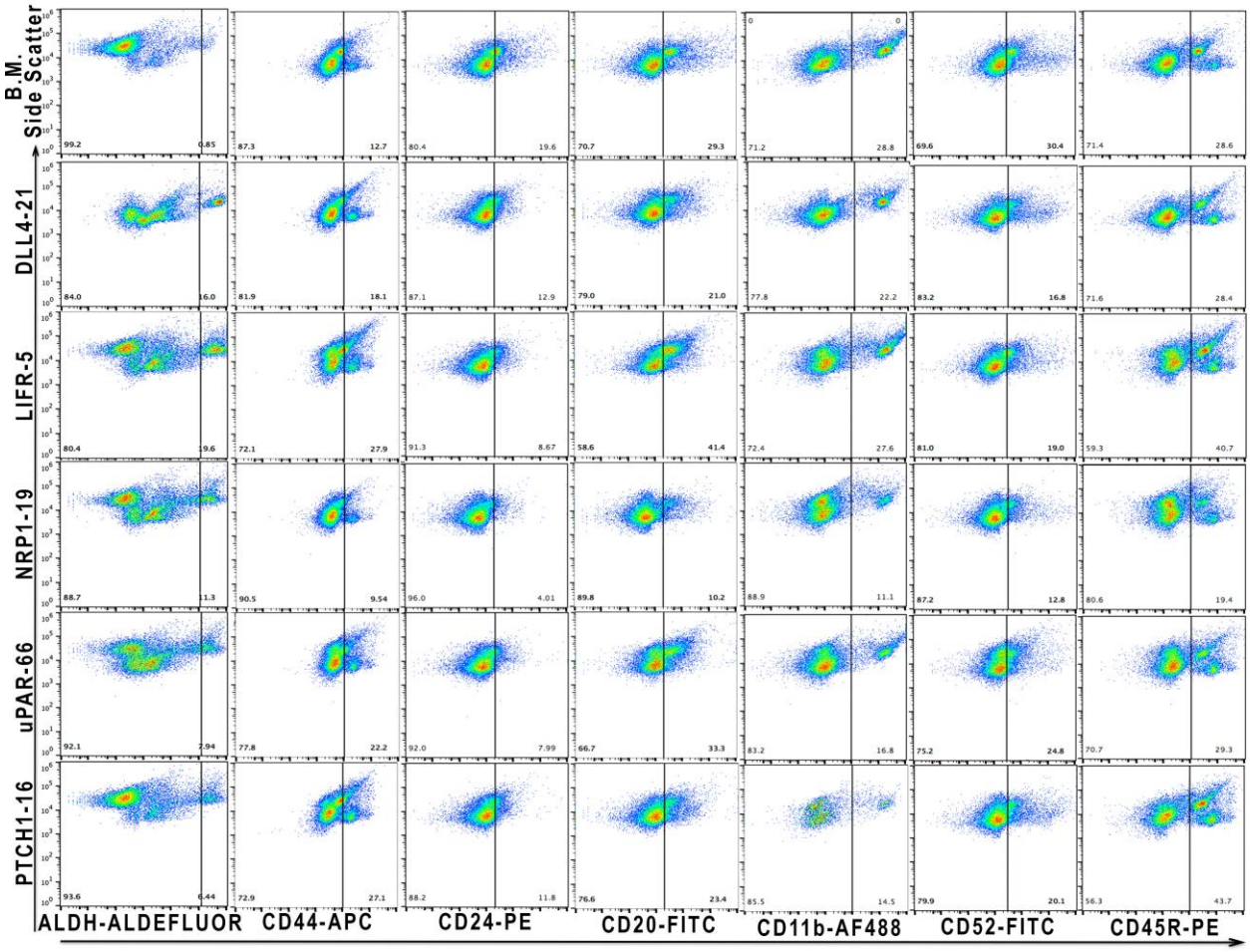

Figure 6.12. Identification of Bone Marrow Whole and Purified Cells. Flow cytometry dot plot analyses of Side Scatter (Y axis) vs. (X-axis) the expression of aldehyde dehydrogenase (ALDH), CD44, CD24, CD20, CD11b, CD52 and CD45R using whole and purified cells by DLL4-21, LIFR-5, NRP1-19, uPAR -66 and PTCH1-16 aptamers.

Moreover, the switchable aptamers allow performing sequential isolation of receptor (+) cells from mice bone marrow (**Figure 4.13**).

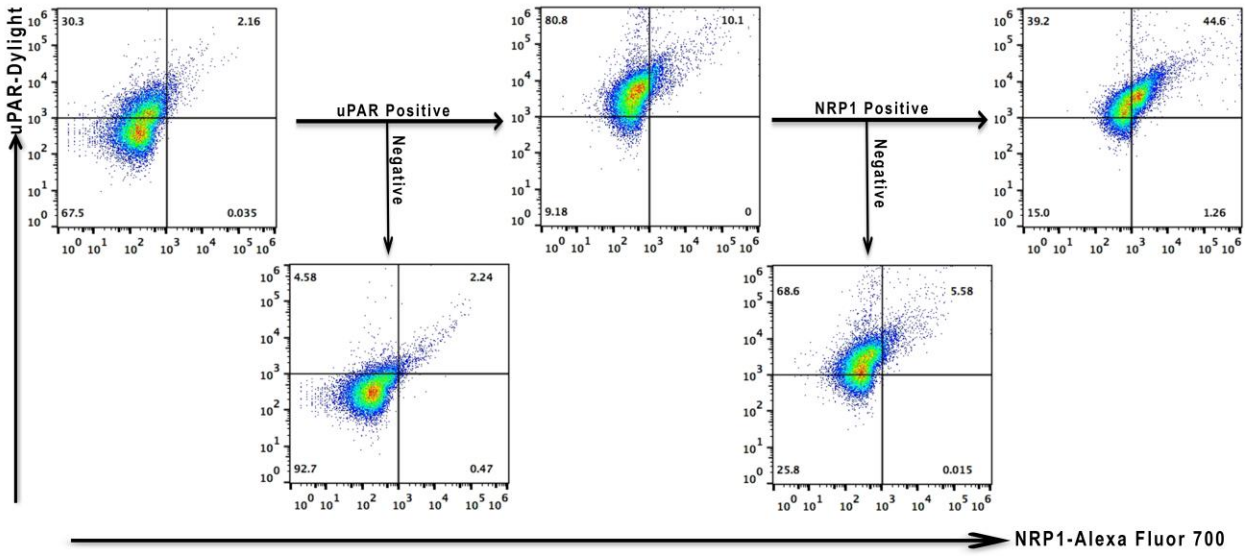

Figure 4.13. Flow cytometric analysis of mice bone marrow during sequential isolation of receptor (+) cells. Two sequential steps of purification had been applied by biotinylated aptamer and streptavidin-coated magnetic beads. Mice bone marrow cells were purified by biotinylated uPAR-66, and the yielded cells had been subjected to purification by NRP1-19. The origin and product cells of each step were incubated with antibodies against uPAR and NRP1, followed by flow cytometric analysis.

4.5. Conclusion

In this study, we present a new class of capture molecules called SwAps aptamers which can be used to isolate specific cells expressing target receptors, LIFR, NRP, DLL4, uPAR or PTCH1 from a mixture of cells and whole bone marrow. Here we applied aptamers in the isolation of specific cells from bone marrow using an aptamer with high specificity. The EDTA switchable aptamers can significantly facilitate the isolation and enrichment or depletion of cells expressing target receptors. The target cells can be separated and purified free of additives. In future, we plan to identify binding partners and their epitopes for aptamers using mass spectrometry analysis.

Chapter 5

Aptamers to detect and sort cells expressing Axl receptor tyrosine kinase

5.1. Objectives

We aimed to generate EDTA switchable aptamers to the cells expressing Axl receptor tyrosine kinase and apply the aptamers in sorting the receptor positive cells from peripheral whole blood leukocytes.

Contributions

Shahrokh M. Ghobadloo and Dr. Maxim V. Berezovski (supervisor) conceived the idea and designed the research. Shahrokh M. Ghobadloo performed experiments. Dr. Gleb G. Mironov performed mass spectrometry analysis.

5.2. Background

Recent discoveries made Axl a significant candidate for diagnosis and target for treatment of various diseases such as cancer,[153] autoimmune,[154] inflammation,[155] viral infections and T-cell disorders[156]. Axl is a member of TAM (Tyro3, Axl, and Mertk) family of receptor tyrosine kinases[157] and involves in cell migration, survival, growth, aggregation and guards cells from apoptosis and inflammation.[157] Axl is an important target for diagnosis and a target for treatment of human diseases such as aggressive cancer and virus infections. The crucial role of Axl in Th cells inflammatory response[158] and survival of T lymphocytes[159] has been recently described. The detection of Axl expressing cells is essential for diagnosis of related disorders. Also, the binding ligand to Axl receptor can trigger cellular responses such as aggressiveness of cancer cells or immune responses of immune cell.[157, 158] This led us to develop aptamers to the Axl receptor and tested them on cells expressing Axl receptor and whole human leukocytes. Moreover, the immune phenotypes of aptamer positive cells were investigated through multicolor fluorescently labeled aptamer probes and antibodies. The results of LC- Orbitrap Fusion Tribrid mass spectrometer revealed Axl tyrosine kinase as the aptamer target protein.

5.3. Materials and methods

Cell lines

The human embryonic kidney (HEK293) cell line was obtained from Clontech Laboratories and cultured in Dulbecco's modified Eagle medium complemented with 10% fetal bovine serum. The transfected cells expressing Axl receptor were inducted with Doxycycline (500 ng/mL) in complete media.

Antibodies

A FITC conjugated antibody against CD3 (Stemcell Technologies, Cat#60011FI.1), PCy7 conjugated antibody against CD4 (Biolegend, Cat#344611), PE-conjugated antibody against Axl receptor (R&D Systems, FAB154P) and primary antibody against Axl receptor (R&D Systems, Cat#MAB6965) were used in this study. Dylight 488 (DI-1488) conjugated antibody against rabbit IgG was obtained from Vector Laboratories.

Construction of Axl gene into the pLVX-TRE3G vector

Bacteria holding plasmid (pDONR223-AXL) with an open reading frame of Axl was obtained from addgene (Cat# 23945)[160]. Bacteria were cultured and the vectors were extracted to make cDNAs of Axl using CloneAmp HiFi PCR Premix (Clontech Laboratories, Inc. Cat. # 639298) and Axl forward primer (ATGGCGTGGCGGTGCCCCA) and reverse primer (TCAGGCACCATC CTCCTGCCCT) with 15 bp extensions homologous to the pLVX-TRE3G vector ends, gccccccgggacgcgt for forward primer and ctacccggtagaattc for reverse primer. We digested pLVX-TRE3G vector with MluI (New England Biolabs, cat# R0198S) and EcoRI

((New England Biolabs, cat# R0101S) restriction enzymes at 37°C for 3 hours to create a linearized vector. The linearized vector was cleaned by 1% Agarose gel and extracted with the GeneJet Extraction Kit (Thermo Scientific, Cat#K0692). Fusion HD Cloning Kits (Clontech Laboratories, Inc. Cat. #639648) were used to clone the PCR products into pLVX-TRE3G.

Transformation

Competent cells (50 μl) were incubated with cloned pLVX-TRE3G reaction mixture (2.5 ng). The mixture was placed on ice for 30 minutes and heat shocked for 45 seconds at 42°C and then moved on ice for an extra 1–2 minute. Then, Super Optimal Broth with Catabolite repression (SOC) medium was added (final volume of 500 μl). The cell mixtures were cultured on agar medium containing ampicillin (100 μg/ml).

Lentivirus production and transduction

A lenti-X^{TM} Tet-On 3G Inducible Expression System was employed (Clontech, Cat#631187) for lentiviral construction. Axl was sub-cloned into the pLVX-TRE3G vector operating the In-Fusion HD (Clontech, Cat# 638909). Lentiviruses were produced by transfecting 293T cells and pLVX-TRE3G- Axl using the Lenti-X HTX Packaging System (Clontech, Cat#631187). Virus particles were collected 48 hours after transfection. HEK293 cells were infected with the pLVX-Tet3G and selected with G418 (Clontech; Cat#631307) (1 mg/mL). A 10 cm plate of the selected cells was infected with the pLVX-TRE3G-Axl viruses and selected with puromycin (Clontech; Cat#631305) (25 μg/mL). Doxycycline (Clontech) was added to the cultures at 500 ng/mL to induce Axl expression.

Immunofluorescence staining

Cells were fixed with 4% paraformaldehyde and permeated with 0.25% Triton X-100 (Sigma, St. Louis, MO). The cells were blocked with 10% fetal bovine serum (Gibco, CA) and incubated with primary antibody against Axl at room temperature for 1 hour. The cells were then incubated with Dylight 488-conjugated secondary antibodies for 1 hour. After washes, cells were counterstained with 4′,6′-diamidino-2-phenylindole (DAPI; Sigma), and studied under a fluorescence microscope or confocal microscope (Nikon).

Validation of Axl receptor expression: Flow cytometric study

To study Axl receptor expression non-transfected, transfected and induced cells were prepared into single-cell suspensions and incubated with antibody against Axl. The samples were analyzed on a Beckman Coulter FC500 flow cytometer.

Oligonucleotides

We applied a single-stranded DNA library with 100 base lengths including a 60 variable internal region flanked by two 20 mer PCR primer sequences which designed from Liu's laboratory at Harvard University[136]; the library was made with 5′ CTCCTCTGACTGTAACCACG787878786666787878787866678787878786666787878786678787878 GCATAGGTAGTCCAGAAGCC3′ where 6 is a combination that makes 1 : 1 : 1 : 1 A/C/G/T, 7 is a combination that makes 45 : 5 : 45 : 5 A/C/G/T, and 8 is a combination that makes 5 : 45 : 5 : 45 A/C/G/T. All oligonucleotides were obtained from IDT DNA Technologies, USA.

DNA aptamer selection

The single-stranded DNA library which was applied to SELEX was 100 base length including a 60 variable internal region flanked by two 20-nt PCR primer sequences which was designed in Liu's laboratory at Harvard University[136]; the library was described in the previous section, Oligonucleotides.

The ssDNA library was denatured at 95°C for 10 minutes and snap cooled on ice. ssDNA library was incubated with the cells expressing Axl receptor to allow ssDNAs to bind to Axl-positive cells for 1 hour at 37°C. Next, the cells were washed with PBS with Ca^{2+}/Mg^{2+} and spun down at 200 g by centrifuge to remove the supernatant holding unbound ssDNAs. The ssDNAs bound to the cell surface was gathered by heating at 95°C for 5 minutes. The gathered ssDNA was incubated with non-transfected HEK293T cells for negative selection to eliminate non-specific ssDNA (1 hour at 37°C). ssDNA in the supernatant was retained. Positive selection was followed by one round of negative selection for ten rounds. ssDNAs were gathered after each selection and amplified by PCR (twenty-five cycles) for the following round using Thermo Scientific Phire Hot Start II DNA Polymerase (Thermo Scientific). The PCR tube had mixture of ssDNA template, 50 μL of the PCR reaction mixture with 1x Phire Reaction Buffer, 3% Dimethyl sulfoxide (DMSO), 200 μM dNTPs, 1 μL of the Phire Hot Start II DNA Polymerase (Thermo Scientific), 0.5 μM of 5'-Cy5-conjugated forward primer and 0.5 μM 5´-phosphorylated reverse primer. The following program was applied to the thermal cycler: melting at 95°C for 30 seconds, annealing at 58°C for 15 seconds, and extending at 72°C for 10 seconds. To digest the 5´-phosphorylated reverse strand and produce ssDNA, Lambda Exonuclease (New England Biolabs, Cat#M0262S) was used, according to manufacturer protocol. Aptamer selections enriched sequences that possess significant binding.

Whole blood leukocyte

Whole blood of healthy human was used to isolate leukocyte by Lymphoprep (Stemcell Technologies; Cat# 07801) gradient centrifugation to remove erythrocytes.

Next-generation sequencing and phylogenetic tree analysis

Best binder pools were amplified by PCR using barcode primers and purified using 4% agarose gel (Invitrogen) and the GeneJET Gel Extraction Kit (Thermo Scientific, Canada, Cat# K0691). All products were pooled in equimolar amounts (each 200 ng) and sequenced by Eurofins MWG Operon LLC, a Eurofins Genomics company, for two times read of an Illumina MiSeq paired-end for 150 bases. We got a total number of 20 million reads (forward read and reverse read) by Illumina sequencing. The documents, in fastq files, were uploaded on the Galaxy project platform (https://usegalaxy.org) and transformed to FASTA[150]. Then data in FASTA format was parted and organized considering to their barcodes. The FASTA data was collapsed and grouped based on their common motifs. The most abundant sequences in each group were studied using MEME (http://meme.nbcr.net/meme/) and a phylogenetic tree was analyzed running Clustal Omega (http://www.ebi.ac.uk/Tools/msa/clustalo/). The evaluated sequences were categorized into four groups based on shared motif and one sequence from each cluster sent to synthesize IDT by DNA Technologies, USA.

Flow cytometric assay of the aptamer binding affinity

To quantify EC_{50} of Axl aptamer (50% of the aptamers bound to cells), HEK293 cells expressing Axl was incubated with the Cy5 labeled Apt (Aptamer)-Axl-1615 (0, 50, 100, 200

and 400 nM). After washes, they were analyzed by flow cytometry, Beckman Coulter Gallios Flow Cytometer. Kaluza analysis software was used to analyze the data. Following deducting the mean fluorescence values of the control sample, the mean fluorescence intensity were used to measure the EC_{50}.

Biomarker Purification

The whole blood leukocyte cells were lysed via hypotonic buffer on ice (4°C) for 30 min[161]. The hypotonic buffer was 50 mM Tris-HCl (pH 7.5) with Halt Protease Inhibitor (Thermo Scientific, Cat#78430]. Following three washes with hypotonic buffer, cells were incubated with 1 mL PBS with Ca^{2+}/Mg^{2+} including 1% Triton X-100 on ice for 30 min. The 25G needle facilitated the lysing. They were centrifuged at 17,000 g for 5 minutes at 4°C. The supernatant was incubated with yeast RNA (1mg/mL) followed by incubation with 5' biotin conjugated Apt-Axl-1615 (150 pmol). Another sample was incubated with 5' biotin conjugated ssDNA library as a control on ice for 30 minutes. The subsequent complexes of protein-ssDNAs were incubated with streptavidin-coated magnetic beads (2 mg) on ice for 15 minutes and harvested on a magnet holder. After four washes with (1 mL of PBS containing with Ca^{2+}/Mg^{2+}), EDTA (20 mM) was added to elute proteins in 30 µL of water. Using a magnet holder, the subsequent supernatant was collected.

Proteins identification

The proteins were run on 12% sodium dodecyl sulfate-polyacrylamide gel electrophoresis (SDS-PAGE) and stained with QC Colloidal Coomassie Stain (161-0803). The Apt-Axl-1615 captured-protein bands were cut and digested *in situ* by Pierce Trypsin Protease, MS Grade

(Thermo Scientific, Cat#90057) based on the manufacturer's protocol. The digested peptides were cleaned using a pipet tip packed with Pierce C18 (Thermo Scientific, Cat# 87782). Peptides were collected with 10 μL of 50% methanol/1% formic acid and studied by Thermo Scientific™ Orbitrap Fusion™ Tribrid™ mass spectrometer.

5.4. Results and Discussion

Axl receptor transfection

For selecting aptamers to receptor Axl, we planned a cell-SELEX approach[147] as an *in vitro* evolution process of affinity ligands, which needs Axl receptor positive cells and Axl receptor negative cells. The generated aptamers by cell-SELEX can recognize the receptor in its natural folding in its native conditions.[147-149] The Axl receptor positive cells were made by transduction of human embryonic kidney (HEK293) operating lentiviral gene transfer system. Axl receptor expression was induced on the transfected cells via adding Doxycycline. The expression of Axl receptor on the cell membrane was validated by immunofluorescence and flow cytometry analysis (**Figure 5.1**).

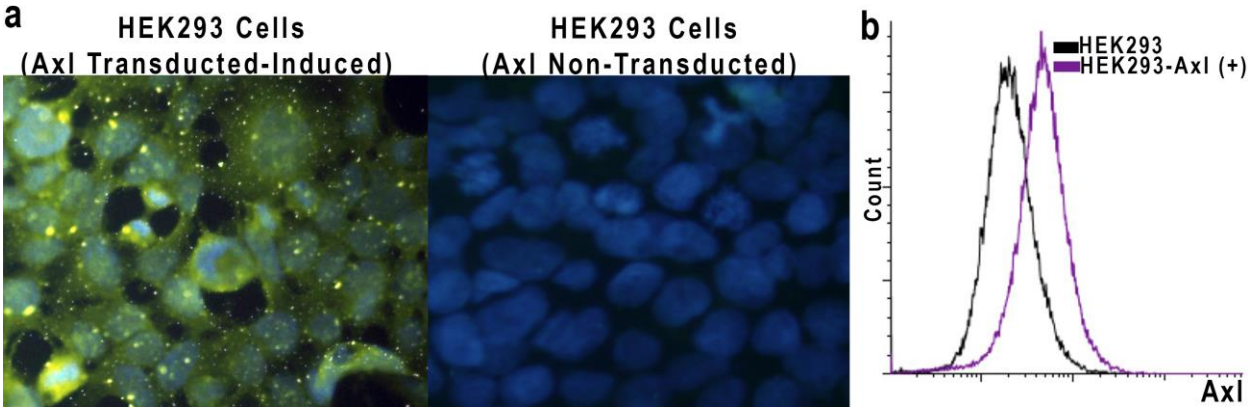

Figure 5.1. Immunofluorescences (a) and flow cytometric (b) test of Axl receptor expression. (a) The immunofluorescences of transfected HEK293 cells with and without induction by doxycycline. The fixed cells after incubation with primary antibody against Axl and two washes were incubated with dylight 488 conjugated secondary antibody. DAPI was used to stain DNA. Photos were captured by Nikon A1RsiMP confocal microscope at 25X magnification. (b) Flow cytometric study of expressing Axl receptor on transfected HEK293 cells after induction (purple) to expressing Axl receptor and without induction.

Axl receptor aptamer selection

The receptor positive and negative cells were used in ten rounds of cell-SELEX. Cy5 conjugated single strand DNA (ssDNA) pool product of each cycle was evaluated for specific binding to Axl receptor positive cell by flow cytometric examination. The evolved aptamer pools displayed stronger binding to the cells expressing Axl receptors compared to ssDNA library **(Figure 5.2)**.

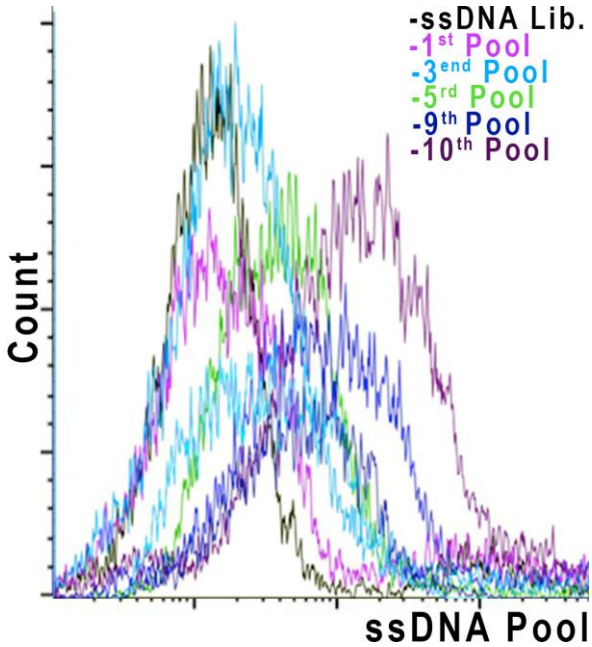

Figure 5.2. ssDNA pools binding to Axl receptor expressing cells. The bindings of Cy5 conjugated ssDNA pool of each round of selection and ssDNA library (initiated ssDNA) to the transfected HEK293 cell expressing Axl receptor were investigated using flow cytometry.

As shown in **Figure 5.2**, the aptamer pools of the 9th and 10th round had the highest binding. These pools were barcoded and after purification were submitted to next generation sequencing (NGS) for the two times read 150bp MiSeq. The results in fastq format were organized, filtered, clustered, and analyzed for the phylogenetic tree and common motifs using the Galaxy software. The analyzing processes resulted in four groups based on their common motifs. The most abundant sequence from each cluster is presented in **Table 5.1**. **Figure 5.3** presents the sequence alignment of aptamers against Axl. The secondary structure of oligonucleotides was assessed based on their sequences free energy minimization[162] using RNAstructure web server **(Figure 5.4)**.

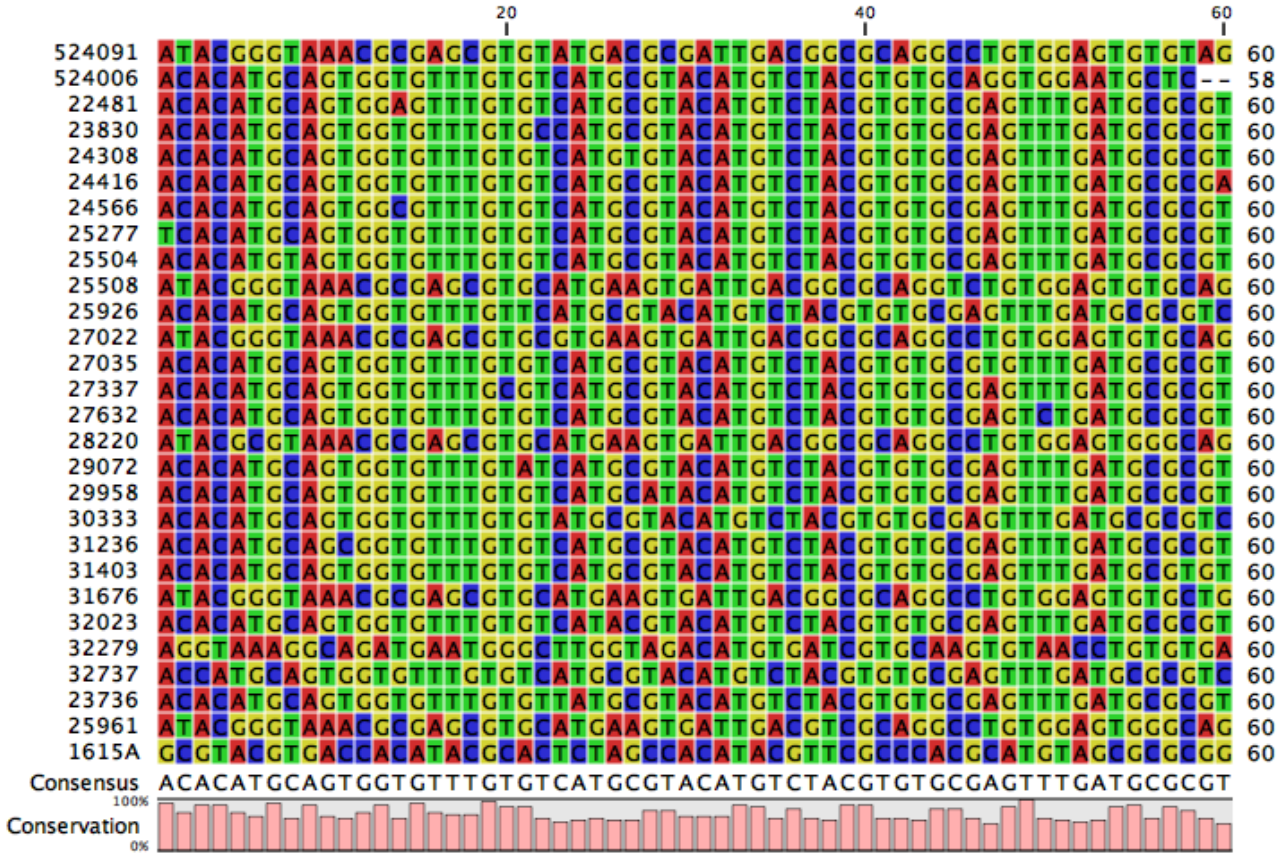

Figure 5.3. Sequence alignment of the selected aptamers against Axl.

Table 5.1. Axl aptamers sequences.

Aptamer	Sequence
Apt-Axl-1615	CTCCTCTGACTGTAACCACGGCGTACGTGACCACATACGCACTCTAGCCA
	CATACGTTCGCCCACGCATGTAGCGCGCGGGCATAGGTAGTCCAGAAGCC
Apt-Axl-25926	CTCCTCTGACTGTAACCACGACACATGCAGTGGTGTTTGTTCATGCGTAC
	ATGTCTACGTGTGCGAGTTTGATGCGCGTCGCATAGGTAGTCCAGAAGCC
Apt-Axl-22481	CTCCTCTGACTGTAACCACGACACATGCAGTGGAGTTTGTGTCATGCGTA
	CATGTCTACGTGTGCGAGTTTGATGCGCGTGCATAGGTAGTCCAGAAGCC
Apt-Axl-25504	CTCCTCTGACTGTAACCACGACACATGTAGTGGTGTTTGTGTCATGCGTA
	CATGTCTACGTGTGCGAGTTTGATGCGCGTGCATAGGTAGTCCAGAAGCC

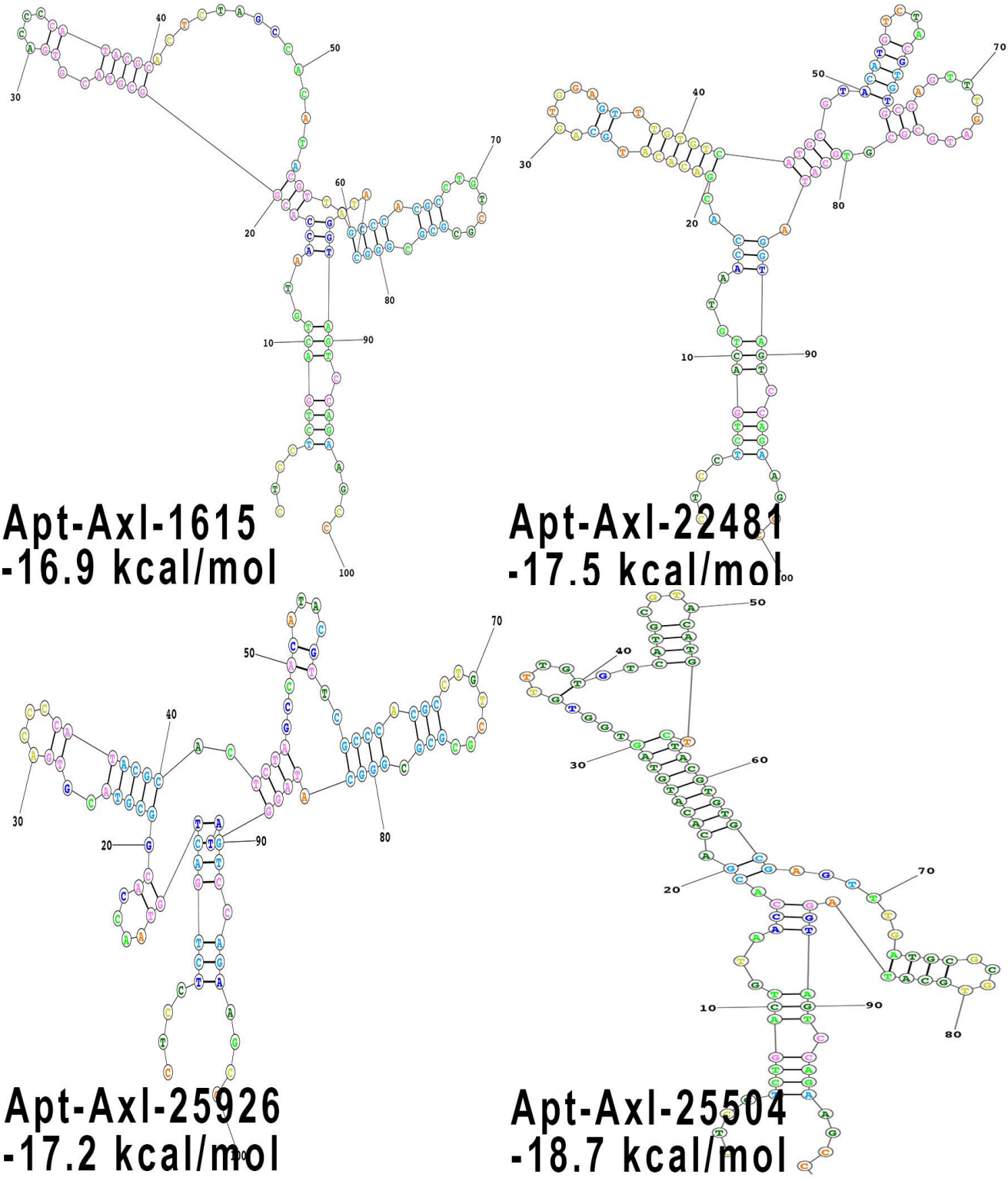

Figure 5.4. Secondary aptamers structure and minimum free energy (kcal/mol). Aptamers structure and minimum free energy were assessed through RNAstructure web software[162].

Aptamers Binding to Axl

The four Cy5-conjugated aptamers were synthesized for binding assessment. A flow cytometric approach assessed the binding of each aptamer to Axl receptor positive and negative cells compared to ssDNA library. Apt-Axl-1615 provided the highest specific binding (**Figure 5.5**).

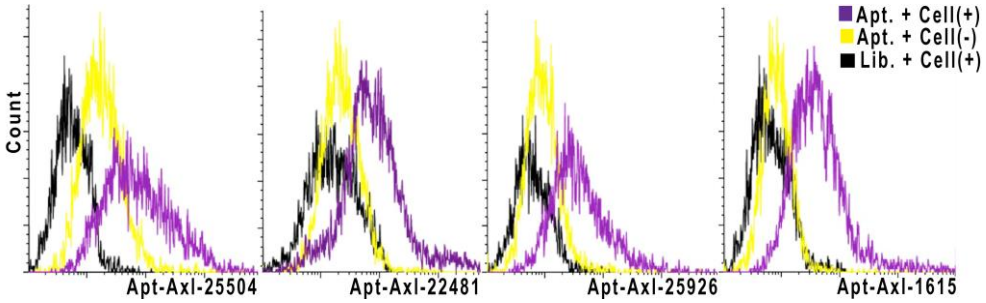

Figure 5.5. Specific binding of the Axl aptamers labeled with fluorochrome Cy5 at its 5' –end. Aptamers and the initial ssDNA library was conjugated with Cy5 fluorochrome and applied to evaluate their cell binding to cultured HEK293 cells and HEK cells expressing Axl (after induction of transfected cells) by flow cytometry analysis. Black represents Axl-positive cells stained with the ssDNA library; yellow represent Axl negative cells stained with the indicated aptamers and purple represents Axl-positive cells stained with the indicated aptamers.

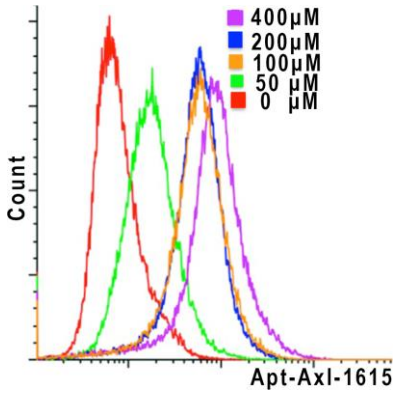

Figure 5.6. Flow cytometric analysis of the titration of Apt-Axl-1615 and Axl positive cell interactions. The Axl receptor-expressing cells were incubated with Cy5 conjugated Apt-Axl-1615 at different concentrations in PBS (with Ca^{2+}/Mg^{2}) at room temperature for 30 minutes, washed and analyzed by flow cytometry to measure the apparent Kd for each clone.

Fluorescence microscopy was used to further investigate the binding of Apt-Axl-1615. Ries, J. et al. demonstrated that small probes facilitate high-resolution microscopic imaging since small probes make the closest possible distance between fluorophores and epitope.[163] Aptamers as small probes can be ideal for this microscopic imaging purposes. We tested Cy5-conjugated Apt-Axl-1615 along with anti-Axl antibody on live cells expressing the receptor (**Figure 5.7**). Adding Apt-Axl-1615 to the medium resulted in specific live cell labeling.

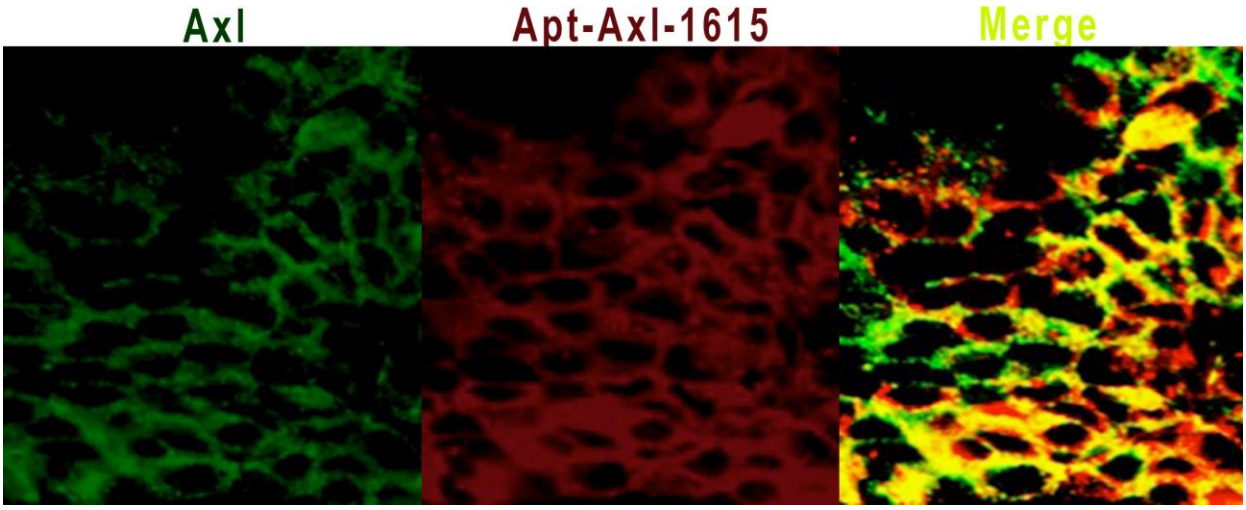

Figure 5.7. Microscopic studies of aptamers binding to live cells. Live cells expressing Axl receptor were incubated with Cy5-conjugated Apt-Axl-1516 and antibody against Axl. The secondary antibody against the primary antibody was conjugated by dylight 488; aptamers and antibodies present similar profiles. Photos were captured by Nikon A1RsiMP confocal microscope at 25X magnification.

Sorting Apt-Axl-1615 target cells from blood cells by FACS

To validate Apt-Axl-1615 target cell populations in biologic heterogeneous tissue, we sorted Apt-Axl-1615 positive cells from whole blood leukocyte using Fluorescence Activated Cell Sorting (FACS). Whole blood leukocytes were incubated with the Cy5-labeled aptamers

(Apt-Axl-1615) in PBS with Ca^{2+}/Mg^{2+}. After washing, the aptamer positive cells were gated and sorted using FACS. The sorted cells were stained by anti-Axl antibody then analyzed using a flow cytometric approach (**Figure 5.8**). Cy5-conjugated Apt-Axl-1615 bound 11.3% of human whole blood leukocytes. 98.6% of the sorted cells were aptamer positive; 1.4% of the sorted cells could release the bound aptamers during or after sorting. Antibody staining against Axl presented 93.8% of the sorted cells double positive for the aptamer and antibody. 4% aptamer negative population can be because of losing the bound aptamers during sorting, incubating and washing the cells. 2.2% of the sorted cells were antibody negative, which can be because of non-specific binding of the aptamer.

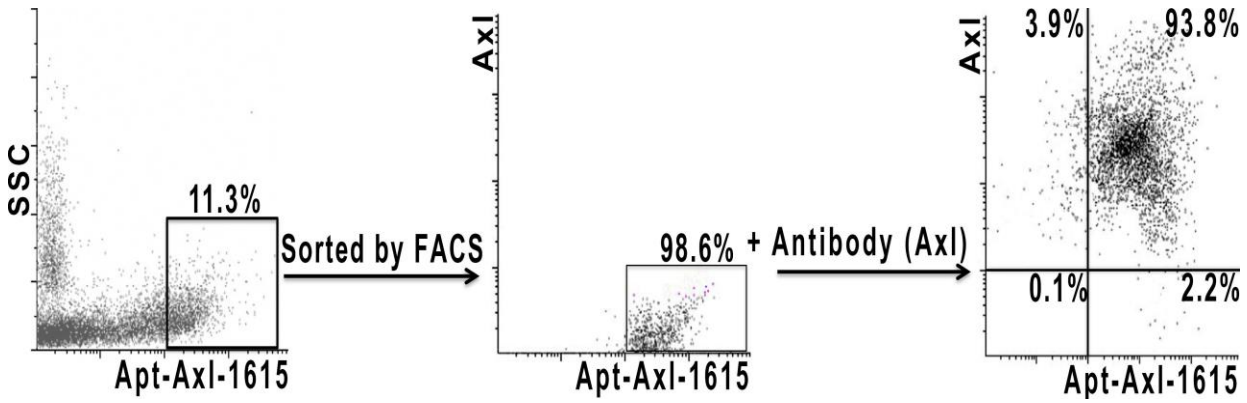

Figure 5.8. FACS cell sorting assay of Apt-Axl-1615 positive cells in whole blood leukocyte. Cy5-conjugated Apt-Axl-1615 positive cells were gated inside scattering vs. Apt-Axl-1615 and applied to sort by FACS. The sorted cells were stained with PE-conjugated antibody against Axl receptor for flow cytometry.

Identification of Apt-Axl-1615 target cells in whole blood leukocyte

We further investigated Apt-Axl-1615 target cells in human whole blood leukocyte by multicolor staining with antibodies against CD3, CD4, and Axl (**Figure 5.9**). As **Figure 5.9** demonstrates, a PE-conjugated antibody against Axl and Cy5-conjugated Apt-Axl-1615 co-

stained 12% of the whole blood leukocytes. The Axl receptor-positive population (12% of whole blood leukocytes) binds to 78% of CD3+CD4+, 16% of CD3+CD4-, 4% of CD3-CD4- and 2% of CD3+CD4-. Whole blood leukocytes also were investigated using flow cytometry with monoclonal antibodies against Axl receptor, CD3, and CD4. In this study, we present DNA aptamers that can be used to detect, bind and isolate Axl-expressing cells in whole blood leukocytes.

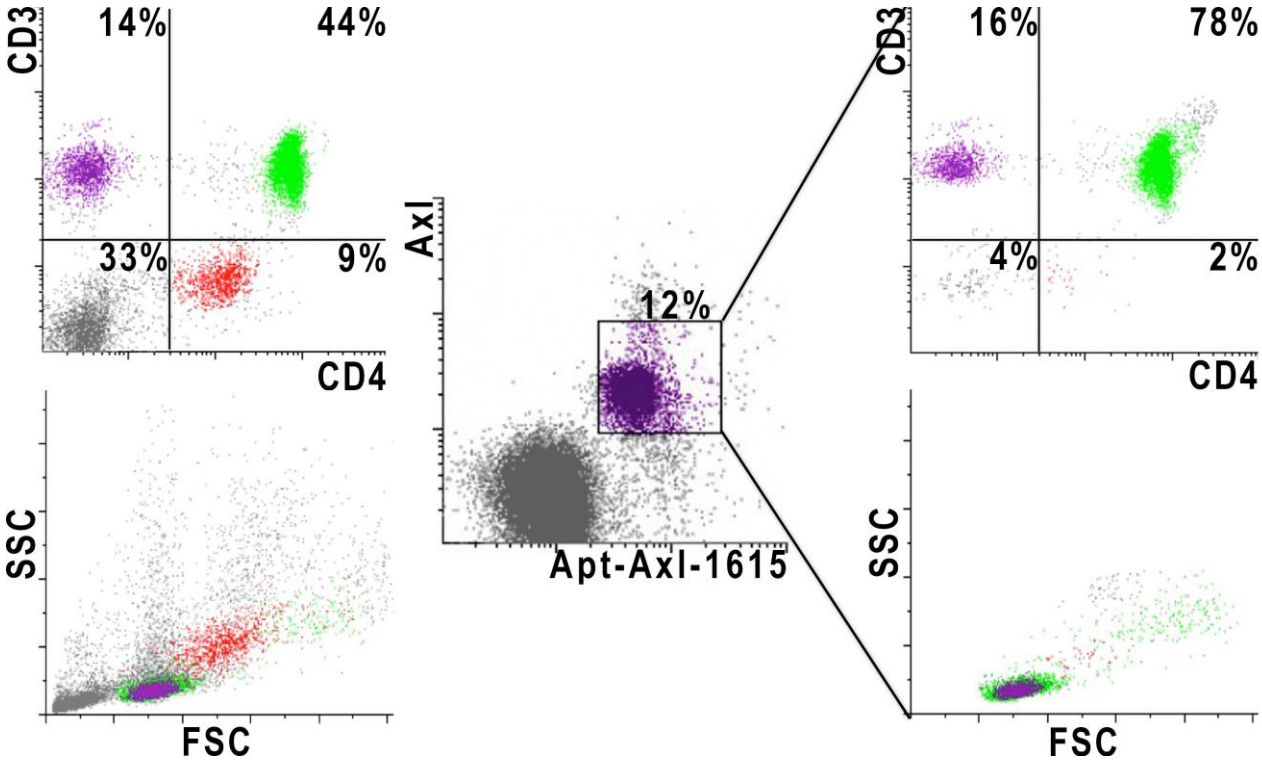

Figure 5.9. Identification of Apt-Axl-1615 positive cells in human whole blood leukocytes. To assess the content of aptamer positive cells, flow cytometric dot plot of Side Scatter (Y axis) vs. Forward Scatter (X-axis) were used to present distinct red blood cells, debris, lymphocytes, and granulocytes. The majority of the cells in the gate of aptamer and Axl antibody positive cell populations appeared in CD3+CD4- (16%) and CD3+CD4+ (78%) cell populations.

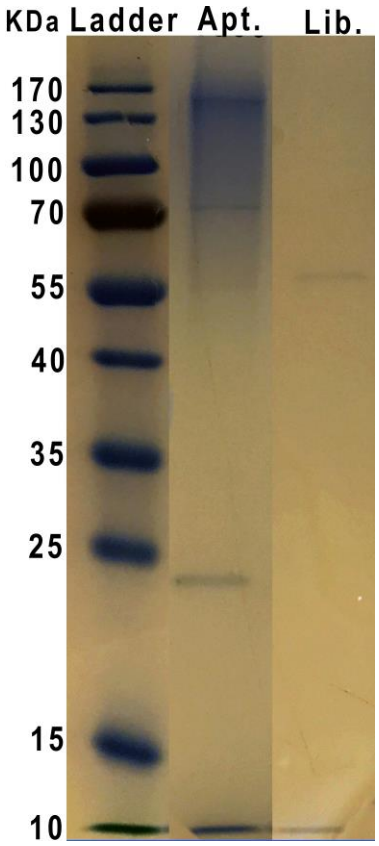

Figure 5.10. SDS-PAGE of the isolated proteins from whole blood leukocyte membrane proteins using biotinylated Apt-Axl-1615 and streptavidin-coated magnetic beads. Lane 1 is the protein marker (10–170 kDa); lane 2 is Apt-Axl-1615 bound target proteins; lane 3 is ssDNA library bound target proteins.

Apt-Axl-1615 target molecule

We used biotinylated Apt-Axl-1615 to isolate its target molecules for mass spectrometry analysis. The membrane proteins of lysed whole human blood leukocytes extracted in PBS (with Ca^{2+}/Mg^{2+}) buffer. After incubation of 5′-biotinylated Apt-9 with the leukocyte membrane proteins, streptavidin-coated magnetic beads were applied to isolate Apt-Axl-1615 and its bound targets. They were washed with PBS (with Ca^{2+}/Mg^{2+}) buffer. The targets bound to streptavidin-coated aptamers were collected after heating at 95°C for 5 minutes. The eluted target proteins were run on 12% SDS-PAGE after heating in the loading buffer. Captured Apt-Axl-1615 bands on the gel were cut for in-gel digestion by trypsin for investigation using nanoLC-Thermo

Scientific Orbitrap Fusion Tribrid mass spectrometer. Axl as a main target and fibronectin type III with Ig-like as co-binder are identified. Axl is a transmembrane receptor of molecular mass 100 to 140 kDa with an extracellular, N-terminal, and an intracellular, C-terminal tyrosine kinase domain.[157] As shown in **Figure 5.8**, approximately 94% of the aptamer positive cells in whole blood leukocytes are identified as Axl membrane protein positive cells by the antibody. The aptamer positive cells in whole blood leukocyte were sorted by FACS followed by staining and analysis by flow cytometry.

5.5. Conclusion

This study presented an Axl DNA aptamer with similar specificity and sensitivity to Axl antibodies. Our results suggested that the Axl-specific aptamer could replace the antibody against Axl in immunofluorescence, flow cytometric and cell sorting studies. Also, multicolor staining of whole human blood leukocytes shows that the Axl aptamer can be used together with antibodies in multi-parameter flow cytometry and immunofluorescences analyses. The generated aptamer isolated Axl receptor expressing cells from a very heterogeneous population such as whole blood leukocyte. Blood is the main focus of study for diagnosis and therapy. The Apt-Axl-1615 was used in combination with antibodies for multicolor cell phenotyping analysis in human peripheral whole blood leukocytes. It will be fascinating to explore the use of Axl aptamer in diagnosis of Axl-associated diseases.

Chapter 6

Aptamer technology discovered CD107a in response to PD-1 expression

6.1. Objectives

Our object at the beginning was to select EDTA switchable aptamers to the cells expressing programmed cell death protein 1 (PD-1). However, we achieved to generate an aptamer to the cells expressing PD-1 but the molecular target of the aptamer was determined CD107a on HEK293 cells membrane as a result of PD-1 expression.

Contributions

Shahrokh M. Ghobadloo and Dr. Maxim V. Berezovski (supervisor) conceived the idea and designed the research. Shahrokh M. Ghobadloo performed all the experiments. Dr. Gleb G. Mironov performed the mass spectrometry experiments.

6.2. Background

In this study, we engaged Cell-SELEX method to distinguish the proteins present on the membrane of human embryonic kidney (HEK293) cells as a result of programmed cell death protein 1 (PD-1) expression. PD-1 has important roles in cancer, immune evasion, and viral infection.[164-167] T cells, natural killer cells, B cells, monocytes, and dendritic cells express PD-1 after activation.[167] PD-1 has an influence on transcription factors involved in cell function such as cell survival signals and differentiation.[167] It has been reported that PD-1 expression induces CD28, IL-2 and Bcl-xl.[167]

In this study, engaging Cell-SELEX and liquid chromatography- Orbitrap Fusion Tribrid mass spectrometer (LC-MS) revealed lysosomal-associated membrane protein 1 (CD107a) as a result of PD-1 expression in cell line HEK293.

6.3. Materials and methods

Cell lines

Cell line HEK293 was obtained from Clontech Laboratories. The cells were cultured in Dulbecco's modified Eagle medium supplemented with 10% fetal bovine serum. The transfected cells expressing PD-1 were inducted with Doxycycline (500 ng/mL) in complete media.

Construction PD-1 gene into the pLVX-TRE3G vector

Bacteria holding plasmid with an open reading frame of PD-1 were obtained from Genecopoeia (Cat# B0169). Bacteria were cultured, and the vectors were extracted. PD-1 forward primer (ATGCAGATCCCACAGGCGC) and reverse primer (TCAGAGGGGCCAAGAGCAGT) with 15 bp extensions homologous to the pLVX-TRE3G vector ends (gcccccgggacgcgt for forward primer and ctacccggtagaattc for the reverse primer) were used for amplification. pLVX-TRE3G vector was digested by MluI (New England Biolabs, cat# R0198S) and EcoRI ((New England Biolabs, cat# R0101S) restriction enzymes at 37°C for 3 hours to provide linearized vector. The linearized vector was cleaned through 1% Agarose gel and extracted with the GeneJet Extraction Kit (Thermo Scientific, Cat#K0692). The PCR products were cloned into pLVX-TRE3G using Fusion HD Cloning Kits (Clontech Laboratories, Inc. Cat. #639648).

Transformation

The plvx-tre3g reaction mixture (2.5 ng) were incubated with competent cells (50 µl). Then, they were placed on ice (30 minutes) and were heat shocked (45 seconds) at 42°C and then moved on ice for an extra 2 minute. Super Optimal Broth with Catabolite repression (SOC) medium was added (final volume of 500 µl). Then, the cell mixtures were cultured on agar medium holding ampicillin (100 µg/ml).

Lentivirus production and transduction

A lenti-X^{TM} Tet-On 3G Inducible Expression System was employed (Clontech, Cat#631187) for lentiviral construction. PD-1 was sub-cloned into the pLVX-TRE3G vector using the In-Fusion HD (Clontech, Cat# 638909). Lentiviruses were produced by transfecting 293T cells and pLVX-TRE3G- PD-1 using the Lenti-X HTX Packaging System (Clontech, Cat#631187). Virus particles were collected 48 hours after transfection. HEK293 cells were infected with the pLVX-Tet3G and selected with G418 (Clontech; Cat#631307) (1 mg/mL). A 10 cm plate of the selected cells was infected with the pLVX-TRE3G-PD-1 viruses and selected with puromycin (Clontech; Cat#631305) (25 μg/mL). Doxycycline (Clontech) was added to the cultures at 500 ng/mL to induce PD-1 expression.

Immunofluorescence staining

The cells were fixed with 4% paraformaldehyde and permeated by 0.25% Triton X-100 (Sigma, St. Louis, MO). The cells were blocked with 10% fetal bovine serum (Gibco, CA) and incubated with primary antibody against PD-1 at room temperature (1hour). The cells were then incubated with Dylight 488-conjugated secondary antibodies (1 hour). After washes, cells were counterstained with 4′,6′-diamidino-2-phenylindole (DAPI; Sigma), and studied under a fluorescence microscope or confocal microscope (Nikon).

Evaluation of PD-1 expression: flow cytometric analysis

To detect PD-1, non-transfected, transfected and induced cells were prepared into single-cell suspensions and incubated with antibody against PD-1. The samples were analysed on a Beckman Coulter FC500 flow cytometer.

Oligodeoxynucleotides

Cell-SELEX was started using ssDNA library single-stranded DNA library that is 100 bases in length including a 60 variable internal region flanked by two 20 mer PCR primer sequences which were designed in Liu's laboratory at Harvard University[136]; the library was made with 5′ CTC CTC TGA CTG TAA CCA CG7 878 787 866 667 878 787 878 666 787 878 787 866 667 878 787 878 666 787 878 78G CAT AGG TAG TCC AGA AGC C3′ where 6 is a combination that makes 1 : 1 : 1 : 1 A/C/G/T, 7 is a combination that makes 45 : 5 : 45 : 5 A/C/G/T, and 8 is a combination that makes 5 : 45 : 5 : 45 A/C/G/T

DNA aptamer selection

The ssDNA library in PBS with Ca^{2+}/Mg^{2+} was used for selection. Before the selection the ssDNA library was denatured at 95°C for 10 minutes and snap cooled on ice. The ssDNA library (1 μM) was incubated with the cells expressing PD-1 receptor to allow ssDNAs to bind to PD-1 positive cells for 1 hour at 37°C. Next, the cells were washed with PBS with Ca^{2+}/Mg^{2+} and spun down at 200 g by centrifuge to remove the supernatant holding unbound ssDNAs. The ssDNAs bound to the cell surface were gathered by heating at 95°C for 5 minutes. The gathered ssDNA was incubated with non-transfected HEK293T cells for negative selection to eliminate non-specific ssDNA (1 hour at 37°C). The unbound ssDNA in the supernatant was collected and used for the follwing PCR apmlification. A positive selection was followed by one round of a negative selection for ten rounds. The collected ssDNA was gathered after each selection and amplified by PCR (twenty-five cycles) for the following round using Thermo Scientific Phire Hot Start II DNA Polymerase (Thermo Scientific). The PCR tube contained a ssDNA template,

50 µL of the PCR reaction mixture with 1x Phire Reaction Buffer, 3% Dimethyl sulfoxide (DMSO), 200 µM dNTPs, 1 µL of the Phire Hot Start II DNA Polymerase (Thermo Scientific), 0.5 µM of 5'-Cy5-conjugated forward primer and, 0.5 µM 5´-phosphorylated reverse primer. The following program was applied to the thermal cycler: melting at 95 °C for 30 seconds, annealing at 58°C for 15 seconds, and extending at 72°C for 10 seconds. To digest the 5´-phosphorylated reverse strand and produce ssDNA, Lambda Exonuclease (New England Biolabs, Cat#M0262S) was used, according to manufacturer protocol.

Whole blood leukocytes

Stemcell Technologies kindly provide us whole human healthy blood to isolate leukocytes by Lymphoprep (Stemcell Technologies; Cat# 07801) gradient centrifugation to remove erythrocytes.

Next-generation sequencing and phylogenetic tree analysis

Best binder pools were amplified by PCR using barcode primers and purified using 4% agarose gel (Invitrogen) and the GeneJET Gel Extraction Kit (Thermo Scientific, Canada, Cat# K0691). All products were pooled in equimolar amounts (each 200 ng) and sequenced by Eurofins MWG Operon LLC, a Eurofins Genomics company, for the two times read of an Illumina MiSeq paired-end for 150 bases. We obtained a total number of 20 million reads (forward read and reverse read) by Illumina sequencing. The documents, in fastq files, were uploaded on the Galaxy project platform (https://usegalaxy.org) and transformed to FASTA[150]. Then data in FASTA format was parted and organized based on their barcodes. The FASTA data was collapsed and grouped based on their common motifs. The most abundant sequences in each

group were studied using MEME (http://meme.nbcr.net/meme/) and a phylogenetic tree was analyzed running Clustal Omega (http://www.ebi.ac.uk/Tools/msa/clustalo/). The evaluated sequences were categorized into four groups based on shared motifs. One DNA sequence from each group was synthesized for the following flow cytometrical analysis.

Flow cytometric assay of the aptamer binding affinity

To quantify EC_{50} of each aptamer (the concentrartion of an apatmer when 50% of all cells are bound), HEK293 cells expressing PD-1 (100,000 cells per sample) were incubated with the Cy5-labeled aptamer (0, 50, 100, 200 and 400 nM). After the washing steps, they were analyzed by flow cytometry, Beckman Coulter Gallios Flow Cytometer. Kaluza analysis software was used to analyze the data. The mean fluorescence intensity deducting the mean fluorescence value of a control sample was used to measure EC_{50}.

Membrane proteins extraction

Whole blood leukocyte cells were lysed via hypotonic buffer on ice (4°C) for 30 min[161]. The hypotonic buffer contained 50 mM Tris-HCl (pH 7.5) with Halt Protease Inhibitor (Thermo Scientific, Cat#78430]. Following three washes with hypotonic buffer, they were incubated with 1 mL PBS with Ca^{2+}/Mg^{2+} including 1% Triton X-100 on ice for 30 min. The lysing was facilitated by 25G needles. They were centrifuged at 17,000 g for 5 minutes at 4°C. The supernatant was incubated with yeast RNA (1 mg/mL) followed by incubation with 5' biotin-conjugated aptamer (200 pmol). Another sample was incubated with 5' biotin-conjugated ssDNA library as a control on ice for 30 minutes. The subsequent complexes of protein-ssDNAs were incubated with streptavidin-coated magnetic beads (2 mg) on ice for 15 minutes and harvested on

a magnet holder. After four washes with 1 mL of PBS containing with Ca^{2+}/Mg^{2+}, EDTA (20 mM) was added to elute proteins in 30 µL water. Using a magnet holder, the subsequent supernatant was collected.

Proteins identification

The proteins were run on 12% sodium dodecyl sulfate-polyacrylamide gel electrophoresis (SDS-PAGE) and stained with QC Colloidal Coomassie Stain (161-0803). The biotinylated aptamer captured protein bands were cut and digested *in situ* by Pierce Trypsin Protease, MS Grade (Thermo Scientific, Cat#90057) based on the manufacturer's protocol. The digested peptides were cleaned using a pipet tip packed with Pierce C18 (Thermo Scientific, Cat# 87782). Peptides were collected with 10 µL of 50% methanol/1% formic acid and analyzed by Thermo Scientific™ Orbitrap Fusion™ Tribrid™ mass spectrometer.

6.4. Results and discussion

Expressing PD-1 in HEK293 cell line and aptamer selection

Bacteria holding plasmid with an open reading frame of PD-1 was obtained from Genecopoeia (Cat# B0169). Bacteria were cultured, and the vectors were extracted to make cDNAs of PD-1 using CloneAmp HiFi PCR Premix (Clontech Laboratories, Inc. Cat. # 639298). HEK293 cell line was transfected using lentiviral Tet-On 3G Inducible expression systems. The transfected cells were induced by Doxycycline. The expression of PD-1 on the cell membrane was confirmed by immunofluorescence and flow cytometry analysis (**Figure 6.1**).

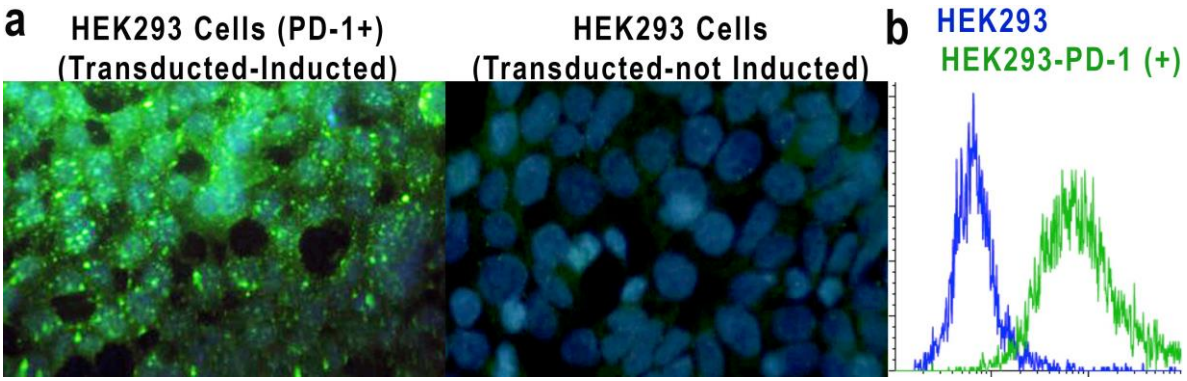

Figure 6.1. Immunofluorescences (a) and flow cytometric analyses (b) validation of PD-1 expression. (a) The immunofluorescences of transfected HEK293 cells after induction by doxycycline and transfected HEK293 cells without induction were studied. The cells were fixed and incubated with primary antibody anti PD-1; after two washes, dylight 488 conjugated secondary antibody was added. Blue color presents DAPI, which stained DNA. Photos were captured by Nikon A1RsiMP confocal microscope at 25X magnification. (b) Flow cytometric analysis of PD-1 expression was achieved in transfected HEK293 cells after induction (green) and without induction (blue).

Cell-SELEX [147] was used to select bound aptamers to the membrane of PD-1 positive cells. The single strand DNAs (ssDNAs) with binding affinity to HEK293 cells negative to PD-1 were removed from the selection. Consequently, the developed aptamers bind to proteins on the membrane of PD-1 positive cells, which is not on the PD-1 negative cell membrane. The binding affinity of Cy5-conjugated ssDNA pool product of each round of selection were assessed, and the aptamer pools of the round 11 and 12 were barcoded using forward primer and submitted for the next generation sequencing (NGS) for the two times read of 150bp MiSeq. The NGS fastq files were organized, filtered, clustered, and analyzed for the phylogenetic tree and common motifs through the Galaxy web software. The resulting sequences were grouped according to their common motifs and the most abundant sequence of each cluster was synthesized with Cy5 fluorochrome at 5' (**Table 6.1)**. RNAstructure web server was used to figure out the possible

secondary structure of the synthesized aptamer based on free energy minimization[162] **(Figure 6.2)**.

Table 6.1. The selected aptamers and their corresponding sequences.

Aptamer	**Sequence**
Apt-46050	CTCCTCTGACTGTAACCACGGTACACATAGCCATGTGAGCGCGCCGCGTG GATGTCCGCACGCATGCGTGTAGTACGTGCGCATAGGTAGTCCAGAAGCC
Apt-65664	CTCCTCTGACTGTAACCACGGTACACATAGTCATGTGAGCGCGCCGCGTG GATGTCCGCACTCATGCGTTTCGTACGTGCGCATAGGTAGTCCAGAAGCC
Apt-93104	CTCCTCTGACTGTAACCACGGTACACATAGCCATGTGAGCGCGCCGCGTG GATGTCCGCACTCATGCGTTTCGTACGCGCGCATAGGTAGTCCAGAAGCC
Apt-95215	CTCCTCTGACTGTAACCACGGTACACATAGCCATGTGAGCGCACCGCGTG GATGTCCGCACTCATGCGTTTCGTACGTGCGCATAGGTAGTCCAGAAGCC

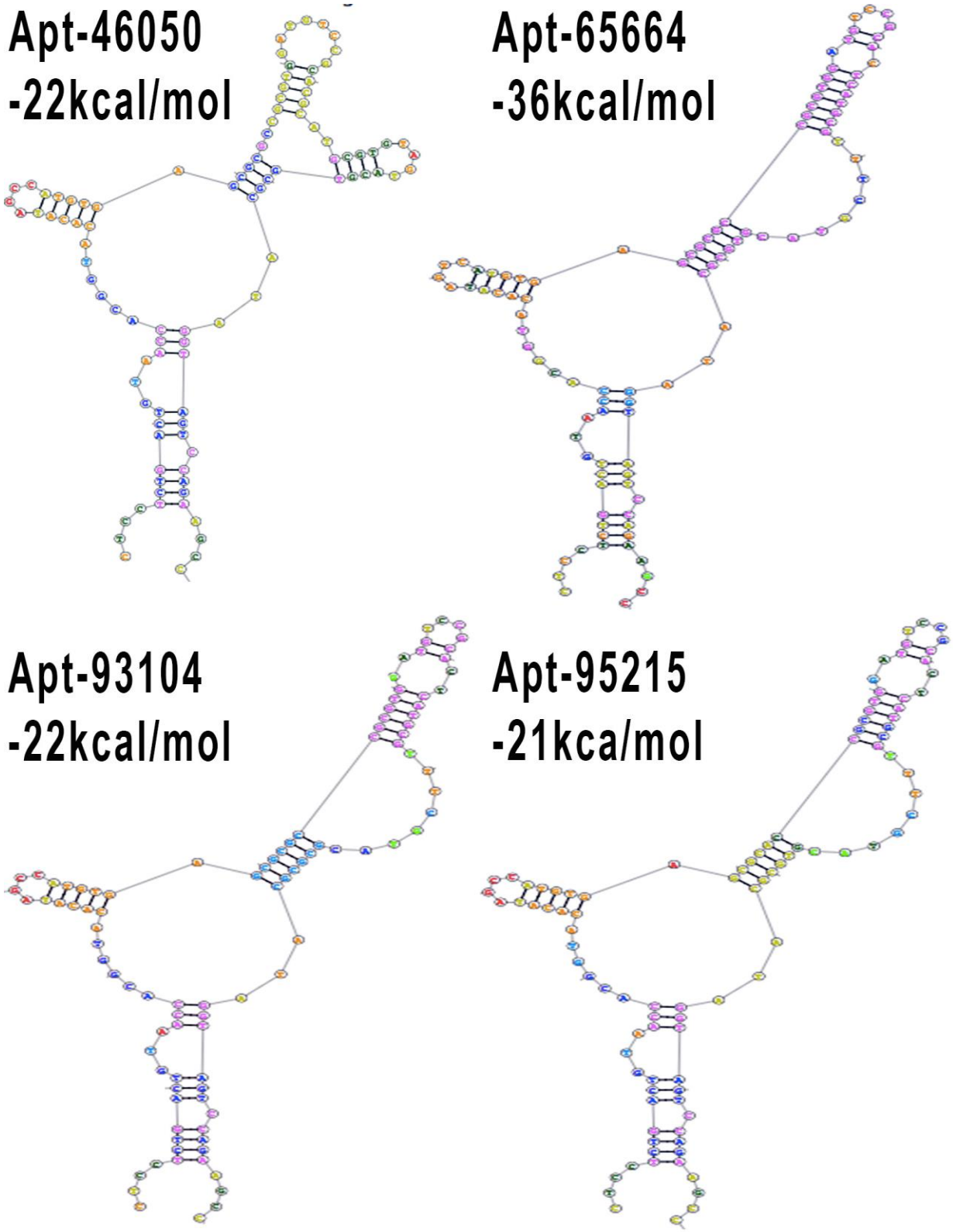

Figure 6.2. The secondary aptamers structure and minimum free energy (kcal/mol). Aptamer structure and minimum free energy was estimated using RNAstructure web software[162].

Aptamer Binding

The binding of the generated aptamer conjugated with Cy5 to the cells expressing PD-1 and not expressing PD-1 was assessed by flow cytometric analysis. Apt-46050 had the highest specific binding to the cells expressing PD-1 in comparison to negative cells (**Figure 6.3**).

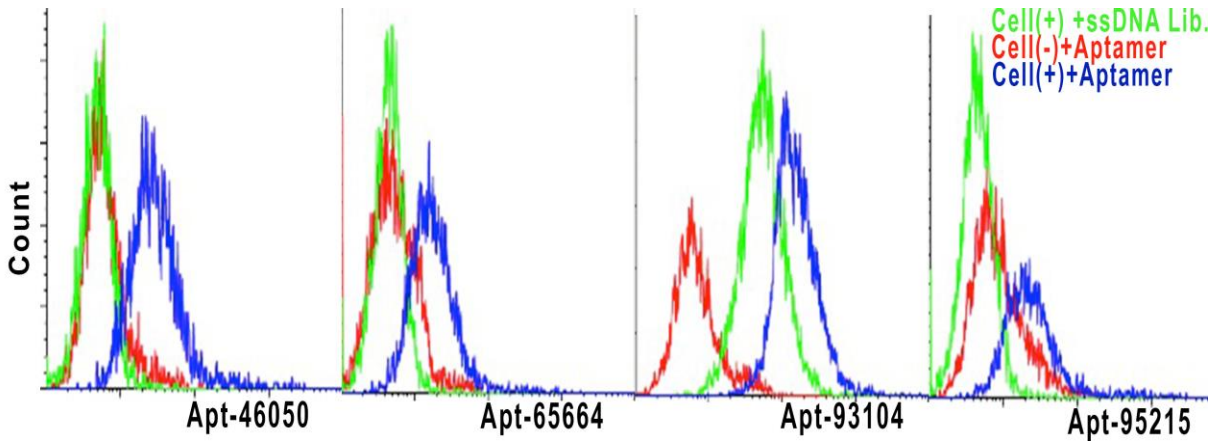

Figure 6.3. Binding of selected aptamers to the HEK293 cells expressing PD-1. The bindings of Cy5-conjugated aptamers and the ssDNA library was tested by flow cytometry.

Apt-46050 target molecule

Biotinylated Apt-46050 was applied to isolate the aptamer target proteins on the cell surface for mass spectrometry investigation. The membrane proteins were extracted in PBS (with Ca^{2+}/Mg^{2+}) buffer from lysed whole human blood leukocytes. Following incubation of 5′-biotinylated Apt-46050 with cell membrane proteins, the aptamer, and bound proteins were isolated operating streptavidin-coated magnetic beads and magnet. After these washes, they were heated at 95°C (5 minutes). The supernatants were collected on the magnet. After heating in the loading buffer under reducing condition, they were run on 12% sodium dodecyl sulfate-polyacrylamide gel electrophoresis (SDS-PAGE). The protein bands on the gel were cut and

after in-gel digestion with trypsin were subjected to proteomic investigation using nanoLC-Thermo Scientific Orbitrap Fusion Tribrid mass spectrometer. Lysosomal-associated membrane protein 1 (LAMP-1) also known as CD107a as a main target of Apt-46050 was recognized.

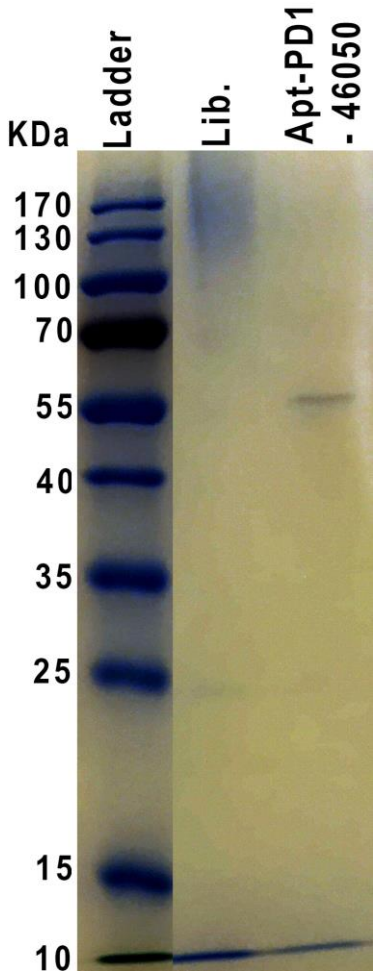

Figure 6.4. SDS-PAGE of the isolated proteins from whole blood leukocyte membrane proteins using biotinylated Apt-46050 and streptavidin-coated magnetic beads. Lane 1 is the protein marker (10–170 kDa); lane 2 is ssDNA library bound target proteins; lane 3 is biotinylated Apt-46050 bound target proteins.

Apt-46050 target cells in blood cells

To identify the cell target of Apt-46050 in whole human blood, whole blood leukocytes were incubated with the Cy5-conjugated Apt-46050 in PBS with Ca^{2+}/Mg^{2+} and tested by an antibody against PD-1 and CD107a using a flow cytometric approach (**Figure 6.5**). Cy5-conjugated Apt-46050 bound 9% of human whole blood leukocytes; 6% of leukocytes were PD-1 positive and 8% of leukocytes were CD107a positive. The results describe that both Apt-46050 and antibody against CD107a target the same population of human blood cells while 7% of Apt-46050 positive cells are PD-1 negative cells and 5% of PD-1 positive cells are Apt-46050 negative.

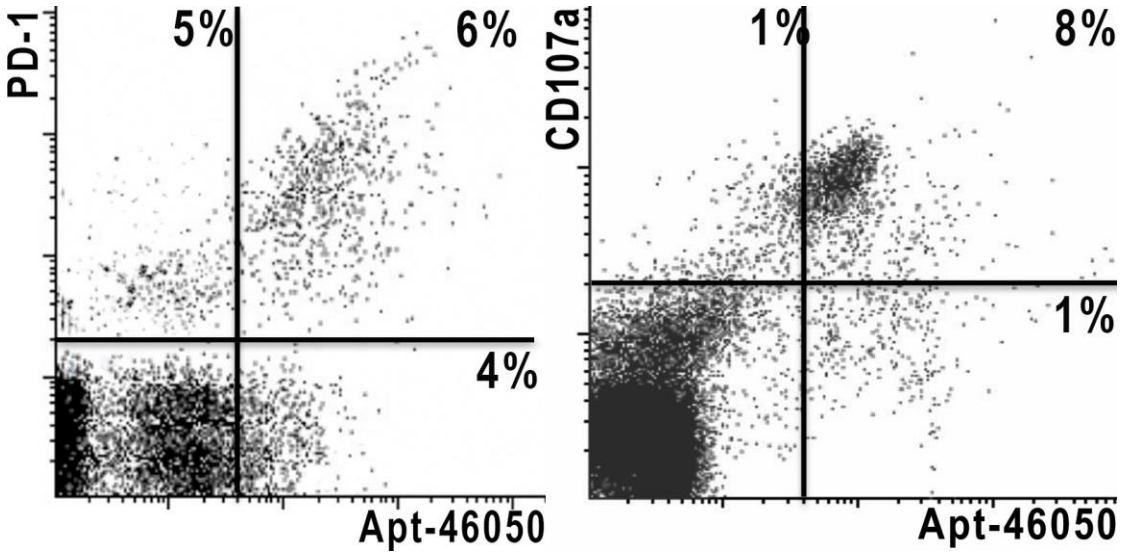

Figure 6.5. Flow cytometric analysis of Cy5-conjugated Apt-46050 positive cells in human whole blood leukocyte using anti- PD-1 and anti- CD107a antibody.

Apt-46050 target cells population in whole blood leukocytes

For analysis on Apt-46050 target cells in human whole blood leukocytes by multicolor staining with antibodies against CD3 and CD4 (**Figure 6.6**).

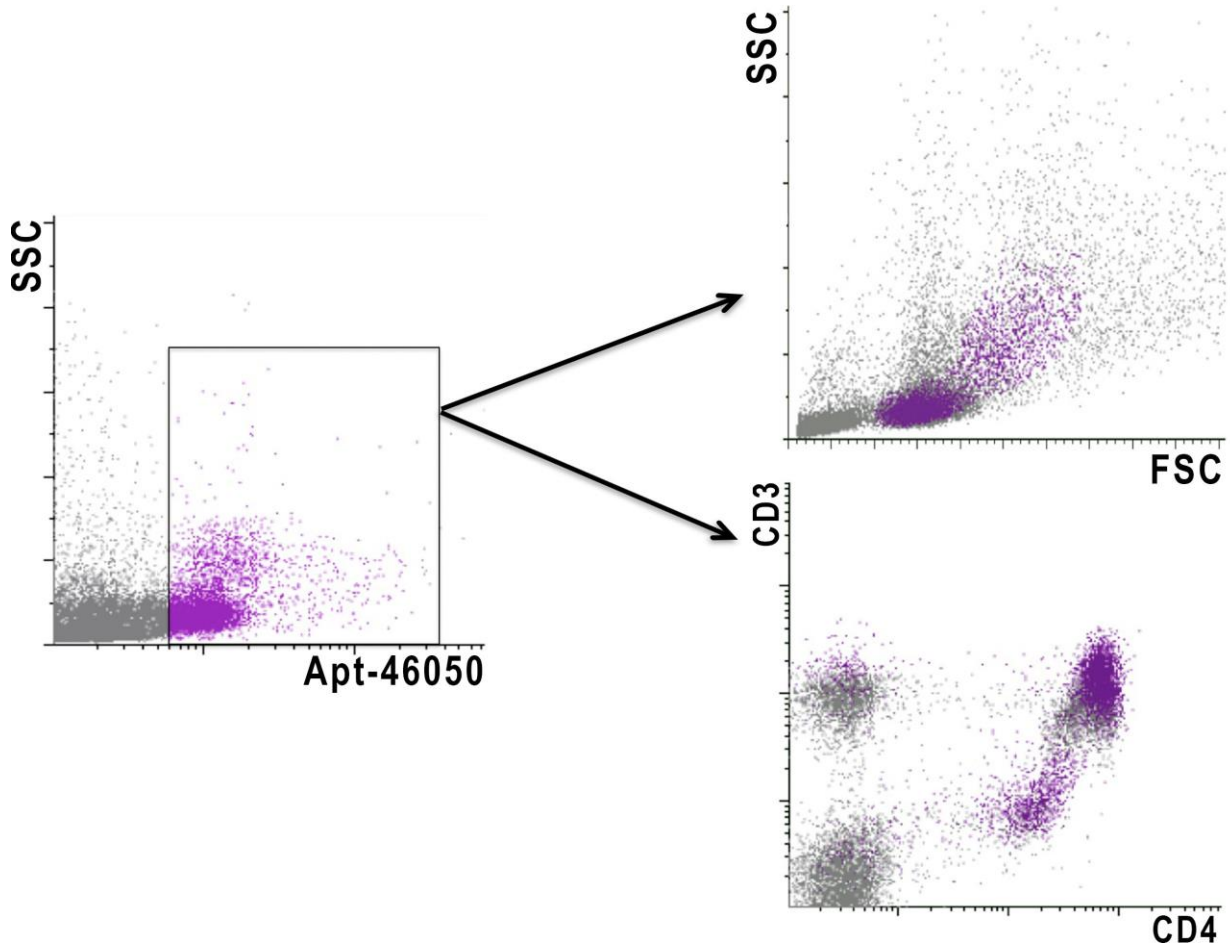

Figure 6.6. Detection of aptamer positive cells in human whole blood leukocytes. Flow cytometric dot plot analysis of Side Scatter (Y axis) vs. Forward Scatter (X-axis) was applied to distinguish red blood cells, debris, lymphocytes, and granulocytes. The aptamer positive cell population was gated and a purple color was applied to a dot plot of CD4 vs. CD3 to evaluate the content of aptamer positive cells subpopulations which majority of them are presented in CD3+/CD4+.

The aptamer positive cells were purple color gated on Side Scatter (SSC) and Forward Scatter (FSC) as well as CD3 and CD4 dot plot chart. As **Figure 6.6** shows on SSC and FSC plot, Apt-46050 positive cells are part of lymphocytes and monocytes. The dot plot of CD3 and CD4 shows the higher portion of aptamer positive cells in order respectively in CD3+CD4+,

CD3-CD4+, and CD3+CD4- cells. In this study, we present DNA aptamers that detect CD107a on the membrane of the HEK293 cells as a consequence of expressing PD-1.

Cell-SELEX aptamer selection with LC-MS proteomics empowers us to detect variation on cell membranes as responses as a consequence of gene expression. This study presented CD107a as a result of expressing PD-1 in cell line HEK293. Previous reports indicate the expression association between PD-1 and CD107a after stimulation with Env and Gag peptide panels.[168] It was shown that PD-1 mediates IL-2 [167]. Research also revealed that IL-2 triggers the expression of CD107a in CD56+ natural killer cells and T cells. The expression of CD107a after IL-2 expression is associated with cytotoxicity activity of lymphocytes.[169]

LC-MS identified CD107 as a protein target of Apt-46050. Multicolour staining of whole human blood leukocytes shows that Apt-46050 can be used in combination with antibodies in multi-parameter flow cytometry to detect cell expressing CD107. Flow cytometry-based detection of CD107a has been recognized as a clinical monitoring marker of activation of lymphocytes and natural killer cells. It is also involved in metastases and differentiation of cancer cells.[169-172] Natural killer cells exposed to HIV have a greater level of CD107a which connects with arbitrated cytolytic activity and cytokine secretion.[173] CD107a expresses on the membrane of tumor-cytolytic T cells; this is used to detect and isolate them from blood samples of patients.[174] Apt-46050 can be used to detect tumor-cytotoxic T lymphocytes and activated natural killer cells and monocytes to monitor immune cells responses to vaccination and immune potency.

6.5. Conclusion

This study discovered CD107a as a result of PD-1 expression in cell line HEK293. The results show that CD107a was expressed on the cell surface upon PD-1 expression. However, further studies are needed to confirm this result using methods such as western blotting to determine the transcriptional level by RT-PCR and the localization using immunofluorescence.

Overall, Cell-SELEX aptamer selection coupled to LC-MS proteomics facilitates the detection of cell membrane variation in responses to gene expression.

Chapter 7

Monocyte marker identification and pure positive isolation

7.1. Objectives

In the previous chapters, we observed diverse performance of the aptamers under influence of conditions of aptamer selections and solutions. Factors such as proteins, ions, and pH can have controls on aptamers binding. Here, we attempt to generate aptamers, which binds to an exclusive molecule on a target cell in its native biological environment. First, we expect robust results of aptamer applications because the aptamer selection conditions and application environment are the same. Therefore, the selected aptamer will be more specific to the target cells in its natural physiological tissue. Second, this selection strategy can result in a biomarker,

exclusive to the target cells against the other cells in the tissue. Accordingly, we developed DNA aptamers to monocytes in peripheral whole blood leukocytes using Fluorescence Activated Cell Sorting (FACS) and SELEX. LC- Orbitrap Fusion Tribrid mass spectrometer determined CD91 as a binding partner of the aptamer on monocytes.

Contributions

Shahrokh M. Ghobadloo and Dr. Maxim V. Berezovski (supervisor) conceived the idea and designed the research. Shahrokh M. Ghobadloo performed the experiments. Dr. Gleb G. Mironov ran the mass spectrometry experiments.

7.2. Background

Many manufacturing processes of biological materials are required to separate live cells from non-processed samples, such as whole blood, umbilical cord blood, bone marrow, feces and ascites, or from processed samples such as buffy coat, peripheral blood mononuclear cells (PBMC), tissue digests or cell cultures. The existing cell separation methodologies can be classified into two main groups. The first group is based on the physical criteria of the cells in the sample like size, shape, and density differences and includes filtration and centrifugation techniques.[175] These methods are commonly used for debulking heterogeneous samples. The second group of cell separation methodologies is based on biochemical cell surface characteristics and biophysical criteria. It comprises affinity methods such as capture on affinity solid matrix (beads, plates, fibers),[176] fluorescence-activated cell sorting (FACS)[177] and magnetic cell isolation.[178]

The affinity separation methods for isolation of cell populations are based on the use of antibodies against differentially expressed cell-surface antigens. Typically, antibodies are covalently linked to a fluorescent molecule (in immunofluorescent technology, FACS), a particle (in immunomagnetic technology), a support matrix (immunoadsorbents in chromatography or bottom of a vessel in panning).

Immunomagnetic separation is the technology of choice to isolate high yields of pure, viable and functional cells in a fast manner. There are two main strategies in the separation: "negative isolation", where unwanted cells are depleted, and "positive isolation" of the cell of interest.[59]

In depletion methods, the unwanted cells are magnetically labeled, retained in a magnetic separator, and eliminated from the cell mixture. The target cells pass through the separator and are collected as the enriched, unlabeled fraction. This method is usually carried out for the removal of unwanted cells, in cases when no specific antibody is available for target cells, or when labeling of the target cells is not desirable. However, if target cells are present in very low concentration, depletion methods may give low yield and purity due to non-specific loss of the cells to be isolated, or due to an insufficient removal of unwanted cells.

Positive isolation is the most direct and specific way to isolate the target cells from a heterogeneous cell suspension. The target cells are magnetically labeled, retained in a magnetic separator and finally eluted as the enriched fraction after removal of the magnet. However, the challenge when performing positive cell isolation is that the cells of interest may be affected and/or altered during the isolation process. In most systems, antibody-coated magnetic beads remain on the cells throughout the duration of downstream experiments; thus, the binding of antibodies or ligands to cell surface antigens can lead to clustering of receptors, triggering of signalling pathways (positive or negative signals) or blocking of receptor functions. Positive cell

isolation without bead removal is used for some downstream applications, such as nucleic acid or protein analysis. However, in order to perform other downstream applications, i.e., flow cytometry, cell cultures, cellular therapy, it is necessary to remove the micron-sized beads, otherwise, they interfere with the applications.

Not many solutions have been explored to remove beads from cells.[179] There are two solutions mostly often used: 1) detachment of the beads and a primary antibody from the cell surface with an anti-antibody or peptide, and 2) detachment of the beads alone with generic release mechanisms, i.e., enzymatic cleavage or biotin displacement. In the first approach, the anti-antibody (raised against the primary antibody) or the synthetic peptide mimicking the surface marker out-compete the binding between the primary antibody and the marker. This method requires precise knowledge of surface antigens and leaves the cells contaminated with excess of the anti-antibodies or peptides in solution. The second approach is based on affinity-competition of a biotin analogue to an avidin/streptavidin analogue or protease cleavage of antibodies from beads. The main disadvantage is that the displacement and cleavage still leave the primary antibody on the cell surface.

To achieve isolation of ultrapure cells free of antibodies and beads, we describe here an emerging technology for detection, purification, fractionation and isolation of live target cells. The technology is called *Aptamer-Facilitated Cell Purification* (AptaCEP) and based on aptamers with switchable affinity (SwAps) mediated by ethylenediaminetetraacetic acid (EDTA). These aptamers bind to cells in presence of Ca^{2+} or Mg^{2+}, and release the pure and intact cells when EDTA or EGTA is added into a solution (**Figure 7.1**). Previously, we have shown that addition of EDTA-switchable aptamers to Vesicular Stomatitis virus enabled the

isolation of the virus with high yield and purity.[180] The virus was active and showed good infectivity in cell-based assays.

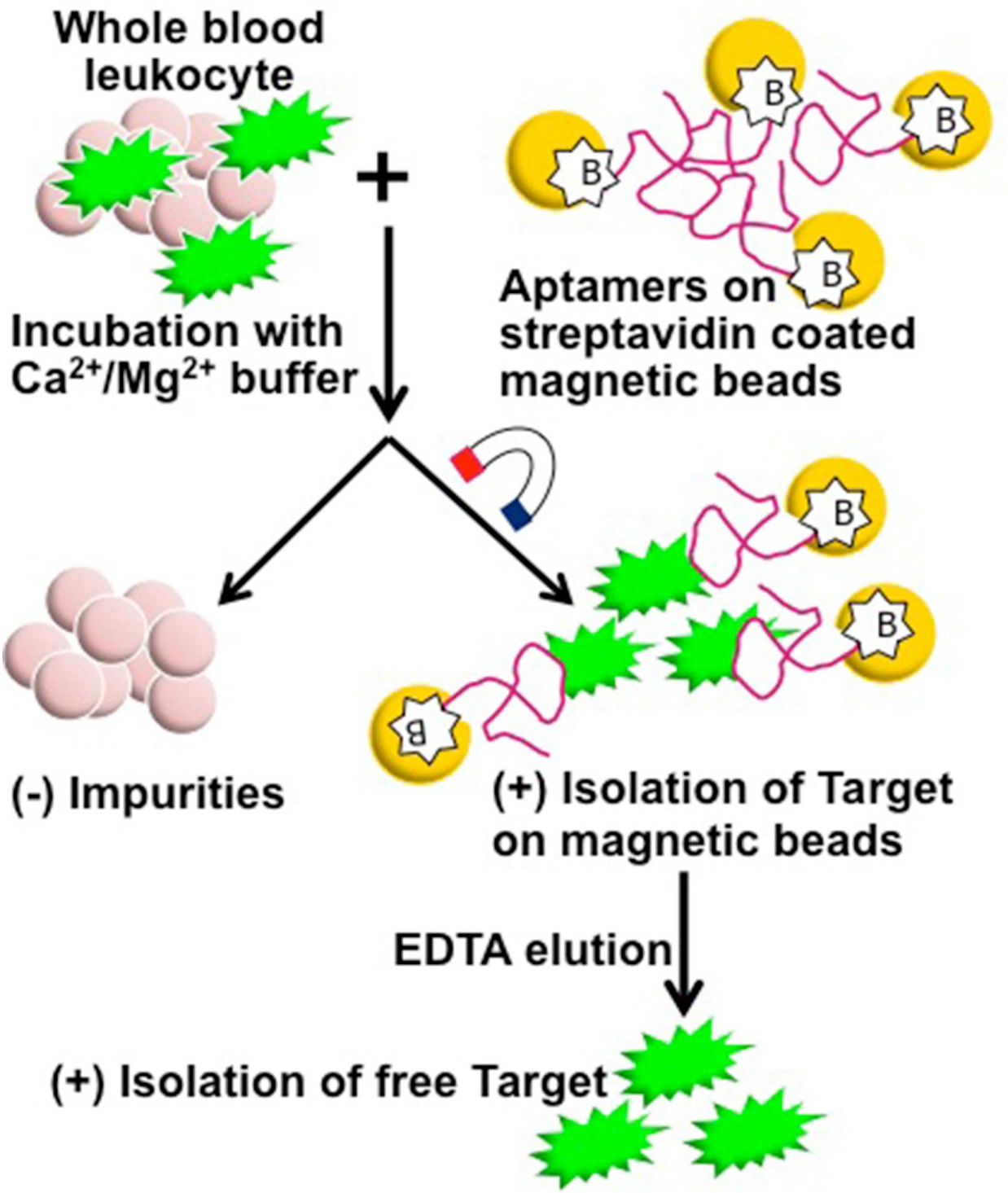

Figure 7.1. Aptamer-Facilitated Cell Purification.

We selected EDTA-switchable aptamers to monocytes from human blood using a combination of Fluorescence-Activated Cell Sorting and Systematic Evolution of Ligands by Exponential Enrichment (FACS-SELEX) techniques. The aptamer clones were then used to isolate biomarkers from monocytes followed by mass spectrometry (MS) analysis of the pull-down proteins. The analysis revealed a known biomarker of monocytes called alpha-2-macroglobulin receptor (CD91). The aptamers were also proven to be highly efficient in purifying probe-free monocytes from whole blood leukocytes by FACS or magnetic beads. As a result, this represents, to the best of our knowledge, the first report of a positive isolation of viable cells with switchable aptamers.

7.3. Materials and methods

Antibodies

A PE-conjugated antibody against CD14 (Anti-CD14-PE) from Stemcell Technologies (Cat# 60004PE), FITC-conjugated antibody against CD3 (Anti-CD3-FITC) from Stemcell Technologies (Cat#60011FI.1), and PCy7-conjugated antibody against CD4 (Anti-CD4-PCy7) were obtained.

Whole blood leukocytes

Whole blood of healthy human was obtained from Stemcell Technologies. Whole blood leukocytes were isolated by standard procedures using Lymphoprep (Stemcell Technologies, 07801) gradient centrifugation to remove erythrocytes.

Oligodeoxynucleotides

The single-stranded DNA (ssDNA) library (5'- CTCCTCTGACTGTAACCACG -N40- GGCTTCTGGACTACCTATGC -3') included a randomized region of 40 nucleotides flanked by two constant regions complementary to primer annealing and PCR amplification. All oligodeoxynucleotides were purchased from IDT DNA Technologies, USA.

Aptamer FACS Cell SELEX

The ssDNA library (1 μM) in PBS with Ca^{2+} (0.9 mM) and Mg^{2+} (0.49 mM) was used for selection **(Figure 7.1)**. Whole human blood leukocytes were blocked by adding yeast RNA 1 mg/mL. After denaturation at 95°C for 5 minutes, the samples was quickly cooled on ice. The ssDNA library was then incubated with whole human blood leukocytes to allow ssDNA to bind to the cells' membranes for 45 minutes on ice. The cells were incubated for an additional 15 minutes on ice with a conjugated antibody against CD14 (Anti-CD14-PE). Then, the cells were rinsed using PBS with (Ca^{2+}/Mg^{2+}) and spun down at 200 RCF using a tabletop centrifuge. The supernatant containing unbound DNAs and antibodies was removed. Beckman Coulter MoFlo Astrios EQ Cell Sorter was used to sort monocyte. Monocytes in leukocyte were identified by setting a gate on the population within the Forward Scatter vs. Side Scatter and anti-CD14-PE vs. Side Scatter. The sorting logic of "1" with 1% threshold and 2,000 events per second were applied to sort monocytes. EDTA was added to sorted monocytes to collect the EDTA switchable aptamers. DNA was collected and purified by 4% agarose gel then amplified by PCR for the next round. Twenty-five cycles of PCR were performed for the amplification of single-stranded DNA (ssDNA) using Thermo Scientific Phire Hot Start II DNA Polymerase (Thermo Scientific, Cat# F-122L). In addition to the DNA template, the 50 μL PCR reaction mixture was

comprised of 1x Phire Reaction Buffer, 3% Dimethyl sulfoxide (DMSO), 200 μM dNTPs, 1 μL of the Phire Hot Start II DNA Polymerase (Thermo Scientific, Cat# F-122L), 0.5 μM of 5'-Cy5-labeled forward primer and 0.5 μM 5´-phosphorylated reverse primer. The following program was used for the thermal cycler: melting at 95 °C for 30 s, annealing at 58°C for 15 s, and extending at 72°C for 10 s. After PCR, Lambda Exonuclease (New England Biolabs, Cat#M0262S) was used to digest the 5´-phosphorylated reverse strand generating ssDNA (**Figure 7.2**). After12 rounds of aptamer selection, aptamer pools became enriched for sequences that possess significant binding. The binding of Cy5-conjugated ssDNA of pools from each selection was monitored simultaneously during sorting.

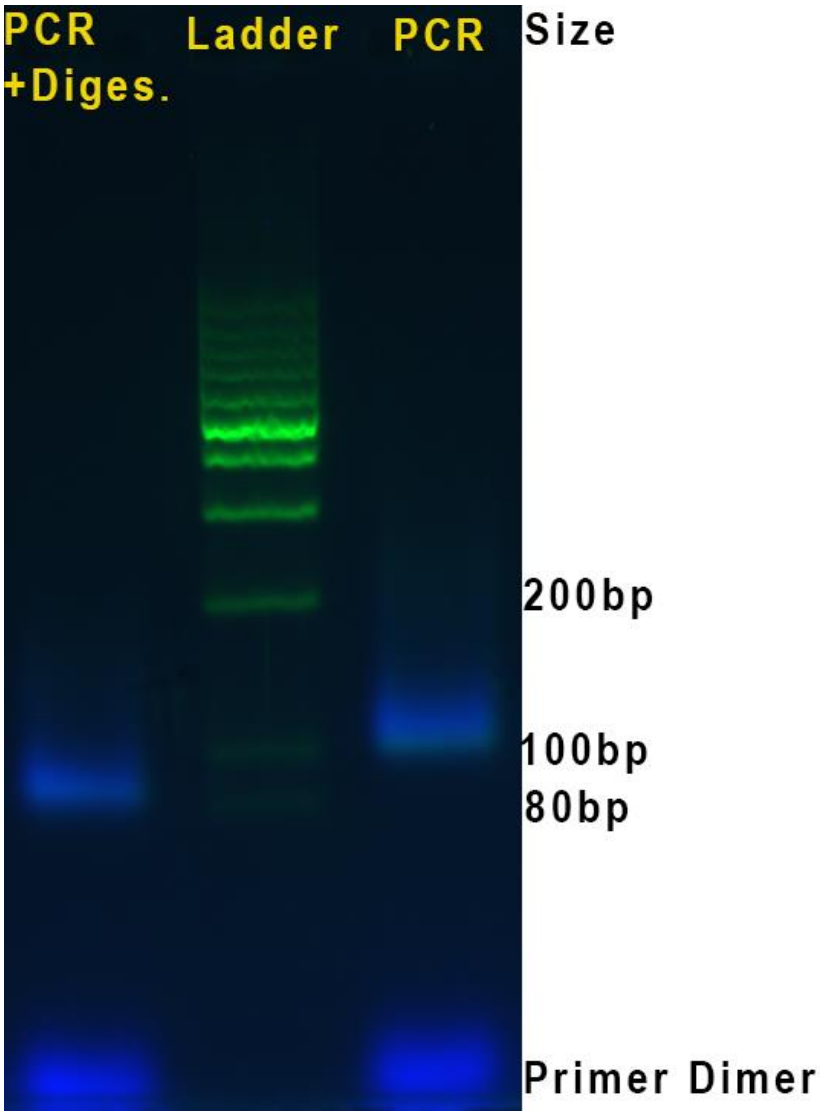

Figure 7.2. PCR products of eluted Cy5 labled DNA from the selection before and after digestion with Lambda Exonuclease. Lambda Exonuclease digests the 5´-phosphorylated reverse strand and generates ssDNA. The PCR had been done with Cy5 forwad prime. The 4% agarose gel was stained with GelRed.

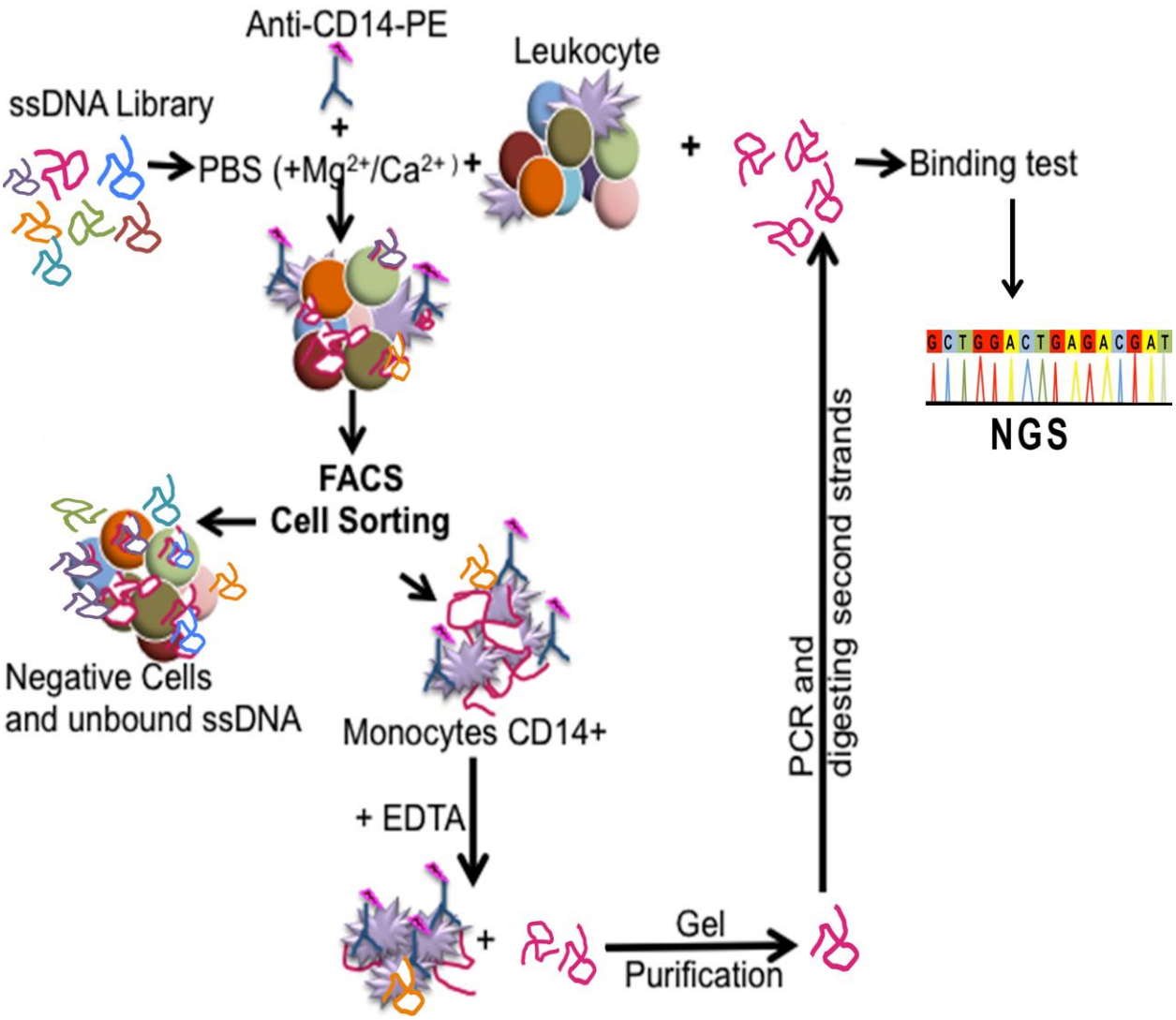

Figure 7.3. FACS–Cell SELEX aptamer production. After staining whole blood leukocyte with ssDNAs and antibodies, monocytes were sorted by FACS. EDTA eluted cell bound ssDNAs. The ssDNAs were amplified using PCR. After digesting a complimentary strand, the resulting ssDNA was applied for the next selection cycle.

Next-generation sequencing and phylogenetic tree analysis

PCR of the best binder pools was performed with primers having unique barcodes. The PCR products were purified using 4% agarose gel (Invitrogen) and the GeneJET Gel Extraction Kit (Thermo Scientific, Canada, Cat# K0691). All products were mixed in equimolar amounts (each 200 ng) and sequenced by Eurofins Genomics company; two times read of an Illumina

MiSeq paired-end with read lengths of 150 bases. We obtained a total number of 20.46 million reads (forward read and reverse read) by Illumina sequencing. The data, in fastq files, were uploaded onto the Galaxy project platform (https://usegalaxy.org) and converted to FASTA[150]. Then data in FASTA format was split and sorted according to their barcodes. The FASTA data was collapsed to analyze the abundance of each sequence. The most abundant sequences were investigated for common motifs using MEME (http://meme.nbcr.net/meme/) and a phylogenetic tree was build operating Clustal Omega (http://www.ebi.ac.uk/Tools/msa/clustalo/). The analyzed sequences were sorted into 21 groups based on common motifs. One sequence from each cluster was chemically synthesized.

Flow cytometric assay of the aptamer affinity

To measure the concentration of aptamers (EC_{50}) at which 50% of cells are bound, whole blood leukocytes (10,000,000 cells per sample) were incubated with the Cy5-conjugated aptamers (0, 50, 100, 200 and 400 nM), anti-CD14-PE, anti-CD3-FITC and anti-CD4-PCy7 on ice for 30 minutes. Then, they were washed and analyzed by a Beckman Coulter Gallios flow cytometer. Data were evaluated using Kaluza analysis software. After deducting the mean fluorescence value of the control sample, the average fluorescence intensity (MFI) of monocytes bound with Cy5-aptamers **(Figure 7.8)** was used to measure the EC_{50}.

Cell isolation with aptamers and streptavidin magnetic beads

Biotinylated aptamers (200 nM) in PBS (1 mL) with Ca^{2+} (0.9 mM) and Mg^{2+} (0.49 mM) were incubated with whole human blood leukocytes on ice for 30 minutes. The cells were washed with PBS ($+Ca^{2+}/Mg^{2+}$) and then incubated with 50 μL streptavidin-coated magnetic

beads (10mg/mL) (Thermo Scientific, cat#88817) in PBS (+Ca^{2+}/Mg^{2+}) on ice for additional 10 minutes. To isolate the captured cells, the tubes were exposed to a magnet holder on ice; the solution was decanted, and the tubes were washed three times with PBS (+Ca^{2+}/Mg^{2+}) to discard non-bound cells. To detach the cells from magnetic beads, EDTA (20 mM) in PBS without Ca^{2+}/Mg^{2+} was added to each tube. After 10 minutes, the tubes were placed on a magnet holder. Then, the free cells were collected in supernatant for further assays.

Biomarker purification

We used a hypotonic buffer to lyse the cells[161]. The buffer contained 50 mM Tris-HCl (pH 7.5) with Halt Protease Inhibitor (Thermo Scientific, Cat#78430]. Following washing and centrifuging at 2,000 g for 10 minutes, the hypotonic buffer lysed whole blood leukocytes (10,000,000 cells) on ice (4°C) for 30 min. After three washes with hypotonic buffer, the pellet was incubated with 1 mL PBS with Ca^{2+}/Mg^{2+} comprising 1% Triton X-100 on ice for 30 min. To facilitate the cell lysing, 25G needles were used. After centrifugation (17,000 g, 5 min, 4°C), the supernatant was incubated with masking RNA (yeast RNA 1 mg/mL) followed by incubation with 5' biotinylated Apt-9 (1 μM) and in a separate sample, 1 mL 5' biotinylated ssDNA library (1 μM) as a control on ice for 30 min. The resulting protein-ssDNAs complexes were incubated with 2 mg of streptavidin coated magnetic beads on ice for 15 min and collect on a magnet holder. The collected complex of magnetic beads, ssDNA and proteins were washed four times with 1 mL of PBS containing Ca^{2+}/Mg^{2+}. EDTA (20 mM) was added to the beads to elute proteins in 30 μL water. After placing the sample on the magnet holder, the subsequent supernatant was collected for the following SDS-PAGE analysis and mass spectrometry identification.

Proteins identification

The proteins were separated by 12% sodium dodecyl sulfate-polyacrylamide gel electrophoresis (SDS-PAGE) and stained with QC Colloidal Coomassie Stain (cat#161-0803). The aptamer-purified protein bands were excised and digested *in situ* by Pierce Trypsin Protease, MS Grade (Thermo Scientific, cat#90057) according to the manufacturer's protocol. The extracted peptide was purified using a ready-to-go pipet tip filled with Pierce C18 Tips spherical silica reversed phase material (Thermo Scientific, Cat# 87782). Peptides were eluted with 10 μL of 50% methanol/1% formic acid and analyzed by Thermo Scientific™ Orbitrap Fusion™ Tribrid™ mass spectrometer.

7.4. Results and discussion

Selection of DNA Aptamers with Switchable Binding to Monocytes

DNA aptamers are single-stranded DNA (ssDNA) molecules selected from a diverse (10^{15}) synthetic library of statistically unique 80-nt oligonucleotides for their affinity to molecular targets. Calcium and magnesium ions at 0.01^{-1} mM range stabilize secondary and tertiary structures of ssDNA.[181] Monovalent cations, divalent cations neutralize the polyanionic backbone and facilitate the formation of multiple DNA conformers.[182, 183] The original selection of aptamers to proteins on cells was pioneered by Gold and co-authors in 1998.[184] Mayer et al.[24] and Berezovski et al.[185] employed FACS in SELEX to enrich aptamer positive live cells.

We utilized FACS to accomplish both positive and negative selections of Cell-SELEX by target cells, monocytes, sorting from heterogeneous tissue, whole human leukocyte, after incubating with ssDNA library. This approach made both negative and positive selections possible with one

round of a target cell population sorting from its heterogeneous biological environment. Also, aptamers were selected to targets in their natural environment as well as in competition with other naturally present other cells. To obtain aptamers with switchable binding, we eluted the bound ssDNAs by adding EDTA (20 mM). These aptamers have a switchable functionality allowing them to bind to their targets in the presence of Mg^{2+} (0.49 mM) and Ca^{2+} (0.9 mM) ions and to release their targets once the ions are removed. To allow for this functionality, an additional step in the cell-SELEX process was added using a strong chelating agent, EDTA.

Aptamer selection starts with a naive ssDNA library. In our case, this library had a randomized region of 40 nucleotides flanked by two primer-hybridization sites. To reduce the effect of natural DNA binding to CD14+ monocytes and phagocytosis on aptamer selection, we were selecting aptamers at 0°C in the presence of masking RNA. Whole blood leukocytes (5×10^6 cells) were incubated with masking RNA (1 μg/μL) to block possible nonspecific binding sites and then washed and incubated with Cy-5 labeled ssDNA library (1 μM) at 0°C. After the washing steps, whole blood leukocytes were sorted by FACS to isolate highly pure monocytes based on the side scatter, forward scatter and CD14+ cells properties (**Figure 7.4**).

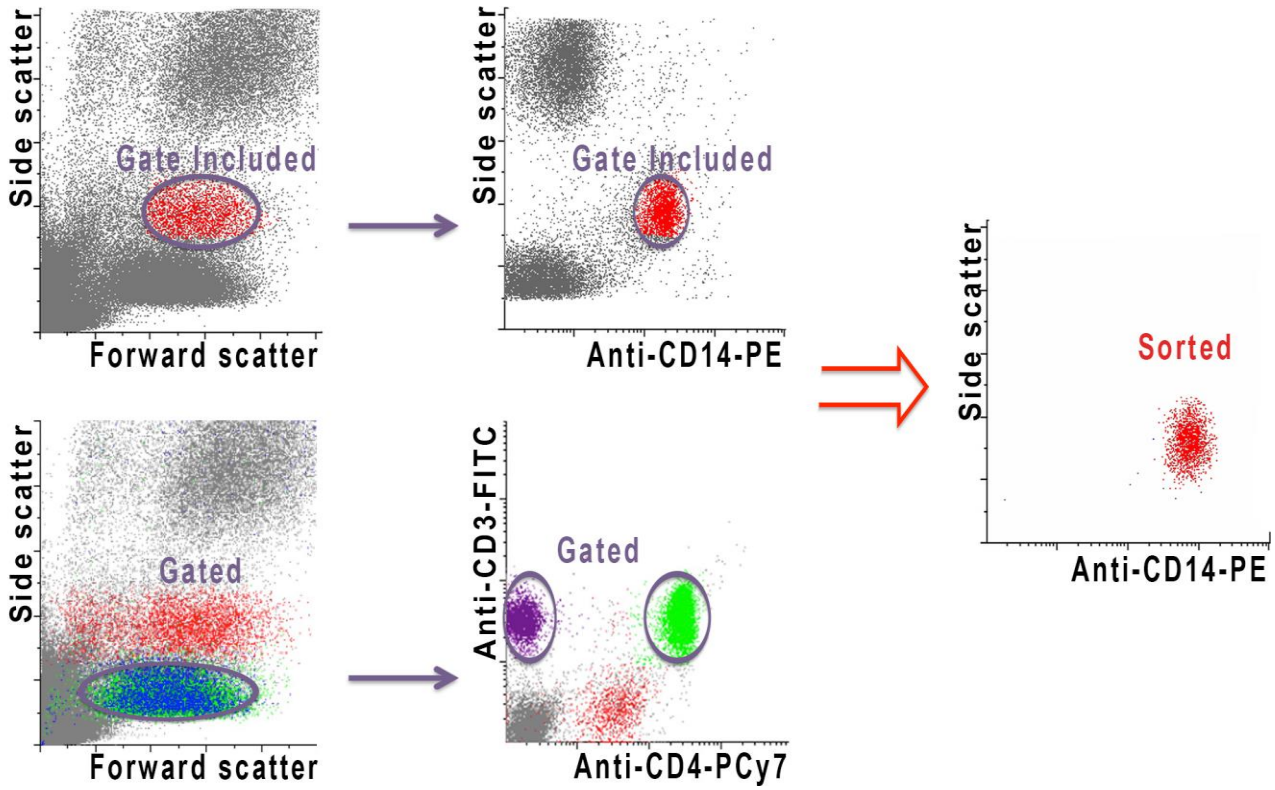

Figure 7.4. Settings for sorting monocytes from whole blood leukocytes by FACS. Whole blood leukocytes were stained with anti-CD14-PE, anti-CD3-FITC, and anti-CD4-PCy7. For the sorting step, monocytes were gated on Side scatter vs. Anti-CD14-PE and Side scatter vs. Forward scatter. To detect other cell populations in sorted monocytes, CD3+CD4+ (green) and CD3+CD4-(purple) were used. The sorted cells were then analyzed.

Vital and dead cells were separated through their scattering characteristics on FACS. Adding EDTA to a final concentration of 20 mM eluted the bound ssDNA to monocyte. Then, the cells were spun down, and supernatant containing ssDNA was collected. A fraction of the ssDNA was amplified using PCR with 5´-Cy5 fluorescent forward primer and 5´-phosphorylated reverse primer. Lambda exonuclease was used to digest a reverse strand and generate single-stranded aptamer and then ssDNA was purified by 4% agarose gel. The second and following aptamer selection rounds were similar except for aptamer concentration was reduced and the number of washes were increased. Increasing the number of washes after binding and decreasing

incubation time improved the binding strength of aptamers. The concentration of the DNA pool was reduced from 200 nM at the beginning of the selection to 50 nM at the 12th round of selection. Monitoring the degree of binding of monocyte-specific aptamer pools was performed by FACS. The aptamer binding increased till round 10 when saturation was achieved. The complete FACS-Cell SELEX process is demonstrated in **Figure 7.3**. **Figure 7.5** demonstrates the gating strategy to measure the binding of the aptamers. The binding of each DNA pool to monocytes in whole blood leukocytes was verified by the flow cytometric analysis (**Figure 7.6**).

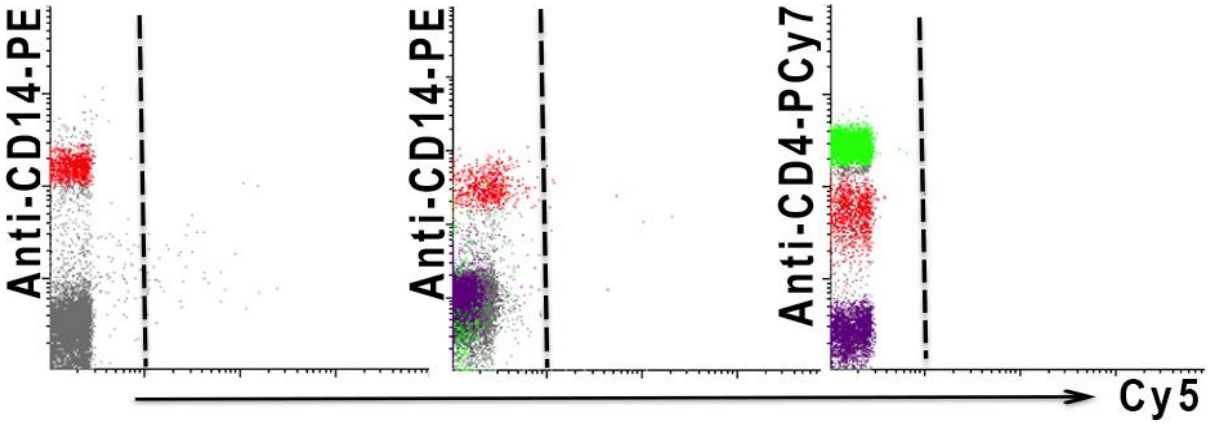

Figure 7.5. The gating strategy to evaluated the binding of the aptamers. Red color, green and purpel colores correspod to CD14 + monocytes, T-helper (CD3+/CD4+) cells and T-cytotoxic (CD4-/CD3+) cell, respectively.

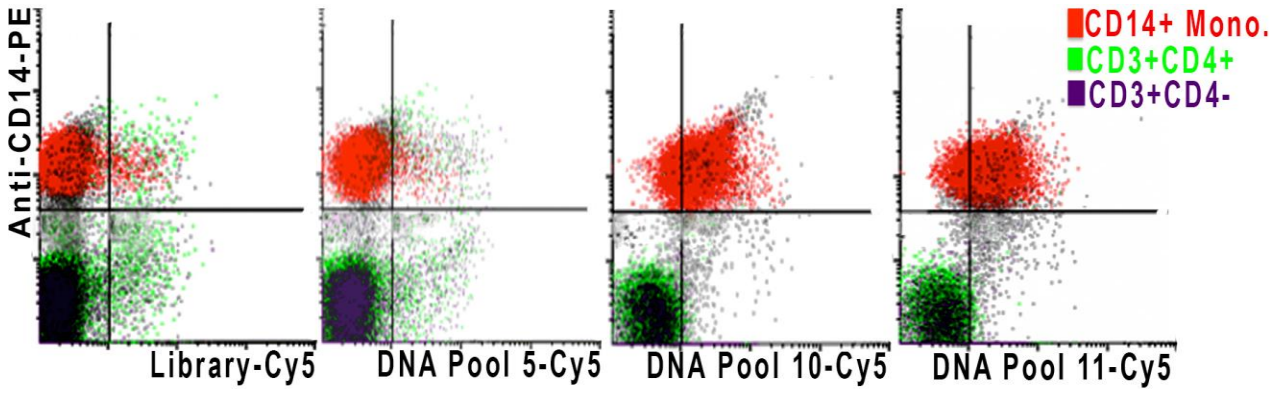

Figure 7.6. Whole blood leukocyte cell populations were stained with Cy5-labeled aptamer pools after rounds 5, 10, 11. The dot plot illustrates the fluorescence intensity distribution of cells incubated with Cy5-labeled ssDNA (ssDNA-Cy5). Red, green and purple populations represent monocytes CD14+, T-helper cells (CD4+ and CD3+) and Cytotoxic T cell (CD4- and CD3+) respectively. The colours were referred to the dot plots through CD3 vs. CD4, CD14 vs. SSC dot plots as shown at **Figure 7.4**.

The DNA pools with the most specific binding were barcoded, purified and submitted for next generation sequencing for two times read with 150bp length using MiSeq Next-Generation Sequencing System. The resulting fastq files were analyzed using the Galaxy software[150]. Error and noise level sequences were removed. Then, the sequences were clustered and grouped based on their common motifs. The leading 21 sequences **(Table 7.1)** were identified from 21 groups based on their abundance and homology.

Table 7.1. An example of the common motifs which resulted in Apt-2, Apt-6 and Apt-9.

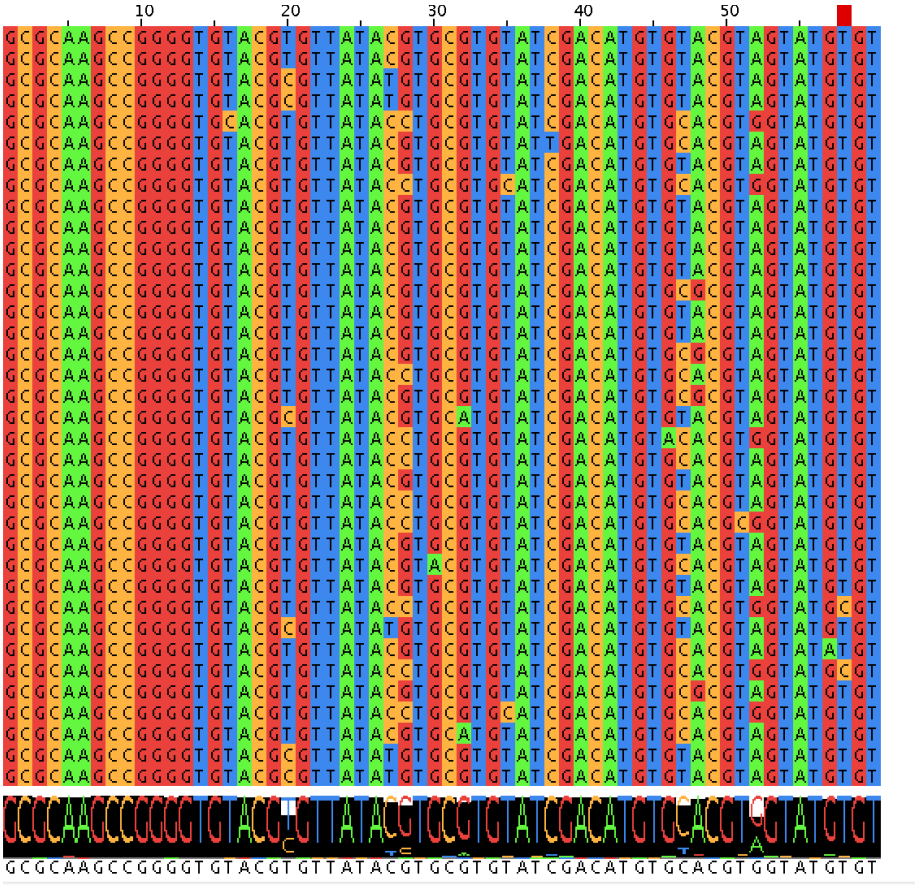

Table 7.2. The developed aptamers sequences to monocyte.

Name	Sequence
1	AGTCTCAGCTCCTCTGACTGCAACCACTTCGTGGTTACAGTCAGAGGAGGTCAGTCA
2	TCCTAGCGAGCATGCCTCCTCTGACTGTATCCACGGCGCAAGCCGGGGTGTACGTGTTAT
3	GTAGCTATGGCCACGTGCACATTCAGTATGCACGTTAATGCTCGCATGTCGTACGCGTGG
4	GTAGCTATGGCCACGTGCACATTCAGTATGCACGTTAATG
5	TGACGCGACTGTGCCTCCTCTGACTGTAATCACG
6	GCGCAAGCCGGGGTGTACGTGTTATACGTGCGTGTATCGACATGTGCACGTGGTATGTGT
7	GTCGTCTTTGTGTAGTATGTACCGTACGAGTTTGTGTGC
8	TGCCTACGTAGGGAAGTGCGCACCCGAGTTAGACCGATTG
9	GCGCAAGCCGGGGTGTACGTGTTATACGTGCGTGTATCGA
10	AAGTGGTTGCCGTGTACACATACCACGTGCACATGTCGATACACGCACGTATAACGCGTA
11	CCCAATCCCGCACCACGTGCATGCCACGCCCACGCATGAGTACACACGTACGGCGCATGT
12	CCCAATCCCGCACCACGTGCATGCCACGCCCACGCATGAG
13	AAGTGGTTGCCGTGTACACATACCACGTGCACATGTCGAT

14	GTTGATTGTGACCCTCATCGCGAGCAAGGACAGATGGGTG
15	AAGTGGTTGCAGTGTACACATACCACGTGCACATGTCGA
16	GCGCAAGCCGGGGTGTACGCGTTATACGTGCGTGTATCGACATGTGCACGTAGTATGTGT
17	TGACGCGACTGTGCCTCCTCTGACTGTAATCACGAAGTGGTTGCAGTGTACACATACCAC
18	TACACGCACGTATAACACGTA
19	TGACGCGACTGTGCCTCCTCTGACTGTAATCACGGCGCAAGCCGGGGTGTACGTGTTATA
20	TACACGCAGGTATAACACGTA
21	GCGCAAGCCGGGTGTACGTGTTATACGTGCGTGTATCGACATGTGCACGTGGTATGTGTA

The secondary structure of oligonucleotides was estimated based on their sequence and free energy minimization[186]. The aptamers structure and minimum free energy (kcal/mol) were estimated via RNAstructure web server (**Figure 7.7**)[162].

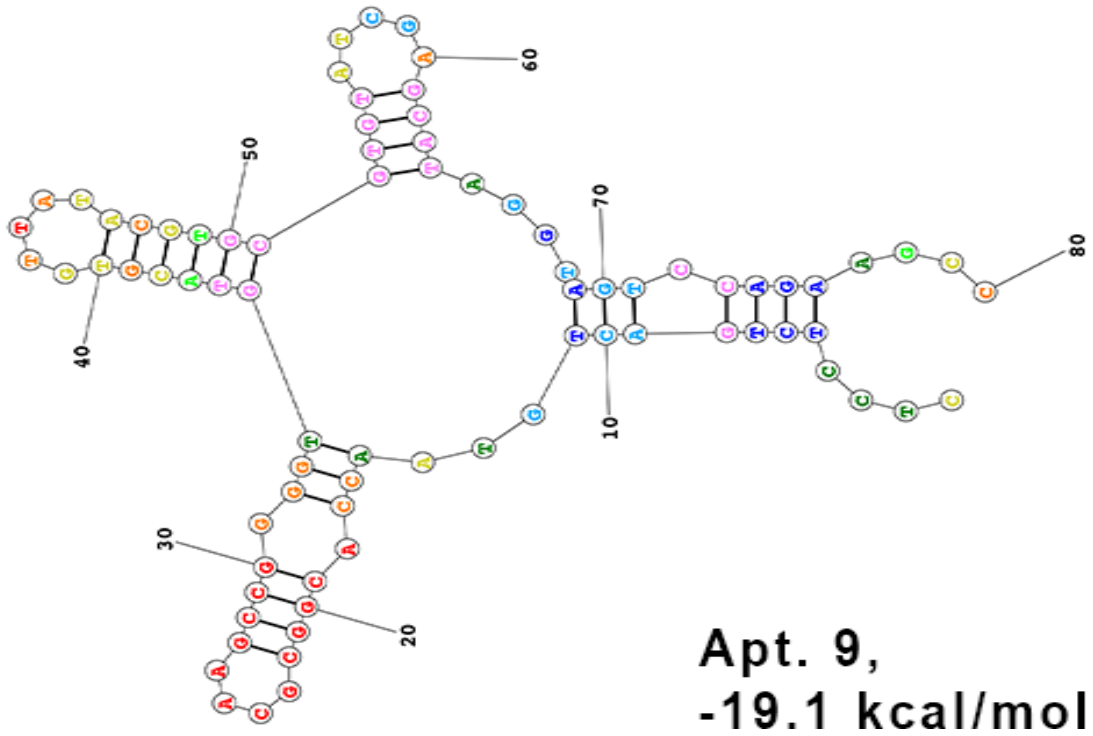

Figure 7.7. Secondary structure and minimum free energy (kcal/mol) of Apt-9. Aptamer-9 structure and minimum free energy were estimated via RNAstructure web software[162]. Next-generation sequencing identified the sequences after FACS Cell SELEX.

Twenty one aptamer clones were synthesized and tested for their affinity to monocytes in whole blood leukocytes (**Figure 7.7**). Apt-9 clone showed the highest binding and most specificity to monocytes (**Figure 7.8**). As shown in **Figure 7.10,** adding EDTA to the final concentration of 20 mM reduce Apt-9 binding.

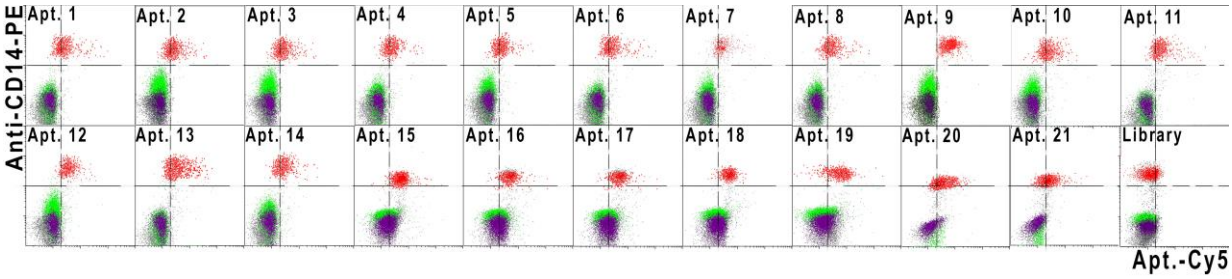

Figure 7.8. Binding of selected aptamers to monocyte in whole blood leukocyte. Cy5-labeled aptamers individually (200 nM) with anti-CD14-PE, anti-CD3-FITC, and anti-CD4-PCy7 were applyed to whole blood leukocytes in 200 µL of PBS with Ca^{2+}/Mg^{2+} for 30 min. After washing and re-suspension in 500 µL of PBS with Ca^{2+}/Mg^{2+}, cell fluorescence was determined by flow cytometry. CD14+ cells, CD3+CD4+ and CD3+CD4- were gated and marked respectively with red, green and purple color (Figure 7.4). The Cy5-labeled ssDNA library was used as a control for nonspecific binding tests.

Binding of apatamers (Apt-1 to Apt-13) to monocytes in whole blood leukocytes was assessed in the range of 0-400 nM to determine the half maximal binding (EC_{50}) concentration (**Figure 7.9).** In the heterogeneous whole blood leukocyte, Apt-9 presented a half maximum binding to monocyte of 115 nM.

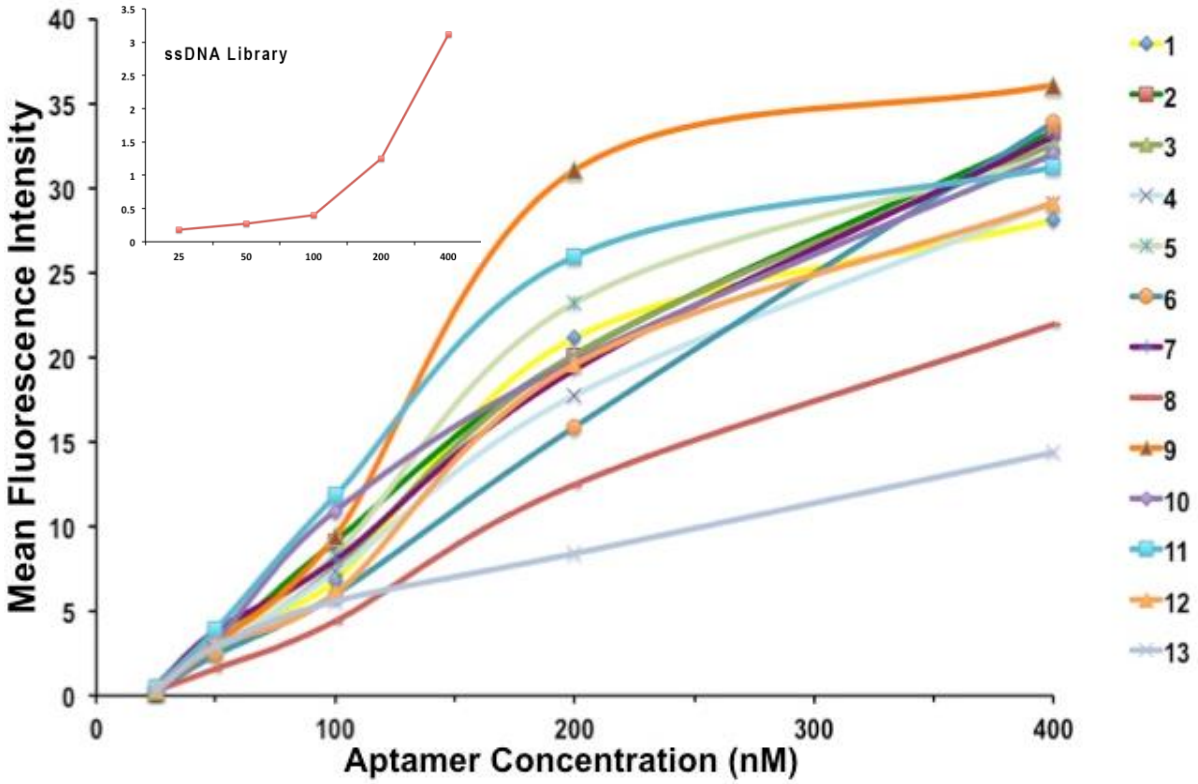

Figure 7.9. Titration curves of aptamer-cell interactions.

Whole blood leukocyte was incubated with corresponding aptamer clones at various concentrations in PBS with Ca^{2+}/Mg^{2} at room temperature for 30 minutes, washed and analyzed using flow cytometry to measure EC_{50} for each clone with binding affinity to monocytes among various cell populations in whole blood leukocyte.

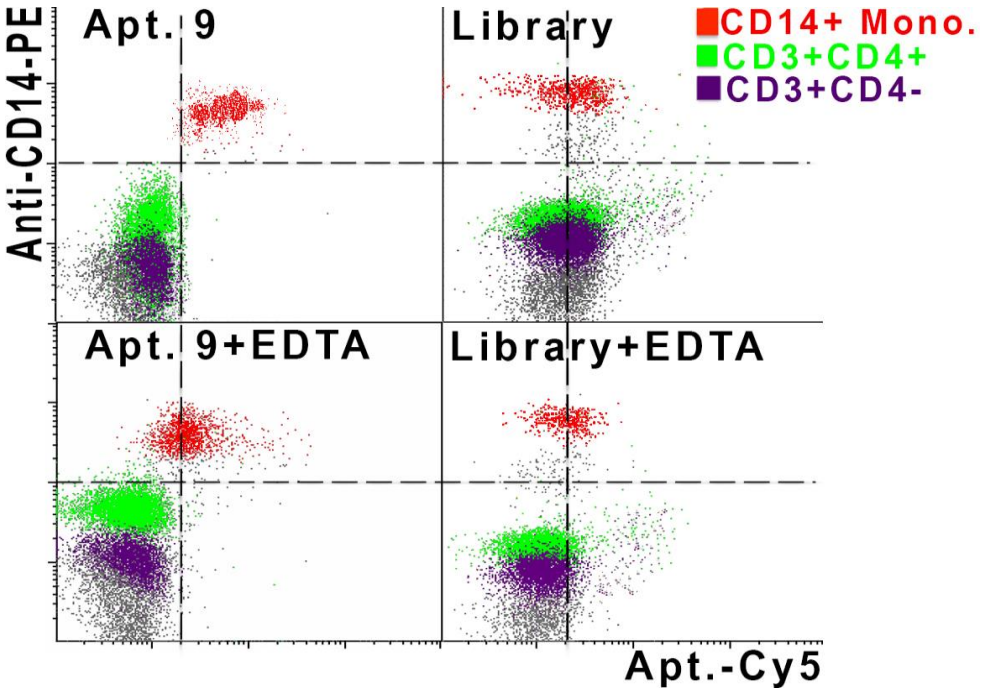

Figure 7.10. Cy5-labeled Apt. 9 (Apt. 9-Cy5) binding to monocyte in whole blood leukocyte and EDTA switchability in comparison to the ssDNA-Cy5 library. The affinity of Apt. 9-Cy5 and ssDNA library-Cy5 was analyzed by flow cytometry, which revealed specific binding of Apt. 9-Cy5 to monocyte in whole blood leukocyte. Binding was reduced upon addition of EDTA (20 mM). The affinity of Apt. 9-Cy5 and ssDNA library-Cy5 was investigated by flow cytometry and revealed specific binding of Apt. 9-Cy5 to monocyte (red dots) in whole blood leukocyte. The binding was reduced upon addition of EDTA (20 mM in total concentration). Red, green, and purple dots represent CD14+monocytes, CD3+CD4+ and CD3+CD4- cell populations respectively. The other cells were presented by the grey dots.

Apt-9 positive cell sorting by FACS

To characterize Apt-9 positive leukocyte cells, we sorted the aptamer positive cells using FACS and then stained them with antibodies against CD14, CD3 and CD4. The sorted cells were compared with whole blood leukocyte before sorting (**Figure 7.11**). The majority of sorted Apt-9 positive cells are CD14 positive as well.

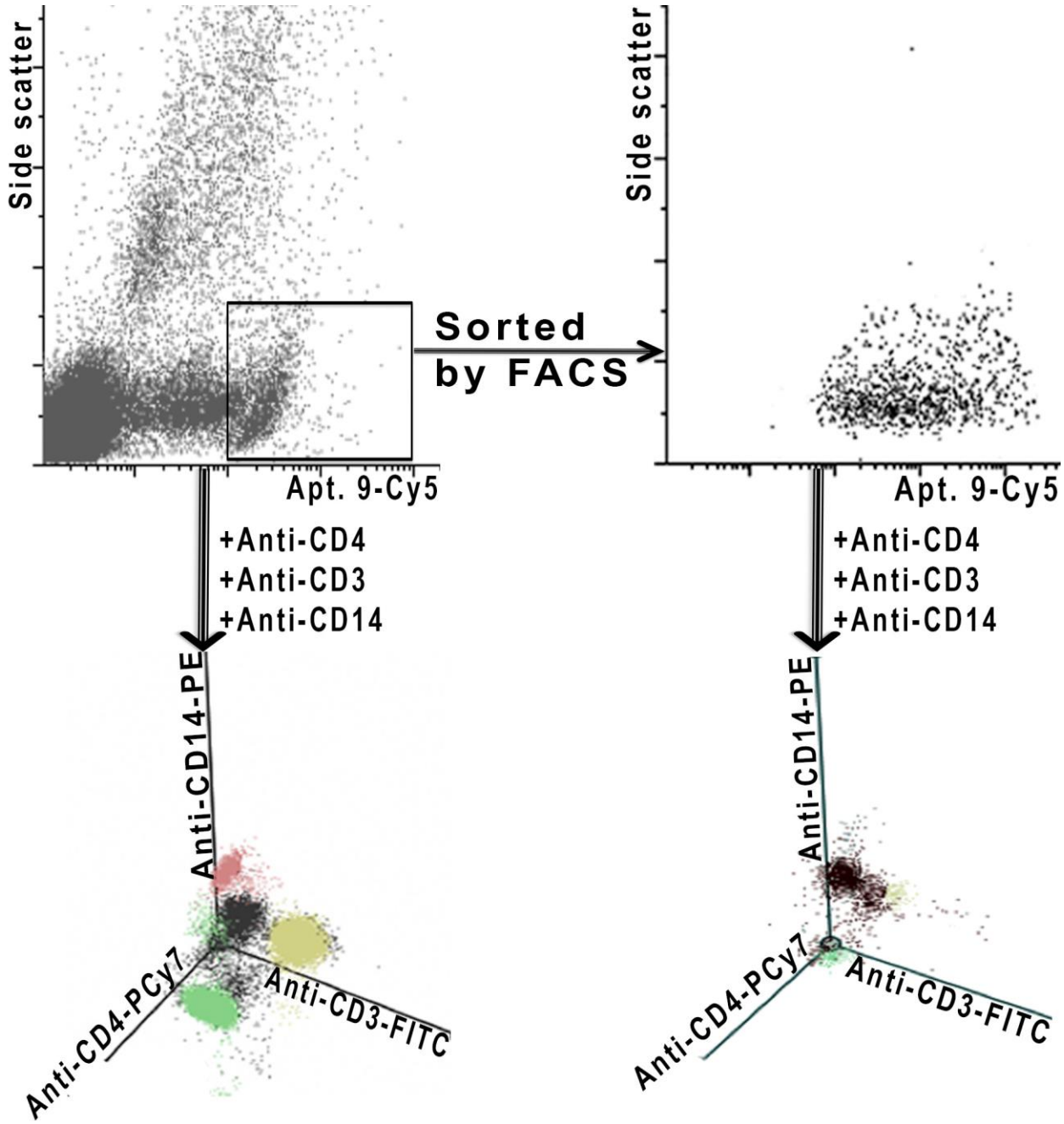

Figure 7.11. Flow cytometric analysis of whole blood leukocyte before and after Apt. 9 bound cell sorting by FACS. Apt. 9-Cy5 bound cells were gated inside scattering vs. Apt. 9-Cy5 and sorted by FACS. Whole blood leukocyte before and after sorting by FACS was incubated with antibodies against CD14, CD4, and CD3 and followed by flow cytometry.

Isolation and identification of Apt-9 molecular target

The identifying Apt-9 target protein is crucial as a biomarker for monocytes in whole blood leukocyte. Apt-9 selected uniquely to monocytes by FACS Cell SELEX can distinguishes them from other blood cells. The target of Apt-9 was confirmed to be a membrane protein since monocytes lost their binding to Apt-9 after adding EDTA. We used Apt-9 to isolate its binding partner for the following mass spectrometry-based protein identification **(Figure 7.12)**.

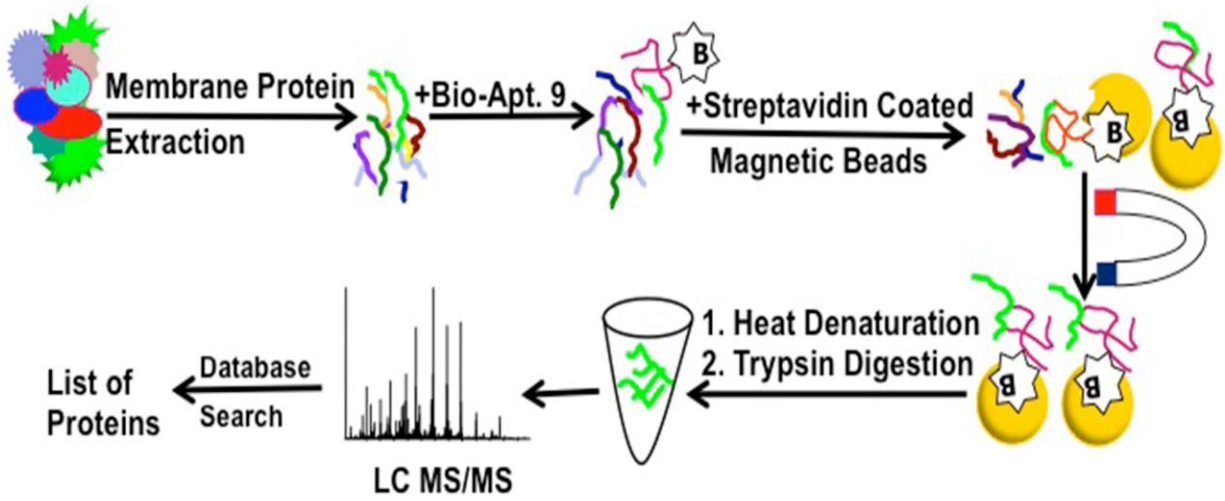

Figure 7.12. Scheme of Aptamer-facilitated biomarker discovery (AptaBiD).

For this, whole human blood leukocytes were lysed, and the membrane proteins were dissolved in PBS ($+Ca^{2+}/Mg^{2+}$) buffer with a surfactant. Then, 5′-biotinylated Apt-9 was incubated with the solubilized leukocyte membrane proteins in the presence of masking RNA to block potential non-specific binding sites. Streptavidin-coated magnetic beads were used to isolate Apt-9 and its targets on a magnet holder. The proteins bound to Apt-9 were pulled out using a magnet. They were washed three times with PBS ($+Ca^{2+}/Mg^{2+}$) buffer to remove unbound proteins and, then, were resuspended in pure water and heated to dissociate protein-

aptamer-streptavidin coated magnet beads complexes. Beads were then pulled out by a magnet. The solution holding the released proteins was collected, heated in the loading buffer and run on 12% SDS-PAGE (**Figure 7.13**).

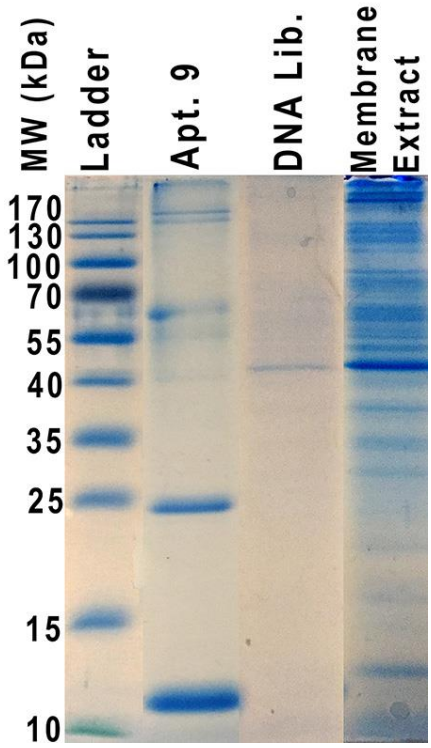

Figure 7.13. SDS-PAGE of the isolated proteins from whole blood leukocyte membrane proteins using biotinylated Apt-9 and streptavidin-coated magnetic beads. Lane 1 is the protein marker (10–170 kDa); lane 2 is Apt. 9 bound target proteins; lane 3 is ssDNA library bound target proteins, and Lane 4 is protein whole cell lysates.

As controls, ssDNA library was applied instead of the aptamer pools. Captured Apt-9 bands on the gel were compared to DNA library (control experiments) captured bands and cut for in-gel digestion by trypsin for experimentation employing nanoLC-Thermo Scientific Orbitrap Fusion Tribrid mass spectrometer. Results of the control experiments were deducted

from experiments with Apt-9 to get possible biomarker. Among the list of proteins, alpha-2-macroglobulin receptor (CD91) is the only cell surface transmembrane protein. S100a9, Filamin A, Serpin, annexin I and Hsp90 were recognized as co-binders with CD91.

We used antibodies against the proteins to evaluate CD91 as the target protein of Apt-9 on the cells. Flow cytometric analysis indicated that Apt-9, CD91, and CD14 dominantly target same population, monocytes (**Figure 7.14 a, b, c**). Flow cytometry results showed no significant competition between CD91 antibody and Apt-9 in the same staining experiments, revealing that they are not binding to the same epitope of CD91.

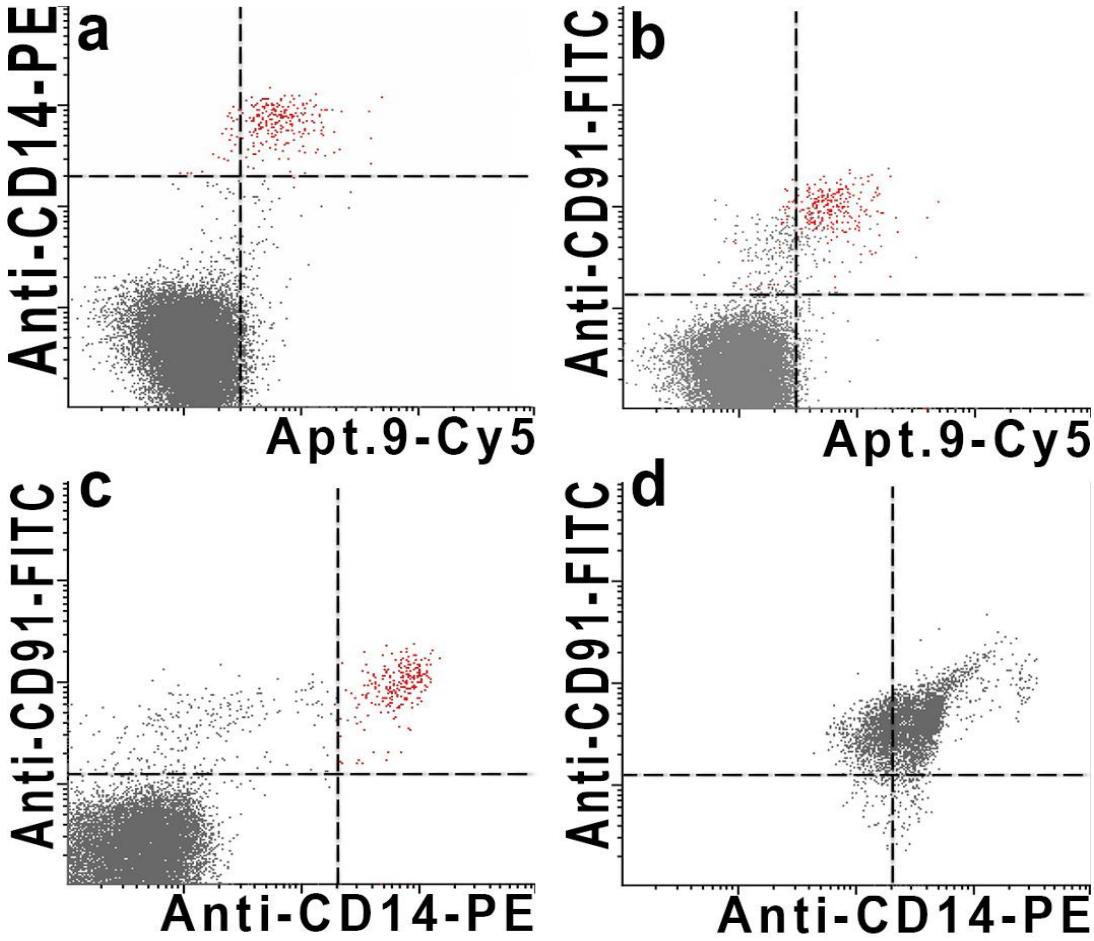

Figure 7.14. A flow cytometric assessment of Apt. 9-Cy5 target cells association in whole blood leukocyte samples with (a) CD14+ cells and (b) CD91+ cells and (c) co-stained CD14+ and CD91+ cells. Red colored cell are monocytes. (d) Flow cytometric analysis of cells captured by biotinylated Apt. 9 and pulled down by streptavidin-coated magnetic beads. The isolated cells were released by addition of EDTA and incubated with PE-conjugated antibody against CD14 (Anti-CD14-PE), and FITC-conjugated antibody against CD91 (Anti-CD91-FITC) for flow cytometric analysis.

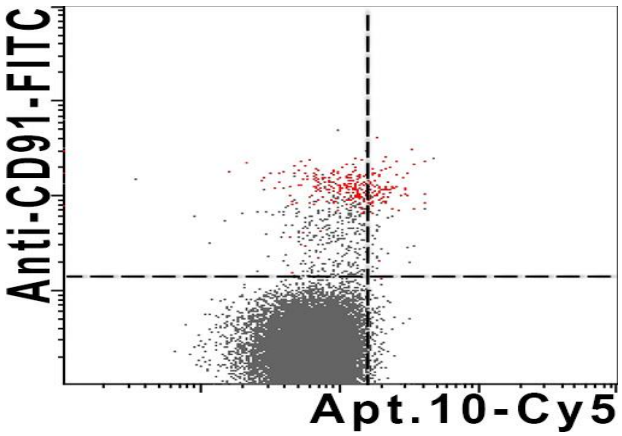

Figure 7.15. A flow cytometry assay of Apt. 10 and FITC conjugated antibody against CD91 population in blood leukocyte. According to mass spectrometry results, CD91 is a target protein for Apt. 9 but not for Apt. 10.

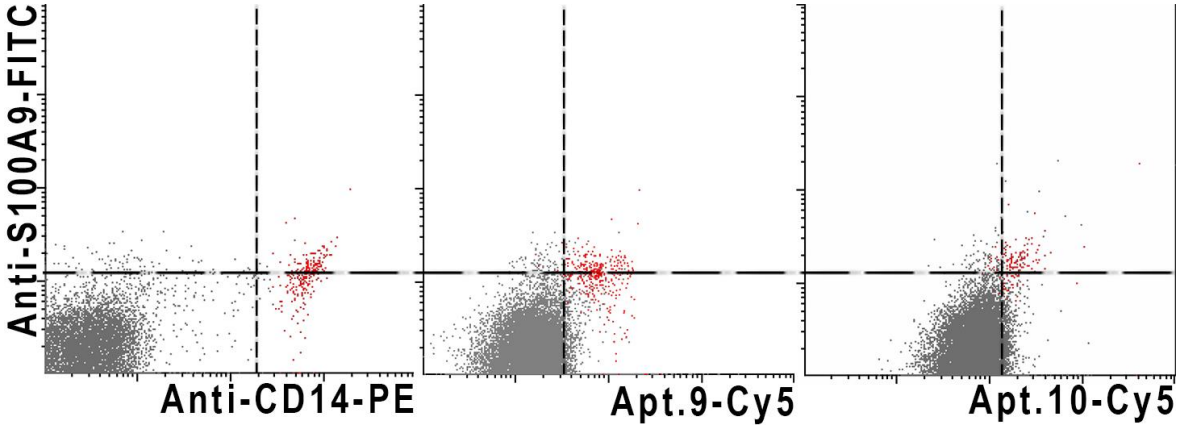

Figure 7.16. Target cell populations of Apt. 9 and Apt. 10 compared to the targets of antibody against S100A9.

Positive cell isolation with Apt-9 and magnetic beads

Here, we tested the capability of Apt-9 to isolate its target cells from a human leukocyte using magnetic beads using biotinylated Apt-9 and streptavidin-coated magnetic beads. First, we synthesized a 5'-biotinylated Apt-9. Biotin makes a bridge to bind the aptamer and streptavidin-coated beads. Second, the biotinylated Apt-9 was incubated with whole human blood leukocyte

in the presence of masking tRNA to block possible non-specific sites. After two washes and removal of unbound aptamers, the cells were incubated with streptavidin-coated magnetic beads. Third, a magnet was used to pull down magnetic bead-bound cells. Fourth, after three washes, the bound cells were released by adding EDTA to a final concentration of 20 mM. The isolated cells free of additives (aptamer and beads) were collected. The isolated cells were stained with antibodies against CD14 and CD91 for analysis by flow cytometry (**Figure 7.14D**). The cells isolated by Apt-9 compared to the whole blood leukocytes before isolation (**Figure 7.14 C**), showed the enrichment of the monocytes expressing both CD14 and CD91. CD91 can be considered as a potential marker for monocytes because Apt-9 targeting CD91 was able to detect monocytes among whole blood leukocytes.

EDTA switchable aptamer, Apt-9, was proven to be a viable alternative to antibodies in positive cell isolation. Furthermore, the isolated cells were free of impurities such as beads.

FACS – Cell SELEX empowered us to develop EDTA switchable aptamers to capture monocyte and provide pure cells without additives after isolation. Engaging mass spectrometry with FACS – Cell SELEX provided a unique marker of monocyte in a heterogeneous tissue of whole blood leukocytes. Among the selected aptamers, Apt-9 was the most specific aptamer for the positive isolation of monocytes from whole blood leukocytes with EDTA switch-ability to reveal intact monocytes. This approach facilitated the isolation of pure monocytes without additives such as magnetic beads and aptamers. Mass spectrometry identified CD91 as a possible candidate target molecule as well as S100a9, Filamin A, Serpin, annexin I and Hsp90 as co-binders with the generated aptamer and CD91 in human leukocyte membrane proteins.

In addition to generating EDTA switchable aptamers, FACS Cell SELEX and mass spectrometry achieved the identification of CD91, as an exclusive monocyte marker, as well as

co-binder proteins in blood leukocytes. Even though CD14 has been well known as a monocyte biomarker, it is not consistent on monocytes in different physiological states. CD33[187] and CD64[188] are suggested for identifying monocytes, but their expression varies in monocyte cells too[189]. Hudig et al. reported that CD91 expression on cell membranes is consistent and distinctively restricted to monocytes among blood cells [189].

CD91 as a multi-ligand receptor[190] is a direct cell surface receptor of Hsp90[187, 191]. Its interactions with filamin A protein was defined by proteomic approaches[192]. Wolfgang Nacken et al. stated that S100A9 expression is restricted to neutrophils and monocytes. S100A9 translocates from the cytosol to membrane in monocytes[193]. Paramita Chakraborty et al. detected S100A9 on monocytes[194]. While they described the binding of S100A9 and annexin I, they could not find the receptor that binds S100A9[193]. Nicolas J. Goulding et al. reported annexin I as a specific, saturable, trypsin-sensitive and calcium-dependent binder to monocytes, deprived of binding to lymphocytes[193, 195]. Later Eue et al. defined CD91 ligand, α_2-macroglobulin, as a binder partner for S100A9 monomer in endothelial cells [196]. CD91 is also reported as the best-characterized receptor for serpin[197]. The results that have been reported in the literature are comparable with the targets of Apt-9 and CD91, as an exclusive membrane marker of monocyte in human whole blood leukocytes.

Current positive isolation methods suffer from the persistence of additives after solitary confinement, which can alter cellular function and affect downstream applications. Also, present techniques target CD14 as a monocyte biomarker. CD14 is an inconsistent monocyte marker due to its presence on granulocytes and its variable expression in different physiological states of monocytes, which result in losing subpopulations of monocytes. Here, we show that Apt-9 with EDTA switchable binding to CD91 acts as an effective substitute to antibodies. Apt-9 binds

selectively to monocytes in the presence of Mg^{2+} and Ca^{2+} while releasing the captured cells upon addition of EDTA, allowing separation of cell in a straightforward and non-toxic way.

7.5. Conclusion

FACS cell-SELEX is an evolutionary approach involving high-affinity binding of ligands to targets on cells of the target cell population in a heterogeneous sample based on side scatter, forward scatter and fluorescent markers. This approach generates a spectrum of aptamers to the targets that discriminate between cell types in their natural folding and dynamic form existing in their physiological environment. This technique is efficient, rapid, and robust. The main problem of positive immunomagnetic and FACS isolation is in irreversible antibody binding, which can be solved by using EDTA-switchable aptamers. In addition to pure cell isolation and marker identification, the generated aptamers in FACS cell-SELEX can by potentially applied as probes in microscopic and flow cytometric studies, to track cells *in vivo* and as therapeutic agents to diseased tissues.

Chapter 8

Carbohydrate-based ice recrystallization inhibitors increase infectivity and thermostability of viral vectors

8.1. Objectives

The objective was to test the impact of carbohydrate-based ice recrystallization inhibitors (IRIs) on the potency of the viral vectors to the possible elimination of the cold chain and apply them to stabilize the potency of Vaccinia virus, Vesicular Stomatitis virus (VSV) and Herpes virus-1 (HSV-1).

Contributions

Shahrokh M. Ghobadloo and Maxim V. Berezovski conceived the idea and designed the research. Shahrokh M. Ghobadloo performed experiments. Anna K. Balcerzak, Chantelle J. Capicciotti and Jennie G. Briard synthesized carbohydrate-based ice recrystallization inhibitors and prepared Figure 5.2. Dr. Ana Gargaun performed capillary electrophoresis experiments. Gleb Mironov performed mass spectrometry experiments to study virus-small molecule binding. Shahrokh M. Ghobadloo and Anna K. Balcerzak wrote the paper. Robert N. Ben and Maxim V. Berezovski edited the manuscript and supervised the study.

8.2. Background

Vaccination is a public health success story saving 3 million lives each year. Many vaccines contain live attenuated viruses that have been cultivated under conditions that disable their virulent properties or closely-related but less dangerous viral vectors to produce a broad immune response or/and an anti-cancer (oncolytic) effect. The inability of viral vaccines to retain sufficient thermostability has been a significant obstacle to global vaccination programs and viral-based therapy.[88, 89] Elevated temperatures damage live viruses and while cryopreservation is the preferred method of storage, freezing dramatically reduces the titer of the virus. Furthermore, exposure to low temperatures associated with cryopreservation results in virus agglomeration, rendering the vaccine ineffective.[89, 94, 95] The World Health Organization has mandated that, for a vaccine to be considered "effective", less than 1 Log_{10} decrease in the original titer is tolerated. Several approaches like biomineralization, addition of silk or albumin have been applied but unfortunately, they often have multi-step preparation protocols or cause unwanted immune responses.[94, 95, 114, 117, 199-202] Consequently, novel methods for the preservation

of vaccines are urgently required. We employed carbohydrate-based ice recrystallization inhibitors to eliminate the cold chain and stabilize the potency of Vaccinia virus, VSV and HSV-1. The impact of these IRIs was tested on the potency of the viral vectors using a plaque forming unit assay following room temperature storage, cryopreservation with successive freeze-thaw cycles and lyophilization.

In this work, we examined the activity and thermostability of three live viral vectors from vesicular stomatitis virus (VSV), Vaccinia virus and herpes simplex virus type 1 (HSV-1), all of which are popular candidates for cancer vaccine development. For example, VSV-Δ51, has been shown to possess potent oncolytic properties[203] against a large number of potential tumor types.[72] VSV is a small bullet-shaped negative-strand RNA virus from the Rhabdoviridae family.[204] VSV selectively attacks tumor cells by taking advantage of defects in the interferon pathway.[77] Subsequently, VSV has been considered for clinical trials by Recombinant DNA Advisory Committee of NIH.[105, 205-207] Furthermore, VSV is being developed as a vaccine shuttle for an array of viral pathogens, such as HIV-1,[206] Ebola virus,[207] hepatitis B[104] and C[105]. JX-594 strain of Vaccinia virus is a member of the poxvirus family and has a large linear double-stranded DNA genome of approximately 200 kbp in length that encodes ~ 250 genes. It has several attributes that make it particularly well suited as an anticancer therapeutic.[208] Vaccinia virus is designed to attack cancer through three diverse mechanisms of action: 1) the lysis of cancer cells through viral replication, 2) the reduction of the blood supply to tumors through vascular targeting and destruction, and 3) the stimulation of the body's immune response against cancer cells. An attenuated HSV-1 strain, known as talimogene laherparepvec is a DNA oncolytic virus currently being studied for the treatment of melanoma and other advanced cancers by Amgen.

With the announcement of positive results in March 2013, it is the first oncolytic virus to be proven effective in a Phase III clinical trial.

8.3. Materials and methods

Compounds

The following compounds were assessed for their ability to preserve viral vectors: Ornithine–glycine–glycine-galactose (OGG-Gal), N-octyl-D-galactonamide (NOGal), N-octyl-D-gluconamide (NOGlc), N-octyl-D-galactonamide (NOGal), N-butyl-gluconamide, β-octyl-galactopyranoside, N-methyl-N-octyl gluconamide, sodium Nα-hexanoyl-Nε-decanoyl-L-lysinate, sodium Nα,Nε-bis(hexanoyl)-L-lysinate, sodium Nε-dodecanoy-L-lysinate, Nα-hexanoyl-Nε-hexyl-L-lysinate, N-octyl-β-D-galctopyranoside, L-lysine decyl ester dihydrochloride, L-lysine tetradecyl ester dihydrochloride, and L-lysine tetradecyl ester dihdrochloride.

Biological Experimental Details

U2OS and Vero cells were grown in Dulbecco's Modified Eagle Medium (DMEM) supplemented with 10% fetal bovine serum (FBS).

VSV Propagation

VSV, a recombinant VSV expressing the yellow fluorescent protein (YFP) or red fluorescent protein (RFP) was obtained from Dr. John Bell’s laboratory. VSV was propagated on Vero cells in the presence of 10% FBS. At 24 h post infection, the cell culture supernatant was

collected, and the cell debris was removed by centrifugation at 3,000 g for 20 min at 4 ºC. The virus was aliquoted and stored at -80 ºC after titration.

VSV Titration

The VSV plaque forming units were determined on a monolayer of Vero cells grown in 12- well culture plates. The cells were inoculated in duplicates of serial virus dilutions for 60 min at 37 ºC. Thereafter, Dulbecco's Modified Eagle Medium (DMEM, Invitrogen, CA) with 1% low melting agarose was added to each well, and the cells were incubated at 37 ºC. The cells were surveyed 24 h after infection using an Alfa Innotech Imaging System, Version 3.0.3.0 and the infectious virus titers were calculated based on the number of YFP- or RFP positive plaques per well and expressed as plaque forming units per milliliter (PFU mL^{-1}).

HSV-1 Titration

A sample of serial diluted HSV-1 expressing GFP in 250 μL of serum-free medium was added to a Vero cell monolayer (0.4×10^6 cells per well) in a 12-well culture plate. Inoculated cells were incubated for 1 h at 37 °C in a 5% CO2 humidified incubator and then cells were overlaid with 1 mL of fresh 1% agarose liquefied in DMEM. After 24 h of incubation, infected cells were visualized using Alfa Innotech Imaging System, Version 3.0.3.0 for GFP fluorescence. Also, a standard plaque assay was achieved, where the same plates were fixed with methanol−acetic acid fixative (3:1 ratio), stained with Coomassie Brilliant Blue R solution, and white plaques were counted.

Vaccinia virus propagation

Vaccinia virus was propagated in U2OS monolayer cultures at 37°C. Cells were infected with Vaccinia virus for 1 hour in DMEM at 37°C.The media was then replaced with fresh DMEM containing 10% FBS. After 48 hours, the supernatant of the infected cells was harvested by centrifugation at 650 g for 30 minutes at 4 °C. The pellets were then suspended in DMEM, and the virus was subsequently used as the stock of Vaccinia.

Vaccinia virus titration

The serial dilutions of Vaccinia virus were added to U2OS cells maintained in 12-well plates. Following virus binding to the cells at 37◦C for 1 hour, virus inoculum was aspirated and an overlay solution (a mixture of 1:1 volumes of 3% carboxymethylcellulose: 2x DMEM, 20% FBS) was added. After 48 hours of incubation, cells positive for GFP fluorescence were visualized by using Alfa Innotech Imaging System, Version 3.0.3.0. Also, a standard plaque assay was performed, where the overlay was removed, and the cell monolayer was stained with crystal violet for enumeration of the virus plaques.

Test to the co-infected cells by the viruses

Equimolar concentrations of YFP and RFP-expressing VSV were incubated with and without the compound for 1 hour at 37 ℃ and then used to infect cells plated on a chamber slide. After 1 hour of infection, cells were washed and overlaid with 0.5% low melting agarose with DMEM and supplemented with 10% FBS. After 24 hours of incubation at 37 °C in a 5% CO2 humidified incubator, cells were washed and analyzed by fluorescence microscopy. The cells expressing YFP, RFP, or both YFP and RFP were counted and analyzed.

Vaccinia virus incubation with NOGlc at 22 °C and analysis by capillary electrophoresis

Two aliquots of Vaccinia virus were prepared, with PBS, and with 40.67 µM NOGlc, and incubated at room temperature for 12 days. Prior to separating each sample by capillary electrophoresis, they were stained with 2.0 µM YOYO-1 fluorescent nucleic acid dye (Invitrogen, CA). As a control, a sample from the two aliquots of Vaccinia virus was stained with 2.0 µM YOYO-1 dye and subjected to separation by capillary electrophoresis without any incubation (Day 0).

A ProteomeLab PA 800 capillary electrophoresis system from Beckman-Coulter, Brea, USA, was used to separate Vaccinia virus. Fluorescence was induced by a 488-nm Ar-ion laser and detected at 520±10 nm. A bare silica-fused capillary was used, 60 cm in total length with 50 cm from injection to the detection point, an outer diameter of 365 µm and an inner diameter of 75 µm. The injections were done by a pressure pulse with hydrodynamic injection volumes of 39 nL. The electric field during the separation was 250 V cm^{-1}, with the positive charge at the inlet and ground at the outlet. The capillary temperature was maintained at 15 °C for the duration of the experiment. The run buffer was 25 mM sodium tetraborate at pH 9.84. Prior to each injection, the capillary was rinsed by applying 20.0 psi of 100 mM HCl, 100 mM NaOH, ddH2O, and 25 mM Borax for 2.5 minutes each. 32 Karat^{TM} software (Beckman-Coulter, Brea, USA) was used for recording the electropherograms and final electropherograms were produced by Excel (Microsoft).

Air-dried Vaccinia virus and VSV infectivity assay

Vaccinia virus or VSV suspended in DMEM with or without the selected compounds was added to flat-bottom 12-well culture dishes. The suspension was directly added to the polystyrene bottom of the wells. The virus was dried under a laminar flow for 60 minutes before the plate was covered with a lid and kept at room temperature. The dried virus was resuspended in DMEM and titrated on Vero cells. The infectivity of Vaccinia virus (600,000 PFU mL^{-1}) suspended in selected IRIs, which were dried under a laminar flow for 60 min before being covered with a lid and kept at room temperature, are depicted in (**Figure 8.1b**). The results of the plaque-forming assay show that Vaccinia virus in the presence of NOGlc was twice as infective as the control. In the same way to determine the effectiveness of IRIs at stabilizing air-dried VSV, a solution of OGG-Gal with VSV (4×1010 PFU mL^{-1}) was dried under laminar flow for 60 min at room temperature. The assay indicated that OGG-Gal is 30% more effective at protecting VSV than the control (**Figure 8.1**).

Assessing Ice Recrystallization Inhibition (IRI) Activity

Sample analysis for IRI activity was performed using the "splat cooling" method as previously described.[209] In this method, the analyte was dissolved in phosphate buffered saline (PBS) solution and a 10 μL droplet of this solution was dropped from a micropipette through a two meter high plastic tube (10 cm in diameter) onto a block of polished aluminum precooled to approximately -80 °C. The droplet froze instantly on the polished aluminum block and was approximately 1 cm in diameter and 20 μm thick. This wafer was then carefully removed from the surface of the block and transferred to a cryostage held at -6.4 °C for annealing. After a period of 30 min, the wafer was photographed between crossed polarizing filters using a digital

camera (Nikon CoolPix 5000) fitted to the microscope. A total of three images were taken from each wafer. During flash freezing, ice crystals spontaneously nucleated from the supercooled solution. These initial crystals were relatively homogeneous in size and quite small. During the annealing cycle, recrystallization occurred, resulting in a dramatic increase in ice crystal size. A quantitative measure of the difference in recrystallization inhibition of two compounds X and Y is the difference in the dynamics of the ice crystal size distribution. Image analysis of the ice wafers was performed using a novel domain recognition software (DRS) program.[210] This processing employed the Microsoft Windows Graphical User Interface to allow a user to visually demarcate and store the vertices of ice domains in a digital micrograph. The data was then used to calculate the domain areas. All data was plotted and analyzed using Microsoft Excel. The mean grain (or ice crystal) size (MGS) of the sample was compared to the MGS of the control PBS solution for that same day of testing. IRI activity is reported as the percentage of the MGS (% MGS) relative to the PBS control, and the % MGS for each sample was plotted along with its standard error of the mean. Large percentages represent a large MGS, which is indicative of poor IRI activity.

8.4. Results and discussion

We examined thirteen compounds to preserve Vaccinia virus, HSV-1 and VSV at room temperature storage, during successive freeze-thaw cycles and lyophilization, and identified three promising ice recrystallization inhibitors, ornithine-glycine-glycine-galactose (OGG-Gal), N-octyl-D-gluconamide (NOGlc) and N-octyl-D-galactonamide (NOGal) (**Figure 8.2a**). All of these compounds demonstrate the ability to inhibit ice recrystallization[94, 211] and significantly increase the infectivity and thermostability of the viruses. OGG-Gal is a C-linked analogue of

naturally occurring antifreeze glycoproteins (AFGPs)[212] which allow arctic fish to survive in sub-zero temperatures.[213] OGG-Gal has been shown to be a potent inhibitor of ice recrystallization without the property of thermal hysteresis,[212] which can be detrimental to biological samples at low temperatures. Until recently, many structure-function studies of native AFGPs were only assessed for thermal hysteresis activity and not ice recrystallization activity.[214] However, more recent studies have explored the relationships between AFGP analogues and IRI activity.[215] The open-chain carbohydrates or alditols, NOGlc and NOGal, are hydrogelators that are capable of immobilizing water molecules into three-dimensional networks having morphologies of fibers.[216, 217] Their ability to inhibit ice recrystallization was assessed using the standard "splat-cooling" assay[209, 212] in which ice crystal size was determined using photographs of frozen ice wafers after a 30 min annealing time at -6.4 °C. The mean grain ice crystal size was determined using domain recognition software[210] and compared to a phosphate buffered saline (PBS) solution as a control. As illustrated in **Figure 8.2b**, OGG-Gal is an extremely potent IRI at a concentration of 5.5 μM. In comparison, alditol NOGlc exhibits potent IRI activity only at 500 μM. Shortening the hydrophobic side chain in NOGlc results in a loss of IRI activity, indicating that the amphiphilic nature of these alditols is an essential property.[218] Interestingly, replacing the glucose alditol portion of NOGlc with a galactose alditol portion (NOGal) results in weak to moderate IRI activity, indicating that the stereochemical arrangement of the hydroxyl groups in the polyol component is an essential structural feature necessary for potent IRI activity as these two compounds only differ by one single stereocentre (indicated by boxes in **Figure 8.2a**).

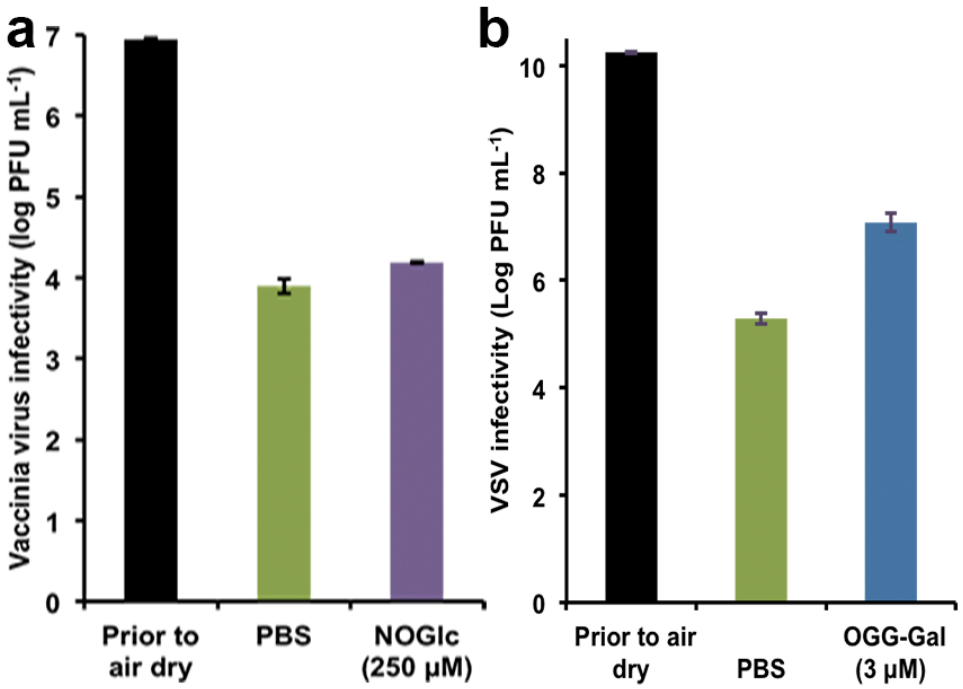

Figure 8.1. Air-dried viral vectors infectivity. a) air-dried Vaccinia virus in NOGlc solution b)VSV in OGG-Gal solution. Error bars indicate standard deviation (Microsoft Excel, version 2011). Reprinted with permission from[198].

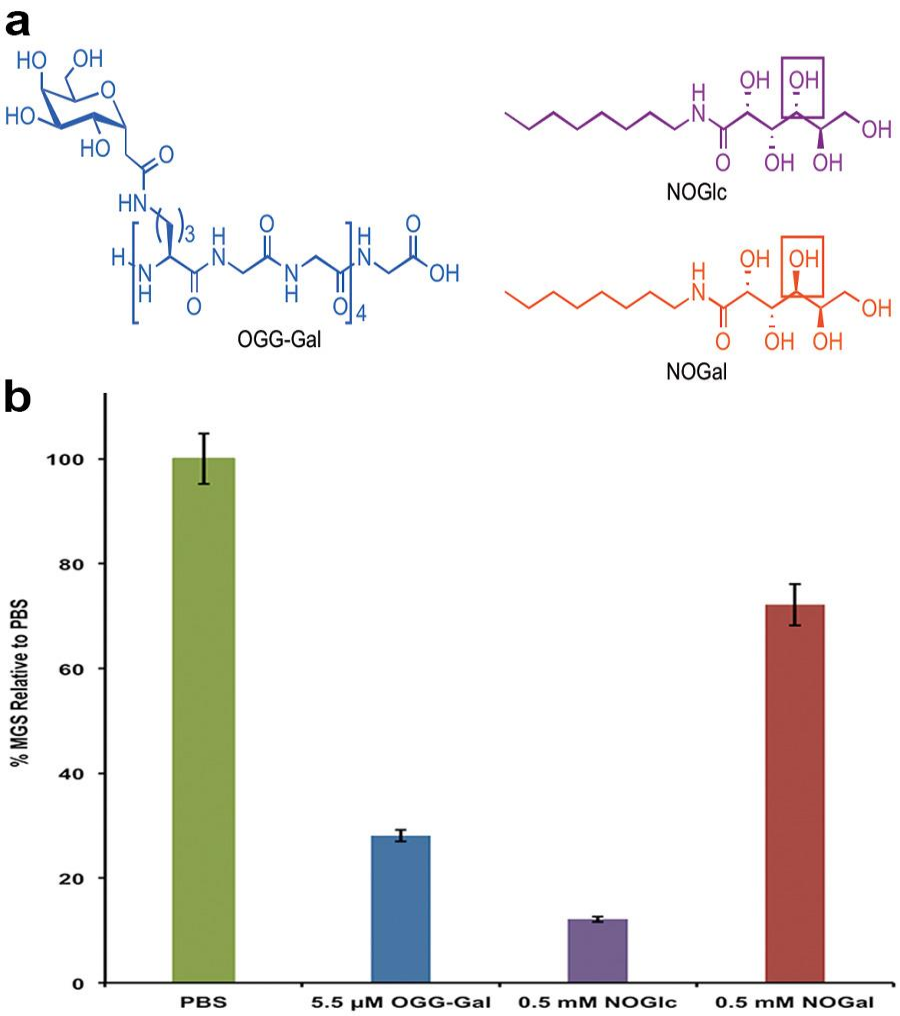

Figure 8.2. a) Structures of ice recrystallization inhibitors OGG-Gal, NOGlc and NOGal. Boxes highlight differences in stereochemistry. b) Ice recrystallization inhibition activity. The mean grain ice crystal sizes (MGS) are compared to a PBS standard. Error bars indicate standard error of the mean. Error bars indicate standard deviation (Microsoft Excel, version 2011). Reprinted with permission from[198].

It is hypothesized that the mechanism by which these compounds inhibit ice recrystallization is though the disruption of the bulk water present between ice crystal boundaries.[219] As ice crystals grow, all solutes are excluded, and the ice recrystallization inhibitors (IRIs) are concentrated at the interface of two ice crystals, where the interface consists of semi-ordered ice (quasi-liquid layer) separated by a layer of bulk water. It is thought that the hydration shell of the IRIs disrupts the ordering of bulk water, therefore, causing an increase in

energy for the transfer of water molecules from bulk water to the ice lattice. Although the structure and molecular weights of OGG-Gal and the small IRIs is significantly different, the mechanism for ice recrystallization is thought to be the same. Further studies must be performed to determine the toxicity and immunogenicity of these compounds in animals.

The most potent compound resulting in stabilization of Vaccinia virus and HSV-1 at room temperature is NOGlc. Vaccinia virus and HSV-1 with and without 250 μM NOGlc were stored at 22 ºC and the infectivity of the viruses was determined counting plaque-forming units (PFU) in a cell-based assay. Three parallel experiments had been done in duplicate assay. The averages and standard deviations were calculated using Microsoft Excel, version 2011. These data are represented by curves of logarithmic infectivity versus time (**Figure 8.3**). As a control, the infectivity of Vaccinia virus in PBS declined more than 1 Log10 PFU mL-1 in the first 8 days of storage and the ability to infect host cells was completely lost after 40 days. However, in the presence of NOGlc the infectivity decreased by only 0.2 Log10 PFU mL-1 after 40 days storage at room temperature (**Figure 8.3a**).

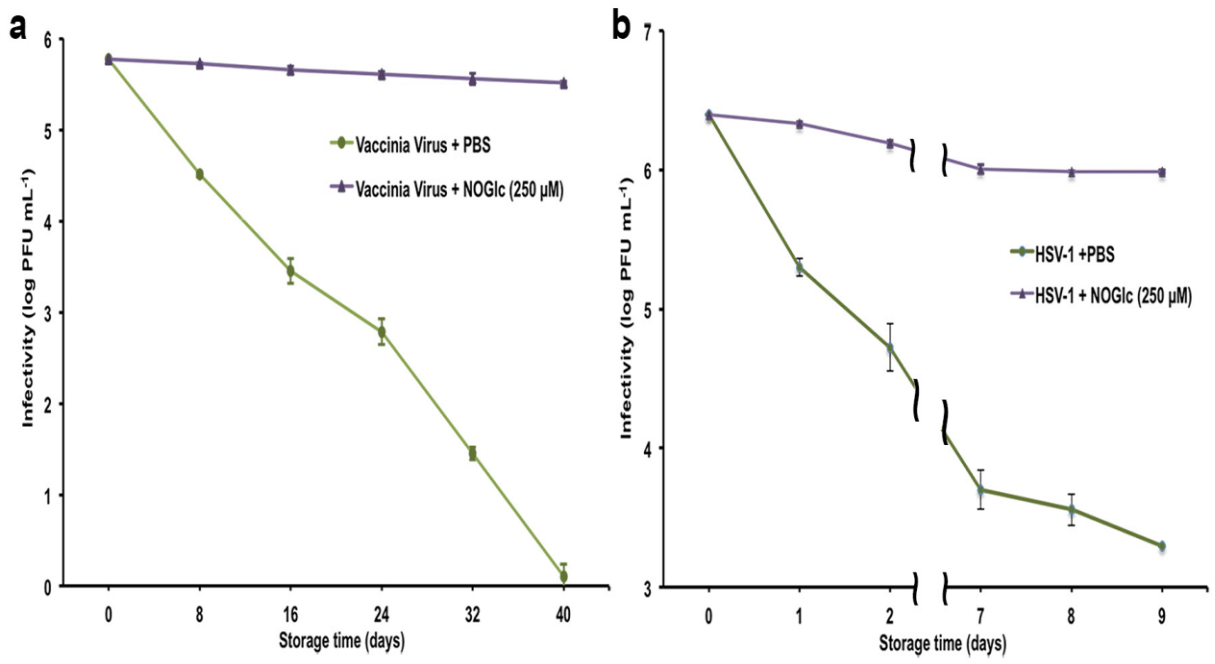

Figure 8.3. NOGlc impact on stored virus at 22 °C: a) Vaccinia virus infectivity during 40 days. b) HSV-1 infectivity during 9 days. Error bars indicate standard deviation (Microsoft Excel, version 2011). Reprinted with permission from[198].

These results were confirmed by viral quantitative capillary electrophoresis (viral qCE),[122] where the intact virus particles were separated from free DNA present after virus degradation (**Figure 8.4**).

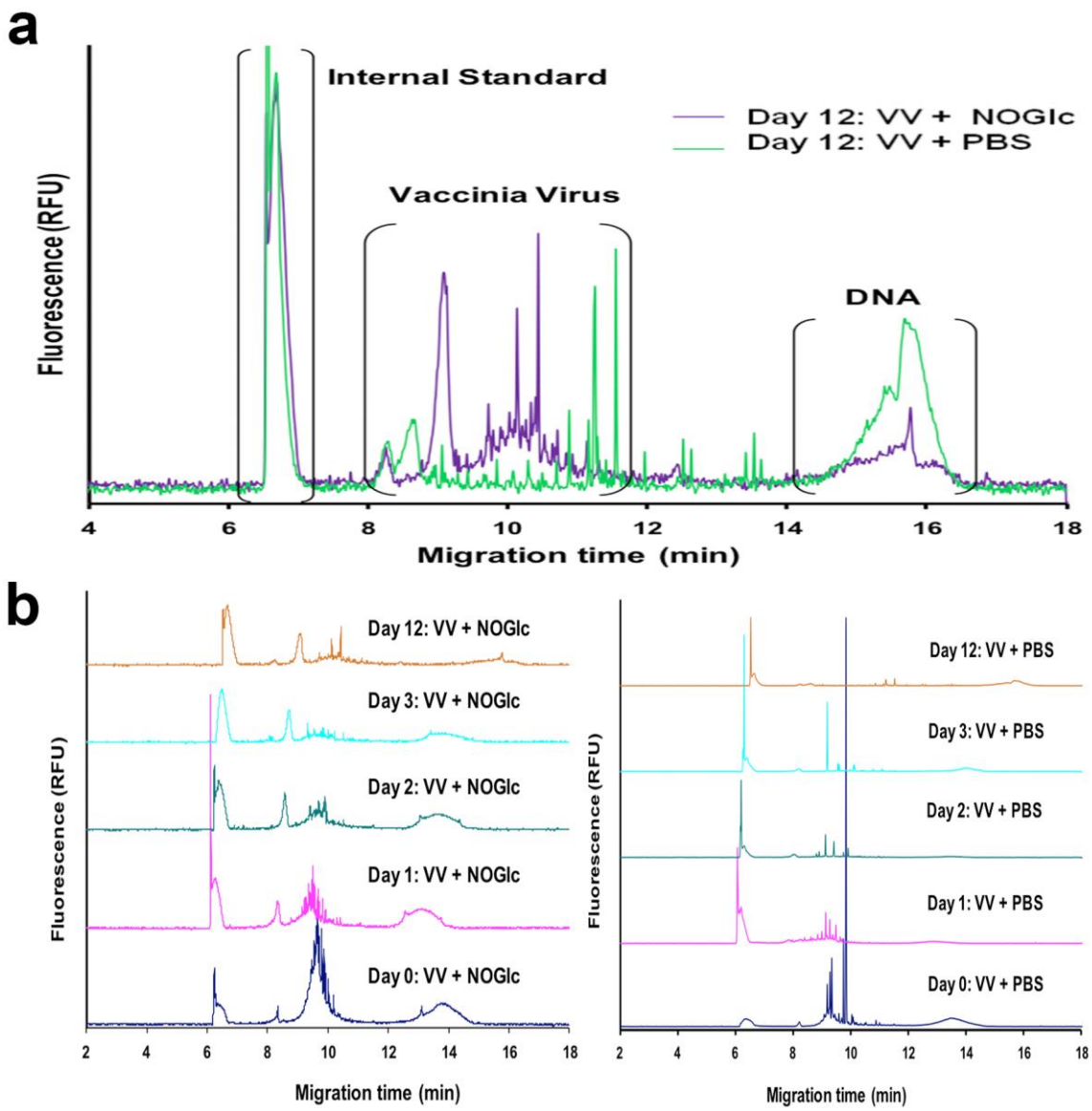

Figure 8.4. Electropherograms for Vaccinia virus separated by capillary electrophoresis (CE) and detected by laser induced fluorescence after incubation with PBS or NOGlc at 22 °C for 12 days. A) Vaccinia virus separated by CE after 12 days of incubation with NOGlc and PBS. B) Separation of Vaccinia virus by CE on various days of incubation with NOGlc and PBS. All samples were stained with YOYO®-1 dye. CE separations were performed in a 60 cm long capillary under 250 V cm-1 in 25 mM borax buffer at 15 °C. Reprinted with permission from[198].

Vaccinia virus degraded slower when incubated with NOGlc than with PBS as more Vaccinia virus peaks and less DNA was observed. We also tested the ability of NOGlc to stabilize HSV-1 at ambient temperature. While the reduction of untreated HSV-1 infectivity was

1 Log10 PFU mL^{-1} after one day, NOGlc treated HSV-1 lost only 0.05 Log10 PFU mL^{-1} of its infectivity on the first day and only 0.41 Log10 PFU mL^{-1} after 9 days, the maximum number of tested days for HSV-1. The experiments had been done three times in parallel. The assays were duplicated. The averages and standard deviations were calculated using Microsoft Excel, version 2011 (**Figure 8.3b**).

While working with Vaccinia virus and VSV we found that even after multiple exposures to −20ºC temperatures, the addition of carbohydrate-based IRIs prevented the damage caused by successive freezing and thawing. For instance, Vaccinia virus treated with OGG-Gal, NOGal and NOGlc lost 0.3, 1.3 and 0.5 Log10 PFU mL^{-1} respectively after 10 freeze-thaw cycles, compared with 1.7 Log10 PFU mL^{-1} lost in a control experiment with PBS (**Figure 8.6a**). Titration experiments demonstrate that the protective effect and ultimately the infectivity of Vaccinia virus was improved with increasing concentrations of NOGlc. The maximum protective effect with NOGal for Vaccinia virus was observed at 62.5 nM (**Figure 8.5a and Figure 8.5b**).

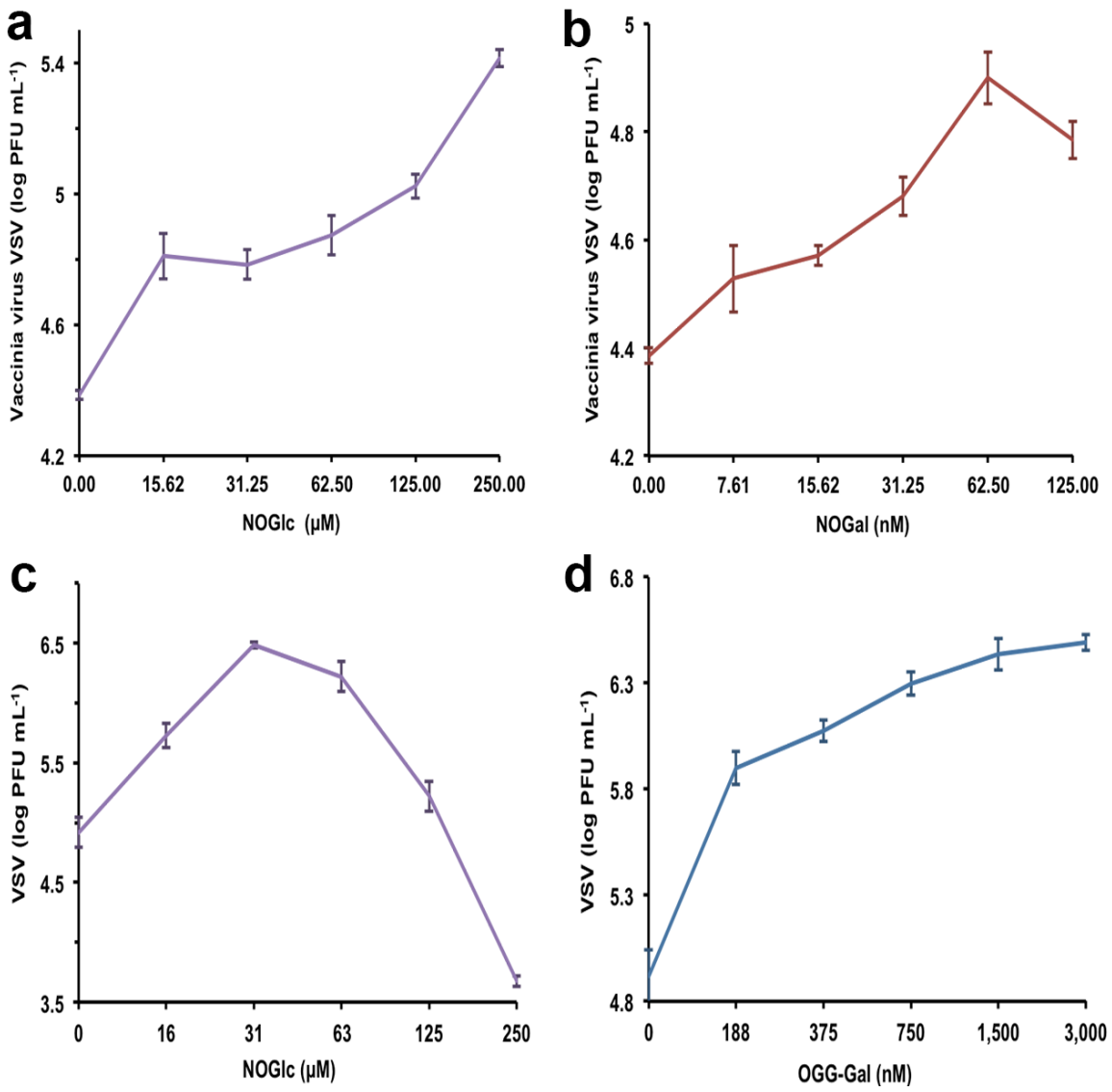

Figure 8.5. Dosage effect assessment by number of plaques formed. a) Vaccinia virus treated with NOGlc b) Vaccinia virus treated with NOGal c) VSV treated with NOGlc d) VSV with OGG-Gal. Error bars indicate standard deviation (Microsoft Excel, version 2011). Reprinted with permission from[198].

The infectivity of VSV in the presence of OGG-Gal and NOGlc was almost 2.1 Log10 higher than a control after 10 freeze-thaw cycles (**Figure 8.6b**). Titration experiments revealed the maximum protection of VSV at 31 μM of NOGlc and 3 μM of OGG-Gal (**Figure 8.5d and Figure 8.5c**).

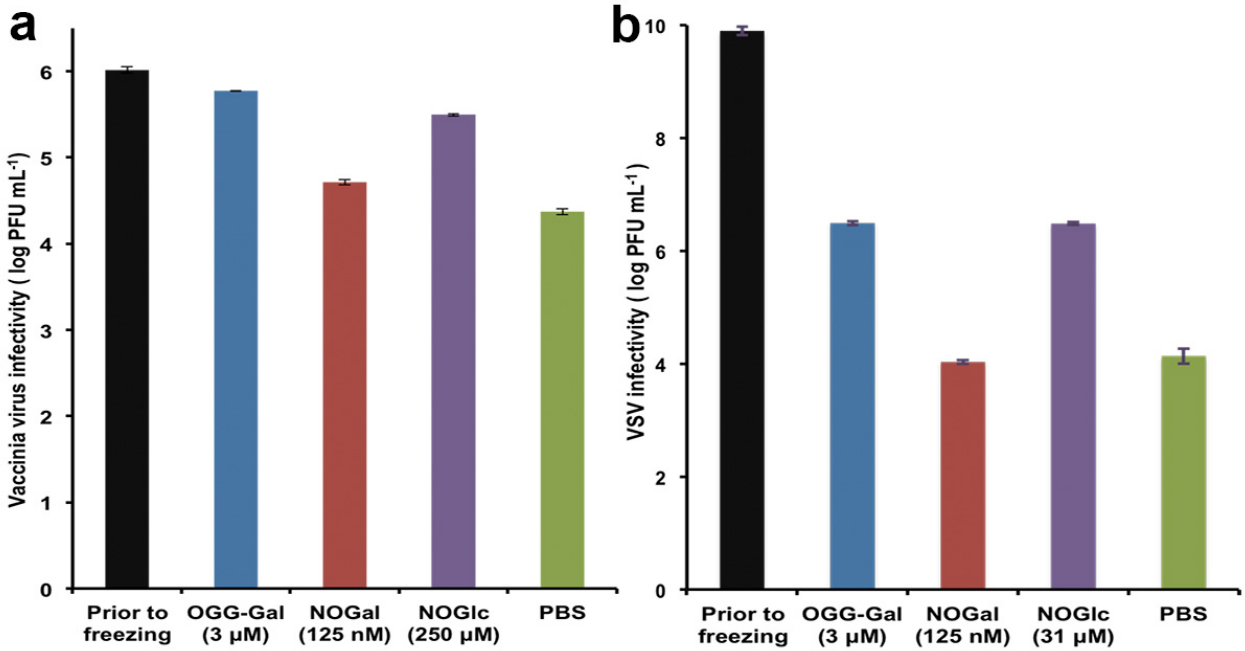

Figure 8.6. The impact of ice recrystallization inhibitors on viral vector infectivity after 10 freeze-thaw cycles on a) Vaccinia virus and b) VSV. Error bars indicate standard deviation (Microsoft Excel, version 2011). Reprinted with permission from[198].

Regardless of how effective a vaccine may be in the laboratory unless the suspension can be stabilized for storage and distribution, its commercial potential will be limited. Lyophilization (freeze-drying) is a well-established technique used in the pharmaceutical industry for stabilizing high-cost, labile bio-products, such as vaccines. We examined the ability of our carbohydrate-based IRIs to preserve Vaccinia virus and VSV during the lyophilization process. As controls, we had tested 2% bovine serum albumin, fetal calf serum, and glycerol as preservers just prior the test virus lyophilization. The recovery of the test viruses was the same as diluted viruses in PBS. Prior to lyophilization, Vaccinia virus infectivity was 6 Log10 PFU mL^{-1} but in the presence of OGG-Gal, NOGal, NOGlc and PBS Vaccinia virus infectivity was reduced by 0.68, 1.37, 1.06 and 2 Log10 PFU mL^{-1}, respectively (**Figure 8.7a**). OGG-Gal showed the most promising result with only 0.68 Log10 PFU mL-1 reduction compared to 2 Log10 of PBS

control. The infectivity of VSV in the presence of OGG-Gal, NOGal, NOGlc and PBS was reduced by 5-6 Log10 PFU mL^{-1} (**Figure 8.7b**).

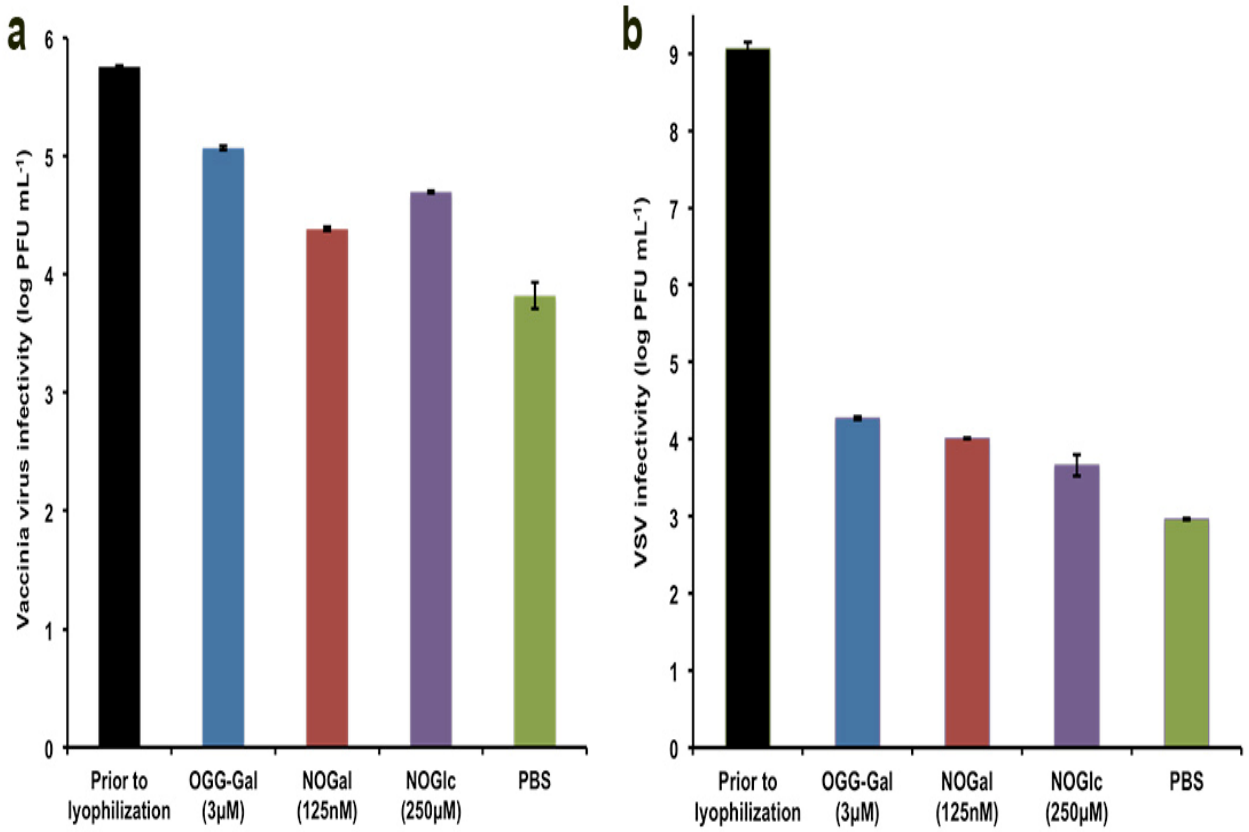

Figure 8.7. Effect of ice recrystallization inhibitors on viral vectors infectivity after lyophilisation of a) Vaccinia virus and b) VSV. Error bars indicate standard deviation (Microsoft Excel, version 2011). Reprinted with permission from[198].

The question of why do these compounds protect viral vectors appears to be complex, as the same compounds provide protection with both storage methods. It is accepted that the majority of damage to bio-materials during cryopreservation is due to ice recrystallization that occurs during the storage and thawing cycles (assuming adequate dehydration during the rate controlled freezing process as described by Mazur's two stage hypothesis of cryoinjury). In lyophilization, samples are flash frozen, and ice crystals are removed by sublimation. Under

both conditions, it seems reasonable that the ability of an ice recrystallization inhibitor to mitigate ice growth would be beneficial and ultimately protect against cryoinjury in both processes. However, another reason for decreased infectivity in cryopreserved and lyophilized samples is aggregation or agglomeration of virus particles. Consequently, we evaluated the impact of OGG-Gal on VSV co-infecting after one freeze-thaw cycle using two different VSV expressing either yellow fluorescent protein (YPF) or red fluorescence protein (RFP). Galasso G. et al. using electron microscopy showed that when a cell monolayer is infected with a low proportion of virus, one active viral particle can infect one cell and an aggregation several infectious particles lead only one cell infection.[123] An overlay of 1% Agarose restricts the spread of the virus to neighbor cells. Hence, in this assay, a single virus with either RFP or YFP will infect a single host cell. In instances where aggregation of the virus particles occurs, multiple virus particles enter the cell, and both red and yellow fluorescence is observed. After viral infection of cells with a mixture of two viruses, we detected fluorescent proteins and their localizations inside the cells (**Figure 8.8**). In the presence of OGG-Gal, the agglomeration of VSV dropped almost 2 times from 34±3.8% to 16±3.0% (**Figure 8.8b**).

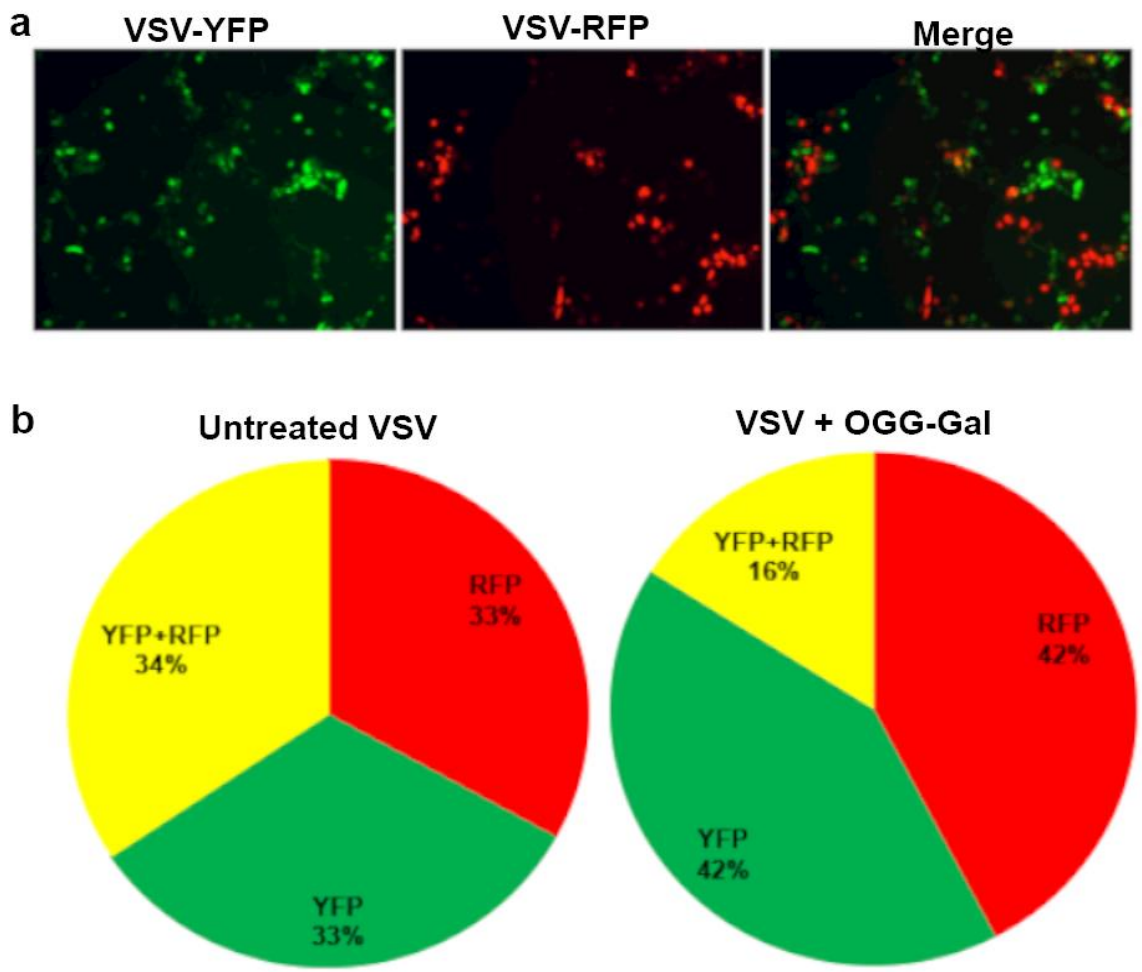

Figure 8.8. Cells infected with a mixture consisting of equal amounts of VSVs expressing YFP and RFP; a) cells expressing YFP, RFP, and both YFP and RFP, respectively. b) Percentage of cells infected by YFP, RFP, and both YFP and RFP for untreated, and OGG-Gal treated VSV. The palque forming assay had been done after one freeze-thaw cycle. Reprinted with permission from[198].

It is interesting to note that direct addition of the carbohydrate-based IRIs to a virus sample increases its infectivity by approximately 20% (**Figure 8.9**).

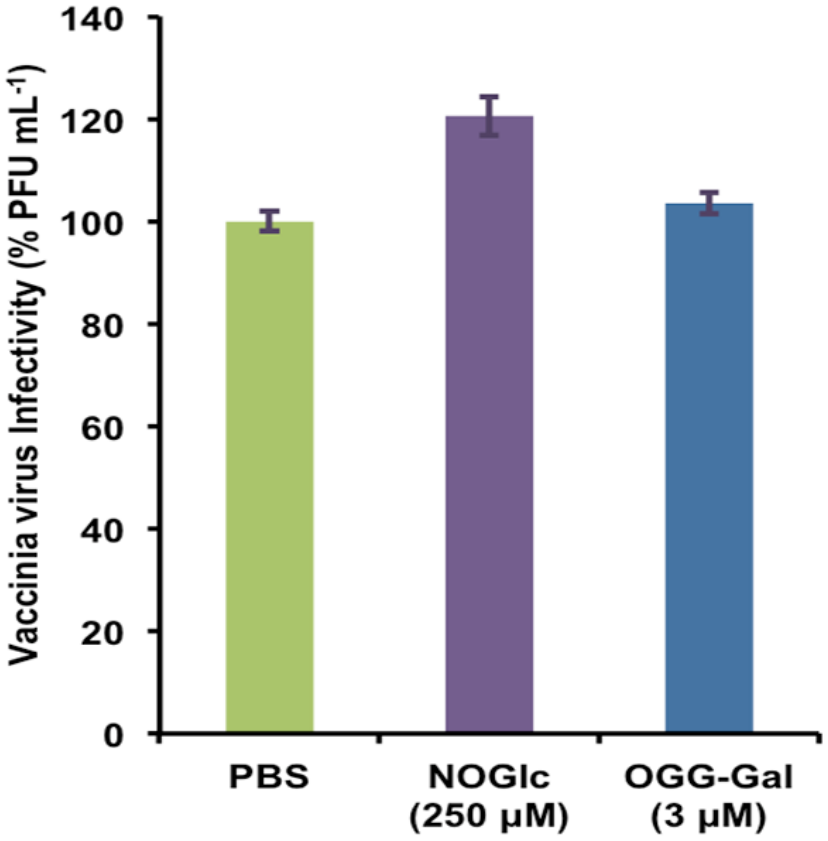

Figure 8.9. Vaccinia virus infectivity after 1 hour incubation in NOGlc and OGG-Gal solution and PBS control. Error bars indicate standard deviation (Microsoft Excel, version 2011). Reprinted with permission from[198].

These results suggest the compounds increase virus active units and stabilize individual virus particles in the solution. The abilities of OGG-Gal and NOGlc to stabilize and preserve three different viruses during cryopreservation, lyophilization and room temperature storage are summarized in **Table 8.1**.

Table 8.1. The capacity of OGG-Gal, NOGal and NOGlc to recover three different viruses throughout cryopreservation, lyophilization and room temperature storage.

		OGG-Gal	NOGal	NOGlc
Room Temperature	Vaccinia virus[1]	NS	NS	↑↑↑↑↑↑↑↑↑↑
	VSV[2]	NS	NS	NS
	HSV-1[3]	NS	NS	↑↑↑↑↑
Freeze-Thaw	Vaccinia virus[4]	↑↑	↑	↑↑
	VSV[4]	↑↑↑↑	NS	↑↑↑↑
	HSV-1[4]	NS	NS	NS
Lyophilization	Vaccinia virus	↑↑	↑	↑↑
	VSV	↑↑	↑↑	↑
	HSV-1	NS	NS	NS

↑ - represents recovered infectivity in 0.5 Log_{10} PFU mL^{-1} compare with PBS control

NS - no significant effect was observed

[1] after 40 days at RT

[2] after 5 days at RT

[3] after 9 days at RT

[4] after 10 freeze-thaw cycles

Reprinted with permission from[198].

Considering the structural differences between OGG-Gal, a high-molecular weight glycopeptide, and NOGlc, a small-molecule non-ionic surfactant, it is interesting to see very little difference in infectivity. Both compounds are equally effective at protecting against cryo-injury

after ten successive freeze-thaw cycles. Furthermore, both of these compounds are most effective with Vaccinia virus but less effective in VSV. In contrast, NOGal is not effective (infectivity is identical to the PBS control). The IRI activity of small molecules is presented in **Figure 8.2b** Ice recrystallization inhibition is defined as the prevention of the re-organization of smaller ice crystals into larger ice crystals. This would occur during the thawing phase in the freeze-thaw cycles. Both OGG-Gal and NOGlc are potent inhibitors of ice recrystallization. NOGlc is effective at 0.5 mM. Given the effectiveness of this compound to inhibit ice recrystallization, which is a significant cause of cellular damage during cryopreservation, it seems likely that NOGlc (and OGG-Gal) may directly inhibiting cryoinjury of the virus particle. In contrast, NOGal does not inhibit ice recrystallization (despite the fact that it differs from NOGlc by only one stereocentre) to any appreciable extent and fails to protect Vaccinia virus and VSV against the cryoinjury associated with successive freezing-thawing. This result is also consistent with the hypothesis that inhibiting ice recrystallization injury in the virus particle is beneficial. Ice crystals can damage a large virus more than a small virus. For cryopreservation, the best compounds are amphiphilic molecules possessing a hydrophilic head group and a hydrophobic tail group, as seen in the alditol structure NOGlc.

Maintaining the stability of viral vectors is an obstacle to global vaccination programs and viral-based therapy.[88, 89, 91, 119, 122] Unfortunately, most vaccines lose 50% of their activity when constructed and stored for one hour at room temperature.[98, 200, 220] The transportation, storage, and use of them consequently present challenges, particularly in developing countries. Unlike former efforts, direct addition of NOGlc is easy, economical and robust. Our results show that NOGlc protects significantly Vaccinia virus and HSV-1 infectivity at room temperature (**Figure 8.3**).

8.5. Conclusion

In conclusion, according to WHO requirement for vaccines cold chain management, NOGlc increases the shelf life of Vaccinia virus from four days to more than forty days and HSV-1 from a day to more than nine days. NOGlc has the opportunity to eliminate the cold chain from viral vector vaccine management.

Acknowledgements

We are most grateful to Dr. John C. Bell and Dr. Fabrice Le Boeuf for providing herpes virus type I and vesicular stomatitis virus expressing fluorescent proteins.

Chapter 9

Conclusions and Future Directions

The primary focus of this thesis was in the development of several aptamer technologies for virus and cell isolation and biomarker discovery of monocytes.

The second chapter described the application of aptamers with binding affinity to VSV to protect the oncolytic virus from nAbs. When the protective capacity of aptamers with binding affinity to VSV and binding affinity to its nAbs was assessed, the constructed quadramer structure of the aptamers provided superior protection against VSV infectivity (76% recovery).

In Chapter 3, we aimed to evaluate the efficiency of aptamers and their constructed structure with high avidity to preserve VSV from freeze-thaw damage. One of the main obstacles of global vaccination is viral vector stability. The results show that the tetrameric structure can preserve 1.4 Logs of the virus infectivity more than controls after 60 freeze-thaw cycles. This

finding is a new application of aptamers that can be used to preserve a virus from freezing damage.

In Chapter 4, we generated EDTA switchable aptamers capable of capturing a receptor positive cell and releasing the cell upon adding EDTA. To provide negative and positive cells expressing LIFR, NRP1, DLL4, uPAR, or PTCH1, we transduced the HEK293 cell line using the lentivirus packaging system. In the cell-SELEX method, the ssDNA library was incubated with positive cells in the presence of Ca^{2+} and Mg^{2+}; the bound ssDNAs from positive cells were collected after adding EDTA. The generated aptamers were successful in positive cell isolation from heterogeneous tissue and mice bone marrow.

In Chapter 5, even though we tried to select EDTA switchable aptamers using the modified Cell-SELEX method as in Chapter 4, the generated aptamer could not be detached from Axl positive cells by adding EDTA. One of the possible explanations is the internalization of the aptamer through the Axl receptor. The aptamer successfully targeted Axl positive cells in human whole blood leukocytes and was applied as a probe to sort cells with FACS and for immunofluorescent analysis. Unlike the switchable aptamers, this aptamer was able to bind to its target from the extracted cell membrane proteins. Defining the sequence of sections bound to the target requires testing the truncated forms of the aptamer in the future experiments.

In contrast to the previously generated aptamers, the aptamer selection in Chapter 6, that targeted the cells expressing PD-1, generated an aptamer to CD107a. This study discovered CD107a as a result of PD-1 expression on the HEK293 cell line membrane. Even though this result was repeated three times, further study is necessary to confirm this result at a transcriptional level using RT-PCR and at a protein level using western blot and proteomic mass spectrometry.

In Chapter 7, we applied all the knowledge we gathered in the past years about the influence of divers factors on aptamers performance and used cell sorting to develop a novel method of aptamer selection, FACS Cell SELEX, in order to generate a switchable aptamer to bind to monocytes in peripheral whole blood leukocytes for biomarker discovery in its native biological tissue. The developed aptamer has the capability of switchable positive monocyte isolation from whole blood using magnetic beads or FACS. The target of the aptamer was identified as CD91 via mass spectrometry analysis. The surface plasmon resonance method could measure dissociation constant more accurately than the apparent dissociation constant. Future investigations can expand its applications in medicine as well.

In Chapter 8, in parallel experiments with Chapter 3, regarding the importance of viral vector stability for global vaccination, we screened not only aptamers but also carbohydrate-based gelators for preserving VSV, Vaccinia virus, and Herpes virus-1 in common forms of storage. The main and novel outcome of this investigation was the N-octyl-gluconamide effect of increasing the shelf life of the vaccinia virus from four days to more than forty days, and the herpes virus-1 from a day to more than nine days as according to the strict requirements of the World Health Organization. Protecting the viruses with N-octyl-gluconamide is simple and robust; nevertheless, it is necessary to investigate its possible toxicity and side effects during vaccinations.

The Darwinian evolutionary approach of aptamer selection in combination with rational design tactics can direct the evolution of aptamer toward new inventions and discoveries in science and medicine. The advantage of a developed aptamer in a condition can be their disadvantage in a different condition. The aptamer evolutionary selection can be engineered to drive aptamers for a specific strategy. Even though aptamer technology seems straightforward, it

needs to be deeply investigated in both the evolutionary and rational design process to get high affinity and specify and robust results.

List of My Publications:

19. **Shahrokh M. Ghobadloo1,** Gleb G. Mironov, Ben Kingston, Bani Malhotra, Samuel Clarke and Maxim V. Berezovski1*. Aptamers with Switchable Affinity for Positive Cell Purification. (In preparation)
18. **Shahrokh M. Ghobadloo,** Gleb G. Mironov, Nadia Al-Youssef and Maxim V. Berezovski*. Single Strand DNA Oligonucleotides to Detect and Sort Cells Expressing Axl Receptor Tyrosine Kinase. (In preparation)
17. **Shahrokh M. Ghobadloo,** Gleb G. Mironov, Nadia Al-Youssef and Maxim V. Berezovski*. Aptamer Technology Detected CD107a in Response to PD-1 Expression. (In preparation)
16. Nadia L. Al-Youssef, **Shahrokh M. Ghobadloo** and Maxim V. Berezovski*. Inhibition of complement dependent cytotoxicity by anti-CD20 aptamers. RSC Advances 6 (15), 12435-12438. (PhD research work)
15. **Shahrokh M. Ghobadloo**, Ana Gargaun, Rebecca Casselman, Darija Muharemagic, Maxim V. Berezovski*. Aptamer-Facilitated Cryoprotection of Viruses. ACS medicinal chemistry letters 5 (11), 1240-1244. (PhD research work)
14. **Shahrokh M Ghobadloo**, Anna K Balcerzak, Ana Gargaun, Darija Muharemagic, Gleb G Mironov, Chantelle J Capicciotti, Jennie G Briard, Robert N Ben, Maxim V Berezovski*. Carbohydrate-based ice recrystallization inhibitors increase infectivity and thermostability of viral vectors. Sci Rep. 2014;4:5903. doi: 10.1038/srep05903. (PhD research work)
13. Darija Muharemagic, Anna Zamay, **Shahrokh M Ghobadloo**, Laura Evgin, Anna Savitskaya, John C Bell, Maxim V Berezovski*. Aptamer-facilitated Protection of Oncolytic Virus from Neutralizing Antibodies. Mol Ther Nucleic Acids. 2014;3:e167. doi:10.1038/mtna. (PhD research work)

12. Mahmoud Labib, **Shahrokh M. Ghobadloo**, Nasrin Khan, Dmitry M. Kolpashchikov and Maxim V. Berezovski*. Four-Way Junction Formation Promoting Ultrasensitive Electrochemical Detection of MicroRNA. Anal Chem. 2013; 15; 85(20): 9422-7. (PhD research work)

11. Mahmoud Labib, Nasrin Khan, **Shahrokh M. Ghobadloo,** Jenny Cheng, John Paul Pezacki, and Maxim V Berezovski*. Three-Mode Electrochemical Sensing of Ultra-Low MicroRNA Levels. J. Am. Chem. Soc. 2013; 135 (8): 3027–3038. (PhD research work)

10. Darija Muharemagic, Mahmoud Labib, **Shahrokh M. Ghobadloo,** Anna S. Zamay, John C. Bell, and Maxim V Berezovski*. Anti-Fab Aptamers for Shielding Virus from Neutralizing Antibodies. J. Am. Chem. Soc. 2012; 134 (41): 17168–17177. (PhD research work)

9. Nomani H, Mozafari H*, **Ghobadloo SM**, Rahimi Z, Raygani AV, Rahimi MA, Haghi AF, Keshavarz AA. The association between GSTT1, M1, and P1 polymorphisms with coronary artery disease in Western Iran. Mol Cell Biochem 2011; 354(1-2):181-7.

8. Sharifi R, Allameh A*, Biramijamal F, **Mohammadzadeh SH**, Rasmi Y, Tavangar SM, Jamali-Zavarei M. Relationship between genetic polymorphism of glutathione S-transferase-p1 and p53 protein accumulation in Iranian esophageal squamous cell carcinoma patients. Indian J Cancer 2008; 45(1):8-12.

7. M Golshani, G Eslami, **Sh Mohhammadzadeh Ghobadloo**, F Fallah, H Goudarzi, AA Soleimani Rahbar, F Fayaz. Detection of Chlamydia trachomatis, Mycoplasma hominis and Ureaplasma urealyticum by Multiplex PCR in Semen Sample of Infertile Men. Iranian J Publ Health 2007;36 (2): 50-57.

6. **Shahrokh Mohammadzadeh Ghobadloo***, Bahram Yaghmaei, Abdolamir Allameh, Parkhideh Hassani, Babak Noorinayer and Mohammad Reza Zali. Polymorphisms of Glutathione S-transferase M1, T1 and P1 in Patients with HBV Related Liver Cirrhosis, Chronic Hepatitis and Normal Carriers. Clinical Biochemistry 2006; 39(1):46-9. (*Corresponding Author)

5. Farideh Esfandi, **Shahrokh Mohammadzadeh Ghobadloo*** and Gholam Basati. Interleukin-6 Level in Patients with Colorectal Cancer. Cancer Letters 2006; 244(1):76-8. (*Corresponding Author)

4. Hamid Nomani, **Shahrokh Mohammadzadeh Ghobadloo***, Bahram Yaghmaei, Nayeb Ali Rezvanie and Kaveh Yaghmaei. Glutathione S-transferases activity in patients with colorectal cancer. Clinical Biochemistry 2005; 38(7):621-4. (*Corresponding Author)

3. A. Movafagh*, F. Maleki, **S.G. Mohammadzadeh** and S. Fadaei. Association of glutathion S-transferase and chromosomal aberrations as a means to determine occupational exposure. International Congress Series 2005; 1276:197-198.

2. **Shahrokh Mohammadzadeh Ghobadloo***, Bahram Yaghmaei, Valery Bakayev, Hossein Goudarzi, Babak Noorinayer, Farhad Haghighi Rad, Saeed Samiy, Sohrab Aghabozorghi and Mohammad Reza Zali. GSTP1, GSTM1, and GSTT1 Genetic Polymorphisms in Patients with Cryptogenic Liver Cirrhosis. J Gastrointest Surg 2004; 8(4):423-7. (*Corresponding Author)

1. **G. S. Mohammadzadeh**, S. Nasseri Moghadam, M. J. Rasaee, A. B. Zaree, H. Mahmoodzadeh and A. Allameh*. Measurement of glutathione S-transferase and its class-pi in plasma and tissue biopsies obtained after laparoscopy and endoscopy from subjects with esophagus and gastric cancer. Clinical Biochemistry 2003; 36(4):283-8.

References

1. Pinheiro, V. B., Taylor, A. I., Cozens, C., Abramov, M., Renders, M., Zhang, S., Chaput, J. C., Wengel, J., Peak-Chew, S.-Y., and McLaughlin, S. H. (2012) Synthetic genetic polymers capable of heredity and evolution, *Science 336*, 341-344.
2. Rana, T. M. (2007) Illuminating the silence: understanding the structure and function of small RNAs, *Nature reviews Molecular cell biology 8*, 23-36.
3. Zhou, J., and Rossi, J. (2016) Aptamers as targeted therapeutics: Current potential and challenges, *Nature Reviews Drug Discovery*.
4. Burge, S., Parkinson, G. N., Hazel, P., Todd, A. K., and Neidle, S. (2006) Quadruplex DNA: sequence, topology and structure, *Nucleic Acids Research 34*, 5402-5415.
5. Anosova, I., Kowal, E. A., Dunn, M. R., Chaput, J. C., Van Horn, W. D., and Egli, M. (2016) The structural diversity of artificial genetic polymers, *Nucleic Acids Research 44*, 1007-1021.
6. Vogler, E. A. (1998) Structure and reactivity of water at biomaterial surfaces, *Advances in Colloid and Interface science 74*, 69-117.
7. Batabyal, S., Choudhury, S., Sao, D., Mondol, T., and Kumar Pal, S. (2014) Dynamical perspective of protein-DNA interaction, *Biomolecular Concepts 5*, 21-43.
8. Long, S. B., Long, M. B., White, R. R., and Sullenger, B. A. (2008) Crystal structure of an RNA aptamer bound to thrombin, *Rna 14*, 2504-2512.
9. Gelinas, A. D., Davies, D. R., and Janjic, N. (2016) Embracing proteins: structural themes in aptamer–protein complexes, *Current Opinion in Structural Biology 36*, 122-132.
10. Lin, C. H., and Patel, D. J. (1996) Encapsulating an amino acid in a DNA fold, *Nature Structural & Molecular Biology 3*, 1046-1050.
11. Hermann, T., and Patel, D. J. (2000) Adaptive recognition by nucleic acid aptamers, *Science 287*, 820-825.
12. Förster, U., Weigand, J. E., Trojanowski, P., Suess, B., and Wachtveitl, J. (2012) Conformational dynamics of the tetracycline-binding aptamer, *Nucleic Acids Research 40*, 1807-1817.
13. Rohs, R., Jin, X., West, S. M., Joshi, R., Honig, B., and Mann, R. S. (2010) Origins of specificity in protein-DNA recognition, *Annual Review of Biochemistry 79*, 233-269.

14. Mayer, G. (2009) The chemical biology of aptamers, *Angewandte Chemie International Edition 48*, 2672-2689.
15. Ellenberger, T. E., Brandl, C. J., Struhl, K., and Harrison, S. C. (1992) The GCN4 basic region leucine zipper binds DNA as a dimer of uninterrupted α helices: crystal structure of the protein-DNA complex, *Cell 71*, 1223-1237.
16. Holmbeck, S. M., Dyson, H. J., and Wright, P. E. (1998) DNA-induced conformational changes are the basis for cooperative dimerization by the DNA binding domain of the retinoid X receptor, *Journal of Molecular Biology 284*, 533-539.
17. Travers, A. A. (1989) DNA conformation and protein binding, *Annual Review of Biochemistry 58*, 427-452.
18. Smestad, J., and Maher, L. J. (2012) Ion-dependent conformational switching by a DNA aptamer that induces remyelination in a mouse model of multiple sclerosis, *Nucleic Acids Research*, gks1093.
19. Tuerk, C., and Gold, L. (1990) Systematic evolution of ligands by exponential enrichment: RNA ligands to bacteriophage T4 DNA polymerase, *Science 249*, 505-510.
20. Ellington, A. D., and Szostak, J. W. (1990) In vitro selection of RNA molecules that bind specific ligands, *Nature 346*, 818.
21. Krishnan, Y., and Simmel, F. C. (2011) Nucleic acid based molecular devices, *Angewandte Chemie International Edition 50*, 3124-3156.
22. Warren, C. L., Mohandas, A., Chaturvedi, I., and Ansari, A. Z. (2009) Macromolecular Interactions: Aptamers, *eLS*.
23. Vinkenborg, J. L., Karnowski, N., and Famulok, M. (2011) Aptamers for allosteric regulation, *Nature Chemical Biology 7*, 519-527.
24. Raddatz, M. S., Dolf, A., Endl, E., Knolle, P., Famulok, M., and Mayer, G. (2008) Enrichment of cell-targeting and population-specific aptamers by fluorescence-activated cell sorting, *Angew Chem Int Ed Engl 47*, 5190-5193.
25. Szeitner, Z., András, J., Gyurcsányi, R. E., and Mészáros, T. (2014) Is less more? Lessons from aptamer selection strategies, *Journal of Pharmaceutical and Biomedical Analysis 101*, 58-65.

26. Gold, L., Ayers, D., Bertino, J., Bock, C., Bock, A., Brody, E. N., Carter, J., Dalby, A. B., Eaton, B. E., and Fitzwater, T. (2010) Aptamer-based multiplexed proteomic technology for biomarker discovery, *5*, e15004.

27. Eaton, B. E. (1997) The joys of in vitro selection: chemically dressing oligonucleotides to satiate protein targets, *Current Opinion in Chemical Biology 1*, 10-16.

28. Dewey, T. M., Mundt, A., Crouch, G. J., Zyzniewski, M. C., and Eaton, B. E. (1995) New uridine derivatives for systematic evolution of RNA ligands by exponential enrichment, *Journal of the American Chemical Society 117*, 8474-8475.

29. Bruno, J. G. (1997) In VitroSelection of DNA to Chloroaromatics Using Magnetic Microbead-Based Affinity Separation and Fluorescence Detection, *Biochemical and Biophysical Research Communications 234*, 117-120.

30. Mendonsa, S. D., and Bowser, M. T. (2004) In vitro evolution of functional DNA using capillary electrophoresis, *Journal of the American Chemical Society 126*, 20-21.

31. Sefah, K., Shangguan, D., Xiong, X., O'donoghue, M. B., and Tan, W. (2010) Development of DNA aptamers using Cell-SELEX, *Nature protocols 5*, 1169-1185.

32. Bahrami- Samani, E., Vo, D. T., de Araujo, P. R., Vogel, C., Smith, A. D., Penalva, L. O., and Uren, P. J. (2015) Computational challenges, tools, and resources for analyzing co- and post- transcriptional events in high throughput, *Wiley Interdisciplinary Reviews: RNA 6*, 291-310.

33. Beck, A., Vijayanathan, V., Thomas, T., and Thomas, T. (2013) Ionic microenvironmental effects on triplex DNA stabilization: Cationic counterion effects on poly (dT)· poly (dA)· poly (dT), *Biochimie 95*, 1310-1318.

34. McGhee, J. D. (1976) Theoretical calculations of the helix–coil transition of DNA in the presence of large, cooperatively binding ligands, *Biopolymers 15*, 1345-1375.

35. Tan, Z.-J., and Chen, S.-J. (2006) Nucleic acid helix stability: effects of salt concentration, cation valence and size, and chain length, *Biophysical Journal 90*, 1175-1190.

36. Solt, I., Simon, I., Csaszar, A. G., and Fuxreiter, M. (2007) Electrostatic versus nonelectrostatic effects in DNA sequence discrimination by divalent ions Mg^{2+} and Mn^{2+}, *The Journal of Physical Chemistry B 111*, 6272-6279.

37. Proske, D., Blank, M., Buhmann, R., and Resch, A. (2005) Aptamers—basic research, drug development, and clinical applications, *Applied Microbiology and Biotechnology 69*, 367-374.

38. Ng, E. W., Shima, D. T., Calias, P., Cunningham, E. T., Guyer, D. R., and Adamis, A. P. (2006) Pegaptanib, a targeted anti-VEGF aptamer for ocular vascular disease, *Nature reviews drug discovery 5*, 123-132.

39. Zhao, Q., Li, X.-F., Shao, Y., and Le, X. C. (2008) Aptamer-based affinity chromatographic assays for thrombin, *Analytical Chemistry 80*, 7586-7593.

40. Labib, M., Zamay, A. S., Kolovskaya, O. S., Reshetneva, I. T., Zamay, G. S., Kibbee, R. J., Sattar, S. A., Zamay, T. N., and Berezovski, M. V. (2012) Aptamer-based viability impedimetric sensor for bacteria, *Analytical Chemistry 84*, 8966-8969.

41. Kiilerich-Pedersen, K., Daprà, J., Cherré, S., and Rozlosnik, N. (2013) High sensitivity point-of-care device for direct virus diagnostics, *Biosensors and Bioelectronics 49*, 374-379.

42. Gopinath, S. C., Misono, T. S., Kawasaki, K., Mizuno, T., Imai, M., Odagiri, T., and Kumar, P. K. (2006) An RNA aptamer that distinguishes between closely related human influenza viruses and inhibits haemagglutinin-mediated membrane fusion, *Journal of General Virology 87*, 479-487.

43. Berezovski, M. V., Lechmann, M., Musheev, M. U., Mak, T. W., and Krylov, S. N. (2008) Aptamer-facilitated biomarker discovery (AptaBiD), *Journal of the American Chemical Society 130*, 9137-9143.

44. Hawkridge, A. M., and Muddiman, D. C. (2009) Mass spectrometry–based biomarker discovery: toward a global proteome index of individuality, *Annual Review of Analytical Chemistry 2*, 265-277.

45. Ganji, A., Varasteh, A., and Sankian, M. (2016) Aptamers: new arrows to target dendritic cells, *Journal of Drug Targeting 24*, 1-12.

46. Kelly, D. J., and Ghosh, S. (2005) RNA profiling for biomarker discovery: practical considerations for limiting sample sizes, *Disease Markers 21*, 43-48.

47. Chen, Y., O'Donoghue, M. B., Huang, Y.-F., Kang, H., Phillips, J. A., Chen, X., Estevez, M.-C., Yang, C. J., and Tan, W. (2010) A surface energy transfer nanoruler for measuring binding site distances on live cell surfaces, *Journal of the American Chemical Society 132*, 16559-16570.

48. Tang, Z., Parekh, P., Turner, P., Moyer, R. W., and Tan, W. (2009) Generating aptamers for recognition of virus-infected cells, *Clinical Chemistry 55*, 813-822.

49. Xiao, Z., Shangguan, D., Cao, Z., Fang, X., and Tan, W. (2008) Cell- Specific internalization study of an aptamer from whole cell selection, *Chemistry–A European Journal 14*, 1769-1775.

50. Bullinger, L., Döhner, K., Bair, E., Fröhling, S., Schlenk, R. F., Tibshirani, R., Döhner, H., and Pollack, J. R. (2004) Use of gene-expression profiling to identify prognostic subclasses in adult acute myeloid leukemia, *New England Journal of Medicine 350*, 1605-1616.

51. Guo, K. T., SchÄfer, R., Paul, A., Gerber, A., Ziemer, G., and Wendel, H. P. (2006) A new technique for the isolation and surface immobilization of mesenchymal stem cells from whole bone marrow using high- specific DNA aptamers, *Stem Cells 24*, 2220-2231.

52. Gronthos, S., Zannettino, A. C., Hay, S. J., Shi, S., Graves, S. E., Kortesidis, A., and Simmons, P. J. (2003) Molecular and cellular characterisation of highly purified stromal stem cells derived from human bone marrow, *Journal of Cell Science 116*, 1827-1835.

53. Arvidson, K., Abdallah, B., Applegate, L., Baldini, N., Cenni, E., Gomez- Barrena, E., Granchi, D., Kassem, M., Konttinen, Y., and Mustafa, K. (2011) Bone regeneration and stem cells, *Journal of Cellular and Molecular Medicine 15*, 718-746.

54. Mattanovich, D., and Borth, N. (2006) Applications of cell sorting in biotechnology, *Microbial Cell Factories 5*, 12.

55. Tomlinson, M. J., Tomlinson, S., Yang, X. B., and Kirkham, J. (2013) Cell separation: Terminology and practical considerations, *Journal of tissue engineering 4*, 2041731412472690.

56. Petersson, F., Åberg, L., Swärd-Nilsson, A.-M., and Laurell, T. (2007) Free flow acoustophoresis: microfluidic-based mode of particle and cell separation, *Analytical Chemistry 79*, 5117-5123.

57. Orfao, A., and Ruiz-Argüelles, A. (1996) General concepts about cell sorting techniques, *Clinical Biochemistry 29*, 5-9.

58. Almeida, M., Garcia-Montero, A. C., and Orfao, A. (2015) Cell purification: a new challenge for biobanks, *Pathobiology 81*, 261-275.

59. Dainiak, M. B., Kumar, A., Galaev, I. Y., and Mattiasson, B. (2007) Methods in cell separations, *Advances in Biochemical Engineering/Biotechnology 106*, 1-18.

60. Smeland, E. B., Funderud, S., Kvalheim, G., Gaudernack, G., Rasmussen, A. M., Rusten, L., Wang, M. Y., Tindle, R. W., Blomhoff, H. K., and Egeland, T. (1992) Isolation and characterization of human hematopoietic progenitor cells: an effective method for positive selection of CD34+ cells, *Leukemia 6*, 845-852.

61. Rowley, S. D., Loken, M., Radich, J., Kunkle, L. A., Mills, B. J., Gooley, T., Holmberg, L., McSweeney, P., Beach, K., MacLeod, B., Appelbaum, F., and Bensinger, W. I. (1998) Isolation of CD34+ cells from blood stem cell components using the Baxter Isolex system, *Bone Marrow Transplantation 21*, 1253-1262.

62. Labib, M., Zamay, A. S., Muharemagic, D., Chechik, A., Bell, J. C., and Berezovski, M. V. (2012) Electrochemical Sensing of Aptamer-Facilitated Virus Immunoshielding, *Analytical Chemistry 84*, 1677-1686.

63. Lopez, A. D., Mathers, C. D., Ezzati, M., Jamison, D., and Murray, C. (2006) Global burden of disease and risk factors. Washington, DC: World Bank, *Disease Control Priorities Project*.

64. Van Laere, S., Limame, R., Van Marck, E. A., Vermeulen, P. B., and Dirix, L. Y. (2010) Is there a role for mammary stem cells in inflammatory breast carcinoma?, *Cancer 116*, 2794-2805.

65. van Golen, C. M., and van Golen, K. L. (2012) Inflammatory breast cancer stem cells: contributors to aggressiveness, metastatic spread and dormancy, *J Mol Biomarkers Diagn S 8*, 2.

66. Ungerechts, G., Bossow, S., Leuchs, B., Holm, P. S., Rommelaere, J., Coffey, M., Coffin, R., Bell, J., and Nettelbeck, D. M. (2016) Moving oncolytic viruses into the clinic: clinical-grade production, purification, and characterization of diverse oncolytic viruses, *Molecular Therapy-Methods & Clinical Development 3*, 16018.

67. Bourgeois-Daigneault, M.-C., Roy, D. G., Falls, T., Twumasi-Boateng, K., St-Germain, L. E., Marguerie, M., Garcia, V., Selman, M., Jennings, V. A., and Pettigrew, J. (2016) Oncolytic vesicular stomatitis virus expressing interferon-σ has enhanced therapeutic activity, *Molecular Therapy-Oncolytics 3*, 16001.

68. Russell, S. J., Peng, K.-W., and Bell, J. C. (2012) Oncolytic virotherapy, *Nature Biotechnology 30*, 658-670.

69. Wakimoto, H., Kesari, S., Farrell, C. J., Curry, W. T., Zaupa, C., Aghi, M., Kuroda, T., Stemmer-Rachamimov, A., Shah, K., and Liu, T.-C. (2009) Human glioblastoma–derived cancer stem cells: establishment of invasive glioma models and treatment with oncolytic herpes simplex virus vectors, *Cancer Research 69*, 3472-3481.

70. Gaudier, M., Gaudin, Y., and Knossow, M. (2002) Crystal structure of vesicular stomatitis virus matrix protein, *The EMBO Journal 21*, 2886-2892.

71. Barber, G. N. (2004) Vesicular stomatitis virus as an oncolytic vector, *Viral Immunology 17*, 516-527.

72. Barber, G. N. (2005) VSV-tumor selective replication and protein translation, *Oncogene 24*, 7710-7719.

73. Breitbach, C. J., Lichty, B. D., and Bell, J. C. (2016) Oncolytic viruses: therapeutics with an identity crisis, *EBioMedicine 9*, 31-36.

74. Hastie, E., Cataldi, M., Marriott, I., and Grdzelishvili, V. Z. (2013) Understanding and altering cell tropism of vesicular stomatitis virus, *Virus Research 176*, 16-32.

75. Stojdl, D. F., Lichty, B. D., Paterson, J. M., Power, A. T., Knowles, S., Marius, R., Reynard, J., Poliquin, L., Atkins, H., and Brown, E. G. (2003) VSV strains with defects in their ability to shutdown innate immunity are potent systemic anti-cancer agents, *Cancer Cell 4*, 263-275.

76. Ahmed, M., McKenzie, M. O., Puckett, S., Hojnacki, M., Poliquin, L., and Lyles, D. S. (2003) Ability of the matrix protein of vesicular stomatitis virus to suppress beta interferon gene expression is genetically correlated with the inhibition of host RNA and protein synthesis, *Journal of Virology 77*, 4646-4657.

77. Balachandran, S., and Barber, G. N. (2000) Vesicular stomatitis virus (VSV) therapy of tumors, *IUBMB Life 50*, 135-138.

78. Morrison, J., Briggs, S. S., Green, N., Fisher, K., Subr, V., Ulbrich, K., Kehoe, S., and Seymour, L. W. (2008) Virotherapy of ovarian cancer with polymer-cloaked adenovirus retargeted to the epidermal growth factor receptor, *Molecular Therapy 16*, 244-251.

79. Doronin, K., Shashkova, E. V., May, S. M., Hofherr, S. E., and Barry, M. A. (2009) Chemical modification with high molecular weight polyethylene glycol reduces

transduction of hepatocytes and increases efficacy of intravenously delivered oncolytic adenovirus, *Human Gene Therapy 20*, 975-988.

80. Fisher, K. D., and Seymour, L. W. (2010) HPMA copolymers for masking and retargeting of therapeutic viruses, *Advanced Drug Delivery Reviews 62*, 240-245.
81. Miest, T. S., Yaiw, K.-C., Frenzke, M., Lampe, J., Hudacek, A. W., Springfeld, C., Von Messling, V., Ungerechts, G., and Cattaneo, R. (2011) Envelope-chimeric entry-targeted measles virus escapes neutralization and achieves oncolysis, *Molecular Therapy 19*, 1813-1820.
82. Muharemagic, D., Labib, M., Ghobadloo, S. M., Zamay, A. S., Bell, J. C., and Berezovski, M. V. (2012) Anti-Fab aptamers for shielding virus from neutralizing antibodies, *Journal of the American Chemical Society 134*, 17168-17177.
83. Muharemagic, D., Zamay, A., Ghobadloo, S. M., Evgin, L., Savitskaya, A., Bell, J. C., and Berezovski, M. V. (2014) Aptamer-facilitated protection of oncolytic virus from neutralizing antibodies, *Molecular Therapy—Nucleic Acids 3*, e167.
84. Ghobadloo, S. M., Gargaun, A., Casselman, R., Muharemagic, D., and Berezovski, M. V. (2014) Aptamer-Facilitated Cryoprotection of Viruses, *ACS Medicinal Chemistry Letters 5*, 1240-1244.
85. Diallo, J.-S., Vähä-Koskela, M., Le Boeuf, F., and Bell, J. (2012) Propagation, purification, and in vivo testing of oncolytic vesicular stomatitis virus strains, *Oncolytic Viruses: Methods and Protocols*, 127-140.
86. Olfert, E. D., Cross, B. M., and McWilliam, A. A. (1993) *Guide to the care and use of experimental animals*, Canadian Council on Animal Care Ottawa.
87. Jorio, H., Tran, R., and Kamen, A. (2006) Stability of Serum- Free and Purified Baculovirus Stocks under Various Storage Conditions, *Biotechnology progress 22*, 319-325.
88. Brandau, D. T., Jones, L. S., Wiethoff, C. M., Rexroad, J., and Middaugh, C. R. (2003) Thermal stability of vaccines, *Journal of Pharmaceutical Sciences 92*, 218-231.
89. Rexroad, J., Wiethoff, C. M., Jones, L. S., and Middaugh, C. R. (2002) Lyophilization and the thermostability of vaccines, *Cell Preservation Technology 1*, 91-104.
90. Purssell, E. (2015) Reviewing the importance of the cold chain in the distribution of vaccines, *British Journal of Community Nursing 20*.

91. Das, P. (2004) Revolutionary vaccine technology breaks the cold chain, *The Lancet Infectious Diseases 4*, 719.

92. Ohtake, S., Martin, R. A., Yee, L., Chen, D., Kristensen, D. D., Lechuga-Ballesteros, D., and Truong-Le, V. (2010) Heat-stable measles vaccine produced by spray drying, *Vaccine 28*, 1275-1284.

93. Ateudjieu, J., Kenfack, B., Nkontchou, B. W., and Demanou, M. (2013) Program on immunization and cold chain monitoring: the status in eight health districts in Cameroon, *BMC Research Notes 6*, 101.

94. Kristensen, D., Chen, D., and Cummings, R. (2011) Vaccine stabilization: research, commercialization, and potential impact, *Vaccine 29*, 7122-7124.

95. Matthias, D. M., Robertson, J., Garrison, M. M., Newland, S., and Nelson, C. (2007) Freezing temperatures in the vaccine cold chain: a systematic literature review, *Vaccine 25*, 3980-3986.

96. Zhang, J., Pritchard, E., Hu, X., Valentin, T., Panilaitis, B., Omenetto, F. G., and Kaplan, D. L. (2012) Stabilization of vaccines and antibiotics in silk and eliminating the cold chain, *Proceedings of the National Academy of Sciences 109*, 11981-11986.

97. Galazka, A., Milstien, J., and Zaffran, M. (1998) Thermostability of Vaccines: Global Programme for Vaccines and Immunization, *World Health Organization. Geneva*.

98. Knezevic, I. (2009) Stability evaluation of vaccines: WHO approach, *Biologicals 37*, 357-359.

99. Alain, T., Lun, X., Martineau, Y., Sean, P., Pulendran, B., Petroulakis, E., Zemp, F. J., Lemay, C. G., Roy, D., and Bell, J. C. (2010) Vesicular stomatitis virus oncolysis is potentiated by impairing mTORC1-dependent type I IFN production, *Proceedings of the National Academy of Sciences 107*, 1576-1581.

100. Fernandez, M., Porosnicu, M., Markovic, D., and Barber, G. N. (2002) Genetically engineered vesicular stomatitis virus in gene therapy: application for treatment of malignant disease, *Journal of Virology 76*, 895-904.

101. Lichty, B. D., Power, A. T., Stojdl, D. F., and Bell, J. C. (2004) Vesicular stomatitis virus: re-inventing the bullet, *Trends in Molecular Medicine 10*, 210-216.

102. Geisbert, T. W., Daddario-DiCaprio, K. M., Lewis, M. G., Geisbert, J. B., Grolla, A., Leung, A., Paragas, J., Matthias, L., Smith, M. A., Jones, S. M., Hensley, L. E.,

Feldmann, H., and Jahrling, P. B. (2008) Vesicular Stomatitis Virus-Based Ebola Vaccine Is Well-Tolerated and Protects Immunocompromised Nonhuman Primates, *PLoS Pathogens 4*, e1000225.

103. Clarke, D., Cooper, D., Egan, M., Hendry, R. M., Parks, C., and Udem, S. (2006) Recombinant vesicular stomatitis virus as an HIV-1 vaccine vector, *Springer Seminars in Immunopathology 28*, 239-253.
104. Cobleigh, M. A., Buonocore, L., Uprichard, S. L., Rose, J. K., and Robek, M. D. (2010) A vesicular stomatitis virus-based hepatitis B virus vaccine vector provides protection against challenge in a single dose, *Journal of Virology 84*, 7513-7522.
105. Majid, A. M., Ezelle, H., Shah, S., and Barber, G. N. (2006) Evaluating Replication-Defective Vesicular Stomatitis Virus as a Vaccine Vehicle, *Journal of Virology 80*, 6993-7008.
106. Higashikawa, F., and Chang, L.-J. (2001) Kinetic analyses of stability of simple and complex retroviral vectors, *Virology 280*, 124-131.
107. Wallis, C., and Melnick, J. L. (1968) Stabilization of enveloped viruses by dimethyl sulfoxide, *Journal of Virology 2*, 953.
108. Xu, Q., Nomura, T., Ikeda, M., Ohta, M., Kameyama, K. i., Konishi, M., Wu, D., Inumaru, S., and Murakami, K. (2011) Stability of recombinant bovine interferon- γ antiviral activity in the absence of stabilizing additives, *Microbiology and Immunology 55*, 595-598.
109. Chen, H.-Z., Liu, C. Y.-Y., Kost, T. A., and Chao, Y.-C. (2012) Sucrose and fetal bovine serum maintain stability and activity of the budded baculovirus during dehydration, *European Journal of Pharmaceutical Sciences 45*, 311-319.
110. Roche, S., Albertini, A. A. V., Lepault, J., Bressanelli, S., and Gaudin, Y. (2008) Structures of vesicular stomatitis virus glycoprotein: membrane fusion revisited, *Cellular and Molecular Life Sciences 65*, 1716-1728.
111. Gomes, A. M. O., Pinheiro, A. S., Bonafe, C. F. S., and Silva, J. L. (2003) Pressure-induced fusogenic conformation of vesicular stomatitis virus glycoprotein, *Biochemistry 42*, 5540-5546.
112. Luan, P., and Glaser, M. (1994) Formation of membrane domains by the envelope proteins of vesicular stomatitis virus, *Biochemistry 33*, 4483-4489.

113. Silva, A. C., Carrondo, M. J. T., and Alves, P. M. (2011) Strategies for improved stability of Peste des Petits Ruminants Vaccine, *Vaccine 29*, 4983-4991.

114. Vrdoljak, A., McGrath, M. G., Carey, J. B., Draper, S. J., Hill, A. V., O'Mahony, C., Crean, A. M., and Moore, A. C. (2012) Coated microneedle arrays for transcutaneous delivery of live virus vaccines, *Journal of Controlled Release 159*, 34-42.

115. Milstien, J. B., Galazka, A. M., Kartoglu, U. m., and Zaffran, M. (2006) Temperature sensitivity of vaccines.

116. Greenwood, B., Salisbury, D., and Hill, A. V. (2011) Vaccines and global health, *Philosophical Transactions of the Royal Society B: Biological Sciences 366*, 2733-2742.

117. Dietz, V., Galazka, A., Van Loon, F., and Cochi, S. (1997) Factors affecting the immunogenicity and potency of tetanus toxoid: implications for the elimination of neonatal and non-neonatal tetanus as public health problems, *Bulletin of the World Health Organization 75*, 81.

118. Parato, K. A., Breitbach, C. J., Le Boeuf, F., Wang, J., Storbeck, C., Ilkow, C., Diallo, J.-S., Falls, T., Burns, J., and Garcia, V. (2011) The oncolytic poxvirus JX-594 selectively replicates in and destroys cancer cells driven by genetic pathways commonly activated in cancers, *Molecular Therapy 20*, 749-758.

119. Wang, G., Li, X., Mo, L., Song, Z., Chen, W., Deng, Y., Zhao, H., Qin, E., Qin, C., and Tang, R. (2012) Eggshell- Inspired Biomineralization Generates Vaccines that Do Not Require Refrigeration, *Angewandte Chemie 124*, 10728-10731.

120. Imamura, K., Kimura, Y., Nakayama, S., Sayuri, M., Ogawa, S., Hoshino, T., Oshitani, J., Kobayashi, T., Adachi, S., and Matsuura, T. (2013) Characteristics of amorphous matrices composed of different types of sugars in encapsulating emulsion oil droplets during freeze-drying, *Food Research International 51*, 201-207.

121. Diallo, J.-S., Vähä-Koskela, M., Le Boeuf, F., and Bell, J. (2012) Propagation, purification, and in vivo testing of oncolytic vesicular stomatitis virus strains, In *Oncolytic Viruses*, pp 127-140, Springer.

122. Azizi, A., Mironov, G. G., Muharemagic, D., Wehbe, M., Bell, J. C., and Berezovski, M. V. (2012) Viral quantitative capillary electrophoresis for counting and quality control of RNA viruses, *Analytical Chemistry 84*, 9585-9591.

123. Galasso, G., and Sharp, D. (1962) Virus particle aggregation and the plaque-forming unit, *The Journal of Immunology 88*, 339-347.

124. Henderson, G., Murray, J., and Yeo, R. P. (2002) Sorting of the respiratory syncytial virus matrix protein into detergent-resistant structures is dependent on cell-surface expression of the glycoproteins, *Virology 300*, 244-254.

125. Chong, L. D., and Rose, J. K. (1994) Interactions of normal and mutant vesicular stomatitis virus matrix proteins with the plasma membrane and nucleocapsids, *Journal of Virology 68*, 441-447.

126. Li, J. L., Sainson, R. C., Shi, W., Leek, R., Harrington, L. S., Preusser, M., Biswas, S., Turley, H., Heikamp, E., Hainfellner, J. A., and Harris, A. L. (2007) Delta-like 4 Notch ligand regulates tumor angiogenesis, improves tumor vascular function, and promotes tumor growth in vivo, *Cancer Res 67*, 11244-11253.

127. Huyton, T., Zhang, J. G., Luo, C. S., Lou, M. Z., Hilton, D. J., Nicola, N. A., and Garrett, T. P. (2007) An unusual cytokine:Ig-domain interaction revealed in the crystal structure of leukemia inhibitory factor (LIF) in complex with the LIF receptor, *Proc Natl Acad Sci U S A 104*, 12737-12742.

128. Solomon, B. D., Mueller, C., Chae, W. J., Alabanza, L. M., and Bynoe, M. S. (2011) Neuropilin-1 attenuates autoreactivity in experimental autoimmune encephalomyelitis, *Proc Natl Acad Sci U S A 108*, 2040-2045.

129. Memarzadeh, S., Kozak, K. R., Chang, L., Natarajan, S., Shintaku, P., Reddy, S. T., and Farias-Eisner, R. (2002) Urokinase plasminogen activator receptor: Prognostic biomarker for endometrial cancer, *Proc Natl Acad Sci U S A 99*, 10647-10652.

130. Coni, S., Infante, P., and Gulino, A. (2013) Control of stem cells and cancer stem cells by Hedgehog signaling: pharmacologic clues from pathway dissection, *Biochemical Pharmacology 85*, 623-628.

131. Real, C., Remédio, L., Caiado, F., Igreja, C., Borges, C., Trindade, A., Yagita, H., Duarte, A., and Dias, S. (2011) Bone marrow-derived endothelial progenitors expressing delta-like 4 (dll4) regulate tumor angiogenesis, *PloS One 6*, e18323.

132. Graf, U., Casanova, E. A., and Cinelli, P. (2011) The role of the leukemia inhibitory factor (LIF)—pathway in derivation and maintenance of murine pluripotent stem cells, *Genes 2*, 280-297.

133. Zacchigna, S., Pattarini, L., Zentilin, L., Moimas, S., Carrer, A., Sinigaglia, M., Arsic, N., Tafuro, S., Sinagra, G., and Giacca, M. (2008) Bone marrow cells recruited through the neuropilin-1 receptor promote arterial formation at the sites of adult neoangiogenesis in mice, *The Journal of Clinical Investigation 118*, 2062.

134. Pillay, V., Dass, C. R., and Choong, P. F. (2007) The urokinase plasminogen activator receptor as a gene therapy target for cancer, *Trends in Biotechnology 25*, 33-39.

135. Uhmann, A., Dittmann, K., Nitzki, F., Dressel, R., Koleva, M., Frommhold, A., Zibat, A., Binder, C., Adham, I., and Nitsche, M. (2007) The Hedgehog receptor Patched controls lymphoid lineage commitment, *Blood 110*, 1814-1823.

136. Ruff, K. M., Snyder, T. M., and Liu, D. R. (2010) Enhanced functional potential of nucleic acid aptamer libraries patterned to increase secondary structure, *Journal of the American Chemical Society 132*, 9453-9464.

137. Keller, L. H. (2009) Bone Marrow–Derived Aldehyde Dehydrogenase–Bright Stem and Progenitor Cells for Ischemic Repair, *Congestive Heart Failure 15*, 202-206.

138. Boxall, S. A., and Jones, E. (2012) Markers for characterization of bone marrow multipotential stromal cells, *Stem Cells International 2012*.

139. Graham, V. A., Marzo, A. L., and Tough, D. F. (2007) A role for CD44 in T cell development and function during direct competition between CD44+ and CD44–cells, *European Journal of Immunology 37*, 925-934.

140. Schuster-Kolbe, J., Ludwig, H., Adolf, G. R., and Heider, K.-H. (1999) Expression of CD44 isoforms on isolated bone marrow plasma cells and peripheral CD19+ B cells of patients with multiple myeloma and healthy individuals, *Leukemia & lymphoma 34*, 95-103.

141. Van Driel, M., Gunthert, U., Van Kessel, A., Joling, P., Stauder, R., Lokhorst, H., and Bloem, A. (2002) CD44 variant isoforms are involved in plasma cell adhesion to bone marrow stromal cells, *Leukemia 16*, 135-143.

142. Elghetany, M. T., and Patel, J. (2002) Assessment of CD24 expression on bone marrow neutrophilic granulocytes: CD24 is a marker for the myelocytic stage of development, *American Journal of Hematology 71*, 348-349.

143. Algino, K. M., Thomason, R. W., King, D. E., Montiel, M., and Craig, F. E. (1996) CD20 (pan-B cell antigen) expression on bone marrow-derived T cells, *American Journal of Clinical Pathology 106*, 78-81.

144. Pelletier, M., and Girard, D. (2006) Differential effects of IL-15 and IL-21 in myeloid (CD11b+) and lymphoid (CD11b−) bone marrow cells, *The Journal of Immunology 177*, 100-108.

145. Hale, G., Zhang, M.-J., Bunjes, D., Prentice, H. G., Spence, D., Horowitz, M. M., Barrett, A. J., and Waldmann, H. (1998) Improving the outcome of bone marrow transplantation by using CD52 monoclonal antibodies to prevent graft-versus-host disease and graft rejection, *Blood 92*, 4581-4590.

146. Hedlund, G., Hansson, J., Ericsson, P. O., Sjogren, H. O., and Dohlsten, M. (1995) Expression of CD11a and CD45R isoforms defines distinct subsets of CD8+ TCR alpha beta and TCR gamma delta CTL in vivo, *Immunological Reviews 146*, 82-94.

147. Daniels, D. A., Chen, H., Hicke, B. J., Swiderek, K. M., and Gold, L. (2003) A tenascin-C aptamer identified by tumor cell SELEX: systematic evolution of ligands by exponential enrichment, *Proc Natl Acad Sci U S A 100*, 15416-15421.

148. Cerchia, L., Duconge, F., Pestourie, C., Boulay, J., Aissouni, Y., Gombert, K., Tavitian, B., de Franciscis, V., and Libri, D. (2005) Neutralizing aptamers from whole-cell SELEX inhibit the RET receptor tyrosine kinase, *PLoS Biol 3*, e123.

149. Sefah, K., Shangguan, D., Xiong, X., O'Donoghue, M. B., and Tan, W. (2010) Development of DNA aptamers using Cell-SELEX, *Nat Protoc 5*, 1169-1185.

150. Afgan, E., Baker, D., van den Beek, M., Blankenberg, D., Bouvier, D., Čech, M., Chilton, J., Clements, D., Coraor, N., and Eberhard, C. (2016) The Galaxy platform for accessible, reproducible and collaborative biomedical analyses: 2016 update, *Nucleic Acids Research*, gkw343.

151. Burdon, T. J., Paul, A., Noiseux, N., Prakash, S., and Shum-Tim, D. (2010) Bone marrow stem cell derived paracrine factors for regenerative medicine: current perspectives and therapeutic potential, *Bone Marrow Research 2011*.

152. Cohen, D. E., and Melton, D. (2011) Turning straw into gold: directing cell fate for regenerative medicine, *Nature Reviews Genetics 12*, 243-252.

153. Wu, X., Liu, X., Koul, S., Lee, C. Y., Zhang, Z., and Halmos, B. (2014) AXL kinase as a novel target for cancer therapy, *Oncotarget 5*, 9546.

154. Nguyen, K.-Q., Tsou, W.-I., Kotenko, S., and Birge, R. B. (2013) TAM receptors in apoptotic cell clearance, autoimmunity, and cancer, *Autoimmunity 46*, 294-297.

155. Lemke, G., and Rothlin, C. V. (2008) Immunobiology of the TAM receptors, *Nature Reviews Immunology 8*, 327-336.

156. Schmid, E. T., Pang, I. K., Silva, E. A. C., Bosurgi, L., Miner, J. J., Diamond, M. S., Iwasaki, A., and Rothlin, C. V. (2016) AXL receptor tyrosine kinase is required for T cell priming and antiviral immunity, *Elife 5*, e12414.

157. Korshunov, V. A. (2012) Axl-dependent signalling: a clinical update, *Clinical Science 122*, 361-368.

158. Ye, F., Han, L., Lu, Q., Dong, W., Chen, Z., Shao, H., Kaplan, H. J., Li, Q., and Lu, Q. (2011) Retinal self-antigen induces a predominantly Th1 effector response in Axl and Mertk double-knockout mice, *The Journal of Immunology 187*, 4178-4186.

159. Batchu, S. N., Hughson, A., Wadosky, K. M., Morrell, C. N., Fowell, D. J., and Korshunov, V. A. (2016) Role of Axl in T-Lymphocyte Survival in Salt-Dependent HypertensionHighlights, *Arteriosclerosis, Thrombosis, and Vascular Biology 36*, 1638-1646.

160. Johannessen, C. M., Boehm, J. S., Kim, S. Y., Thomas, S. R., Wardwell, L., Johnson, L. A., Emery, C. M., Stransky, N., Cogdill, A. P., and Barretina, J. (2010) COT drives resistance to RAF inhibition through MAP kinase pathway reactivation, *Nature 468*, 968-972.

161. Shangguan, D., Cao, Z., Meng, L., Mallikaratchy, P., Sefah, K., Wang, H., Li, Y., and Tan, W. (2008) Cell-specific aptamer probes for membrane protein elucidation in cancer cells, *Journal of Proteome Research 7*, 2133-2139.

162. Reuter, J. S., and Mathews, D. H. (2010) RNAstructure: software for RNA secondary structure prediction and analysis, *BMC Bioinformatics 11*, 1.

163. Ries, J., Kaplan, C., Platonova, E., Eghlidi, H., and Ewers, H. (2012) A simple, versatile method for GFP-based super-resolution microscopy via nanobodies, *Nature Methods 9*, 582-584.

164. Goodman, A., Patel, S. P., and Kurzrock, R. (2016) PD-1-PD-L1 immune-checkpoint blockade in B-cell lymphomas, *Nature Reviews Clinical Oncology*.

165. Sharma, P., and Allison, J. P. (2015) Immune checkpoint targeting in cancer therapy: toward combination strategies with curative potential, *Cell 161*, 205-214.

166. Mellman, I., Coukos, G., and Dranoff, G. (2011) Cancer immunotherapy comes of age, *Nature 480*, 480-489.

167. Keir, M. E., Butte, M. J., Freeman, G. J., and Sharpe, A. H. (2008) PD-1 and its ligands in tolerance and immunity, *Annu. Rev. Immunol. 26*, 677-704.

168. Pettersen, F., Tasken, K., and Kvale, D. (2010) Combined Env- and Gag- specific T cell responses in relation to programmed death- 1 receptor and CD4+ T cell loss rates in human immunodeficiency virus- 1 infection, *Clinical & Experimental Immunology 161*, 315-323.

169. Aktas, E., Kucuksezer, U. C., Bilgic, S., Erten, G., and Deniz, G. (2009) Relationship between CD107a expression and cytotoxic activity, *Cellular immunology 254*, 149-154.

170. Zaritskaya, L., Shurin, M. R., Sayers, T. J., and Malyguine, A. M. (2010) New flow cytometric assays for monitoring cell-mediated cytotoxicity, *Expert Review of Vaccines 9*, 601-616.

171. Alter, G., Malenfant, J. M., and Altfeld, M. (2004) CD107a as a functional marker for the identification of natural killer cell activity, *Journal of Immunological Methods 294*, 15-22.

172. Agarwal, A. K., and Kalraiya, R. D. (2014) Glycosylation regulates the expression of Lysosome Associated Membrane Protein-1 (LAMP1) on the cell surface, *J Biosci Tech 5*, 556-563.

173. Alter, G., Malenfant, J. M., Delabre, R. M., Burgett, N. C., Xu, G. Y., Lichterfeld, M., Zaunders, J., and Altfeld, M. (2004) Increased natural killer cell activity in viremic HIV-1 infection, *The Journal of Immunology 173*, 5305-5311.

174. Rubio, V., Stuge, T. B., Singh, N., Betts, M. R., Weber, J. S., Roederer, M., and Lee, P. P. (2003) Ex vivo identification, isolation and analysis of tumor-cytolytic T cells, *Nature Medicine 9*, 1377-1382.

175. Chianea, T., Assidjo, N. E., and Cardot, P. J. (2000) Sedimentation field-flow-fractionation: emergence of a new cell separation methodology, *Talanta 51*, 835-847.

176. Edelman, G. M., Rutishauser, U., and Millette, C. F. (1971) Cell fractionation and arrangement on fibers, beads, and surfaces, *Proc Natl Acad Sci U S A 68*, 2153-2157.

177. Givan, A. L. (2004) Flow cytometry: an introduction, *Methods Mol Biol 263*, 1-32.

178. Bonanno, G., Perillo, A., Rutella, S., De Ritis, D. G., Mariotti, A., Marone, M., Meoni, F., Scambia, G., Leone, G., Mancuso, S., and Pierelli, L. (2004) Clinical isolation and functional characterization of cord blood CD133+ hematopoietic progenitor cells, *Transfusion 44*, 1087-1097.

179. CLARKE, S. J. (2014) Compositions and methods for rapid and reversible biomolecular labeling, Google Patents.

180. Wehbe, M., Labib, M., Muharemagic, D., Zamay, A. S., and Berezovski, M. V. (2014) Switchable aptamers for biosensing and bioseparation of viruses (SwAps-V), *Biosens Bioelectron*.

181. Dobi, A., and v Agoston, D. (1998) Submillimolar levels of calcium regulates DNA structure at the dinucleotide repeat (TG/AC)n, *Proc Natl Acad Sci U S A 95*, 5981-5986.

182. Onoda, A., Arai, N., Shimazu, N., Yamamoto, H., and Yamamura, T. (2005) Calcium ion responsive DNA binding in a zinc finger fusion protein, *J Am Chem Soc 127*, 16535-16540.

183. Watanabe, K., and Iso, K. (1984) Magnesium binding and conformational change of DNA in chromatin, *Biochemistry 23*, 1376-1383.

184. Morris, K. N., Jensen, K. B., Julin, C. M., Weil, M., and Gold, L. (1998) High affinity ligands from in vitro selection: complex targets, *Proc Natl Acad Sci U S A 95*, 2902-2907.

185. Berezovski, M. V., Lechmann, M., Musheev, M. U., Mak, T. W., and Krylov, S. N. (2008) Aptamer-facilitated biomarker discovery (AptaBiD), *J Am Chem Soc 130*, 9137-9143.

186. Mathews, D. H., and Turner, D. H. (2006) Prediction of RNA secondary structure by free energy minimization, *Current Opinion in Structural Biology 16*, 270-278.

187. Basu, S., Binder, R. J., Ramalingam, T., and Srivastava, P. K. (2001) CD91 is a common receptor for heat shock proteins gp96, hsp90, hsp70, and calreticulin, *Immunity 14*, 303-313.

188. Dalal, B. I., and Khare, N. S. (2013) Flow cytometric testing for paroxysmal nocturnal hemoglobinuria: CD64 is better for gating monocytes than CD33, *Cytometry Part B: Clinical Cytometry 84*, 33-36.

189. Hudig, D., Hunter, K. W., Diamond, W. J., and Redelman, D. (2014) Properties of human blood monocytes. I. CD91 expression and log orthogonal light scatter provide a robust

method to identify monocytes that is more accurate than CD14 expression, *Cytometry Part B: Clinical Cytometry 86*, 111-120.

190. Morrot, A., Strickland, D. K., de L Higuchi, M., Reis, M., Pedrosa, R., and Scharfstein, J. (1997) Human T cell responses against the major cysteine proteinase (cruzipain) of Trypanosoma cruzi: role of the multifunctional alpha 2-macroglobulin receptor in antigen presentation by monocytes, *International Immunology 9*, 825-834.
191. Binder, R. J., Han, D. K., and Srivastava, P. K. (2000) CD91: a receptor for heat shock protein gp96, *Nature Immunology 1*, 151-155.
192. Song, S., Kole, S., and Bernier, M. (2012) A chemical crosslinking method for the analysis of binding partners of heat shock protein-90 in intact cells, *BioTechniques*, 1.
193. Nacken, W., Roth, J., Sorg, C., and Kerkhoff, C. (2003) S100A9/S100A8: Myeloid representatives of the S100 protein family as prominent players in innate immunity, *Microscopy Research and Technique 60*, 569-580.
194. Chakraborty, P., Bjork, P., Källberg, E., Olsson, A., Riva, M., Mörgelin, M., Liberg, D., Ivars, F., and Leanderson, T. (2015) Vesicular Location and Transport of S100A8 and S100A9 Proteins in Monocytoid Cells, *PloS One 10*, e0145217.
195. GOULDING, N. J., PAN, L., WARDWELL, K., GUYRE, V. C., and GUYRE, P. M. (1996) Evidence for specific annexin I-binding proteins on human monocytes, *Biochemical Journal 316*, 593-597.
196. Eue, I., König, S., Pior, J., and Sorg, C. (2002) S100A8, S100A9 and the S100A8/A9 heterodimer complex specifically bind to human endothelial cells: identification and characterization of ligands for the myeloid-related proteins S100A9 and S100A8/A9 on human dermal microvascular endothelial cell line-1 cells, *International Immunology 14*, 287-297.
197. Yamamoto, T., Davis, C. G., Brown, M. S., Schneider, W. J., Casey, M. L., Goldstein, J. L., and Russell, D. W. (1984) The human LDL receptor: a cysteine-rich protein with multiple Alu sequences in its mRNA, *Cell 39*, 27-38.
198. Ghobadloo, S. M., Balcerzak, A. K., Gargaun, A., Muharemagic, D., Mironov, G. G., Capicciotti, C. J., Briard, J. G., Ben, R. N., and Berezovski, M. V. (2014) Carbohydrate-based ice recrystallization inhibitors increase infectivity and thermostability of viral vectors, *Scientific Reports 4*, 5903.

199. Milstien, J. B., Galazka, A. M., Kartoglu, U. m., Zaffran, M., and Organization, W. H. (2006) Temperature Sensitivity of Vaccines.

200. Greenwood, B., Salisbury, D., and Hill, A. V. (2011) Vaccines and global health, The Royal Society.

201. Organization, W. H. (1998) Global programme for vaccines and immunization, *Immunization policy. Available from: URL:* http://www. *trufax. org/vaccine/who1995program. html# Im3*.

202. Wang, G., Cao, R.-Y., Chen, R., Mo, L., Han, J.-F., Wang, X., Xu, X., Jiang, T., Deng, Y.-Q., and Lyu, K. (2013) Rational design of thermostable vaccines by engineered peptide-induced virus self-biomineralization under physiological conditions, *Proceedings of the National Academy of Sciences 110*, 7619-7624.

203. Cary, Z. D., Willingham, M. C., and Lyles, D. S. (2011) Oncolytic vesicular stomatitis virus induces apoptosis in U87 glioblastoma cells by a type II death receptor mechanism and induces cell death and tumor clearance in vivo, *Journal of Virology 85*, 5708-5717.

204. Lyles, D., and Rupprecht, C. (2007) Rhabdoviridae, *Fields Virology 5*, 1363-1408.

205. Regules, J. A., Beigel, J. H., Paolino, K. M., Voell, J., Castellano, A. R., Muñoz, P., Moon, J. E., Ruck, R. C., Bennett, J. W., and Twomey, P. S. (2015) A recombinant vesicular stomatitis virus Ebola vaccine—preliminary report, *New England Journal of Medicine*.

206. Clarke, D. K., Cooper, D., Egan, M. A., Hendry, R. M., Parks, C. L., and Udem, S. A. (2006) Recombinant vesicular stomatitis virus as an HIV-1 vaccine vector, In *Springer seminars in immunopathology*, pp 239-253, Springer.

207. Geisbert, T. W., Daddario-DiCaprio, K. M., Lewis, M. G., Geisbert, J. B., Grolla, A., Leung, A., Paragas, J., Matthias, L., Smith, M. A., and Jones, S. M. (2008) Vesicular stomatitis virus-based ebola vaccine is well-tolerated and protects immunocompromised nonhuman primates, *PLoS Pathog 4*, e1000225.

208. Jacobs, B. L., Langland, J. O., Kibler, K. V., Denzler, K. L., White, S. D., Holechek, S. A., Wong, S., Huynh, T., and Baskin, C. R. (2009) Vaccinia virus vaccines: past, present and future, *Antiviral Research 84*, 1-13.

209. Knight, C. A., Hallett, J., and DeVries, A. (1988) Solute effects on ice recrystallization: an assessment technique, *Cryobiology 25*, 55-60.

210. Jackman, J., Noestheden, M., Moffat, D., Pezacki, J. P., Findlay, S., and Ben, R. N. (2007) Assessing antifreeze activity of AFGP 8 using domain recognition software, *Biochemical and Biophysical Research Communications 354*, 340-344.

211. Williams, K. A. (2011) Synthesis and Characterization of Monosaccharide-derived Low Molecular Weight Gelators.

212. Czechura, P., Tam, R. Y., Dimitrijevic, E., Murphy, A. V., and Ben, R. N. (2008) The importance of hydration for inhibiting ice recrystallization with C-linked antifreeze glycoproteins, *Journal of the American Chemical Society 130*, 2928-2929.

213. Harding, M. M., Anderberg, P. I., and Haymet, A. (2003) 'Antifreeze'glycoproteins from polar fish, *European Journal of Biochemistry 270*, 1381-1392.

214. Tachibana, Y., Fletcher, G. L., Fujitani, N., Tsuda, S., Monde, K., and Nishimura, S. I. (2004) Antifreeze glycoproteins: elucidation of the structural motifs that are essential for antifreeze activity, *Angewandte Chemie 116*, 874-880.

215. Wilkinson, B. L., Stone, R. S., Capicciotti, C. J., Thaysen- Andersen, M., Matthews, J. M., Packer, N. H., Ben, R. N., and Payne, R. J. (2012) Total synthesis of homogeneous antifreeze glycopeptides and glycoproteins, *Angewandte Chemie International Edition 51*, 3606-3610.

216. Pfannemüller, B., and Welte, W. (1985) Amphiphilic properties of synthetic glycolipids based on amide linkages. I. Electron microscopic studies on aqueous gels, *Chemistry and Physics of Lipids 37*, 227-240.

217. Fuhrhop, J. H., Schnieder, P., Boekema, E., and Helfrich, W. (1988) Lipid bilayer fibers from diastereomeric and enantiomeric N-octylaldonamides, *Journal of the American Chemical Society 110*, 2861-2867.

218. Capicciotti, C. J., Leclère, M., Perras, F. A., Bryce, D. L., Paulin, H., Harden, J., Liu, Y., and Ben, R. N. (2012) Potent inhibition of ice recrystallization by low molecular weight carbohydrate-based surfactants and hydrogelators, *Chemical Science 3*, 1408-1416.

219. Tam, R. Y., Ferreira, S. S., Czechura, P., Chaytor, J. L., and Ben, R. N. (2008) Hydration Index□ A Better Parameter for Explaining Small Molecule Hydration in Inhibition of Ice Recrystallization, *Journal of the American Chemical Society 130*, 17494-17501.

220. Kissmann, J., Ausar, S. F., Rudolph, A., Braun, C., Cape, S. P., Sievers, R. E., Federspiel, M. J., Joshi, S. B., and Middaugh, C. R. (2008) Stabilization of measles virus for vaccine formulation, *Human Vaccines 4*, 350-359.